Coalesce Research Group

APPROVED PROVIDER #782310

13th International Conference on

MATERIALS SCIENCE AND ENGINEERING

October 22-24, 2025

In Collaboration with

Research Institute of Semiconductor Physics and Microelectronics at The National University of Uzbekistan, Tashkent, Uzbekistan

Institute of Materials Science of Uzbekistan Academy of Sciences

Contact Us:

Phone: +1-718-543-9362

Whatsapp: +1-864-275-0927

Coalesce Research Group

33 Market Point Dr,

Greenville, SC 29607, USA

Scientific Program

Wi-Fi Details:

Username: Conference hall
Password: Ispmconferencehall

Scientific Program

Wednesday
October 22, 2025

13th International Conference on

Materials Science and Engineering

Day-1 | October 22, 2025	
Conference Hall: Conference Hall	
08.00 - 08.45	Registration
08.45 - 09.00	Introduction
Keynote Presentations	
09.00 - 09.15	Introduction Keynote Speech
	Inom Madjidov, Rector of National University of Uzbekistan named after Mirzo Ulugbek, Uzbekistan
09.15 - 09.50	Remote THz Biosensor
	Janez Trontelj, University of Ljubljana, Slovenia
09.50 - 10.25	Buckybowl as A New Motif for 2.5-Dimensional Materials
	Hidehiro Sakurai, The University of Osaka, Japan
10.25 - 11.00	General Behavior and Mechanisms of Dendritic Crystal Formation in Evaporated Biological Solutions and its Applications
	Yao Xiong Huang, Jinan University, China
Network & Refreshments (11.00 - 11.10) @ Coffee Area	
11.10 - 11.25	About Physical- Technical Institute of Uzbekistan Academy of Sciences
	Khusniddin Olimov, Director of The Physical-Technical Institute, Uzbekistan
11.25 - 12.00	Design and Performance of Novel Thermally Conductive Polymer Composites Filled with Graphite Materials
	Shulin Bai, Peking University, China
12.00 - 12.20	Nanocrystals Produced by Nuclear Reactions in Lithium Fluoride Crystals
	Ibragimova Elvira, Institute of Nuclear Physics of Uzbekistan Academy of Sciences, Uzbekistan
12.20 - 12.35	The Bandgap Value of The Si3MnS Phase in a Si Supercell (1X1X3)
	Mavlyanov Abdulaziz, Deputy Director of Institute of Semiconductor Physics and Microelectronics, National University of Uzbekistan, Uzbekistan
Oral Presentations	
Chair:	**Andrej Štrukelj, University of Maribor, Slovenia**
Chair:	**Miroslav Premrov, University of Maribor, Slovenia**
Chair:	**Shulin Bai, Peking University, China**
Chair:	**Janez Trontelj, University of Ljubljana, Slovenia**
Chair:	**Sharifa Utamuradova, Director of the Institute of Semiconductor Physics and Microelectronics, National University of Uzbekistan, Uzbekistan**
Sessions:	Materials Science and Applications | Materials Science and Engineering | Mechanical and Civil Engineering | Engineering
12.35 - 13.00	Floating Zone Melting Synthesis and Characterization of High Entropy Boride Powders
	Hasan Goçmez, Kutahya Dumlupinar University, Turkey
Group Photo (13.00 - 13.10)	
Lunch (13.10 - 14.00) @ Lunch Area	

13th International Conference on

Materials Science and Engineering

14.00 - 14.25	Effect of Laser Textured Micro-patterns on The Corrosion Susceptibility of NiTi Alloy in Simulated Body Fluid
	Mariam Maroof, Motilal Nehru National Institute of Technology Allahabad Prayagraj, India
14.25 - 14.50	Numerical Analysis of Light-timber Frame Wall Elements with Various Sheathing Material
	Jelena Vilotijević, Andrej Štrukelj and Miroslav Premrov, University of Maribor, Slovenia
14.50 - 15.15	Composite Coatings from Cobalt Alloys with Specified Physical and Mechanical Properties
	Gauhar Mussabek and Gulmira Yar Mukhamedova, Al-Farabi Kazakh National University, Kazakhstan
15.15 - 15.40	The Impact of Metallic Modification and Glued Bed Technology on Sorbent Properties
	Agata Mlonka Medrala, AGH University of Krakow, Poland
15.40 - 16.05	Silicon Surface Engineering with Plasmonic and Up-conversion Coatings for Photovoltaic Applications
	Alma Dauletbekova, L.N. Gumilyov Eurasian National University, Kazakhstan
Network & Refreshments (16.05 - 16.15) @ Coffee Area	
16.15 - 16.40	Evaluating Crumb Rubber Implementation in South African Asphalt Industry towards Sustainable Waste Tyre Management
	Mohamed M H Mostafa, University of KwaZulu-Natal, South Africa
16.40 - 17.05	Reusing Construction Waste as Pavement Material
	Bojan Žlender, University of Maribor, Slovenia
Poster Presentations	
Poster Judge	**Arkadii Arinstein, Technion - Israel Institute of Technology, Israel**
Poster Judge	**Chien-Hsiang Chang, National Cheng Kung University, Taiwan**
Poster Judge	**Janez Trontelj, University of Ljubljana, Slovenia**
MSEPP - 01	Change of Copper Wire Microstructure in The Process of Deformation by A New Method
	Andrey Volokitin, Karaganda Industrial University, Kazakhstan
MSEPP - 02	Spectrophotometric Determination of Ceftriaxone with Pre-Solid-Phase Extraction using A Copper Trimesinate-Graphene Oxide Nanocomposite
	Victoria N Naumkina, Southern Federal University, Russia
MSEPP - 03	Development of Cryogels based on Natural Polymers using Click Chemistry and Cryopolymerization Methods
	Kudaibergen Gulshakhar and Akhmetkarimova Zhanar, National Center for Biotechnology, Kazakhstan
MSEPP - 04	Solid-phase Extraction of Azorubin and Ponceau with A Mixed-ligand Complex based on Nickel Terephthalate and 2,2'-Dipyridine
	Maria A Chernomorova, Southern Federal University, Russia

13th International Conference on

Materials Science and Engineering

MSEPP - 05	Electrochemical Characterization of $(Ti_{0.2}Zr_{0.2}Hf_{0.2}Nb_{0.2}Ta_{0.2})B_2$ Powders for Supercapacitor Applications
	Mustafa Tuncer, Kutahya Dumlupinar University, Turkey
MSEPP - 06	Cryogenic Cooling of AISI 304 Steel Wire in The Drawing Process
	Volokitina Irina Evgenievna, Karaganda Industrial University, Kazakhstan
MSEPP - 07	Radiation Damage Caused by Swift Heavy Ions in YAG:Nd^{3+} Single Crystals
	Baubekova Guldar, L.N. Gumilyov Eurasian National University, Kazakhstan
MSEPP - 08	Color Center Generation and Annealing Kinetics in BaF_2 Irradiated with Swift Heavy Ions
	Daurzhan Kenbayev, Shakarim University, Kazakhstan
MSEPP - 09	Obtaining and Studying the Properties of Silicides of the Mo-Si System
	Akhmedova Nilufar, Institute of Semiconductor Physics and Microelectronics, National University of Uzbekistan, Uzbekistan
MSEPP - 10	Universal Camera for The EG-2 Linear Accelerator
	Saydimov Yakubbay, Institute of Semiconductor Physics and Microelectronics, National University of Uzbekistan, Uzbekistan
MSEPP - 11	The Effect of Impure Clusters on The Structural Properties of Si Doped Cu
	Turmanova Raymash, Institute of Semiconductor Physics and Microelectronics, National University of Uzbekistan, Uzbekistan
MSEPP - 12	Formation of Impurity Defects in Si Doped with Ni and Fe
	Khaytimmetov Nodir, Institute of Semiconductor Physics and Microelectronics, National University of Uzbekistan, Uzbekistan
MSEPP - 13	Lithium Nobate ($LiNbO_3$) Thin Films Produced by Magnetron Ion Sputtering in The MSIR System
	Azamatov Zakirjan, Institute of Semiconductor Physics and Microelectronics, National University of Uzbekistan, Uzbekistan
MSEPP - 14	Investigate of Morphology of Silicon Doped with Pd Atoms
	Rakhmanov Dilmurod, Institute of Semiconductor Physics and Microelectronics, National University of Uzbekistan, Uzbekistan
MSEPP - 15	Effect of Gamma Irradiation on The Structure of Tin-Doped Silicon Monocrystals
	Bokiev Bakhodir, Institute of Semiconductor Physics and Microelectronics, National University of Uzbekistan, Uzbekistan
MSEPP - 16	Structural Features of Single-Crystal Silicon with Scandium and Yttrium Impurities
	Khamidjonov Islomjon, Institute of Semiconductor Physics and Microelectronics, National University of Uzbekistan, Uzbekistan
MSEPP - 17	Influence of Cooling Rate on Structural and Electrophysical Changes in Zirconium-Doped Silicon (Si<Zr>)
	Ismoilov Shukhratjon, Institute of Semiconductor Physics and Microelectronics, National University of Uzbekistan, Uzbekistan

13th International Conference on

Materials Science and Engineering

MSEPP - 18	Analysis of Mn-Related Defects in Si by using X-Ray Diffraction **Matchonov Khusniddin, Institute of Semiconductor Physics and Microelectronics, National University of Uzbekistan, Uzbekistan**
MSEPP - 19	Structural Analysis of Monocrystalline Silicon Doped with Lutetium **Bahronkulov Zavkiddin, Institute of Semiconductor Physics and Microelectronics, National University of Uzbekistan, Uzbekistan**
MSEPP - 20	Influence of 60Co γ-Quanta and Electrons on The Process of Radiation Defect Formation in Silicon Doped with Ytterbium Atoms **Bekmuratov Mansur, Institute of Semiconductor Physics and Microelectronics, National University of Uzbekistan, Uzbekistan**
MSEPP - 21	Deep Centers and Their Influence on The Electrophysical Properties of Dysprosium-doped Silicon **Norkulov Shakhriyor, Institute of Semiconductor Physics and Microelectronics, National University of Uzbekistan, Uzbekistan**
MSEPP - 22	The Role and Importance of Capacitive Semiconductor Electronic Modules in Modern Protection Systems **Murodov Sherali, Institute of Semiconductor Physics and Microelectronics, National University of Uzbekistan, Uzbekistan**
MSEPP - 23	The Role and Importance of Semiconductor Modules in Ensuring Technical Safety of Facilities **Rashidov Sunnatillo, Institute of Semiconductor Physics and Microelectronics, National University of Uzbekistan, Uzbekistan**
MSEPP - 24	Kinetics of Clearance on Bismuth Films in the $CdTe_2$ Light-sensitive System **Khaydarov Bunyodbek, Ferghana State University, Uzbekistan**
MSEPP - 25	Theoretical Calculation of Photodetector Parameter Selection for A Gas-Discharge Cell **Khaydarov Zokirjon, Ferghana State University, Uzbekistan**
MSEPP - 26	Optical and Photoelectric Properties of Solar Cells based on p-CdTe-n-CdS and p-CdTe-n-CdSe Heterostructures with Deep Impurity Levels **Ergashev Ravshanbek, Ferghana State University, Uzbekistan**
MSEPP - 27	Thermoelectric Generators for Power Supply of Automation Equipment in Industrial Enterprises **Latipova Mukhayyo, Ferghana State Technical University, Uzbekistan**
MSEPP - 28	Influence of γ-Quanta on The Electrophysical Parameters of Silicon Avalanche Transit Time Diodes **Tagaev Marat, Karakalpak State University, Uzbekistan**
MSEPP - 29	Investigation of The Optical and Electrical Properties of Sb_xSe_y Films Deposited at Different Source Evaporation Temperatures **Kuchkarov Kudratjon, Institute of Physics and Technology named after S.A. Azimov, Academy of Sciences of the Republic of Uzbekistan, Uzbekistan**
MSEPP - 30	Combined Diffusion of Ga and P Mixture Atoms in Silicon **Turekeev Xojaaxmetjan, Karakalpak State University, Uzbekistan**

13th International Conference on

Materials Science and Engineering

MSEPP - 31	Influence of Temperature and Magnetic Field on The Density of Energy States in The Conduction Band of Quantum Well Semiconductor Materials
	Dadamirzaev Muzaffar, Namangan State Technical University, Uzbekistan
MSEPP - 32	γ-Al_2O_3 and Dehydration of Alcohols
	U.A.Karimova, Academician Y.H. Mammadaliyev Institute of Petrochemical Processes of the Ministry of Science and Education of The Republic of Azerbaijan, Azerbaijan
MSEPP - 33	Morphological Characterization of $(GaAs)_{1-x-y}(Ge2)_x(ZnSe)_y$ Solid Solutions
	Zaynobidinov Sirojiddin, Andijan State University, Uzbekistan
MSEPP - 34	Morphology of Nickel Impurity Accumulations in Silicon
	Sobirova Shirin, Institute of Semiconductor Physics and Microelectronics, National University of Uzbekistan, Uzbekistan
MSEPP - 35	Optoelectronic Device for Information Protection in Fiber-Optic Communication Lines
	Nabiev Davronjon, Institute of Semiconductor Physics and Microelectronics, National University of Uzbekistan, Uzbekistan
MSEPP - 36	Study of the Optical Properties of Cotton Fibers
	Mamadalimov Abdugafur, Institute of Semiconductor Physics and Microelectronics, National University of Uzbekistan, Uzbekistan
MSEPP - 37	Physical Process of Temperature Distribution as A Time Dependence in A Solid, with A Non-stationary Heat Flow
	Kasimakhunova Anarkhan, Ferghana State Technical University, Uzbekistan
MSEPP - 38	Photocatalytic, Structural and Optical Properties of Undoped and Doped Zinc Oxide Nanostructures
	Esbergenova Amugul, Institute of Semiconductor Physics and Microelectronics, National University of Uzbekistan, Uzbekistan
MSEPP - 39	Formation of Cu-Ni-Sn Precursors on A Flexible Metal Foil to Obtain Semiconductor $Cu_2NiSn(S,Se)_4$ Thin Films
	Fayzullaev Kakhramon, Institute of Semiconductor Physics and Microelectronics, National University of Uzbekistan, Uzbekistan
MSEPP - 40	Nanocrystals Produced by Nuclear Reactions in Lithium Fluoride Crystals
	Ibragimova Elvira, Institute of Nuclear Physics of Uzbekistan Academy of Sciences, Uzbekistan
MSEPP - 41	Preliminary Testing of A Photovoltaic Installation with A Dual-axis Solar Tracking System
	Daminov Sultonjon, Institute of Semiconductor Physics and Microelectronics, National University of Uzbekistan, Uzbekistan
MSEPP - 42	Investigation of the Temperature-dependent Photovoltaic Behavior of Silicon Heterojunction Solar Cells with Gallium- and Phosphorous-doped Silicon Substrates
	Ataboev Omonboy, Institute of Semiconductor Physics and Microelectronics, National University of Uzbekistan, Uzbekistan

Day-1 Concludes followed by Certificate Distribution

13th International Conference on

Materials Science and Engineering

Day-2 | October 23, 2025	
Conference Hall: Conference Hall	
Keynote Presentations	
09.00 - 09.35	Enhancing Materials Soundness in Different Projects (Performance, Quality, & Life Cycle Costing) through The Value Analysis Tools
	Jamal Alduaij, Chairman, GCC BUREAU, Kuwait
09.35 - 10.10	Machine Learning for Logistics and Transportation Engineering-Gender Disparities in Rural Motorcycle Accidents: A Neural Network Analysis of Travel Behavior Impact
	Ittirit Mohamad, King Mongkut's University of Technology Thonburi, Thailand
10.10 - 10.45	Necessary Revision of Carbon Solid State and Raman Spectroscopy Fundamentals for Comprehensive Mastering of More Performing Advanced Materials Applications
	Stephane Neuville, Independent Scientific Consultant, France
10.45 - 11.20	Imitation Modeling. The Behavior Analysis of The Mixture of Two Oppositely Charged Polyelectrolytes with The Help of A Macroscopic Mechanical System
	Arkadii Arinstein, Technion - Israel Institute of Technology, Israel
Network & Refreshments (11.20 - 11.30) @ Coffee Area	
11.30 - 11.50	Effect of Radiation on The Electrophysical Properties of Silicon, doped With Palladium Atoms
	Rakhmanov Dilmurod, Institute of Semiconductor Physics and Microelectronics, National University of Uzbekistan, Uzbekistan
11.50 - 12.10	The Role and Importance of Semiconductor Modules in Ensuring Technical Safety of Facilities
	Rashidov Sunnatillo, Institute of Semiconductor Physics and Microelectronics, National University of Uzbekistan, Uzbekistan
Oral Presentations	
Chair:	**Chien-Hsiang Chang, National Cheng Kung University, Taiwan**
Chair:	**Janez Trontelj, University of Ljubljana, Slovenia**
Chair:	**Arkadii Arinstein, Technion - Israel Institute of Technology, Israel**
Chair:	**Abdulaziz Mavlyanov, Deputy Director of The Institute of Semiconductor Physics and Microelectronics, National University of Uzbekistan, Uzbekistan**
Sessions:	Materials Science and Engineering | Metallurgy, Metals and Mining Materials | Functional Materials: Properties and Applications | Batteries and Solid Electrolyte Materials | Catalysis and Chemical Engineering | Mechanical and Civil Engineering | Polymers & Biopolymers | Other Key Topics
12.10 - 12.35	Theoretical and Spectral Characterization of Biologically Active Ln(III) Complexes
	Irena Kostova, Medical University, Bulgaria
12.35 - 13.00	Morphological Characteristics of Nematic Droplets Doped with Metal Nanoparticles
	Makhsudov Barot Islomovich, Tajik National University, Tajikistan

13th International Conference on

Materials Science and Engineering

Lunch (13.00 - 14.00) @ Lunch Area	
14.00 - 14.25	Defect Engineering of $PbWO_4$ Single Crystals by Heavy Xe Ions
	Ainash Abdrakhmetova, L.N. Gumilyov Eurasian National University, Kazakhstan
14.25 - 14.50	Preparation of Zwitterionic Solid Polymer Electrolytes for Lithium-ion Batteries
	Chien-Hsiang Chang, National Cheng Kung University, Taiwan
14.50 - 15.15	Novel HEM-based Catalysts for Energy and Environmental Applications
	Miran Ceh, Jozef Stefan Institute, Slovenia
15.15 - 15.40	The Mechanism of Heterogeneous Alkaline Deacetylation of Chitin
	Svetlana Derkach, Murmansk Arctic University, Russia
15.40 - 16.05	Valorization of Mining and Metallurgical Waste from Metal Extraction: Global Trends and Initiatives
	Irina Marinova, Institute of Mineralogy and Crystallography, Bulgaria
Network & Refreshments (16.05 - 16.15) @ Coffee Area	
16.15 - 16.40	Orientation-dependent Defect Formation in $MgAl_2O_4$ Crystals under Swift Heavy Ion Irradiation
	Abdirash Akilbekov, L.N. Gumilyov Eurasian National University, Kazakhstan
16.40 - 17.05	Waste Mullite Used for Refractory Lining of The Combustion Furnace
	Rene Sommr, SMS CZ s.r.o, Czech Republic
17.05 - 17.30	High-Entropy Shape Memory Alloys for High or Cryogenic Temperatures Applications
	Aleksei Sibirev, Saint-Petersburg State University, Russia
17.30 - 17.55	Thermal Cycling Stability of the Functional Properties of The NiTi-based Shape Memory Alloys
	Natalia Resnina, Saint-Petersburg State University, Russia
Day-2 Concludes followed by Certificate Distribution	

13th International Conference on

Materials Science and Engineering

Day-3 | October 24, 2025	
Conference Hall: Institute of Materials Science, Uzbekistan	
Keynote Presentation	
10.00 - 10.25	About Institute of Materials Science
	Parpiev Odilkhuja, Director of The Institute of Materials Science, Uzbekistan
Oral Presentations	
Chair:	**Abdulaziz Mavlyanov, Deputy Director of The Institute of Semiconductor Physics and Microelectronics, National University of Uzbekistan, Uzbekistan**
Chair:	**Sharifa Utamuradova, Director of The Institute of Semiconductor Physics and Microelectronics, National University of Uzbekistan, Uzbekistan**
Sessions:	Materials Science and Engineering | Metallurgy, Metals and Mining Materials | Functional Materials: Properties and Applications | Batteries and Solid Electrolyte Materials | Catalysis and Chemical Engineering | Mechanical and Civil Engineering | Polymers & Biopolymers | Other Key Topics
10.25 - 10.50	Hydrogen Storage Technologies
	Payzullakhanov Mukhammad-Sultankhan, Doctor of Technical Sciences, Head of Laboratory of The Institute of Materials Science, Uzbekistan
10.50 - 11.15	Efficient Photocatalysts for Producing Hydrogen using Solar Energy
	Rakhimov Rustam, Doctor of Technical Sciences, Head of Laboratory of The Institute of Materials Science, Uzbekistan
Network & Refreshments (11.15 - 11.30) @ Coffee Area	
11.30 - 11.55	Preliminary Testing of a Photovoltaic Installation with a Dual-Axis Solar Tracking System
	Daminov Sultonjon, Institute of Semiconductor Physics and Microelectronics, National University of Uzbekistan, Uzbekistan
E-Poster Presentations	
MSE-EP 1	Innovative Sensor Technologies for Heavy Metal Ion Detection in Water: The Role of IoT in Sustainable Water Resource Management
	Babankumar S Bansod, CSIR-Central Scientific Instrument Organisation Chandigarh, India
MSE-EP 2	PtNPs-Coated Gold Surface for High-Performance Electrochemical Sensing of Lead in Environmental Samples
	Monika Antil, CSIR-Central Scientific Instrument Organisation Chandigarh, India
MSE-EP 3	The Effect of Mechanical Activation on the Structural and Phase States and Hydrogen Absorption Properties of the LaNi5 Intermetallic Compound- Review
	Nassyrova Anar, NJSC East Kazakhstan University Named after Sarsen Amanzholov, Kazakhstan
MSE-EP 4	Effect of Acidic Environment on the Structure of Composite Coatings Based on Supermolecular Polyethylene
	Perassyl Zhanimkhan, Sarsen Amanzholov East Kazakhstan University, Kazakhstan

13th International Conference on

Materials Science and Engineering

MSE-EP 5	Investigation of Intergranular Corrosion Resistance in Welded Dissimilar Stainless Steels 12X18H10T and AISI 316
	Eldos Akbolatov, Institute of Atomic Energy, Kazakhstan

Lunch (12.30 - 13.30) @ Lunch Area

University Visit 13:30 Onwards

Network & Refreshments followed by University Tour

Day-3 Concludes followed by Certificate Distribution and Vote of Thanks

Day-1
Keynote Presentations

REMOTE TH_Z BIOSENSOR

Janez Trontelj

University of Ljubljana, Slovenia

Abstract

Background: THz waves are a newcomer in remote sensors family. Their advantage is the ability to penetrate the nonconducting material like clothes and not human cells, consequently not hurting the person subject the full body scan.

Objective: In contrary the x ray scanning is damaging by ionizing a healthy cells which can alter their chemical structure and affect its function.

Methods: To obtain relevant info, the affected part of the body should be irradiated by THz waves, the reflected waves should be detected and analyzed.

Results: One of the possible scenarios where THz waves could be the best option is its application at a scene of disastrous earthquake, where a large number of people would be unconscious and laying under debris.

Conclusion: THz sensor system would help to perform a triage by selecting the ones still alive and breathing. The rescuing team should be equipped with a portable THz system with range of 5-10 meters.

Biography

Janez Trontelj is a Head of the Laboratory for Microelectronics at the Faculty of Electrical Engineering, University of Ljubljana. He graduated in 1965 at the Faculty of Electrical Engineering in University of Ljubljana and received his master's and PhD degree in 1969 and 1971, subsequently. He is a principal author of the first scientific book on mixed signal circuit design "Analog Digital ASIC Design" published by McGraw Hill in 1989. He authored or co-authored 26 granted patents, 13 of them being international. The major results of his research work are the development of several microcircuits, as well as magnetic and mechanical microsystems, which are being produced in millions yearly. He is internationally recognized as an expert on magnetic sensor technology, Terahertz sensors and systems. He designed more than a dozen ASICs with integrated smart sensor systems, SoCs or SiPs used for different applications. He is the recipient of many national awards and is a member of Slovenian Academy of Engineering. He has held several invited talks at eminent conferences. He is a regular member of Sigma Xi Honor Society, and recipient of IAM Scientist Medal Lecture.

BUCKYBOWL AS A NEW MOTIF FOR 2.5-DIMENSIONAL MATERIALS

Hidehiro Sakurai
The University of Osaka, Japan

Abstract

"Buckybowls" refer to a class of organic compounds consisting of fullerene fragments terminated with hydrogen atoms. Among them, two pristine structures are known: corannulene, with five-fold symmetry, and sumanene, with three-fold symmetry. In particular, sumanene has attracted attention due to its symmetry, making it a promising candidate for applications across various fields. In the realm of two-dimensional materials, theoretical studies suggest that sumanene derivatives can effectively modulate the band gap of graphene. When intercalated into bilayer graphene, they function as efficient piezoelectric conversion elements. Moreover, the synthesis of covalent organic frameworks (COFs) incorporating the sumanene motif enables the construction of non-planar carbon network architectures. These materials can be considered "2.5-dimensional" materials, offering added functionality beyond conventional two-dimensional systems. In this presentation, I will introduce the chemistry of sumanene and explore its potential as a 2.5D material.

Biography

Hidehiro Sakurai received his Ph.D. degree from U. Tokyo in 1994. After Assistant Professor in Tokyo (1994– 1996, 1998–2000), JSPS Postdoctoral fellow at U. Wisconsin (1996–1998), and an Associate Professor in Osaka U. (2000-2004), he moved to the Institute for Molecular Science (IMS). In 2014, he returned to U. Osaka. Professor Sakurai has studied various topics in physical organic chemistry, and his current research interests include the science of buckybowls, and nanometal catalysts.

GENERAL BEHAVIOR AND MECHANISMS OF DENDRITIC CRYSTAL FORMATION IN EVAPORATED BIOLOGICAL SOLUTIONS AND ITS APPLICATIONS

Yao-Xiong Huang
Jinan University, China

Abstract

With AI aided analysis, we revealed the onset and dynamic process, the behavior, and general rules of the dendritic crystal growth in evaporated biological solutions as a function of temperature, pH value, and the concentrations of their major components (NaCl, KCl, $NaHCO_3$, and D-glucose). We proposed the crystallization mechanism for each of them at various conditions and indicated the factors that control the formation of dendritic crystals. We showed that at a temperature ranging from 20 to 40°C, only the solution mixed with crystalline and amorphous substances could form dendritic crystals. The rise in temperature and decreasing pH from the neutral value would reduce the pattern divergence induced by different components and concentrations. Increasing the content of the crystalline substances would make the dendritic crystals thicker and have less branching. The dendritic crystals are mainly composed of the salt with the highest ratio R of concentration/solubility. The crystal structure of the salt also determines the shape of the dendrites. The amorphous substances mainly distribute at the edge of the dried spot to form a ring and deposit in the gaps between the dendritic crystals or the growing tips of the dendrites. This study suggests that based on the behavior of the dendrite growth, it is possible to use the methods of dendrite formation and pattern analysis to replace analytical instruments for some solution physicochemical tests in different aspects of biomedicine or grow dendritic crystals with desired patterns for various applications.

Biography

Yao-Xiong Huang, at the present is a Professor of biomedical engineering and Medical physics. in the Department of Biomedical Engineering, Jinan University. He also has been the Member of the Academic Degree Committee of the State Council of China; the Vice President of the Chinese Society of Medical Physics; the Member of the Science Committee of International Organization of Medical Physics; and the chairman of the Science Committee of Asia-Oceania Federation of Organization for Medical Physics. His specialty: Biophysics, biomedical engineering, physics, medical physics, photobiology, and laser medicine. Since 1978, he has engaged in the researches on Laser medicine, nano-biotechnology, medical imaging, optoelectronics, microscope imaging and spectroscopy, cellular and tissue engineering, and nano-nuclear medicine. He has published over 400 papers and five academic books, and is the owner of 36 patents.

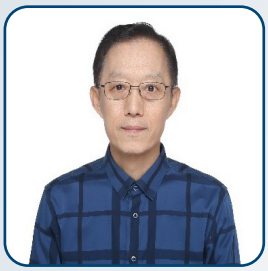

DESIGN AND PERFORMANCE OF NOVEL THERMALLY CONDUCTIVE POLYMER COMPOSITES FILLED WITH GRAPHITE MATERIALS

Shulin Bai

Peking University, China

Abstract

With the 5G and information technology development, the miniaturization and high power of devices generate huge heat which threatens gravely the operation and span life of device. Therefore, heat management is required by developing thermal interface materials (TIMs) with high thermal conductivity (TC), which can dissipate heat timely and effectively. Our work focus on developing new composite materials with super high TC. The graphite film (GF) and graphite foam (GFoam) are employed as filler, and silicon rubber (SR) as matrix. A simple stacking and vertically cutting method is developed to construct a TIM with both high TC and soft compressibility. The prepared 75 vol% (GFoam(600):GF=1:1)/SR composite has Tc of 235.86 W m^{-1} K^{-1}, thermal resistance of 0.611°C cm^2 W^{-1}, and compressive modulus as low as 2.22 MPa. In this composites, GF provides high thermal pathway, while GFoam guarantees high flexibility. When the composite is applied for temperature control of LED, it shows an excellent thermal management performance, leading to a 27.4°C temperature drop of the working temperature of LED.

Biography

Shu-Lin Bai obtained his PhD degree from Ecole Centrale des Arts et Manufactures de Paris, France in 1993, MS degree from Dept. of Engineering Mechanics in 1986 and BS degree in 1983 from Dept. of Materials Engineering of Dalian University of Technology, China. He joined Peking University from 1996. His expertise is in the area of polymer matrix composites filled with particles (graphene, CNTs, BN, SiO2, etc.) and fibers (carbon fiber, glass fiber, etc.), specially on processing and characterization including thermal, electrical and mechanical properties. He has published about 200 journal papers. His current research focuses on design, manufacture and thermal/ electrical/ mechanical properties of nanofillers filled polymer nanocomposite, as well as processing and application of long fiber reinforced thermoplastics (LFT). He is founder, chairman/co-chairman of Asia-Europe Symposium on Processing and Properties of Reinforced Polymers for many times.

THE BANDGAP VALUE OF THE SI3MNS PHASE IN A SI SUPERCELL (1X1X3)

Sharifa Utamuradova, Abdulaziz Mavlyanov* and Gulhayo Abdurazzakova
Research Institute of Semiconductor Physics and Microelectronics, Uzbekistan

Abstract

Background: The Si lattice with a diamond structure scaled up to a supercell (1X1X3) where impurity atoms of S and Mn are located in substitutional positions in the first coordination shell in the lattice has been chosen as a research object. The reason behind choosing for quantum-chemical calculations Si3MnS was that interesting physical properties and rich polymorphism have prompted many laboratories to study MnS nanocrystals in view of their possible application as photoluminescent components, catalysts, as anode material for lithium-ion batteries, and also as supercapacitors.

Objective: To model and quantum-chemically calculate hypothetical Si3MnS structure that represents a "hybrid" of the cubic lattice of silicon Si and sphalerite ZnS. To calculate the forbidden bandgap energy of Si3MnS phase in Si supercell (1X1X3).

Methods: All calculations were performed using the Quantum ESPRESSO suit for first-principles electronic-structure modelling and calculations. Before the calculation, the parameters for the Si3MnS phase in a scaled-up supercell (1X1X3) were entered. To calculate the density of electron states (DOS) for phase Si3MnS in the supercell (1X1X3), the density functional theory (DFT) method was used in the Quantum ESPRESSO software package with Hubbard U correction (DFT+U).

Results: By checking the DOS (density of states) output file, we were able to extract the values needed to calculate the forbidden band gap. The Fermi level was determined:

E (eV) dos(E) Int dos(E) EFermi = 7.049 eV

Near the Fermi level of 7.049 eV, all subsequent DOS values equal to zero were tracked. Incidentally, after several mathematical operations we have been able to determine the bandgap which accounted 1.14 eV.

Conclusion: A model and results of quantum-chemical calculation of a hypothetical phase of Si3MnS, similar to the cubic structure of F43m-β-MnS were proposed. The bandgap value Eg of the Si3MnS phase obtained in quantum-chemical numerical calculation of the electron position was presented.

Biography

Mavlyanov Abdulaziz is an electronics engineer graduating from Tashkent State Technical University, majoring in Semiconductors and Dielectrics in 1990-1995. PhD in 2018 in Semiconductor Physics. Certificate of Senior Scientific Researcher in 2020. Since 2025- Acting Deputy Director at the Research Institute of Semiconductor Physics and Microelectronics. The activities consist in performing scientific research, as well as general overview and monitoring of lab research and administrative activities. The research interests are in: high temperature annealing and doping of silicon with various impurities; study of photoconductivity of single crystal silicon samples doped with Mn and some AII and BVI impurity atoms; quantum chemical modelling and calculation of basic matrix of silicon with new phases and cells; structural and morphology studies of silicon samples.

Day-1
Oral Presentations

FLOATING ZONE MELTING SYNTHESIS AND CHARACTERIZATION OF HIGH ENTROPY BORIDE POWDERS

Hasan Goçmez

Kütahya Dumlupınar University, Turkey

Abstract

Most research is concentrated on advancing novel electrode materials that will produce superior performance and low cost. In this study, fiber-shaped high entropy borides $(Ti_{0.2}Zr_{0.2}Hf_{0.2}Nb_{0.2}Ta_{0.2})B_2$ compositions have been successfully synthesized by zone melting methods. The TiB_2, ZrB_2, HfB_2, NbB_2 and TaB_2 powders were used as initial materials. In the final product, the fibers of HEBs were obtained with a high surface area. X-ray powder diffraction (XRD), Scanning electron microscopy (SEM), Transmission electron microscopy (TEM), Electron paramagnetic resonance (EPR) and SEM-EDX techniques have been used to investigate phase content, microstructure and composition, respectively. The XRD analysis of the powders confirmed the presence of $(Ti_{0.2}Zr_{0.2}Hf_{0.2}Nb_{0.2}Ta_{0.2})B_2$. in their compositions.

Biography

Hasan Göçmez, PhD, received the B.E. degree in the Department of Metallurgical and Material Science from the University of Middle east Technical, Turkey, in 1977, and the M.Tech. and Ph.D. degrees in Material/Ceramic Engineering from the Rutgers University, USA, in 1997 and 2001, respectively. He has experience with ceramic processing, nanomaterials and photovoltaic materials. He is professor in Department of Metallurgical and Material Engineering at Dumlupinar University, Turkey.

EFFECT OF LASER TEXTURED MICRO-PATTERNS ON THE CORROSION SUSCEPTIBILITY OF NITI IN SIMULATED BODY FLUID

Mariam Maroof
Motilal Nehru National Institute of Technology Allahabad, India

Abstract

Background: The surface properties of Nitinol (NiTi) based biomedical devices influences their long-term corrosion performance once implanted inside the human body. Among the surface modification techniques, laser-texturing has proved to be a cutting-edge technology in enhancing NiTi characteristics by formation of thin surface layer that retards Ni ion diffusion.

Objective: To investigate the electrochemical behavior and passive film characteristics of 0.2mm thick biomedical grade NiTi sheet under contact with simulated-body-fluid (SBF).

Methods: Two micro-patterns (HC: honeycomb, S: square) were laser-textured on NiTi surface. Samples were divided into two sub-groups as per texture-densities (TD): high TD-honeycomb (HC-h): 50%, low TD-honeycomb (HC-l): 25%, high TD-square (S-h): 36%, low TD-square (S-l): 18%. Electrochemical assessment was carried out in SBF by first monitoring open circuit potential (OCP) followed by electrochemical impedance spectroscopy (10^{-2} – 105Hz). Corrosion behaviour was evaluated via. potentiodynamic polarization test (PP, −1.0 v to +1.0 v). Finally, surface chemical composition was analyzed using X-ray photoelectron spectroscopy (XPS).

Results: Laser-textured NiTi showed improved OCP such that high TD achieved maximum improvement in OCP (S-h: −0.197v, HC-h: −0.18v). S-l exhibited largest while S-h had smallest capacitive arc in Nyquist plots. As observed from bode-impedance plot, square texture (S-l: 2.48 × 105 Ωcm^2, S-h: 2.35 × 105 Ωcm^2) had higher impedance as compared to honeycomb texture (HC-l: 2.31 × 105 Ωcm^2, HC-h: 2.01 × 105 Ωcm^2), indicating more difficulty in charge transfer through surface. PP curves exhibited decrease trend of Icoor: S-h<S-l<HC-l<HC-h<P. This undoubtedly illustrates that corrosion resistance significantly enhances due to laser-texturing on NiTi. Furthermore, all laser-textured NiTi exhibited very high polarization-resistance (1.5 to 15 times of Pristine) that supports Icoor results. XPS analysis of passive film composition supports corrosion results as there are TiO_2 and NiO layers that effectively shields laser-textured NiTi substrate from corrosion in biological fluid.

Conclusion: Present study provides foundation for enhancement of corrosion-resistance of thin NiTi sheet based biomedical devices through laser-texturing.

Biography

Mariam Maroof received her bachelor's degree in Mechanical engineering from A.P.J Abdul Kalam Technical University (AKTU), India in 2018 and master's degree in Material science and engineering from Motilal Nehru National Institute of Technology Allahabad (MNNIT-A), India in 2020. She is currently pursuing PhD from MNNIT-A. Her current area of research includes preparation and analysis of laser marked/textured Superelastic NiTinol, along with design and analysis of biomedical device in the field of dentistry. She is motivated and looking forward for research opportunities in further improving her skills in the area of surface modification techniques of NiTinol based devices. She is ready to contribute her undivided effort in the field of STEM.

NUMERICAL ANALYSIS OF LIGHT-TIMBER FRAME WALL ELEMENTS WITH VARIOUS SHEATHING MATERIAL

Jelena Vilotijević, Andrej Štrukelj and Miroslav Premrov
University of Maribor, Slovenia

Abstract

This paper numerically analyses many different parameters with the most sensitive impact on the in-plane lateral behaviour of Light timber-framed (LTF) wall elements. Different types of the sheathing material (fibre-plaster boards, OSB, or even reinforced concrete) with a various thickness of the boards are parametrically studied. Among that, an additional option with the Light steel frame (LSF) load-bearing structure as a possible lateral strengthening wall element in mid-rise timber building is especially analysed. The semi-analytical procedure using the Modified γ-Method simultaneously considers bending, shear and timber-to-framing connection flexibility, while assuming stiff-supported wall elements as prescribed by Eurocode 5 standard.

In the study a particular emphasis is placed on the sliding deformation between sheathing boards and the timber frame caused by a fastener`s flexibility and which can significantly reduce the overall racking stiffness of LTF wall elements. The influence of fasteners spacing (s) on sheathing-to-framing deformation and overall racking stiffness of the prefabricated wall element is comprehensively analysed using a semi-analytical approach with the Modified γ-Method deeply analysing a different bending and shear behaviour in a case of a different sheathing material. For specially selected parametric values of fasteners spacing (S = 50, 75, 100, 150 mm) a parametrical FEM study using a special 2D Hinge layer is additionally performed to validate the developed semi-analytical expressions for the racking stiffness.

The results obtained by the Modified γ-Method demonstrate that reducing the fastener spacing (s) can significantly improve the stiffness of OSB LTF wall elements, while it is less useful for FPB elements used in mid-rise timber buildings. The inclusion of RC sheathing on one side of the LTF element demonstrates an important potential to increase in-plane racking stiffness, making it a viable solution for strengthening in prefabricated multi-storey timber buildings.

By comparing the obtained results between LTF and LSF elements it can be evidently concluded that the lateral stiffness of LSF wall elements is essentially higher and demonstrates also more sensitive behaviour in dependence of the fasteners spacing.

Biographies

Jelena Vilotijević, M.Sc. Civil Engineering, has been employed since 2023 at the Faculty of Civil Engineering, Transportation Engineering, and Architecture of the University of Maribor as a young researcher and assistant at the Chair of Building Structures. As part of her doctoral studies, which she is pursuing under the supervision of Prof. Dr. Miroslav Premrov, she focuses her research on Advanced Approaches in the Design of Hybrid Timber Structures in Seismic Areas. In her research, she actively collaborates with colleagues from the Chair of Structural Mechanics. Already during and immediately after her studies, she gained teaching experience as an external collaborator in courses at the chairs of Building and Steel Structures, where she participated in exercises and lectures. Today, as an assistant, she is involved in teaching courses related to structural design, while also integrating research and teaching with mentorship —she has co-supervised three published master's theses. In the field of research, she is the author of one scientific article in an international journal with an impact factor (Assessment of In-Plane Timber Floor Stiffness as Structural Diaphragms: A Numerical Approach to Lateral Load Response, 2024), co-authored with Prof. Dr. Miroslav Premrov. She has also participated in two international conferences, where she presented the results of her research. Her master's thesis (Allplan Bridge for Creating Geometric and Analytical Models and Structural Analysis on the Case Study of the Kozarica Viaduct, 2022) focused on the use of modern software tools in modeling and analyzing bridge structures. The thesis was carried out in collaboration with the company Ponting d.o.o. Maribor, Slovenia, where she was employed from 2021 to 2023. Prior to

that, she worked at the design office Geoprom d.o.o. in Podgorica, Montenegro. In 2022, she participated in the international competition Competition for the Conceptual Architectural Design of a Sports Hall in Cetinje, Montenegro, where she was responsible for the structural calculations and, together with the team, won 2nd place.

Andrej Štrukelj was elected to the rank of full professor in the field of Civil Engineering in 2017. He is a regular member of the Senate of the Faculty of Civil Engineering, Transportation Engineering and Architecture at the University of Maribor, and Head of the Chair of Operative Construction. He is the author or co-author of 41 research papers, most of which are indexed in the SCI database and cover topics in civil engineering structures. At the beginning of his academic career, he focused on the problem of dynamic soil–structure interaction, which was also the subject of his doctoral dissertation. In 1996, he broadened his research and professional activities to include civil engineering materials, operational construction, and experimental analysis of structures. In his current research, he collaborates with colleagues from the Chair of Building Structures and the Chair of Structural Mechanics on European and national research projects. Professionally, he works with many of Slovenia's leading design bureaus specializing in bridge structures. His present focus is on the development of innovative methods for electronic and optical measurement of mechanical quantities and the monitoring of bridge structures. In addition, in the field of mechanical engineering, he is engaged in industrial diagnostics, addressing problems related to stress analysis and vibration transmission. He frequently applies theoretical research results to the practical challenges of construction. He is also a member of the Chamber of Engineers of Slovenia and a certified engineer in the areas of design, supervision, and execution of construction works.

Miroslav Premrov was elected in 2009 in the full professor degree for »Timber Structures« and »Concrete Structures«. From 2009 to 2019 he was a dean of the Faculty of Civil Engineering, Transportation Engineering and Architecture at University of Maribor. Miroslav Premrov is since 2007 a head of Chair of Building Structures at University of Maribor, Faculty of Civil Engineering, Transportation Engineering and Architecture. In the period from 2017 to 2023 year 2017 he was an elected member of European Monitoring Committee (EMC) of largest European Engineering Association FEANI. Miroslav Premrov is the author or co-author of 71 research papers indexed by SCI impact factor and reviewer for the most reputable international journals from the field of civil engineering structures. He is an editorial board member of five international journals with an impact factor. From the year 1999 he has been actively dealing with the problems of strengthening in composite timber elements used in multi-storey prefabricated timber buildings.

COMPOSITE COATINGS FROM COBALT ALLOYS WITH SPECIFIED PHYSICAL AND MECHANICAL PROPERTIES

Gauhar Mussabek and Gulmira Yar Mukhamedova
Al-Farabi Kazakh National University, Kazakhstan

Abstract

Background: The energy security of any country is based on several factors, including the network of national energy-generating enterprises and the developed industrial basis for energy-accumulating devices and energy source production. Utilization of electrochemical methods favors the interactions in the chain "process parameters – composition and structure of the material – properties – functions – applications." Because of this, it is possible to fabricate deposits with varied qualitative and quantitative compositions and desirable functional properties, such as microhardness, wear resistance, thermal resistance, chemical resistance, and corrosion resistance, as well as catalytic activity.

Objective: To study the influence of the electrolysis parameters on the quality, composition, morphology, catalytic properties, and corrosion resistance of ternary Co-Mo-Zr coatings.

Methods: The composition and microstructure of composite electrolyte coatings (CECs) were investigated using optical metallography methods, spectrometric and X-ray diffraction analysis, scanning electron microscopy, and atomic force microscopy. Gravimetric and potentiodynamic methods were used to study the corrosion properties. Physical and mechanical properties were studied using microhardness measurements and tribological testing methods.

Results: A series of diffraction lines for α-Co on X-ray diffraction patterns for Co-Mo-Zr deposits on steel substrates was obtained. No other phases, including intermetallic compounds, were found in the coatings' structure. Testing of the catalytic activity of the synthesized Co-Mo-Zr coatings was also performed in the model reaction of carbon (II) oxide conversion to carbon (IV) oxide. the temperature dependencies at the platinum plate catalyst with ω(Pt)=100 at.% the oxidation of CO begins at 190°C, while 100 % conversion degree is achieved at 250°C.

Conclusion: Corrosion of cobalt-based electrolytic coatings, as follows from the nature of the alloying components, proceeds predominantly with hydrogen depolarization in an acidic medium and in neutral and alkaline conditions under oxygen action. This research has been funded by the Committee of Science of the Ministry of Science and Higher Education of the Republic of Kazakhstan (Grant No AP23484310).

Biographies

Gulmira Yar-Mukhamedova - Professor, Doctor of Physics & Mathematics Sciences, Corresponding Member of the Higher School's National Academy of Sciens. Her innovative and scientific activity includes actual directions for Kazakhstan: optimization of the technology for obtaining protective coatings and materials with improved functional properties, physical, technological, and ecological aspects of extractive and processing industries, electroplating, galvanochemical design of new composite systems, and nanomaterials of strategic importance. Generation materials with adjustable physical, chemical, and operational characteristics, which are based on natural and anthropogenic raw materials and demonstrate a synergistic effect for optimizing industrial processes and power engineering. She leads scientific projects on the development of nanotechnology for the synthesis of functional materials, with the aim of transferring advanced foreign experiences and technologies to specific scientific, technical, and educational spheres. She also supervises the introduction of dual-degree Master's and PhD programs in collaboration with leading universities in Europe and the USA. In accordance with the agreement, she with outstanding scientists from Great Britain, Germany, and Poland to improve the quality of education and training for PhD students. Gauhar Mussabek is a Professor-Researcher at the Faculty of Physics and Technology, Al-Farabi Kazakh National University (Kazakhstan), and Head of the Laboratory of Advanced Materials and Composite Coatings Technology. She received her Bachelor's degree in Physics in

2007 and her Master's degree in Physics in 2009 from Al-Farabi KazNU, where she also earned her PhD in Physics in 2013 for her work on the formation and optical properties of silicon nanocrystals and multilayer structures. Her research focuses on silicon- and carbon-based nanomaterials, optical spectroscopy, and hydrogen generation using nanostructured silicon. Dr. Mussabek completed a postdoctoral fellowship at Al-Farabi KazNU (2019–2022) and maintains active collaborations with national and international research groups. She is widely recognized for her commitment to interdisciplinary science, innovative teaching, and the development of smart nanomaterials for advanced energy, sensing, and environmental technologies.

THE IMPACT OF METALLIC MODIFICATION AND GLUED BED TECHNOLOGY ON SORBENT PROPERTIES: THERMAL STABILITY

Agata Mlonka-Mędrala
AGH University of Krakow, Poland

Abstract

Adsorption chillers represent an attractive low-emission cooling technology that utilizes the reversible adsorption of a refrigerant (typically water) onto a solid sorbent. This study presents methods for enhancing the properties of sorbents used in adsorption processes through metallic modification and the formation of glued beds. The addition of metallic additives aims to increase the thermal conductivity of sorbents, leading to more efficient heat and mass transfer during adsorption and desorption cycles. An alternative strategy, based on the use of glued beds, enables the formation of structures with improved thermal and mechanical contact, thereby enhancing the operational durability of sorption systems. Special attention was given to the use of thermally conductive adhesives to reduce thermal contact resistance at the interface between the silica gel and the heat exchanger surface, further improving heat transfer efficiency. Three different additives were tested in this study: polyurethane resin, hydroxyethylcellulose, and epoxy resin, each combined with copper and graphite flakes. The epoxy resin was diluted using benzyl alcohol, a non-reactive additive (not chemically reacting with the resin), which decreases viscosity, improves the wetting of thermally conductive fillers, but also affects the curing time and may influence the final properties of the material. Detailed investigations into both the thermal stability and long-term stability of the modified materials were carried out. The thermal stability studies analysed the behavior of sorbents at elevated temperatures, while long-term tests evaluated their performance and structural integrity under repeated adsorption-desorption cycling conditions. The results demonstrate that careful selection of modification techniques, including the application of thermally conductive adhesives can significantly improve the efficiency, durability, and operational lifespan of sorption materials, opening new prospects for their application in thermal energy management systems.

Biography

Agata Mlonka-Mędrala (Ph.D) is currently an Associate Professor at the Faculty of Energy and Fuels of AGH University of Krakow. She is the author of more than 80 papers in peer-reviewed scientific journals and conference proceedings. She has participated in many international research projects and scholarships (Queen's University Ionic Liquid Laboratory in the United Kingdom; Technical University of Denmark in Denmark; Royal Institute of Technology (KTH) in Sweden; Lund University in Sweden, DBFZ German Biomass Research Center gGmbH in Germany, Xi'an Jiaotong University in China). Her research interests are high and low-temperature corrosion in industrial processes, thermochemical conversion of biomass and alternative fuels, new advanced carbon materials synthesis, analysis and description using advanced instrumental techniques and laboratory-scale corrosion studies in simulated environments.

SILICON SURFACE ENGINEERING WITH PLASMONIC AND UP-CONVERSION COATINGS FOR PHOTOVOLTAIC APPLICATIONS

Alma Dauletbekova
L.N. Gumilyov Eurasian National University, Kazakhstan

Abstract

Background: Si has long dominated photovoltaic technologies, yet its efficiency is limited by surface recombination and incomplete absorption of the solar spectrum, particularly in the ultraviolet (UV) and infrared (IR) regions. Various strategies, including "black silicon," plasmonic nanostructures, and rare-earth–doped up-conversion layers, have been developed to extend the absorption range and improve device performance. However, many of these methods require additional composite layers or complex fabrication steps, limiting compatibility with standard Si processing.

Objective: To develop dual-side nanostructured coatings on Si wafers that enable broadband absorption from near-UV to near-IR, improve photoelectric response, and remain fully compatible with existing silicon technologies.

Methods: A p-type Si wafer with an n^{++} top layer (~100 nm) was used as the substrate. On the front surface, a 15 nm mesoporous Si (meso-PS) layer was produced by electrochemical etching in hydrofluoric acid solution, followed by the deposition of Ag nanoparticles (30–60 nm) to enhance absorption below 500 nm. On the back surface, a 0.5 μm meso-PS layer filled with TiO_2:Er/Yb and larger Ag nanoparticles (140–220 nm) was fabricated to enable IR up-conversion and reduce heating effects. Morphological parameters of Ag nanoparticles were studied by SEM, while optical performance was assessed under 980 nm laser irradiation.

Results: The dual-side coatings significantly increased the absorption of optical radiation across the near-UV to near-IR range. Enhanced photoelectric characteristics were observed under IR excitation, confirming effective up-conversion. The backside structure also demonstrated athermality, reducing unwanted heating during illumination.

Conclusion: The proposed fabrication method enables efficient, broadband, and thermally stable surface modification of Si wafers using processes fully compatible with current technologies. These coatings represent a promising route to improving the performance of silicon-based photodetectors and solar cells.

Biography

Alma Dauletbekova is a Research Professor of the Department of Technical Physics at L.N. Gumilyov Eurasian National University, Astana, Kazakhstan, and a foreign member of the Latvian Academy of Sciences. Her research focuses on radiation resistance of materials, nanomaterials, track technologies, and ion-beam modification of solids. Prof. Dauletbekova is the author of five monographs, two textbooks, and more than 80 papers in international journals, with over 850 citations (h-index 19, Google Scholar, 2025). She has supervised more than 10 PhD theses and numerous master's and bachelor's projects. Her research has been supported by national and international grants, including projects on nanostructures, scintillation materials, and optoelectronic applications. She has received several national awards, including the Satpayev Prize (2020) and the "Best University Teacher" distinction (2010, 2015, 2022). Prof. Dauletbekova actively collaborates with Latvian, Estonian and Japanese scientists, strengthening international scientific networks.

EVALUATING CRUMB RUBBER IMPLEMENTATION IN SOUTH AFRICAN ASPHALT INDUSTRY TOWARDS SUSTAINABLE WASTE TYRE MANAGEMENT

Mohamed M H Mostafa
University of KwaZulu-Natal, South Africa

Abstract

Background: South Africa faces escalating environmental and public health challenges due to the accumulation of over 150,000 tonnes of waste tyres annually. Traditional disposal methods, including landfilling and illegal dumping, contribute to pollution, fire hazards, and resource wastage. Crumb rubber modified (CRM) asphalt presents a sustainable solution by repurposing waste tyres into road construction materials, yet adoption remains limited despite global advancements.

Objective: This study evaluates the technical feasibility, environmental benefits, and socioeconomic barriers to integrating crumb rubber into South Africa's asphalt industry, proposing strategies to enhance waste tyre management and promote circular economy principles.

Methods: A mixed-method approach was employed, combining a systematic literature review of global CRM asphalt practices, analysis of secondary data from government reports and industry publications, and a case study of South Africa's waste tyre management frameworks, including the defunct REDISA Plan and current Waste Bureau (WB) initiatives.

Results: Findings reveal that CRM asphalt improves pavement durability, reduces noise pollution, and lowers CO_2 emissions by 39.7% compared to conventional asphalt. However, barriers such as high initial costs, fragmented legislation, inadequate funding, and limited public awareness hinder large-scale adoption. South Africa's recycling rate stagnates at 20–32%, contrasting sharply with the EU's 95% recovery rate. Policy gaps, bureaucratic inefficiencies, and misallocation of tyre levies further exacerbate challenges.

Conclusion: Accelerating CRM asphalt adoption requires robust legislative frameworks, targeted funding for recycling infrastructure, public-private partnerships, and enhanced stakeholder education. Aligning South Africa's strategies with successful EU models, such as Extended Producer Responsibility (EPR), could mitigate stockpiling, reduce environmental impacts, and foster sustainable road infrastructure development. This study underscores the urgency of integrating waste-derived materials into engineering solutions to address both environmental and infrastructural demands.

Biography

Mostafa is a Civil Engineer by qualification and holds a PhD from the University of Liverpool, UK in Pavement Engineering. He is the head of the ACL Cluster (Agriculture Engineering & Civil Engineering and Land Surveying) at University of KwaZulu-Natal. He is also the Chair and Director for KZNDoT Chair in Sustainable Transportation. Professor Mostafa is an experienced academic with multinational experience, having started his academic career in Egypt before moving to the UK and relocating to South Africa. His primary expertise lies in sustainable transportation research, including, but not limited to, asphalt pavement materials, smart transportation, geotechnical pavement applications, and resilient infrastructure. His research includes incorporating non-conventional materials, e.g. recycled or waste, in pavement. Furthermore, he considers pavement modelling, pavement life cycle assessment, pavement management systems, pavement sensing, and climate change effects on roads. He has published more than 100 articles in journals and conference proceedings. His scholarly activities include serving as an editorial member and reviewer for multiple journals and examination of multiple national and international PhDs. Mohamed has graduated 25 PG students to date while supervising many more. He is also the founder and chair of the Sustainable Transportation Research group (STRg) at UKZN.

REUSING CONSTRUCTION WASTE AS PAVEMENT MATERIAL

Bojan Žlender
University of Maribor, Slovenia

Abstract

Background: Sustainable construction is becoming increasingly important as it reduces environmental impact, and promotes using recycled materials. An important aspect of sustainable construction is the reuse of construction waste, primarily from excavated soil and the demolition of structures. Demolition projects generate large quantities of waste that must be properly processed for reuse. Despite the environmental and economic benefits, the reuse of construction waste faces various challenges, including regulatory, organizational, logistical, and technical barriers. Regulatory challenges arise from complex legislation and the lack of clear guidelines for the reuse of excavated soil. Organizational challenges relate to planning and coordination between stakeholders, while logistical constraints include transport and storage difficulties. On the technical side, the lack of standardized test methods makes it difficult to assess the geochemical and geotechnical properties required for reuse.

Methods: To evaluate the improvement of soil properties by hybrid waste materials, various laboratory tests were performed, including the standard Proctor test, unconfined compressive strength test, California Bearing Ratio (CBR) test and cyclic triaxial tests. The aim was to determine key parameters for the design and construction of road pavements and to demonstrate that the use of hybrid waste materials contributes significantly to the sustainability of road infrastructure.

Results: The study confirmed that mixing construction waste with primary materials improves the mechanical properties of pavement structures. The optimal mixture depends on project-specific and environmental conditions, but hybrid mixtures have been shown to achieve high load-bearing capacity and durability.

Conclusion: The reuse of construction waste in road construction significantly reduces the need for newly produced materials, improves pavement stability and contributes to more efficient waste management. Successful implementation requires close cooperation between regulators, investors, designers, and contractors to fully realize the potential of construction waste as a valuable secondary resource in modern construction.

Biography

Bojan Žlender is a professor and researcher at the University of Maribor, Faculty of Civil Engineering, Transportation Engineering and Architecture. He has been head of the Laboratory of Soil Mechanics since 1995 and head of the Institute of Geotechnics since 2012. His research focuses on soil mechanics investigations and geotechnical engineering. He is the author of over 150 scientific publications and co-editor of the journal Acta Geotechnica Slovenica. He is also a reviewer for numerous international journals and an active member of several professional organizations, including the Slovenian Geotechnical Society (SloGeD), the International Society for Soil Mechanics and Geotechnical Engineering (ISSMGE), the International Association for Engineering Geology and Environment (IAEG), the International Geosynthetics Society (IGS) and others. He is also a certified engineer by the Slovenian Chamber of Engineers (IZS) and has extensive experience in all aspects of geotechnical engineering design and construction.

Day-1
Poster Presentations

SPECTROPHOTOMETRIC DETERMINATION OF CEFTRIAXONE WITH PRELIMINARY SOLID-PHASE EXTRACTION BY COPPER TRIMESINATE – GRAPHENE OXIDE NANOCOMPOSITE

Victoria N. Naumkina
Southern Federal University, Russia

Abstract

Background: Solid-phase extraction (SPE) is an effective method for extracting, separating and concentrating antibiotics from the environment that enter wastewater from pharmaceutical plants, medical institutions, livestock farms, while metal-organic frameworks (MOFs) are popular sorbents. To expand the practical application of MOFs, a promising direction is the creation of their composites with other materials, in particular with graphene oxide (GO). In such composites, separated and functionalized graphene sheets will enhance dispersion interactions, and MOFs will increase the pore volume in which adsorbates can be stored.

Objective: Synthesis of copper trimesinate/graphene oxide (Cu-BTC/GO) composites with 10% GO content and its use as a sorbent for solid-phase extraction of the antibiotic ceftriaxone.

Methods: The composite was synthesized in situ in two stages: obtaining GO with subsequent introduction of trimesic acid, sodium hydroxide and copper salt into the synthesis procedure. The obtained composites were studied by SEM, X-ray diffraction, IR spectroscopy. The dependence of solid-phase extraction on the sorbent mass, initial concentration of the antibiotic, temperature and contact time was studied. The optical density of the solutions was measured using a spectrophotometer at a wavelength of λ_{max} = 270 nm.

Results: Results indicate that the composite is highly effective, especially with a high initial antibiotic concentration. The maximum adsorption capacity was achieved at 975.4 mg/g. Equilibrium reached within 180 minutes; the most adsorption happened in the first 60 minutes. Lowering the temperature from 308 K to 278 K reduced the contact time needed.

Conclusion: Maximum extraction efficiency was recorded as 98.3 ± 0.3% under optimized conditions. This high efficiency suggests the potential of Cu-BTC/GO composites for environmental problems and chemical analysis applications. The work was supported by the Russian Science Foundation (Grant No. 22-13-00260).

Biography

Victoria Naumkina graduated from the Chemistry Department of SFedU in 2022. Under the supervision of I.E. Uflyand, she has been engaged in research on the topic "Nanocomposites Based on Copper, Nickel, Cobalt Trimesinate, and Graphene Oxide as Sorbents for Solid-Phase Extraction of Organic Pollutants." During this time, she studied the extraction of various organic dyes, as well as the antibiotics tetracycline from cow's milk and ceftriaxone from aqueous solutions.

CHANGE OF COPPER WIRE MICROSTRUCTURE IN THE PROCESS OF DEFORMATION BY A NEW METHOD

Andrey Volokitin
Karaganda State Industrial University, Kazakhstan

Abstract

Background: In today's high-tech world, where material requirements are constantly growing, especially in industries such as mechanical engineering, metallurgy, aerospace and aerospace, low-alloy copper alloys are steadily replacing pure copper, demonstrating undeniable advantages in strength, reliability and durability. This is due to their unique physical and mechanical properties, allowing for the creation of more efficient and durable components. However, the constant search for new technologies that can further improve the performance of copper materials remains a challenge for researchers and engineers.

Objective: Study of changes in microstructure of copper wire in the process of deformation by a new method.

Methods: The wire was passed through a rotating equal-channel step die and conventional drawing at room temperature. Deformation was carried out on a B–I/550 M mill. The reliability of the results was confirmed by a large number of experiments using a combination of standard and modern research methods.

Results: There is a significant increase in strength: the tensile strength more than doubles, from 302 to 635 MPa. This means that deformed wire can withstand twice as much load before breaking as undeformed wire. The yield strength, which characterises the onset of plastic deformation, also increases, rising from 196 to 306 MPa, which is an increase of approximately 56%. However, the increase in strength is achieved at the expense of reduced ductility: the relative elongation before failure decreases from 42% to 27%.

Conclusion: The present article is devoted to a detailed analysis of an innovative approach to the creation of copper wire with significantly improved mechanical properties based on the formation of a controlled gradient microstructure. The key difference of the proposed method is the symmetric distribution of structural changes within the wire.

Biography

Andrey Volokitin has been engaged in scientific research in the field of metal science and metal forming for over 15 years. He holds a PhD in Technical Sciences and the title of Associate Professor. Over the years, he has published more than 200 articles, 75 of which are included in the Scopus and Web of Science databases, with an H-index of 15 for Scopus and 11 for Web of Science.

DEVELOPMENT OF CRYOGELS BASED ON NATURAL POLYMERS USING CLICK CHEMISTRY AND CRYOPOLYMERIZATION METHODS

Kudaibergen Gulshakhar and Akhmetkarimova Zhanar
National Center for Biotechnology, Kazakhstan

Abstract

Background: Cryogels are 3D macroporous materials formed as a result of cryogelation of monomers/polymers in a solvent below the freezing point (up to -20°C). Gelatin (Gel) is a biopolymer derived from animal collagen, considered to be denatured collagen. Hyaluronic acid (HA) is an anionic non-sulfated GAG widely distributed in connective, epithelial and nervous tissues. The "click" chemistry method is used, which leads to the rapid formation of covalent bonds, also its often used for bioengineering due to its simplicity and the formation of a minimum amount of by-products.

Objective: Synthesis and study of physicochemical properties of cryogels based on gelatin and hyaluronic acid.

Methods: the methods of cryopolymerization, "click" chemistry, IR, NMR spectroscopy, scanning electron microscopy, differential scanning calorimetry.

Results: Polymers based on gelatin and hyaluronic acid were obtained by cryopolymerization and "click" chemistry methods and characterized. Optimal synthesis conditions for each type of polymers have been determined. The functional group was determined by IR spectroscopy, the modified prepolymers were identified by NMR spectroscopy. The physico-chemical properties of cryogels, such as swelling, pore volume, gel fraction, density, and degradation have been studied. The results of studying the surface morphology of the synthesized polymers were obtained by scanning electron microscopy. The thermogravimetric analysis of the synthesized cryogels was carried out.

Conclusion: Cryogels based on GelHA were synthesized using "click" chemistry methods. Modified forms of Gel and HA were preliminarily obtained by grafting unsaturated double bonds with further photoinitiation of cryogels. The presence of double bonds was identified by ^{1}H NMR spectroscopy. The effect of "thiol-ene" groups (cross-linking agent 4-arm-PEG-SH) on UV polymerization and physicochemical properties of cryogels were studied. SEM showed the porous surface of the synthesized cryogels, the average size of which varied within 89–203 μm. According to the results of the study, it was found that cryogels have the most suitable properties for use in *in vivo* studies.

Biographies

Kudaibergen Gulshakhar Kudaibergenkyzy, PhD, Assoc. Professor. She has experience in the production and application of natural and synthetic polymers, cryogels and hydrogels, complexes of humic acids and their derivatives, nanocomposites with the participation of carbon nanotubes, polymer-metal nanocomposites, magnetically controlled sorbents, the production of polyester resins and copolymers based on them.

Gauhar Mussabek is a Professor-Researcher at the Faculty of Physics and Technology, Al-Farabi Kazakh National University (Kazakhstan), and Head of the Laboratory of Advanced Materials and Composite Coatings Technology. She received her Bachelor's degree in Physics in 2007 and her Master's degree in Physics in 2009 from Al-Farabi KazNU, where she also earned her PhD in Physics in 2013 for her work on the formation and optical properties of silicon nanocrystals and multilayer structures. Her research focuses on silicon- and carbon-based nanomaterials, optical spectroscopy, and hydrogen generation using nanostructured silicon. Dr. Mussabek completed a postdoctoral fellowship at Al-Farabi KazNU (2019–2022) and maintains active collaborations with national and international research groups. She is widely recognized for her commitment to interdisciplinary science, innovative teaching, and the development of smart nanomaterials for advanced energy, sensing, and environmental technologies.

SOLID-PHASE EXTRACTION OF AZORUBIN AND PONCEAU WITH A MIXED-LIGAND COMPLEX BASED ON NICKEL TEREPHTHALATE AND 2,2'-DIPYRIDINE

Maria A Chernomorova
Southern Federal University, Russia

Abstract

Background: Environmental pollution is increasing worldwide due to population growth and industrial development. One of the main pollutants are synthetic azo dyes, they can enter the environment from wastewater from the food and pharmaceutical industries, so the problem of the presence of dyes in surface and groundwater is relevant. Solid-phase extraction is the most commonly used method for extracting and concentrating dyes. Metal-organic frameworks (MOFs) are promising materials for use as solid-phase extractants.

Objective: Synthesis of mixed-ligand complex "nickel terephthalate – 2,2'-dipyridyl" and study of the possibility of its use in solid-phase extraction of azo dyes.

Methods: A green method for the synthesis of MOFs with preliminary preparation of nickel terephthalate and its subsequent complexation with 2,2'-dipyridyl was developed. The dependence of solid-phase extraction on the sorbent mass, initial concentration of the studied objects, temperature, pH.

Results: It was found that under experimentally optimized conditions, the degree of dye extraction reaches 90%. The efficiency of ponceau 4R extraction is higher at lower temperatures. At the same time, temperature does not significantly affect the extraction of azorubine. A study of the effect of solution acidity showed that the degree of azorubine extraction does not depend on the pH of the solution. Ponceau 4R is most completely extracted from alkaline solutions.

Conclusion: A mixed-ligand MOF based on nickel terephthalate and 2,2'-dipyridine is an effective extractant for removing azo dyes from aqueous media. The maximum extraction value is 224 and 70 mg/g for azorubin and ponceau 4R, respectively.

This work was supported by the Russian Science Foundation (Grant no. 22-13-00260).

Biography

Chernomorova Maria graduated from the Chemistry Department of SFedU in 2022. Under the supervision of I.E. Uflyand, she studies solid-phase extraction of personal hygiene products using a metal-organic framework in combination with spectrophotometric determination. She studies the use of metal-organic framework structures for the determination and separation of organic dyes and the determination of cephalosporin antibiotics.

ELECTROCHEMICAL CHARACTERIZATION OF (TI0.2ZR0.2HF0.2NB0.2TA0) B_2 POWDERS FOR SUPERCAPACITOR APPLICATIONS

Mustafa Tuncer
Kütahya Dumlupınar University, Turkey

Abstract

This study investigated the electrochemical performance of the high-entropy ceramic powders by a zone melting method for a potential electrode in supercapacitor devices. Two types of electrodes were used for measurements via the two-electrode method with symmetric and asymmetric devices. HEBs were utilized as working electrodes for both symmetric and asymmetric devices, and carbon-based materials were used as the other working electrodes for asymmetric devices. Electrochemical characterization (CV, PEIS, GCPL) of powders was) were performed using the multi-channel potentiostat [**Figure 1**].

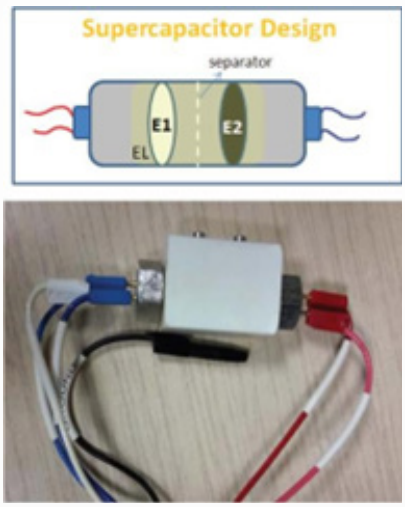

Figure 1: High-Capacitance Hybrid Supercapacitor based on Multi-Colored Fluorescent Carbon-Dots.

Biography

Mustafa Tuncer, PhD, received the B.E. degree in the Department of Ceramic Engineering from the University of Dumlupinar, Turkey, in 2000, and the M.Sc. and Ph.D. degrees in Ceramic Engineering from the University of Dumlupinar, Turkey, in 2003 and 2011, respectively. He has experience with ceramic processing, powder synthesis and photovoltaic materials. He is the faculty member in Department of Metallurgical and Material Engineering at Kütahya Dumlupinar University in Turkey.

CRYOGENIC COOLING OF AISI 304 STEEL WIRE IN THE DRAWING PROCESS

Volokitina Irina Evgenievna
Karaganda State Industrial University, Kazakhstan

Abstract

Background: Wire is one of the most high-demand metal products. It is widely used in the production of electrical wires, ropes, cables and similar products. But every year higher requirements for performance properties are applied to such products, so research on obtaining ultrafine-grained and nanostructures in them has become increasingly relevant. Thermomechanical processing allows controlling the course of structural processes (i.e. influencing grain size, ratio and character of grain boundaries), and therefore determining the final structure, i.e. mechanical properties, of the material already during its processing. In practice, such deformation can lead to a decrease in the grain size in the micrometer area, further refinement using traditional deformation methods is no longer possible.

Objective: The study of the microstructure and mechanical properties of AISI 304 steel wire after deformation by drawing with cryogenic cooling.

Methods: The wire was drawn using the traditional method at ambient temperature and deformed with cooling at cryogen temperature immediately after the wire leaves the drawing. The deformation was carried out at the B–I/550 M mill. The reliability of the results is confirmed by a large number of experiments using a complex of standard and modern research methods.

Results: Metallographic analysis of the deformed wire structure at both temperatures showed a microstructure consisting of a mixture of α-martensite and austenite. When the wire was deformed at cryogenic temperatures, a microstructure with an average grain size of 650 nm was obtained, and at ambient temperature - 2 microns.

Conclusion: In this work, a new combined technology of thermomechanical processing of AISI 304 steel wire has been developed. A special feature of the technology is the cryogenic cooling of the wire immediately after its exit from the die. Compared with traditional wire drawing, the increased ability to plastic deformation, due to the formation of martensite, allows it to be processed with large deformations without intermediate annealing.

Biography

Volokitina Irina Evgenievna has been engaged in research in the fields of metals science, heat treatment and metal forming for more than 15 years. He has a PhD degree and the title of associate professor. Over the years, she has published more than 250 articles, 129 of which are included in the Scopus and Web of Science databases, H-Index for Scopus - 25, H-Index for Web of Science – 21. He has the skills to work on optical, scanning JSM 5910 and transmission JEM 2100 microscopes.

RADIATION DAMAGE CAUSED BY SWIFT HEAVY IONS IN YAG:ND3+ SINGLE CRYSTALS

Baubekova Guldar
L.N. Gumilyov Eurasian National University, Kazakhstan

Abstract

Background: YAG:Nd crystals are the most commonly used laser materials suitable for space deployment, along with some of their characteristics, applications and real deployment examples. In recent years, many experimental investigations on pumping YAG:Nd directly into the upper laser level have already demonstrated great advantages.

Objective: In this study the samples YAG:Nd^{3+} (with a percentage content of Nd^{3+} impurity of 0.6%) single crystal were irradiated at RT with 231-MeV Xe^{132} ions within a fluence range of 10^{11}-10^{14} ion/cm^2.

Methods: X-ray luminescence was measured for YAG:Nd samples that were non-irradiated and Xe-irradiated ions within a fluence range of 10^{12}-10^{14} ion/cm^2, measured at room temperature under identical conditions (voltage 25 kV, current 10 mA). For YAG:Nd samples irradiated to different fluences, photoluminescence spectra were measured at a synchrotron (Maxlab, Germany). X-ray diffraction (XRD) analysis of YAG:Nd samples was performed on a Bruker D6 eco X-ray diffractometer using a copper anode X-ray tube in the 2θ angle range of 30°–110° with a step size of 0.01°.

Results: The obtained X-ray luminescence spectra are characterized by several clearly defined luminescence lines, which are caused by intracenter transitions of neodymium ions (Nd^{3+}) between the split levels of the 4f-configurational terms. The photoluminescence spectra excited by light with a wavelength of 220 nm, as well as the luminescence quenching kinetics for emission at 440 nm (near the emission of F-centers) were measured at a synchrotron. XRD analyses showed that xenon ion irradiation resulted in significant changes in YAG:Nd crystals.

Conclusion: The conducted analysis of X-ray luminescence indicates a high sensitivity of the light characteristics of YAG:Nd to radiation exposure, while the stability of the spectral position of the lines confirms the preservation of the structure of the luminescent centers of neodymium ions.

Biography

Baubekova Guldar - PhD in specialty 6D072300- Technical Physics. Over the past five years, 12 articles have been published in rating scientific journals (articles with impact factor), 10 articles in Journals recommended by Committee for Control in the Sphere of Education and Science, the results of scientific research were reported at 20 international conferences.

COLOR CENTER GENERATION AND ANNEALING KINETICS IN BaF_2 IRRADIATED WITH SWIFT HEAVY IONS

Daurzhan Kenbayev
Shakarim University, Kazakhstan

Abstract

Background: Barium fluoride (BaF_2) is a promising candidate for radiation detection owing to its wide band gap and ultrafast scintillation response. However, irradiation with heavy ions induces color centers that significantly alter its optical performance. Understanding the evolution, stability, and recovery of these defects is critical for deploying BaF_2 in radiation-intensive environments.

Objective: To investigate the formation mechanisms and thermal annealing kinetics of color centers in BaF_2 single crystals irradiated with swift Xe ions, and to determine the corresponding activation energies of defect relaxation.

Methods: BaF_2 single crystals were irradiated with 220 MeV ^{132}Xe ions at room temperature at fluences from 1×10^{11} to 1×10^{14} ions·cm^{-2}. Optical absorption spectra were recorded in the IR–VUV range (190–118 nm). Post-irradiation stepwise thermal annealing was conducted up to 825 K, followed by spectral acquisition at room temperature. The temperature dependence of optical density was fitted using the Arrhenius model to extract activation energies.

Results: Irradiation induced a fluence-dependent increase in absorption across the spectrum. The most stable room-temperature defect was the F_2 aggregate center (absorption peak at ~1.62 eV). A sharp reduction in F_2 concentration was observed between 400–450 K due to recombination with mobile interstitial fluorine ions. Concurrently, absorption bands at 9–10 eV intensified, indicating aggregation of interstitial-type defects. Two dominant annealing stages were identified with activation energies of ~0.32 eV and ~0.53 eV.

Conclusion: Swift Xe ion irradiation generates multiple defect species in BaF_2, with F_2 centers exhibiting the highest stability. Their two-stage thermal recovery reflects distinct recombination pathways. These insights are crucial for engineering radiation-hard BaF_2-based optoelectronic and scintillation systems.

Acknowledgments: This research was funded by the Science Committee of the Ministry of Science and Higher Education of the Republic of Kazakhstan (Grant number: AP19178510).

Biography

Daurzhan Kenbayev is engaged in research and comparative analysis of dose dependencies in the creation of radiation-induced CC's and identification of radiation defects in BaFBr and BaF2 crystals during irradiation with fast heavy ions. He also determines the positive and negative effects of oxygen impurities on the functional properties of barium fluorobromides and develops theoretical models of radiation defects in BaFBr and BaF2 crystals. Daurzhan's approach is characterised by openness and sensitivity to context: it involves interaction with various participants, from students and researchers to practitioners, and promotes dialogue between disciplines. His goal is not only to produce knowledge, but also to ensure its practical application.

Coalesce Research Group

13th International Conference on

Materials Science & Engineering

October 22-24 2025 | Tashkent, Uzbekistan

OBTAINING AND STUDYING THE PROPERTIES OF SILICIDES OF THE MO - SI SYSTEM

S.A. Muzafarova, A.S. Achilov, N.A. Akhmedova*, Z.S. Kenzhaeva, O.Sh. Norkulov, D.M. Tashlanova

Institute of Semiconductor Physics and Microelectronics at the National University of Uzbekistan named after Mirzo Ulugbek, Tashkent, Uzbekistan

Abstract

Background: Molybdenum, like other refractory metals, is characterized by a unique set of physical, mechanical, and chemical properties, which has ensured its wide application in various fields. The heat resistance and thermal shock resistance of the silicide coating on molybdenum are significantly increased if the MoSi2 layer is alloyed with metals, for example, chromium and iron [1-3]. The high heat resistance of the coatings in the temperature range of 1300÷1450 °C is due to the formation of a continuous glassy film of silicon dioxide, which, in the presence of a small amount of alloying elements, becomes more easily fusible compared to an unalloyed film, has greater fluidity, is capable of healing emerging defects, and facilitates the relaxation of thermal stresses during a sharp change in the temperature of the product[4].

According to the equilibrium phase diagram of the Mo - Si state, molybdenum forms a refractory silicide with silicon; in this system there are three compounds: molybdenum disilicide MoSi2, lower molybdenum silicides Mo5Si3 and Mo3Si [5].

Methods: A p- and n- type silicon single crystal with a purity of at least 99.9%, measuring 0.5 x 1.5 cm and 1.4 mm thick, was used as the substrate. Before coating, the silicon substrate surface was cleaned with a cambric cloth soaked in a mixture of polyrite and rectified alcohol diluted in distilled water. New polishing compounds, such as polyrites made from cerium and zirconium dioxides, as well as ready-made suspensions based on silicon and aluminum oxides, are currently widely used in Russia and abroad. After loading the substrates into the working chamber, the surface of the single-crystal silicon substrates was treated with a high-voltage ion source in an argon atmosphere with a 5% oxygen content. The solubility of silicon in solid molybdenum is 3.35 atm. % at 1820 °C and 9 atm. % at 2025 °C. The region of solid solutions based on the Mo3Si compound is practically absent. The physical thickness of the resulting metal layer was calculated based on the optical thickness nh = λ0/4, measured by the interference extrema, and was 1–2 μm. The film deposition rate (nm/min) was determined based on the obtained physical thickness and the coating application time. Next, silicon single crystals with a Mo-coated surface were thermally quenched at various temperatures in quartz ampoules in a vacuum. X-ray diffraction analysis revealed the formation of various types of molybdenum silicide compounds at the Mo - Si interface and within the bulk of the diffuse silicon layer. Silicon atoms replace metallic atoms and form complex crystalline structures in the form of graphite-like networks. Silicides are characterized by layered structures with fairly sharp separations between the layers of metal and silicon atoms, which facilitates shear deformation and reduces creep resistance at elevated temperatures.

Results: The (Mo) phase was assumed to obey Henry's law, and the solubility of solid Mo in (Si) was assumed to be zero. The liquidus is partially speculative due to the lack of experimental data. However, modern thermodynamic calculations show that the enthalpy of mixing in the liquid is strongly negative. The presence of a reaction involving MoSi2, Mo5Si3 and a MoSi2 at 1850°C, which the evaluators consider speculative and require further study.

Three eutectics are realized in the system:

- Mo3Si - Mo5Si3 at 26.4 atm. % silicon and a temperature of 2020 oC;
- Mo5Si3 - MoSi2 at 54 atm. % silicon and a temperature of 1900 oC;
- oSi2 - Si at 98.5 atm. % silicon and a temperature of 1400 oC.

At a temperature of 1850 o C there is a eutectoid $\beta MoSi_2 \leftrightarrow$ Mo5Si3 + $\alpha MoSi_2$ and at 1900 o C peritectic βMoSi2 + P↔ αMoSi2.Silicide Mo3Si is formed by the peritectic reaction Mo + Si = Mo3Si at 2025 ± 20°C, has a cubic structure with a period a = 0.4890 ± 0.0002. Mo3Si has a close- packed cubic structure or something close to it. The highly compact lattice emphasizes the metallic nature of the Mo-Si bond, but covalent bonds between metallic atoms also exist in the phases. The melting point of the silicide Mo5Si3 is 2180+20 oC, the width of the homogeneity region at 1700o C is from 37 to 40.35 at.% silicon. The compound MoSi2 melts at 2020 ± 20 °C, the homogeneity region is from 65.8 to 66.7 at. % silicon, and has a tetragonal structure. Silicide MoSi2 undergoes an allotropic transformation in the temperature range of 1850 ÷ 1900°C. The low-temperature variety α-MoSi2 has a tetragonal structure. The high-temperature β form -MoSi2 has a hexagonal structure with parameters: a = 0.4642 ± 0.0005, c = 0.6529 ±. 0.0005 nm, s/a - 1.406. The MoSi2 boundary on the Mo side is located at 67.1 ± 1.0% (atm.). The low-temperature form α of MoSi2 is a tetragonal cell with 2 Mo and 4 Si atoms. The Si atoms form a framework with Mo in the voids. The structure can also be viewed as consisting of layers parallel to the (010) plane with the closest hexagonal packing. The layers alternate in the order ABAB..., with layer B shifted in the X-axis direction by a/2. The shortest Mo-Si distance is c/3. Silicon atom chains form zigzags passing through the Mo prisms parallel to the X and Y axes.

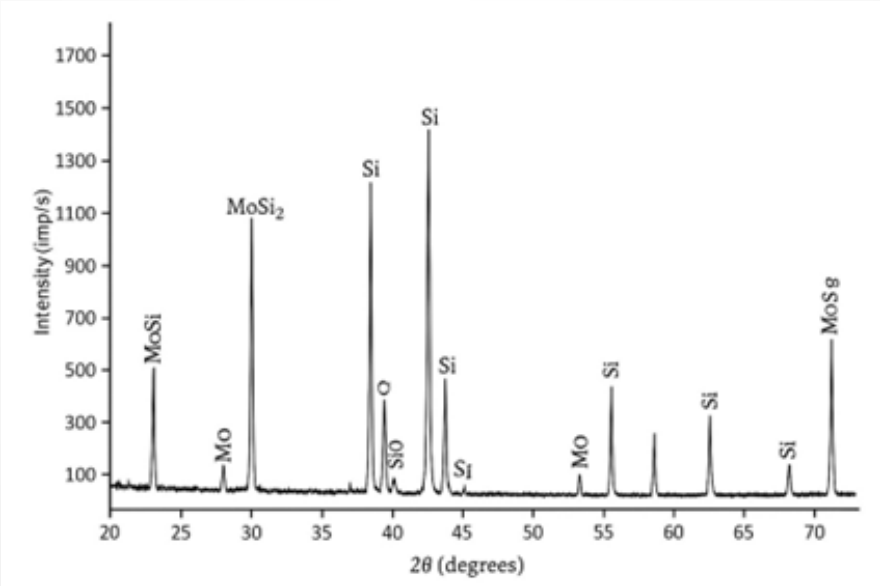

Fig.1. Diffraction pattern of the Mo- Si copper anode structure with Bragg-Brentano focusing

Comparison of the obtained results with a set of reference X-ray diffraction patterns (ASTM) [6] also allowed us to determine the composition of the Mo- Si structure. Figure1 shows an X-ray diffraction pattern of the Mo-Si structure. The lattice parameters of the structure are calculated using the formula

$$d^2 = \frac{a^2}{\hbar^2 + k^2 + l^2} = \frac{a^2}{N} \qquad [1]$$

and the Wulff–Bragg formula:

$$\mathrm{Sin}\theta = \frac{\pi}{2a} N \qquad [2]$$

where, θ is the Bragg angle determined from the X-ray diffraction pattern, and is the Miller index. θ the X-ray diffraction pattern shows the characteristic peaks of the original components of molybdenum MoSi2 and silicon SiO2, which are shown in Fig.1. During the diffusion process, silicon is partially oxidized, leaving residual oxygen in the bulk. As a result, structure and phase formation - crystallization and recrystallization - occur within the single crystal. The adjoining grains of the crystalline substance form a common boundary. The intergranular contact expands, and the process of grain fusion develops.

The protrusions of the chains point toward each other, and the distances between the Si atoms in the protrusions and in the chains are equal, creating a three-dimensional silicon framework. The high - temperature form β, MoSi2, has a hexagonal structure.

Conclusion: Using thicker Mo coatings on the silicon surface does not yield the desired results, as increasing metal thickness leads to cracks appearing in the transition layer of the structure, which leads to a reduction in the service life of the structures. Undesirable diffusion processes at the coating-substrate interface can be significantly slowed by creating barrier layers. Diffusion inhibition is observed when the diffusing element forms multicomponent compounds. A promising approach to protecting molybdenum products from oxidation is the creation of composite multilayer coatings, in which each layer performs a specific function: it provides heat resistance, prevents parasitic interaction between the coating and the substrate, promotes stress relaxation in the coating, and smooths out fluctuations in the system.

During the diffusion process, silicon is partially oxidized with residual oxygen in the volume, resulting in a single crystal structural - and Phase formation -crystallization and recrystallization. Studies of the properties of protective molybdenum silicide components have allowed us to identify the key factors initiating the degradation of the protective properties of single crystals, ensuring their thermal stability, and coatings during high-temperature operation in an oxidizing atmosphere.

Coalesce Research Group

13th International Conference on
Materials Science & Engineering
October 22-24 2025 | Tashkent, Uzbekistan

UNIVERSAL CAMERA FOR THE EG-2 LINEAR ACCELERATOR

Ya.A. Saidimov* and F.B. Umarov
Institute of Semiconductor Physics and Microelectronics at the National University of Uzbekistan named after Mirzo Ulugbek, Tashkent, Uzbekistan

Abstract

Background: This paper presents the technical foundations and experimental results for the creation of a new universal chamber for irradiation and modification of semiconductor materials at the central output of the EG-2 linear accelerator. As a result of modernization, development and installation of a new universal chamber, at the outlet of the central channel, the proton beam current reached 7 μA at a proton energy of 600 keV with an energy resolution of ~50 keV, which opens up wider opportunities for studying the interaction of accelerated protons with the surface of semiconductor materials and for their modification.

Methods: The EG-2 electrostatic linear accelerator is a multicomponent complex with a variety of technical equipment that provides: high voltage from 0.3 to 2 million volts; vacuum equipment systems to ensure high vacuum in the system up to 10-7 mmHg; gas installations with a mixture of gases to fill the accelerator's protective boiler with pipe pressure up to 10 atmospheres, which increases the electrical insulation properties of the system; improved water supply management (closed water supply cycle ~30 l/min) to ensure efficient cooling of all EG-2 components.; an accelerator tube with a high-voltage beam focusing system; an injector with a system for producing high-frequency plasma and removing ions into the accelerator tube; a charger with a conveyor belt for transferring electrostatic charge to a high-voltage conductor (voltage up to 2 million volts) and a shaft with a generator providing power (220 V, 400 Hz) devices located in a high-voltage accelerating electrode, at a voltage of up to 2 million volts. During the operation of this entire complex, at the output we receive a beam of charged ions with proton energy from 0.3 to 2 MeV or alpha particles up to 3.5 MeV (with a high energy resolution of ~ 5 keV) and a beam current from 10 pA to 1.5 μA. These characteristics of the complex make it possible to carry out both applied and fundamental research on it.
Results: The EG-2 accelerator has three beam output channels. The left and right channels with a working magnetic separator have a high energy resolution of 5 keV, but a low beam current of up to 1.5 μA.

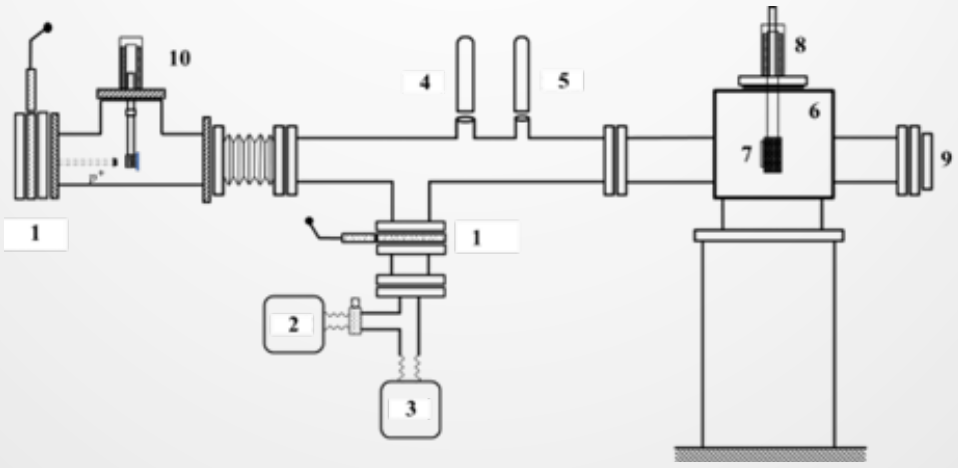

Fig.1. Schematic diagram of the universal camera

On a direct beam with the separator turned off, the energy resolution is ~50 keV, which is not very important when irradiating polypropylene materials, but the beam current can reach 15 μA, and this is important for tasks related to changing the properties of polypropylene materials.
To connect the universal chamber to the ion conductor, a connection diagram was developed, the schematic diagram of which is shown in Fig. 1 (1 is a vacuum gate, 2 is a turbomolecular pump, 3 is a pre-vacuum pump, 4 is a thermocouple pressure gauge converter, 5 is an ionization pressure gauge converter, 6 is an experimental chamber, 7 is an irradiation target, 8 is a target rotation mechanism, 9 is a window for visual inspection, and 10 is a proton beam monitoring unit). After the assembly of the connecting part, the universal chamber system for the EG-2 direct channel, test work was carried out to check the system for low and high vacuum.

Fig. 2. Universal camera docked to the central terminal of the EG-2 accelerator

According to the results of checking the system for low vacuum, several leaks were detected, after which a high vacuum of ~ 10-6 Pa was obtained.
Figure 2 shows a real view of the universal camera connected to the central output of the EG-2 accelerator. After the connection, adjustment work was carried out to set up the camera and test the methodology for measuring and controlling the parameters of the accelerated proton beam. Based on the results of testing and configuration, the camera was calibrated for experimental work on modification of semiconductor materials.

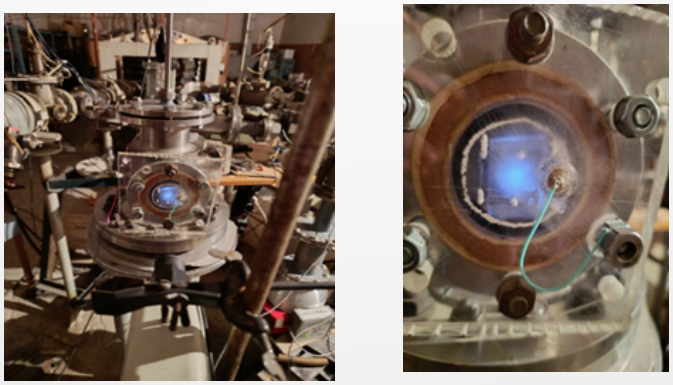

Fig. 3. A proton beam falling on a window for visual inspection

Conclusion: As a result of the modernization, development and installation of a new universal chamber at the outlet of the central channel, the proton beam current reached 7 μA at a proton energy of 600 keV with an energy resolution of ~50 keV, which opens up wider opportunities for studying the interaction of accelerated protons with the environment. surfaces of semiconductor materials and for their modification.

INFLUENCE OF IMPURITY CLUSTERS ON THE STRUCTURAL PROPERTIES OF SAMPLE N-SI<CU>

Nozimjon Turgunov and Raymash Turmanova*
Institute of Semiconductor Physics and Microelectronics at the National University of Uzbekistan named after Mirzo Ulugbek, Tashkent, Uzbekistan

Abstract

This work presents the results of a comprehensive study of the influence of copper impurity clusters on the crystal structure of monocrystalline silicon doped by high-temperature diffusion. Scanning electron microscopy revealed the formation of impurity nanoinclusions of various morphologies with sizes up to ~800 nm, characterized by structural homogeneity and a stable distribution of Cu, Si, O, and C atoms. X-ray diffraction analysis showed a shift of the Si(111) peak, indicating the emergence of elastic lattice deformations, as well as the formation of new phases: SiO_2, SiC, Cu_5Si_4, Cu_2O, and CuP_2. Fourier-transform infrared spectroscopy revealed a decrease in the concentration of optically active carbon by 28% and oxygen by 52%, which is attributed to their redistribution and the formation of stable compounds. The results confirm the high chemical activity of copper in silicon and demonstrate the possibility of precise control over the phase composition and defect structure of the material, which is of significant importance for semiconductor device technology.

Background: In semiconductor device manufacturing technology, the diffusion doping method remains one of the key methods for introducing impurities into the volume of a crystalline semiconductor. Fast-diffusing impurities are predominantly used to obtain doped semiconductor materials. In the silicon lattice, such impurity atoms are typically characterized by limited solubility and a relatively low concentration of electrically active states. In addition, they tend to form various aggregated states due to interaction with atoms of technological impurities [1-7].

Methods: A single-crystal silicon of the KEF grade, grown using the Czochralski method, with a specific resistance of ρ=0.3 Ohm•cm, was used as the initial sample for the experiments. Diffusion of copper elements into silicon was carried out at a temperature of T=1473 K for 5 hours. After diffusion annealing, the samples were cooled using rapid cooling (υcool = 200 K/s).

The structural composition and chemical composition of impurity clusters in n-Si<Cu> samples were studied using a JSM-IT200 scanning electron microscope.

Structural studies were performed using a modern XRD 6100 X-ray diffractometer, using CuKα radiation in step-by-step scanning mode, with a radiation wavelength of λ= 0.15405 nm.

To determine the concentration of optically active oxygen and carbon, we conducted studies using IR Fourier spectroscopy with the FSM 2201 device.

Results: The results of studies of the formation processes of impurity clusters in silicon under certain thermodynamic conditions of diffusion doping showed that the morphological parameters of nickel impurity clusters mainly depend on the temperature and diffusion time, as well as on the cooling rate of the samples after diffusion annealing. As shown by the results in rapidly cooled n-Si<Cu> samples, impurity clusters of various shapes and sizes are observed. The sizes of these impurity clusters reach up to ~800 nm **(Fig. 1).**

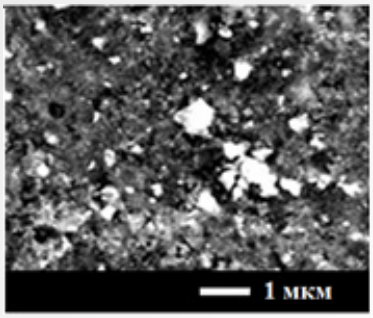

Fig. 1. Impurity clusters of copper in silicon in n-Si<Cu> samples

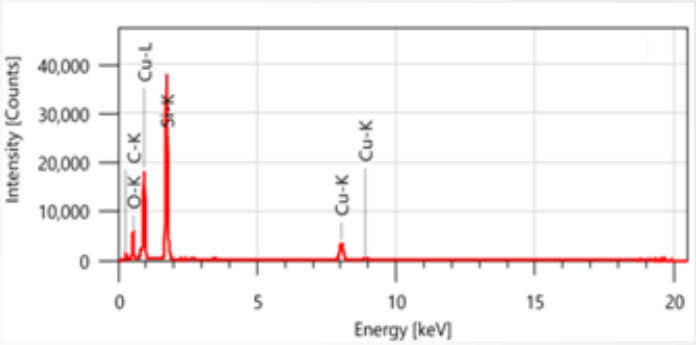

Fig. 2. Full spectrum of elemental composition of spherical impurity microinclusions with a size of ~800 nm in a rapidly cooled n-Si<Cu> sample.

Fig. 2 shows the results of determining the chemical composition of a spherical impurity cluster with a size of ~800 nm, formed in the volume of a rapidly cooled n-Si<Cu> sample after diffusion. As can be seen, the percentage of Cu atoms in the volume of nanoinclusions is 29.53%, Si atoms - 69.76%, oxygen atoms - 0.39%, and carbon atoms - 0.32%. As it turned out, these indicators do not actually change throughout the entire volume of this nanoinclusion.

To determine the structural characteristics of impurity atom clusters formed in silicon single crystals, phase and structural fragments of the initial samples and copper-doped silicon samples were studied using X-ray structural analysis. The peak with the highest intensity is observed in the angle range 2θ=28÷29°C and corresponds to reflection from the crystallographic plane (111) of single-crystal silicon (Si).

Fig. 3 shows an X-ray diffraction pattern of n-Si samples. Analysis of the diffraction pattern indicates the presence of two distinct diffraction peaks, differing in intensity. This reflection is characteristic of a well-ordered silicon crystal lattice and indicates the presence of a dominant Si(111) orientation in the sample under investigation. The second peak, which is significantly less intense, is recorded in the angle range 2θ=25÷26°C. This signal is identified as a reflection from an amorphous or oxide phase—silicon dioxide (SiO_2)—the formation of which is apparently associated with natural or technological oxidation of the sample surface during preparation or processing.

Fig. 4 shows the X-ray diffraction pattern of n-Si<Cu> samples. As can be seen from the diffractogram, the spectrum shows diffraction reflections of varying intensity corresponding to both the silicon matrix and the phases formed on the basis of Cu, O, and C.

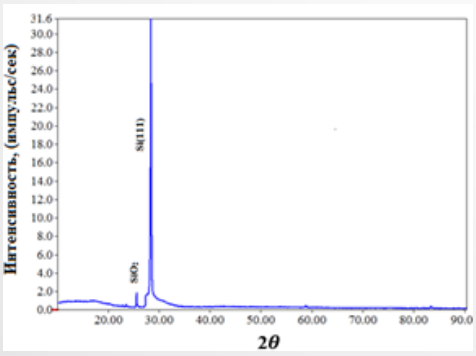

Fig. 3. X-ray diffraction pattern of the initial n–Si sample.

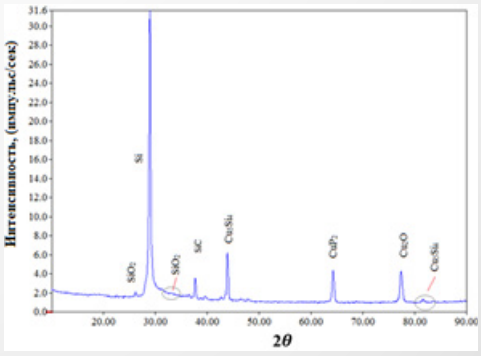

Fig. 4. X-ray diffraction pattern of the n-Si<Cu> sample.

The most intense reflection belongs to single-crystal silicon with crystallographic orientation (111), observed at an angle of 2θ = 28.97°C. It should be noted that after diffusion, this reflex shifts to the large angle region compared to the initial sample (Δθ=0.57°C), which indicates the occurrence of elastic deformations of the Si crystal lattice associated with the introduction of impurity atoms and the formation of a solid solution of substitution or interstitial atoms. The X-ray diffraction pattern also shows a reflection at 2θ=26.15°C, which clearly corresponds to the silicon dioxide (SiO_2) phase that forms when silicon reacts with oxygen during heat treatment. Additionally, a weak peak at 2θ=37.65°C was registered, identified as SiC, indicating chemical interaction between silicon and carbon atoms during high-temperature diffusion. Of particular interest are the reflections corresponding to copper-silicon compounds. In particular, the Cu5Si4 phase manifests itself in two characteristic peaks: the most intense one is recorded at 2θ=43.9°C, and the second, less pronounced one, is observed in the range of 80÷85°C. In addition, at an angle of 2θ=64.25°C, a peak belonging to the CuP2 phase was detected, indicating the possible inclusion of phosphorus in the diffusion doping process. The next registered reflex at 2θ=73÷74°C corresponds to copper oxide Cu_2O, which forms when Cu atoms interact with residual oxygen in the crystal. Thus, analysis of the X-ray diffraction pattern shows that diffusion doping of copper into silicon is accompanied by the formation of a whole complex of phases-from oxides and carbides to silicides and phosphides of copper-which confirms the high chemical activity of impurity atoms under conditions of high-temperature treatment and subsequent cooling.
Fig. 5 shows a fragment of the IR spectrogram of the change in the concentration of optically active carbon in the initial sample and in the n-Si<Cu> samples.

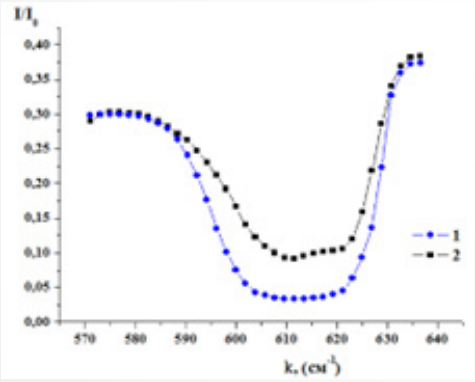

Fig. 4.Graph showing the dependence of the transmittance coefficient on the wave vector. 1-initial sample, 2-sample n-Si<Cu>

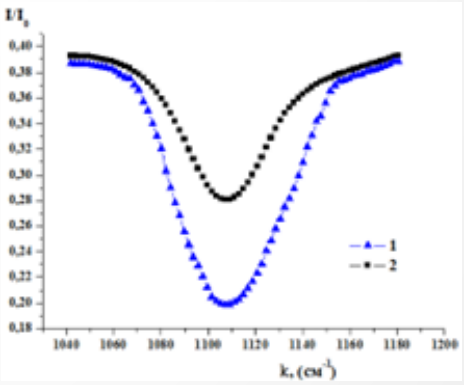

Fig.5. . Graph showing the dependence of the transmittance coefficient on the wave vector. 1-initial sample, 2-sample n-Si<Cu>

Calculations show that in n-Si<Cu> samples, the concentration of active carbon decreases by 28% compared to the initial sample. This is due to the fact that during the diffusion doping of copper, carbon atoms transition to more stable states, forming compounds such as SiC.
Fig. 6 shows a fragment of the IR spectrogram of the change in the concentration of optically active oxygen in the initial sample and in the n-Si<Cu> samples. Calculations show that in n-Si<Cu> samples, the concentration of optically active oxygen decreases by 52% compared to the initial samples due to the formation of stable oxide compounds, such as SiO_2 and Cu_2O.

Conclusion: Thus, the results of the work show that high-temperature diffusion doping of copper into silicon is an effective way to purposefully change its phase composition and defect structure. This opens up opportunities for controlling the morphology, chemical composition, and physicochemical properties of silicon materials. It has been established that impurity nanoinclusions of various morphologies and sizes up to ~800 nm are formed in rapidly cooled n-Si<Cu> samples. X-ray structural studies have shown that diffusion doping with copper leads to a shift in the silicon (111) peak, indicating the occurrence of elastic lattice deformations associated with the introduction of impurity atoms. New phases were identified in the n-Si<Cu> samples: SiO_2, SiC, Cu5Si4, Cu_2O, and copper phosphide CuP2. This confirms the occurrence of complex chemical reactions between impurity atoms and matrix silicon under high-temperature annealing conditions. The results of IR Fourier spectroscopy show that the concentration of optically active carbon in n-Si<Cu> samples decreases by approximately 28%, which is associated with its transition to more stable states, including the formation of SiC. The concentration of optically active oxygen decreases by 52%, indicating redistribution and structural rearrangement of interstitial oxygen with the formation of stable oxide phases SiO_2, Cu_2O. These processes are accompanied by a decrease in the concentration of optically active oxygen and carbon impurities and the formation of stable compounds that determine the thermodynamic and structural stability of the system.

Coalesce Research Group

13th International Conference on

Materials Science & Engineering

October 22-24 2025 | Tashkent, Uzbekistan

FORMATION OF IMPURITY DEFECTS IN SI DOPED WITH NI AND FE

Nozimjon Turgunov and Nodirbek Khaytimmetov*

Institute of Semiconductor Physics and Microelectronics at the National University of Uzbekistan named after Mirzo Ulugbek, Tashkent, Uzbekistan

Abstract

This article examines the structural construction of impurity accumulations of nickel and iron formed in the bulk of n-Si<Ni,Fe> samples. The structural construction of impurity accumulations was studied using X-ray diffraction analysis. It has been established that with rapid cooling υcool = 200 K/s of n-Si<Ni,Fe> samples after diffusion annealing, the formation of various accumulations of impurity atoms is observed in their volume. From the results of X-ray diffraction analysis, it was revealed that structural lines with different intensities are observed in the X-ray diffraction patterns of n-Si<Ni,Fe> samples.

Background: The modern development of micro- and nanoelectronics requires conducting research into the physicochemical properties of semiconductor materials using more high-precision methods. One of the directions of such research is structural analysis, through which we can obtain important information about semiconductor materials. In this field, X-ray spectroscopy methods for studying defective structures in substances are among the most informative, reliable, and widely used [1-3]. One of the most common methods for studying the structural properties of crystalline solids is X-ray structural analysis. With its help, it is possible to study the structural structure of crystals, i.e., to determine the type of crystal lattice and its parameters. If the object of research is multiphase, for example, an alloy consisting of several components, then it is possible to identify each of these phases and determine their percentage content in the alloy [4,5]. In this work, we investigated the structural properties of silicon samples doped with nickel and iron, as well as the peculiarities of the formation of various clusters with the participation of silicon, nickel, iron, and oxygen atoms.

Methods: For the research, we prepared the initial n-Si samples and the doped n-Si<Ni,Fe> samples. The initial sample for the experiments was monocrystalline silicon of the KEF brand, grown by the Chokhralsky method, with a resistivity of 0.3 Ohm·cm. The samples, made in the form of a rectangular parallelepiped with dimensions of 10x5x2 mm, were purified by chemical methods using a HF:HN03 (1:2) solution. Using the VUP-4 unit, where the vacuum value was 10-4 Torr, 0.4 μm thick nickel atoms were deposited on one side of the pre-prepared silicon samples by spraying. On the other hand, iron atoms with a thickness of 0.2÷0.3 μm were applied to these same samples. Simultaneous diffusion of nickel and iron atoms in silicon was carried out in a horizontal SUOL-4 furnace at a temperature of T=1473 K for 5 hours. The temperature in the furnace was controlled within ±3 K using a platinum-platinorodium thermocouple. After diffusion annealing, the samples were cooled using the rapid cooling method (υcool=200 K/s).

To clarify the structural characteristics of the formed accumulations of impurity atoms in silicon monocrystals, the phase and structural fragments of the initial samples and silicon samples doped with nickel and iron simultaneously were investigated using the X-ray structural analysis method. Structural studies were carried out using the modern Malvern Panalytical Empyrean X-ray diffractometer, using CuKα radiation in step-by-step scanning mode, with a radiation wavelength of λ = 0.15405 nm.

Results: The results of structural studies of n-Si<Ni,Fe> samples obtained by rapid cooling υcool =200 K/c after diffusion annealing showed that impurity compounds are formed in their volume. The obtained results were analyzed as follows. Using the obtained results, the distance between the planes in the crystal can be determined using the Wolf-Bragg equation:

$n\lambda=2d\sin\theta$

where: d - interplanar distance, θ - Vulf-Bragg angle n- order of diffraction maximum, λ = 0.15405 nm - wavelength of CuKα-radiation.

The average size of the crystallites in different planes is determined by the Scherer formula:

$L=K\lambda/\beta\cos\theta$

where: K - dimensionless particle shape coefficient (Sherrer constant); λ = 0.15405 nm - wavelength of CuKα-radiation; β - half-height reflection width, θ - Wolf-Bragg angle, L - average crystallite size (nm).

In the obtained X-ray diffraction pattern of the initial sample, only two structural reflections were observed. One of them has the strongest intensity and reflects at an angle of 2θ=28.39° corresponds to Si (111). The average size of the crystallites L and the interplanar distance d in this reflection are 2.84 nm and 0.628 nm, respectively. The second peak, reflected by a weaker intensity, is observed at an angle of 2θ =25.61° and corresponds to the SiO2 compound. The average size of the crystallites and the interplanar distance in this reflection are L=2.55 nm and d=0.347 nm. The narrow width of the structural lines and the absence of other peaks in the diffraction pattern indicate the high degree of perfection of the initial sample's crystal lattice.

The X-ray diffraction pattern of a silicon sample doped with nickel and iron is shown in Figure 1. As can be seen from the radiograph, several structural reflections with different intensities are observed. The largest of these peaks corresponds to monocrystalline silicon with a crystalline orientation (111) (Fig. 2). It reflects at an angle of 28.83° and shifts towards a larger angle compared to the same reflection in the original sample. This shows that the crystal lattice deforms due to the penetration of impurity atoms. In this reflex, the value of L and the value of d are 0.997 nm and 0.619 nm, respectively. In addition, other compounds formed with the participation of impurities from iron, oxygen, phosphorus, nickel atoms, and the matrix element were also observed in the radiograph. The formation of nickel and silicon oxides can also be observed. Compounds formed by iron atoms with nickel atoms were observed at a 44° angle. The average size of the crystallites and the interplanar distance on this structural line are L=0.624 nm and d=1.44 nm. The reflection observed at an angle of 39.52° corresponds to the FeSi compound and the value of L and d in this reflection is 0.769 nm and 1.36 nm, respectively.

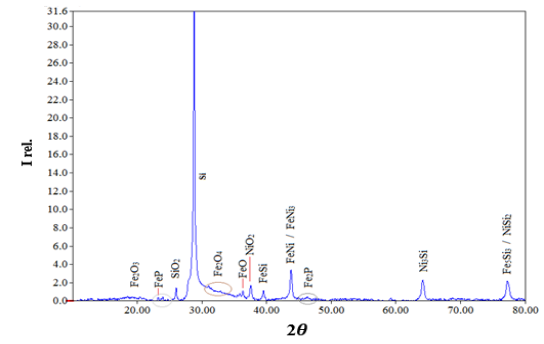

Fig.1. X-ray diffraction pattern of n-Si<Ni,Fe> sample.

The reflection observed at an angle of 64.15° corresponds to the Ni3Si compound and in this reflection, the values of L and d are 0.569 nm and 1.161 nm, respectively. From the radiograph, we can still see the formation of a compound of iron with oxygen in the form of Fe2O4 and FeO. These structural lines are reflected around an angle interval of 30-37°. On the radiograph, weakly intense structural lines are observed and correspond to iron-phosphorus compounds, in the form of FeP and Fe2P. They reflect around 25° and 45° angles, respectively. Another structural line is reflected around the 77° angle. From the crystal structure database (COD-Crystallography Open Database) and literature data, it was found that this peak corresponds to two compounds in the form of Fe5Si3 and NiSi2.

Conclusion: Thus, during high-temperature doping of silicon with nickel and iron impurities, impurity accumulations are formed in the sample volume, consisting of various two-component compounds with the participation of matrix element atoms, atoms of basic and technological impurities, which can migrate along the crystalline structure of silicon. From the obtained results, it was revealed that several types of compounds with different intensities and different 2θ values are formed in n-Si<Ni,Fe> samples. These compounds represent not only the combinations of matrix element atoms and impurity atoms but also the combinations of oxygen with impurity atoms and the combinations of impurity atoms with each other. Among the formed compounds, compounds of phosphorus atoms with impurity Fe atoms are also observed.

Coalesce Research Group

13th International Conference on

Materials Science & Engineering

October 22-24 2025 | Tashkent, Uzbekistan

LITHIUM NIOBATE ($LINBO_3$) THIN FILMS PRODUCED BY MAGNETRON ION SPUTTERING IN THE MSIR SYSTEM

Z.T. Azamatov*, S.A. Muzafarova, A.S. Achilov and A.B. Bakhromov

Research Institute of Semiconductor Physics and Microelectronics at the National University of Uzbekistan. Uzbekistan, 100057, Tashkent, st. Yangi Almazar, 20.

Abstract

Lithium niobate ($LiNbO_3$) thin films were deposited by magnetron ion sputtering in an MSIR system and systematically characterized to assess their suitability for integrated photonics and electro-optic devices. A Z-cut $LiNbO_3$ wafer (thickness d = 0.3 mm) served as the sputtering target. Depositions were carried out in mixed oxygen/argon ambient (40% O_2 / 60% Ar) at a total pressure of 0.58 Pa with a magnetron power of 145 W. Film growth was monitored in situ using a quartz crystal microbalance to track deposition rate and thickness, yielding films in the 75-160 nm range on transparent glass substrates. Post-deposition thermal treatment consisted of two air anneals, 1 h at 550 °C followed by 1 h at 700 °C, to promote crystallization and reduce point-defect disorder. X-ray diffraction revealed the emergence of distinct $LiNbO_3$ reflections after annealing and an increased fraction of crystallites with (001) planes parallel to the surface, indicative of partial texturing. A secondary $LiNb_3O_8$ phase was also observed, consistent with lithium depletion during sputtering. Electrical and optical measurements showed average sheet resistances of ~50 Ω/sq for 160 nm and 100 nm films and ~180 Ω/sq for 75 nm films, while optical transmittance spanned ~85–98%, reaching ~95–100% for the thickest films. Variations in target–substrate spacing affected film stoichiometry: increasing the distance from 20 mm to 120 mm reduced the niobium fraction (from 42.10 wt% to 3.74 wt%) and increased oxygen incorporation, consistent with additional plume-gas interactions in oxygen-rich ambient (~10^{-2} Torr equivalent). These results show that low-power magnetron sputtering with controlled annealing yields crystalline $LiNbO_3$ films with high transmittance; tuning O_2 partial pressure, spacing, and annealing suppresses $LiNb_3O_8$ and improves texture.

Background: Recently, the electronics industry has seen a trend toward integrating silicon technologies with ferroelectrics and creating film and thin-film ferroelectric structures on silicon substrates. However, the properties of bulk materials can differ significantly from those of films [1-3]. The electrophysical properties of LiNbO3 films can be affected, in particular, by the conditions of deposition and growth of the film structure, the composition and quality of the substrate, and the electrode material. The differences between the properties of thin-film structures and those of bulk materials and the influence of various factors on their characteristics remain insufficiently studied.

The development of microelectronics and miniaturization in instrument making entail the need to create and study micro - and nanoscale structures based on ferroelectrics – lithium niobate [4,5]. Recently, the electronics industry has seen a trend towards integrating silicon technologies with ferroelectrics and creating film and thin-film ferroelectric structures on silicon substrates. The properties of bulk materials can differ significantly from those of films. The use of film structures based on lithium niobate with silicon technologies remains very promising.

Methods: The magnetron-ion sputtering method provides the following advantages (Fig. 1) [2,3]:
- high adhesion of films, since the energy of the sputtered particles is an order of magnitude higher than the energy of the evaporated particles;

- maintenance of the stoichiometric composition during sputtering of multicomponent materials; - high utilization rate of the sputtered material;
- production of coatings of uniform thickness (including when deposited on surfaces with a complex profile) in the absence of large agglomerates observed during vacuum evaporation;
- the possibility of creating continuous-action installations and lines, since the targets can have a virtually unlimited supply of sputtered material, and the use of quantitative relationships between various process parameters enables automatic control of the deposition modes of thin-film layers.
Magnetrons use permanent magnets with a field strength of 0.4 T at the poles.

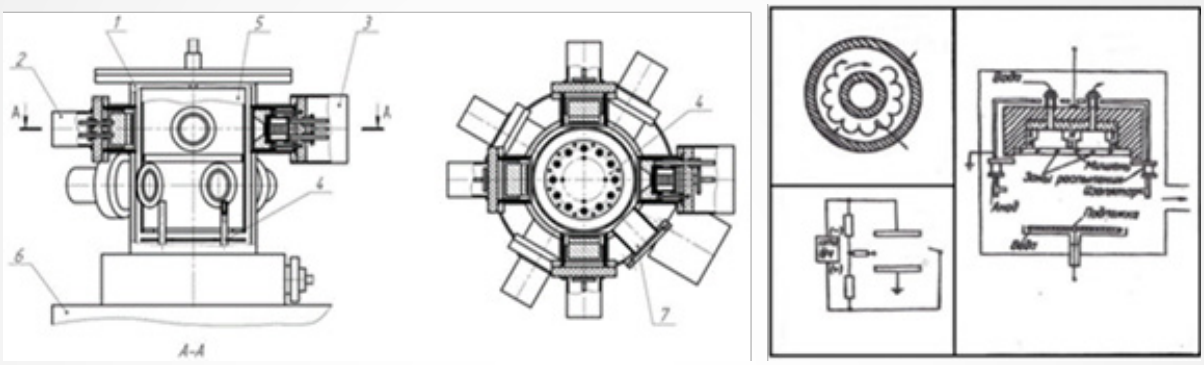

Fig. 1. Diagram of the coating application plant.

1-vacuum chamber; 2-magnetron; 3-ion source; 4-manipulator; 5-screen; 6-vacuum stand; 7-viewing window.

The main type of movement of a charged particle in a plane perpendicular to the magnetic field is cyclotron rotation. The technical characteristics of the gas discharge devices used in this installation are presented in Table 1.

	Current discharge, A	**Voltage combustion discharge, V**	**Minimum working pressure , Torr**
Magnetron	0-0.3	150÷450	2·10-3
Source Hall	0-0.5	300-500	10-3

Table 1. Technical characteristics of the magnetron and ion source.

The combined action of electric and magnetic fields causes a charged particle to drift in a direction perpendicular to both and with a velocity

$$\vec{V} = \frac{\left[\vec{E} \cdot \vec{B}\right]}{B^2} \qquad \vec{V} = \left[\vec{E} \times \vec{B}\right] / B^2 \qquad [1]$$

Where V is the electric field strength, in V/m. The magnitude of the drift does not depend on the charge or mass of the particle and does not lead to charge separation or the generation of a current, since the particles move in the same direction and at the same speed.

As noted above, the MSIR belongs to low-voltage sputtering systems. The supply voltage does not exceed 1000 V, with direct current. The operating voltage is 300÷800 V, a negative potential is usually applied to the target, and the anode has zero potential [2]. The current density on the target is quite high and for an MSIR with a hollow cylindrical cathode it reaches 800 A/m2, with a conical cathode - 1600 A/m2, and for a flat MSIR - up to 2000 A/m2, and the maximum current densities in the central part of the sputtering zone can be significantly higher. The specific power in an MSIR with a hollow cylindrical cathode is 4•105 W/m2 [5]. The maximum permissible power is determined by the target cooling conditions and the thermal conductivity of the sputtered material. LiNbO3 films were deposited on a transparent glass substrate for optical and electrical studies.

Results and discussion: Film structure manufacturers conducted X-ray structural analysis of samples using diffractometers. Bede D1 System (Bede Scientific Instruments, Ltd., UK) and DRON 3. The X-ray diffraction images are shown in Figure 2. For the LiNbO3 film after thermal annealing at 700°C, LiNbO3 peaks were detected. The phases present in the film were LiNbO3 and LiNb3O8.

LiNbO3 film thickness ranged from 75 to 160 nm and was monitored during deposition using a quartz crystal sensor with a preset normalization factor. The advantage of using a quartz crystal sensor is that it allows monitoring not only the thickness but also the deposition rate in the magnetron system. The average surface resistance values were 50 Ω/sq for 160 nm films, 50 Ω/sq for 100 nm films, and 180 Ω/sq for 75 nm films. Transparency ranged from 85 to 98%, while for 160 nm films it reached 95 to 100%. The lower transparency of thinner films is explained by the fact that the interference maximum occurs at a wavelength where absorption is still quite strong.

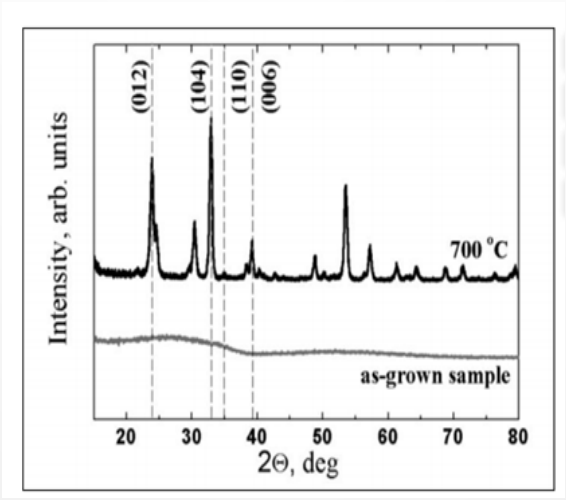

Fig. 2. Results of X-ray structural analysis for LiNbO3 film.

Figure 2 shows that annealing at 700°C increases the proportion of LiNbO3 crystallites with (001) crystallographic planes parallel to the film surface. The formation of the LiNb3O8 phase indicates lithium deficiency. A crystalline structure was observed in the LiNbO3 film after annealing.

Conclusion: The results of the studies showed that LiNbO3 films obtained at a target-substrate distance of 120 mm contain less niobium (3.74 wt.%) compared to films obtained at its base (20 mm) (42.10 wt. %). In addition, with an increase in the distance from the target to the substrate, the oxygen content in the LiNbO3 films increases, which is associated with the intensification of processes in the torch during its expansion in an oxygen atmosphere with a pressure of 10-2 Torr and confirms the uneven distribution of components during magnetron evaporation of the LiNbO3 target.

INVESTIGATION OF MORPHOLOGY OF SILICON DOPED WITH PD ATOMS

Sh.B. Utamuradova and D.A. Rakhmanov*
Institute of Semiconductor Physics and Microelectronics at the National University of Uzbekistan, Uzbekistan

Abstract

This study investigates the surface morphology and topology of n-type silicon (n-Si) single crystals doped with palladium at various temperatures using atomic force microscopy (AFM). AFM analysis reveals that palladium diffusion at 1200 °C markedly smooths the surface of n-type silicon single crystals. The surface roughness parameters are reduced by about 50%, and the initially anisotropic relief becomes more uniform and isotropic.

Background: Silicon remains the cornerstone material of modern micro- and nanoelectronics, thanks to its abundance, well-established single-crystal growth technology, and exceptional electronic properties. However, as semiconductor devices become increasingly complex, there is a growing demand to modify both the surface and bulk characteristics of silicon to enhance its electrical and optical performance. One promising strategy involves surface doping with transition metals, which can form stable silicide compounds with silicon and significantly influence diffusion and surface relaxation processes [1]. Among such systems, silicon–palladium (Si–Pd) combinations are of particular interest. Palladium exhibits strong chemical reactivity toward silicon and is capable of forming various silicide phases. These compounds are characterized by high thermal stability and low electrical resistivity, making them attractive for use in barrier contacts, interconnects, and components of nanostructured devices. The morphology and topology of the silicon surface—shaped during the diffusion of Pd atoms into the substrate at different temperatures—play a crucial role in determining the properties of these systems [2,3]. Therefore, the significance of this work lies in analyzing the morphological and topological transformations of n-type single-crystal silicon surfaces doped with palladium through diffusion under different thermal conditions. The main objective is to establish correlations between heat-treatment parameters, surface relief formation, and the potential impact of the resulting structures on the functional characteristics of silicon materials used in nanoelectronic applications.

Methods: The study was conducted on n-type silicon wafers with a specific resistivity of 40 Ω·cm (KEF-40), produced from single-crystal silicon ingots grown by the Czochralski method. Palladium doping was carried out using a diffusion technique: a thin palladium layer was deposited onto the silicon surface, followed by thermal annealing in evacuated quartz ampoules at 1200 °C for 3 hours. The surface morphology of the n-type single-crystal silicon samples was examined by atomic force microscopy (AFM) both before and after palladium diffusion at 1200 °C. The AFM analysis included the acquisition of two-dimensional (2D) height maps, three-dimensional (3D) surface reconstructions, and line profiles, enabling both qualitative and quantitative evaluation of topographical changes.

Results: AFM images of the initial silicon sample (Fig. 1) revealed a surface with pronounced anisotropy and considerable roughness. The two-dimensional map (Fig. 1a) displays elongated features resembling parallel grooves and ridges, which are likely related to both the mechanical polishing process and natural “step-bunching” phenomena—aggregations of atomic steps on the crystal surface. In the three-dimensional reconstruction (Fig. 1a), the surface relief is characterized by alternating ridge-like

elevations and deep depressions. The maximum height variation reaches approximately 32 nm, while the peak-to-valley (Pt) value is about 17.4 nm. The corresponding line profile (Fig. 1b) further confirms significant height variations over several micrometers. Overall, these results indicate that the untreated silicon surface exhibits substantial roughness and a distinctly directional relief.

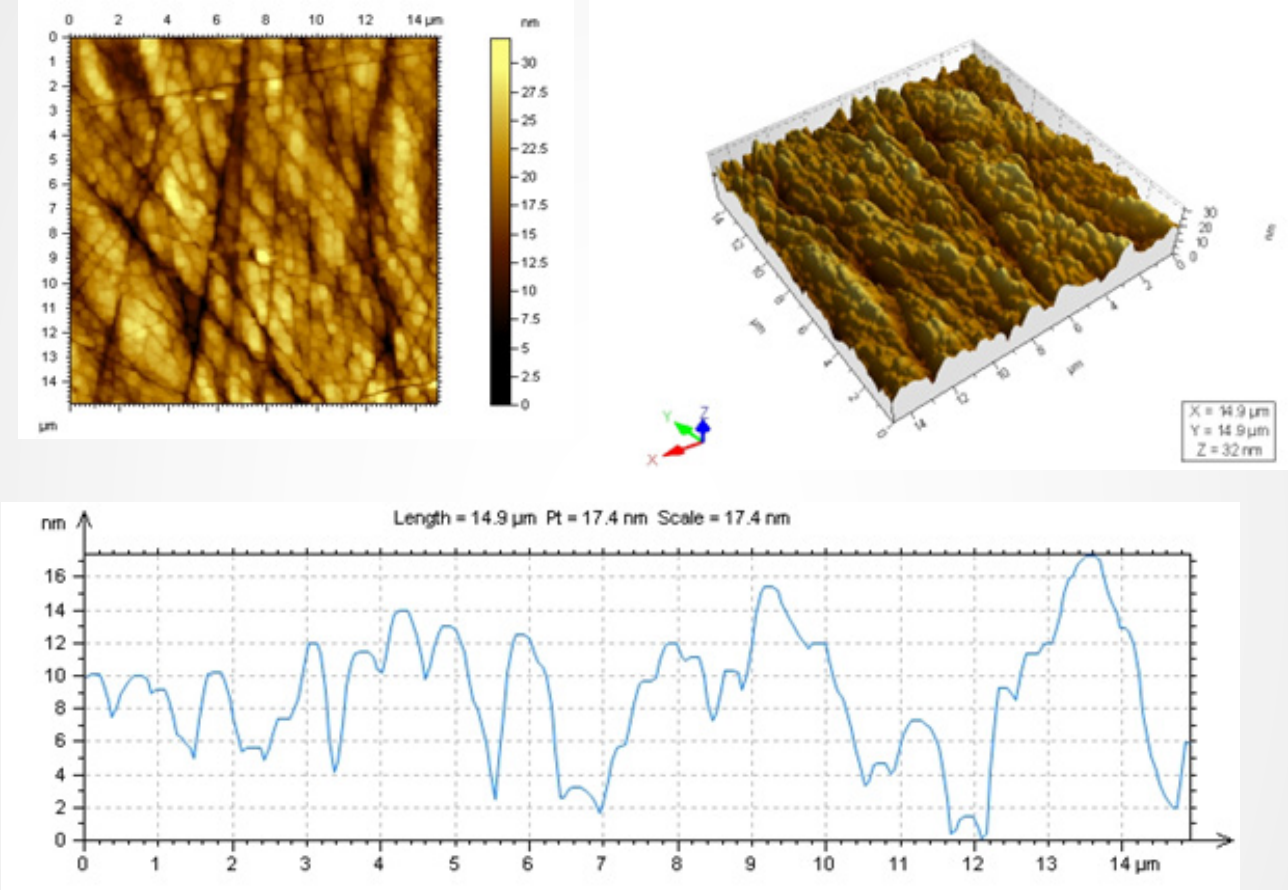

Fig.1. Typical 2D and 3D AFM images of the surface (a), cross-section profile along the main irregularities (b) of an n-type silicon single crystal.

After palladium diffusion at 1200 °C, the silicon surface exhibited a markedly smoother morphology (Fig. 2). The previously observed directional pattern disappeared, and the surface relief became nearly isotropic. The formation of smaller, more uniformly distributed irregularities suggests a significant re-organization of the surface layer structure.

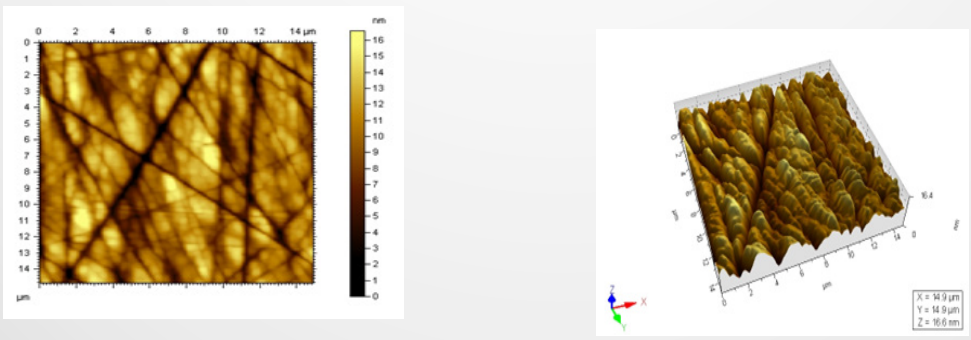

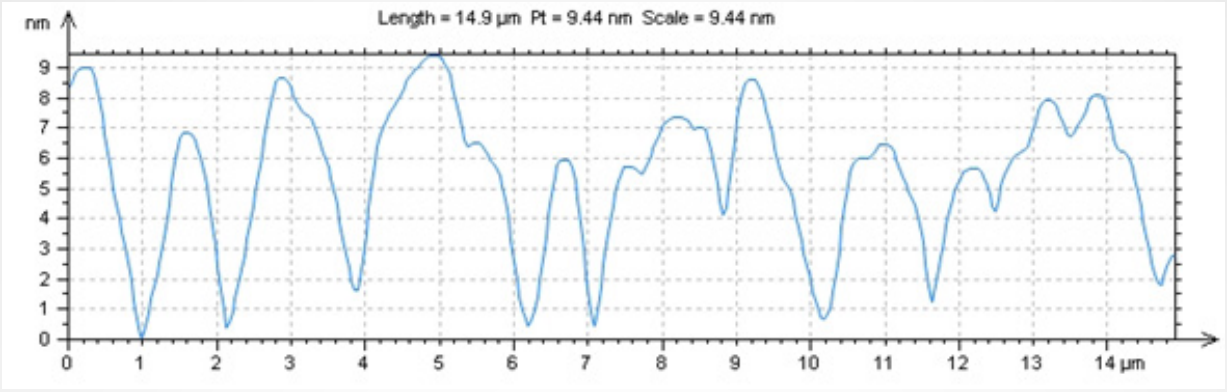

Fig. 2. Typical 2D and 3D AFM images of the surface (a), cross-sectional profile (b) of a single crystal of n-type silicon doped with palladium at 1200 °C.

The maximum surface height variation decreases to approximately 16.6 nm, while the peak-to-valley (Pt) value is reduced to about 9.44 nm—nearly half that of the initial sample. Consequently, increasing the diffusion temperature results in a systematic reduction in surface roughness and a decrease in the amplitude of surface fluctuations. With rising temperature, surface silicon atoms gain higher mobility, leading to material redistribution and the smoothing of large irregularities [4,5]. Palladium further contributes to this process by lowering the surface energy and promoting a more ordered rearrangement of silicon atoms, thereby accelerating surface leveling [6,7]. At elevated temperatures around 1200 °C, the interaction between Pd and Si can initiate the formation of thin silicide layers, which enhances surface stability and suppresses the development of large defects [8]. The observed transition from directional, comb-like patterns to a more uniform relief reflects the minimization of surface free energy and the suppression of step-bunching effects [9,10].

Overall, AFM analysis demonstrates that palladium diffusion at 1100–1200 °C leads to significant smoothing of the n-type single-crystal silicon surface. The roughness parameters are reduced by approximately 50%, and the surface becomes more isotropic. These effects are attributed to enhanced self-diffusion processes, the surfactant action of palladium, and the possible onset of silicide formation. The findings confirm the potential of palladium doping as an effective method for modifying silicon surfaces to improve their electronic and optical performance.

Conclusion: In this study, morphological and topological transformations of single-crystal n-type silicon surfaces doped with palladium through diffusion at 1200 °C were analyzed using atomic force microscopy (AFM). The results show that the initial silicon surface exhibits pronounced anisotropy and relatively high roughness (Pt ≈ 17.4 nm, Z ≈ 32 nm). After palladium diffusion at 1200 °C, a notable reduction in surface roughness (to Pt ≈ 9.44 nm) is observed, accompanied by the smoothing of comb-like features and a partial loss of directional relief.

Therefore, it has been established that high-temperature palladium diffusion promotes systematic surface smoothing, primarily due to the enhancement of surface self-diffusion and the possible initiation of Pd–Si phase formation. These processes contribute to lowering the surface free energy and suppressing anisotropic structural features.

Coalesce Research Group

13th International Conference on

Materials Science & Engineering

October 22-24 2025 | Tashkent, Uzbekistan

EFFECT OF GAMMA IRRADIATION ON THE STRUCTURE OF TIN-DOPED SILICON MONOCRYSTALS

Sh.B.Utamuradova, O.X. Kuldashov and B.R Bokiev*

Scientific Research Institute of Semiconductor Physics and Microelectronics at the National University of Uzbekistan, Tashkent, Uzbekistan

Abstract

This study investigates the effect of gamma irradiation on the structural properties of tin-doped silicon single crystals. In the experiment, n-type and p-type Si<Sn> samples were irradiated with gamma rays from a ^{60}Co source at doses of 10^6 rad and 2×10^6 rad. To determine the structural modifications, X-ray diffraction (XRD) analysis was performed in the Bragg–Brentano geometry within the range of 2θ = 10°–100°. For the n-type Si<Sn> samples before irradiation, a strong (111) reflection was observed at 2θ = 28.6°, with a lattice constant of 0.5431 nm and an average subcrystallite size of 42.7 nm, indicating a high degree of crystalline perfection. After exposure to 10^6 rad of gamma radiation, the (111) peak shifted slightly to 2θ = 28.55°, its intensity increased by a factor of 1.8, the lattice constant expanded to 0.5482 nm, and the subcrystallite size increased to 53.4 nm. In the p-type Si<Sn> samples, the (400) reflection at 2θ = 69.1° initially exhibited an intensity of 0.11×10^4 imp/s. After 2×10^6 rad irradiation, the intensity increased by 1.6 times, the subcrystallite size enlarged from 27.5 nm to 33.9 nm, and the lattice constant slightly increased from 0.5442 nm to 0.5443 nm. The obtained results demonstrate that gamma irradiation causes redistribution and partial annihilation of dislocations, leading to the coarsening of subcrystallites, reduction of internal stresses, and improvement of lattice perfection in Si<Sn> single crystals. The observed increase in reflection intensity and the slight peak shift toward lower angles confirm the ordering and structural enhancement induced by gamma irradiation.

Background: Silicon (Si) is a key semiconductor material in modern micro- and nanoelectronics due to its excellent electrical and structural properties. To enhance its performance, isovalent doping with tin (Sn) and germanium (Ge) is widely used, as these dopants modify the lattice constant and defect structure without changing carrier concentration. Gamma irradiation strongly affects the microstructure of semiconductors by generating and redistributing defects. Studying these effects in doped silicon is important for developing radiation-resistant electronic materials. In this work, tin-doped silicon (Si<Sn>) single crystals were irradiated with ^{60}Co gamma rays at doses of 10^6 and 2×10^6 rad. Structural changes were analyzed by X-ray diffraction (XRD) in the Bragg–Brentano geometry to determine variations in lattice constant, subcrystallite size, and reflection intensity. The results reveal how gamma irradiation influences defect redistribution and improves lattice ordering in Si<Sn> crystals.

Methods: Tin-doped silicon (Si<Sn>) single crystals were investigated to study the effect of gamma irradiation on their structural properties. Both n-type and p-type Si<Sn> samples were prepared by doping high-purity silicon with isovalent tin (Sn) atoms. The samples were cut and chemically polished to obtain smooth mirror-like surfaces suitable for X-ray diffraction (XRD) analysis. Gamma irradiation was carried out using a ^{60}Co radioactive source with photon energy of 1.17 and 1.33 MeV. The samples were exposed to total doses of 10^6 rad and 2×10^6 rad at room temperature. After irradiation, all samples were stored under identical conditions to minimize environmental effects prior to measurement. Structural characterization was performed using X-ray diffraction (XRD) in the Bragg–Brentano geometry within

the 2θ range of 10°–100°. The scanning speed was maintained at 2°/min, and CuKα radiation with a wavelength of λ = 0.154 nm was used as the X-ray source. The diffraction peaks were recorded before and after irradiation to identify any changes in the crystallographic parameters. The average subcrystallite size (L) was determined using the Scherrer equation, L=K·□/□·Cosθ,

where K=0.94K = 0.94K=0.94 is the shape factor, λ=0.154 nm the wavelength of the X-ray radiation, β is the full width at half maximum (FWHM) of the diffraction peak, and θ is the Bragg angle. The lattice constant (a) was calculated from the diffraction data using the Nelson–Riley extrapolation function, x = ½(Cos2θ/Sinθ+Cos2θ/θ), and the linear relation y=kx+b, where the intercept bbb at x→0 corresponds to the true lattice constant. These analyses allowed determination of the changes in subcrystallite size, lattice parameter, and diffraction intensity caused by gamma irradiation in both n-type and p-type Si<Sn> single crystals.

Results: Figure 1 shows the X-ray diffraction (XRD) patterns of n-type Sn-doped silicon (n-Si<Sn>) samples before and after exposure to 10^6 rad of gamma radiation from a ^{60}Co source. Before irradiation, a strong (111) reflection was observed at 2θ = 28.6° (d = 0.3138 nm) with high intensity (1.25×10^4 imp/s) and a narrow FWHM (4.1×10^{-3} rad), indicating high crystalline quality [1]. After irradiation, the (111) peak shifted slightly to 2θ = 28.55°, and its intensity increased by 1.8 times (2.27×10^4 imp/s). The calculated subcrystallite size and lattice constant increased from 42.7 to 53.4 nm and from 0.5431 to 0.5482 nm, respectively. This suggests lattice expansion and defect redistribution under gamma exposure [2].

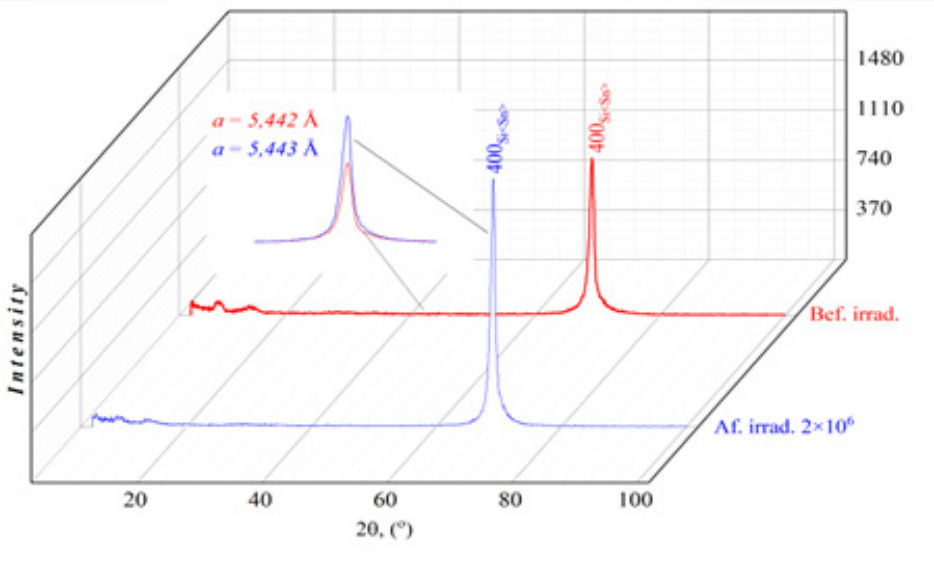

Figure 1. X-ray diffraction patterns of n-Si<Sn> samples before irradiation (red curve) and after exposure to 10^6 rad of gamma radiation (blue curve).

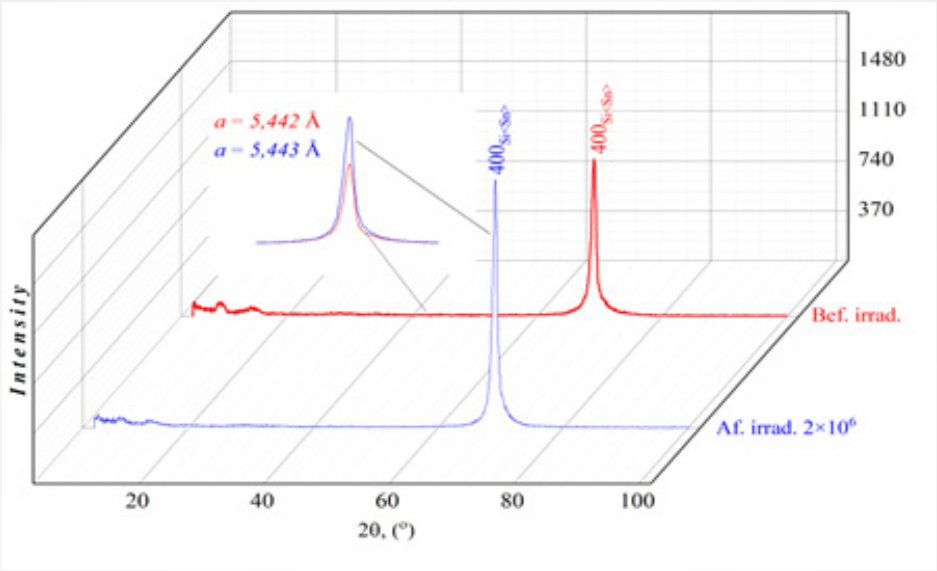

Figure 2. X-ray diffraction patterns of p-Si<Sn> samples before irradiation (red curve) and after exposure to 10^6 rad of gamma radiation (blue curve).

Figure 2 presents the XRD data for p-type Si<Sn> before and after 2×10^6 rad gamma irradiation. Initially, a (400) reflection appeared at $2\theta = 69.1°$ with intensity 0.11×10^4 imp/s and FWHM = 9.3×10^{-3} rad, indicating relatively lower crystalline perfection [3]. After irradiation, the peak shifted to $2\theta = 69.15°$, intensity increased 1.6 times (0.18×10^4 imp/s), and the subcrystallite size enlarged from 27.5 to 33.9 nm, while the lattice constant slightly expanded from 0.5442 to 0.5443 nm. These changes reflect partial recrystallization and reduction of dislocation density [4]. Overall, the results indicate that gamma irradiation promotes defect rearrangement, subcrystallite growth, and improvement of lattice order in both n- and p-type Sn-doped silicon. This finding agrees with previous studies reporting that gamma exposure enhances crystalline perfection and radiation tolerance in isovalently doped silicon materials [2–4].

Conclusion: Gamma irradiation significantly affects the structural properties of tin-doped silicon (Si<Sn>) single crystals. XRD analysis showed that irradiation shifts diffraction peaks to lower angles, increases intensity, and enlarges subcrystallite sizes in both n-type and p-type samples. These effects indicate lattice expansion, dislocation redistribution, and partial recrystallization. As a result, Sn-doped silicon exhibits improved crystalline order and structural stability, making it suitable for radiation-resistant semiconductor applications.

Coalesce Research Group

13th International Conference on

Materials Science & Engineering

October 22-24 2025 | Tashkent, Uzbekistan

STRUCTURAL AND SPECTROSCOPIC FEATURES OF SILICON DOPED WITH YTTRIUM AND SCANDIUM

Khodjakbar S Daliev[1], Jonibek J Khamdamov[2] and Islomjon Kh Khamidjonov[2*]

[1]Branch of the Federal State Budgetary Educational Institution of Higher Education "National Research University MPEI", 1 Yogdu st., Tashkent, Uzbekistan

[2]Institute of Semiconductor Physics and Microelectronics at the National University of Uzbekistan, Tashkent, Uzbekistan`

Abstract

This work presents a structural study of yttrium- and scandium-doped silicon using Raman spectroscopy and X-ray diffraction. Raman spectra obtained with a Bruker SENTERRA II spectrometer revealed both crystalline and amorphous phases, as well as frequency ranges corresponding to Y-Y, Y-Si, and Si-Si vibrations. The spectra indicate significant internal stresses caused by lattice mismatch between yttrium and silicon. X-ray analysis identified near-surface crystallites of SiSc, SiO_2, and Sc_2O_3 with trigonal and cubic symmetries, while bulk regions contained Y_2O_3, SiO_2, Si, and SiY phases. Rapid cooling led to unsaturated bonds due to incomplete ordering of Si-O-Y atoms. The results highlight the effect of elastic stresses and composition variation on the structural stability of silicon-based solid solutions.

Background: In recent years, structured silicon has garnered significant interest, as silicon is a promising material not only for electronics but also for optoelectronics and solar cells [1-3]. The efficiency of rare earth impurities in silicon, along with the manifestation of optical properties in such structures, depends on the spectrum of optically and electrically active centers containing rare earth elements, their total concentration, and the interaction with uncontrolled impurities and thermal defects within the material [2-5]. For many years, Raman scattering has been a widely used technique for studying the structure of silicon [3-9]. Raman spectroscopy is a powerful method for investigating the structure and dynamics of crystal lattices, based on the interaction of electromagnetic radiation with matter. Dynamic fluctuations caused by atomic and molecular vibrations lead to inelastic scattering of light, which is characterized by a shift in the frequency of the scattered radiation relative to the incident radiation. Raman spectra are unique for each substance and provide valuable insights into its structure and energy levels [13].

The basic principles of Raman theory are tied to the forced oscillations of a molecule's dipole moment under the influence of incident light and the modulation of this induced dipole moment by the vibrational movements of the molecule's "skeleton." This method finds broad applications across various fields of science and technology. In material studies, Raman scattering provides information about energy dispersion, structure, bonding, and defects. Structural analysis is often based on the phonon confinement model, which considers the finite size of crystallites by assessing phonon scattering efficiency. Confinement effects in these structures lead to modifications in their electronic, optical, and vibrational properties. While the Raman spectrum of crystalline silicon has been extensively studied, the Raman spectra of silicon doped with rare earth metals remain insufficiently explored. This work aims to investigate the defect structure of yttrium-doped silicon using Raman spectroscopy.

Methods: For this study, n-Si samples with initial resistivity ranging from 0.3 to 100 Ω·cm were selected. Prior to doping, the samples underwent thorough acid-peroxide cleaning, and oxide layers were re-

moved from their surfaces using an HF solution. Following the cleaning process, yttrium impurity films of high purity (99.999%) were deposited onto the clean silicon surfaces through vacuum deposition. The vacuum conditions in the chamber, maintained between 10^{-7} and 10^{-8} Torr, were achieved using an oil-free vacuum pumping system.

Before diffusion annealing, the samples were sealed in evacuated quartz ampoules. Doping with yttrium was carried out using the diffusion method at a temperature of 1200°C for 20 hours, followed by rapid cooling. To ensure a thorough investigation of the interaction between impurity atoms and silicon, it was essential to achieve both uniform doping and maximum impurity concentration. Accordingly, optimal conditions for doping silicon with yttrium were carefully considered.

Results: The spectrum displays a prominent peak at 521 cm^{-1} with a half-maximum width of 8–12 cm^{-1}. This peak is attributed to first-order scattering, which is associated with both transverse optical (TO) and longitudinal optical (LO) phonons. A notable feature of the spectrum is the presence of second-order acoustic phonon scattering at 303 cm^{-1} (TA), though its precise origin remains to be fully understood. It is likely that this peak represents a superposition of transverse and longitudinal acoustic modes. In addition, a broad peak between 920 and 1000 cm^{-1} is observed, which is linked to the scattering of multiple transverse optical phonons, commonly referred to as ~2TO phonons. The exact origin of this broad feature is still debated and requires further investigation. Some researchers propose that this peak results from the superposition of two or more optical modes [5-6]. A Raman microscope is an optical device that combines the advanced technological capabilities of a Raman spectrometer with an optical microscope. This integrated system offers a significant advantage over conventional spectrometers. In this system, the spectral signal is collected from a micron-sized focal region illuminated by an excitation laser, enabling highly localized measurements and spatial scanning over the sample surface. This allows for the acquisition of separate spectra from different points of interest. Micro-Raman mapping provides sample characterization at a level that surpasses traditional optical microscopy. For instance, image data can be used to determine the distribution of components, grain or particle size, changes in crystal structure or phase, the shape and size of internal impurities, the interaction and association of components across phase boundaries, as well as the distribution of internal stresses and strains within the sample.

The crystal lattices of materials in heterostructures (Y-Si) and solid solutions (YxSi1-x) are always different, leading to the development of built-in elastic stresses in the Y, Si, and Y-Si layers of multilayer structures when one material (Y) is grown on a substrate of another material (Si). The magnitude of lattice mismatch plays a crucial role in determining the quality of these structures, as such stresses can result in the formation of structural defects and, in many cases, significantly limit the potential for creating perfect heterocompositions.

When the layer material is a solid solution, the lattice mismatch is less pronounced compared to structures made of pure Si and Y. Changes in composition and material deformation lead to alterations in the crystal structure, which are reflected in the vibrational and phonon spectra [3-8]. It has been previously noted that the difference in Raman phonon bands between crystallites and nanocrystallites primarily concerns their bandwidth, while the Raman frequencies remain very close. This observation supports the attribution of the calculated transition to internal stress [2-9]. The Raman spectrum of the YxSi1-x solid solution (x = 0.25), grown on a Si substrate, was investigated. The thickness of the solid solution layer is 5 μm. In this case, the lattice constant of the YxSi1-x layer falls between the lattice constants of Y and Si. The solid solution contains bonds such as Si-Si, Y-Y, and Y-Si. If the content of one of the compo-

nents of the solid solution (e.g., Y) were zero, the frequency of the Si-Si mode would coincide with the optical phonon frequency in pure Si. In the obtained Raman spectrum, three distinct ranges of Raman shift frequencies can be identified, corresponding to the masses of the constituent elements and the elasticity coefficients of the bonds present. These include vibrations of the Y-Y bonds (around 315 cm^{-1}), Y-Si bonds (957–989 cm^{-1}), and Si-Si bonds (522 cm^{-1}). The main structural line on the silicon diffraction pattern appears at a scattering angle of 2θ = 27.99°, corresponding to the (111) plane. Its high intensity (112,341 $imp \cdot s^{-1}$) and narrow half-width (0.005 rad) indicate a high degree of crystallinity. The presence of second- and third-order reflections ((222) at 57.9° and (333) at 94.68°) suggests micro-distortions in the lattice caused by the uneven distribution of oxygen atoms — the primary background impurity in silicon. These defects form a thin near-surface layer characterized by structural lines typical of silicon dioxide. Calculated lattice parameters (a=b=4.9762 nm, c=5.4321 nm) correspond to a trigonal system (space group P321), with a polycrystalline layer about 1–2 μm thick. Scandium and yttrium doping lead to significant lattice modifications. After diffusion at 1200 °C and rapid cooling, the intensity of the main (111) line decreases, while the forbidden (222) reflection becomes visible, indicating the formation of bulk defects and micro-deformations. The lattice constants decrease to a_Si<Sc>=0.5418 nm and a_Si<Y>=0.5419 nm, confirming structural distortion caused by Sc and Y incorporation.

In the near-surface region, nanocrystallites of SiSc, SiO_2, Sc_2O_3, SiY, and Y_2O_3 compounds form, exhibiting cubic and trigonal symmetries. Rapid cooling promotes the appearance of unsaturated Si–O–Y bonds and small clusters that cause diffuse small-angle scattering. Thus, thermal treatment and rare-earth doping lead to the formation of oxide polycrystalline layers and substantial structural modifications in silicon.

Conclusion: This study provides comprehensive insights into the Raman and X-ray structural characteristics of Si samples and Y_xSi_{1-x} solid solutions with varying yttrium and silicon contents. Raman spectra revealed characteristic peaks corresponding to optical and acoustic phonons, while micro-Raman mapping offered detailed information about the microstructure and composition. Built-in elastic stresses, arising from lattice constant differences between Y and Si, strongly influence the position of Raman lines and contribute to the formation of structural defects that affect the perfection of heterostructures and solid solutions.

For scandium- and yttrium-doped silicon, X-ray analysis showed that prolonged heat treatment followed by rapid cooling leads to the formation of nanocrystallites in the near-surface regions. These crystallites, identified as SiSc, SiO_2, Sc_2O_3, SiY, and Y_2O_3, exhibit cubic, trigonal, and tetragonal symmetries with distinct lattice parameters. Rapid cooling reduces subcrystallite size and induces unsaturated Si–O–Y bonds, forming oxide polycrystalline layers and clusters. The results confirm that doping and thermal treatment significantly modify the crystallinity, phase composition, and structural order of silicon-based materials.

Coalesce Research Group

13th International Conference on

Materials Science & Engineering

October 22-24 2025 | Tashkent, Uzbekistan

INFLUENCE OF COOLING RATE ON STRUCTURAL AND ELECTROPHYSICAL CHANGES IN ZIRCONIUM-DOPED SILICON (SI+ZR)

Sh.A. Ismoilov

Research Institute of Semiconductor Physics and Microelectronics, National University of Uzbekistan, Uzbekistan

Abstract

This paper presents the results of an analysis of the Raman spectra and electrical properties of zirconium-doped silicon (Si+Zr) after heat treatment at temperatures of 700–1200°C for 12 hours. Both p- and n-type samples were studied, subjected to different cooling regimes—slow and fast. Raman and FTIR spectroscopy allowed us to identify features of crystallization, defect formation, and phase transformations, while electrical measurements revealed the effects of zirconium and oxygen on conductivity and carrier mobility.

Background: Zirconium-doped silicon (Si+Zr) has attracted attention as a potential material for microelectronics due to the stability and high dielectric properties of ZrO_2-based oxides. Understanding how the cooling rate affects its structural and electrical characteristics is essential for optimizing fabrication processes. In this study, both p-type and n-type silicon samples doped with zirconium were investigated to determine the influence of different cooling conditions following high-temperature annealing.

Objective: To investigate the effect of cooling rate on the structural, spectroscopic, and electrophysical properties of Si+Zr after thermal annealing at 700–1200 °C.

Methods: Silicon wafers of p-type and n-type conductivity were doped with zirconium and annealed at 700–1200 °C for 12 hours under controlled conditions. Two cooling regimes were applied — slow cooling and rapid quenching. Raman and FTIR spectroscopy were used to analyze crystal quality, defect formation, and Zr–O–Si phase evolution. Electrical measurements were conducted using the Hall method to determine resistivity (ρ), carrier concentration (n), and mobility (μ).

Results: The Raman peak near 520 cm^{-1} corresponds to crystalline silicon. Slow cooling preserved the lattice order, while rapid cooling led to peak broadening and shifting, indicating partial amorphization and defect growth. Additional peaks between 300–400 cm^{-1} and 600–650 cm^{-1} indicated the formation of ZrO_2 and Zr–O–Si phases. The resistivity of Si significantly decreased after Zr diffusion, from 35 Ω·cm to 2.1 Ω·cm for p-type and from 28 Ω·cm to 1.9 Ω·cm for n-type samples. Carrier concentration and mobility increased substantially at 1100 °C under rapid cooling, confirming activation of donor and acceptor centers.

Conclusion: The results demonstrate that the annealing temperature and cooling rate critically determine the structural and electrical properties of Si+Zr. Rapid cooling enhances conductivity and preserves metastable defects, whereas slow cooling leads to stable crystalline phases. These findings provide valuable insights for designing zirconium-doped silicon materials for semiconductor and sensor applications.

ANALYSIS OF MN-RELATED DEFECTS IN SI BY USING X-RAY DIFFRACTION

Sh.B.Utamuradova and Kh.J.Matchonov*
Institute of Semiconductor Physics and Microelectronics at the National University of Uzbekistan

Abstract

A study of the behavior of manganese atoms in the crystal lattice of silicon using an X-ray diffractometer, which is shown in the diffraction pattern Si<Mn>SiO2 and Si<Mn>, several selective structural reflections with different intensities are observed. It is determined that the lattice parameter of the Si<Mn> sample, the value is slightly less than the lattice parameter of the Si<Mn>SiO2 sample, but causes a shift of structural reflections in the Si<Mn> diffraction pattern towards smaller scattering angles.

Background: At present, solid-state electronic devices are used all over the world in almost all areas of science and technology. The field of application of solid-state devices is constantly expanding, fundamentally new devices are being created that stimulate the development of industry in new directions, which requires a significant increase in the perfection of the structure of Si, the main material of modern semiconductor solid-state electronics. In this regard, research aimed at studying the processes of defect formation in Si doped with various impurities and establishing controlled methods for stabilizing the parameters of semiconductor devices is one of the important problems.

Methods: The work is devoted to studying the influence of manganese impurity on X-ray diffraction analysis of silicon. Doping of silicon with manganese atoms was carried out by diffusion from the gas phase in evacuated quartz ampoules at a temperature of 1200 °C for 12 hours.

The used n-Si crystals (ρ=40 Ω·cm) were grown by the Czochralski method. Some samples were subjected to preliminary rapid cooling after high temperature treatment (HTT) at 1100°C for 10 hours. After high-temperature treatment (HTT), the surface of the silicon sample was cleaned with acid (HF÷HNO3; 1÷3).

The control of the structural and phase states of the studied samples was carried out on a third-generation X-ray diffractometer of the Empyrean Malvern type PANalytical L.T.D.

Results and their discussion: X-ray diffraction measurements were carried out in the Bragg-Brentano beam geometry in the range 2θB = from 15° to 140° continuously at a scanning rate of 0.33 deg/min and an angular step of 0.0200 (deg).

On fig. 1 shows the X-ray pattern of Si<Mn> with SiO2. It can be seen that the diffraction pattern contains several selective structural reflections with different intensities. The analysis showed that the surface of the sample corresponds to the crystallographic plane (111).

This is evidenced by the presence on the X-ray pattern from a series of selective reflections (HHH) (where H=1.2.3...), intense lines (111) Si with d/n = 0.3141 (2θ = 28.4°), (222) Si with d/n = 0.1570 (2θ = 58.8°) and (333) Si with d/n = 0.1046 nm (2θ = 94.9°). The beta (β) component of the structural line of the first order (111) Si is visible at the scattering angle 2θ = 25.7°, and the third order at 2θ = 83.3°.

The high intensity (5.8 x 104 imp x sec-1) of the main (111) Si reflection and the narrow width (FWHM

= 3.49 x 10-3 rad) testify to the perfection of crystalline Si with the lattice parameter aSi=0.54265 nm. The sizes of subcrystallites estimated from the width of this peak were LSi~54 nm.

However, the nonmonotonic nature of the inelastic background level at medium scattering angles (2θ = 35 ÷ 90°) of the X-ray pattern, that is, its distorted form, shows the presence of an elastic growth microstress in the silicon lattice. This conclusion is confirmed by the presence of the forbidden reflection (222)Si on the X-ray pattern with d/n = 0.1570 nm for the silicon lattice, the intensity of which is related to the intensity of the main peak (111)Si as I(222)/I(l 11) ≈ 10-3, which is an order of magnitude greater than 10-4, corresponding to uniform distribution of manganese and oxygen in the sample [1].

These facts testify to the inhomogeneous distribution of manganese and oxygen over the interstices of the silicon matrix lattice and the presence of local regions with microdistortions. According to the law of extinction of diffraction reflections, the (222)Si reflection should not be present in the X-ray diffraction pattern of an undistorted grating of a diamond-like structure. It appears only in the presence of distortions (elastic microstress) in the lattice.

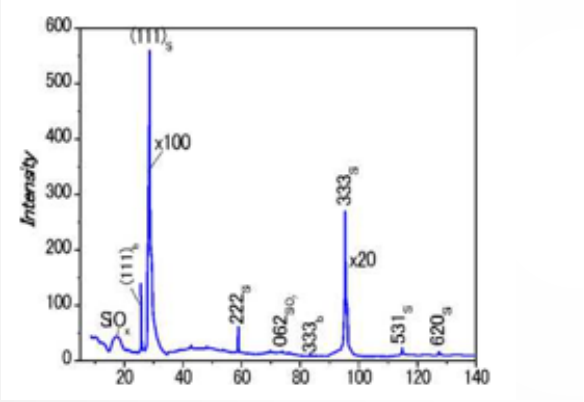

Fig.1. X-ray pattern of Si<Mn> Si<Mn> with SiO_2

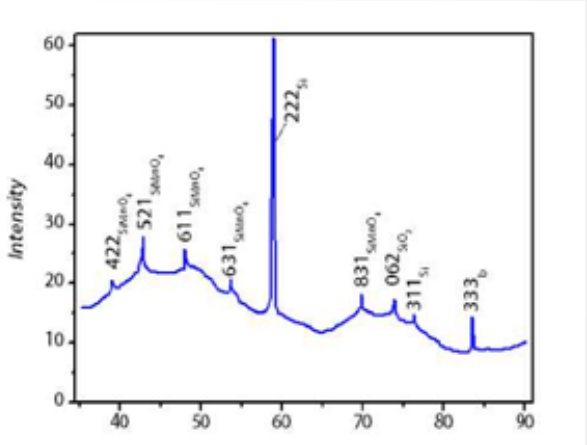

Fig.2. Section of the X-ray diffraction pattern of Si<Mn> Si<Mn> with SiO_2

Good splitting of the (333)Si reflection and weak splitting of the main (111)Si reflection by α1 and α2 radiations show the presence of residual elastic stresses in the silicon matrix lattice, associated with the difference in the ionic radii of silicon, manganese and oxygen atoms r_Si^(4+)=0.042 nm, r_Mn^(+2)=0.08 nm and r_o^(-2)=0.140 nm, respectively [3]. This assumption is confirmed by the presence of an oxygen precipitate in silicon in the crystalline form with a characteristic size LSiO2 ~ 93 nm on the (062)SiO2 X-ray diffraction pattern.

Additional confirmation is the presence of diffuse reflection at medium scattering angles with a maximum of 2θ = 48.3° (FWHM = 1.3x10-1 rad) caused by randomly oriented structural fragments Ld ≈ 1.7 nm in size (Fig. 2). Above the level of this diffuse reflection, five more structural reflections with weak intensity are clearly distinguished. The analysis showed that they are caused by silicon- manganese-oxygen precipitates in silicon, with an average characteristic size LsiMn04 ≈ 28 nm and having diffraction indices - (422)SiMnO4, (521)SiMnO4, (611)siMn04, (631)SiMnO4 and (831)SiMnO4. Processing and analysis of the experimental results of these reflections made it possible to determine the lattice param-

eter of nanocrystallites in SiMnO4, with aexp = 1.002 nm, which is in good agreement with the literature data [1-4]. In addition, in the X-ray pattern at small acattering angles 2θ = 17.3°, a wide (FWHM = 1.25x10-1 rad) diffuse reflection is observed, due to SiOx structural fragments in near¬surface layers with unsaturated bonds. The too wide width of this reflection indicates that the dimensions of the structural fragments caused by this reflection are small and there is no long- range order in their arrangement. Therefore, these structural fragments are not SiOx nanocrystals but clusters. The characteristic dimensions of these clusters were ~ 2.7 nm.

Conclusion: Thus, based on the analysis of the results obtained and the studies carried out, the following conclusions can be drawn:
- high intensity and narrow half-width of the main reflection (111)α gives information about the perfection of the Si<Mn>SiO2 single crystal with the lattice parameter aSi=0.5426 nm and is a diamond-like structure with a cubic lattice (sp. gr. Fd3m);
- it is determined that the lattice parameter of the sample Si<Mn> (aSi = 0.5419 nm), the value is slightly less than the lattice parameter of the sample Si<Mn>SiO2 (aSi = 0.5426 nm), but causes a shift of structural reflections in the diffraction pattern Si< Mn> towards smaller scattering angles;
- self-formation of the SiO2 impurity phase with lattice parameters
$a_{exp} = b_{exp}$ = 0.508428 nm and cexp = 0.7098 nm and sizes from 65 nm to 72 nm was determined at the SiOx boundaries;

Coalesce Research Group

13th International Conference on

Materials Science & Engineering

October 22-24 2025 | Tashkent, Uzbekistan

STRUCTURAL ANALYSIS OF MONOCRYSTALLINE SILICON DOPED WITH LUTETIUM

Kh.S.Daliev and Z.E. Bahronkulov*

Institute of Semiconductor Physics and Microelectronics at the National University of Uzbekistan, Tashkent, Uzbekistan

Abstract

In this work, it was established that the incorporation of lutetium (Lu) atoms into the silicon lattice induces micro-deformations in the crystalline structure, which was confirmed by X-ray diffraction measurements performed on an Empyrean Malvern diffractometer in Bragg–Brentano geometry (2θ = 10–90°, step size 0.020°, scan rate 0.33°/min). It was shown that Lu, when bonded with Si, forms polycrystalline regions belonging to the P6/mmm space group with a hexagonal unit cell (a=b=0.4085 nm, c=0.3803 nm). At the subcrystallite boundaries, Lu_2O_3 nanocrystallites of 15–18 nm in size were detected (space group P3m1, a=b=0.3573 nm, c=0.5843 nm). Prolonged Lu incorporation and rapid cooling lead to the formation of surface fragments associated with SiLuxOy compounds, as well as the crystallization of Lu_2SiO_5 (space group P21/c, a=0.6614 nm, b=0.6614 nm, c=0.9123 nm).

Background: Modern global scientific and technological progress is largely determined by the development of electronics, whose achievements directly depend on advances in fundamental sciences—primarily solid-state physics and semiconductor physics. The latest achievements in these fields are related to the physics of low-dimensional structures and the development of technologies for producing nanostructures with fundamentally new functional capabilities for nano- and optoelectronics, communications, advanced technologies, and measurement instruments. Structured silicon currently attracts significant attention, since Si itself is a highly promising material not only for electronics but also for optoelectronics and solar cells. In this regard, the study of the formation of low-dimensional objects and their influence on the electrophysical, optical, photoelectric, and magnetic properties of semiconductors represents one of the most relevant research directions today.

Methods: Before diffusion annealing, the samples were placed in evacuated quartz ampoules. The diffusion of Lu impurities into the Si bulk was carried out by heating the pre-deposited samples in a diffusion furnace at a temperature of 1250°C for 50 hours, followed by rapid cooling. The structural-phase state of the studied samples was monitored using an Empyrean Malvern X-ray diffractometer. The OriginPro 2019 software was used to determine the peak maxima. X-ray diffraction measurements were performed in the Bragg–Brentano geometry within the 2θ range of 10°–90°, with a continuous scan rate of 0.33°/min and an angular step of 0.0200°.

Results: Figure 1(a) shows the X-ray diffraction pattern of the reference p-Si sample. The diffraction pattern contains several structural reflections of selective nature with varying intensity and two diffuse reflections at small and medium scattering angles. Analysis revealed that the substrate surface corresponds to the <100> crystallographic plane, as evidenced by a series of selective {H00} reflections (H = 2, 4). The intense (200) reflection with d/n = 0.2717 (2θ = 32.67°) and (400) with d/n = 0.1357 (2θ = 68.83°) were clearly identified. The β-component of the main structural (400) line is observed at a scattering angle of 2θ = 61.75°.

The high intensity (1438.2 counts·s-1) and narrow width (FWHM = 1.1×10-2 rad) of the (400) reflection indicate a high crystalline quality of the control p-Si lattice. However, the presence of weak reflec-

tions with indices (100), (101), and (111)—broader compared to (400)Si—indicates the existence of polycrystalline regions within the substrate volume. Furthermore, among the {H00} reflections, two selective (200) reflections are observed. According to extinction rules, this reflection should not appear in an ideal diamond-like silicon lattice [1,2]. The appearance of forbidden (200) and additional (100), (101), and (111) reflections is associated with lattice distortions caused by thermoelastic stresses arising during sample preparation, as well as inhomogeneous oxygen distribution in the silicon lattice [3]. The nonmonotonic behavior of the inelastic background in the 2θ range of 10°–41° is attributed to residual elastic stresses in the matrix lattice. At small scattering angles (2θ ≈ 13.8°), a broad diffuse reflection (FWHM = 9.54×10^{-2} rad) is observed, which is associated with SiOx structural fragments in the near-surface layers containing unsaturated chemical bonds. Thus, among all structural reflections, only the (400) reflection is suitable for determining the lattice parameter of the substrate, as it is the most intense and narrow. The experimental value of the substrate lattice parameter was a(p-Si) = 0.5462 nm.

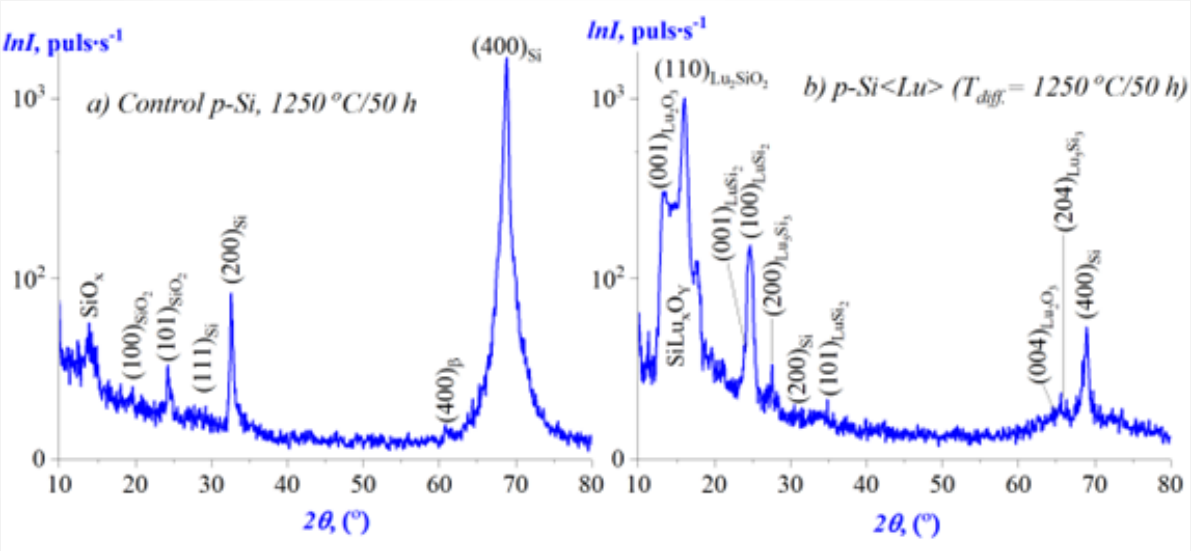

Fig. 1. X-ray diffraction patterns of n-Si: control sample (a) and Lu-doped sample (b).

Figure 1-b shows the X-ray diffraction (XRD) pattern of silicon doped with lutetium atoms. This diffraction pattern differs significantly from that of the reference p-Si sample. As seen from Fig. 1-b, the intensity of the structural reflection corresponding to the main crystallographic orientation (400) decreased by approximately 36 times, and a shift of about 0.08° toward higher diffraction angles was observed. This, in turn, indicates that the incorporation of lutetium (Lu) atoms into the silicon lattice induces stresses in the crystal structure. Based on the experimental results, the lattice constant of silicon containing Lu atoms was determined to be an–Si<Lu> = 0.5401 nm, differing by 0.061 nm from that of undoped silicon. In addition, structural reflections corresponding to crystallographic orientations (001), (100), (101), (200), and (204) were observed on the diffraction pattern. This indicates that the lutetium impurity atoms, by interacting with silicon atoms, form polycrystalline regions consisting of silicide phases with various degrees of crystalline order [1–8]. Based on the experimental data from the observed structural reflections, it was established that these polycrystalline regions belong to the space group P6/mmm and have a hexagonal unit cell with lattice parameters a = b = 0.4085 nm and c = 0.3803 nm. Prolonged thermal treatments followed by rapid cooling of samples can lead to the formation of amorphous-like surface layers on silicon doped with Lu impurity atoms [8–12]. This assumption is sup-

ported by the presence of diffuse reflection at small diffraction angles in the XRD pattern of the p-Si<-Lu> sample, which corresponds to the SiLuxOy compound. As previously noted, such diffuse scattering arises due to the nonuniform and chaotic distribution of oxygen and lutetium atoms near the surface. However, while some oxygen atoms remain randomly distributed, most of them bond with lutetium atoms, forming various crystalline phases [12–15]. Therefore, the diffraction pattern also shows structural reflections corresponding to the crystallographic orientations <001> and <004>. These reflections indicate the formation of small Lu_2O_3 nanocrystallites (15–18 nm in size) at the subcrystallite boundaries.Based on the experimental data from these structural reflections, it was established that the Lu_2O_3 crystallites belong to the space group P3m1 and have a trigonal unit cell with lattice parameters a = b = 0.3573 nm and c = 0.5843 nm.

Conclusion: Thus, the incorporation of lutetium (Lu) atoms into the silicon lattice induces microdistortions in the crystalline structure. It has been established that lutetium impurity atoms, by bonding with silicon atoms, form polycrystalline regions consisting of silicides with varying degrees of crystalline order. These polycrystalline regions belong to the space group P6/mmm and have a hexagonal unit cell with lattice parameters a = b = 0.4085 nm and c = 0.3803 nm. Furthermore, it has been determined that at the subcrystallite boundaries, small Lu_2O_3 crystallites with sizes of 15–18 nm are formed, belonging to the space group P3m1 with a trigonal unit cell having lattice parameters a = b = 0.3573 nm and c = 0.5843 nm.

Coalesce Research Group

13th International Conference on

Materials Science & Engineering

October 22-24 2025 | Tashkent, Uzbekistan

INFLUENCE OF Γ-RAYS FROM $_{60}$CO AND ELECTRONS ON THE PROCESS OF RADIATION DEFECT FORMATION IN SILICON DOPED WITH YTTERBIUM ATOMS

Daliev Kh.S, Daliev Sh.Kh and Bekmuratov M.B*

Institute of Semiconductor Physics and Microelectronics at the National University of Uzbekistan, 20 Yangi Almazar st., Tashkent, 100057, Uzbekistan

Abstract

This work investigates the enhancement of radiation resistance in silicon, which is a key challenge for creating electronic devices operating in extreme conditions. One promising approach is doping silicon with rare earth elements (REE), particularly ytterbium (Yb). It is believed that REE impurities can increase the crystal lattice's resistance to radiation damage by acting as effective sinks for primary point defects, such as vacancies.

Background: It is known that doping single-crystal silicon with rare earth element (REE) impurities leads to an increase in the stability of its parameters under radiation exposure [1]. Many authors explain this effect by the presence of various REE inclusions in the Si lattice, which act as effective sinks for vacancies created by irradiation. However, there is no consensus in the literature regarding the electrical activity of REE impurities and their interaction with radiation defects (RD) and other impurities in silicon. Studies of radiation effects on crystals containing additional impurities, both electrically active and neutral, besides the main doping impurity, are of significant interest [2-3]. It is known that doping single-crystal silicon with rare-earth element (REE) impurities leads to increased stability of its parameters under radiation exposure [4-6]. Many authors explain this effect by the presence of various REE inclusions in the Si lattice, which serve as effective sinks for radiation-induced vacancies. However, there is no consensus in the literature regarding the electrical activity of REE impurities and their interaction with radiation defects (RD) and other impurities in silicon.

Methods: The purpose of this work is to investigate the influence of the rare-earth impurity ytterbium on the formation of radiation defects in silicon under irradiation using deep-level transient spectroscopy (DLTS) methods. To conduct capacitance measurements on the studied samples, diode structures were fabricated according to a known method [13-14]. Measurements and processing of spectra are also described in detail in works [15-16].

Results: The samples under investigation were n-Si doped with Yb during the melt growth process, with an initial resistivity of ρ=20 Ohm·cm. The total concentration of Yb atoms in the volume of monocrystalline Si was determined by neutron activation analysis, ranging from 3·1016 to 7·1017 cm-3 from the beginning to the end of the ingot. The samples were irradiated at room temperature with γ-rays from 60Co with a flux intensity of ~ 3.2·1012 quanta/cm2 s. The energy spectrum of the formed deep levels (DL) was determined from measurements of the DLTS spectra of Si samples doped with Yb during the growth process from the melt and control undoped samples before and after each irradiation cycle. Figure 1 shows the DLTS spectra of control n-Si samples (curve 1) and n-Si samples doped with ytterbium (2) after irradiation with γ-quanta of 60Co. Note that in these samples, N0opt was 7×1017 cm-3. Analysis of the DLTS spectra shows that the introduction of Yb into Si during the growth process from the melt does not lead to the formation of any deep levels in the bandgap of silicon. As can be seen from the DLTS spectra (Fig. 1, curves 1 and 2), as a result of γ-irradiation, both in the control n-Si samples

and in the n-Si<Yb> samples, a new level is introduced with ionization energy and electron capture cross-section σ =1×10-14 cm2. The values of the parameters of this DL correspond to known radiation defects - vacancy-oxygen complexes (A-centers). Analysis of the measured spectra reveals that the presence of Yb leads to a slowdown in the radiation defect formation process: the concentration of A-centers in n-Si<Yb> samples is 4-5 times lower than in the control samples. Moreover, the higher the ytterbium concentration, the lower the concentration of radiation defects. The features of radiation defect formation in "oxygen-free" silicon doped with ytterbium were also investigated. E_c-0.43 эВMeasurements of the DLTS spectra of the control samples of "oxygen-free" silicon (Figure 2, curve 1) showed that γ-radiation introduces, in addition to A-centers, another characteristic radiation defect - the E-center with an ionization energy and electron capture cross-section of σ_n=1.8·10^(-15) ⟦cm⟧^(-2). The concentration of E-centers in these samples at a radiation dose of Φ=3.2·1012 quanta/cm2 is 4.2×1013 cm-3 and the concentration of A-centers is ≈ 2.5×1013 cm-3, approximately an order of magnitude lower than the concentration of A-centers in "oxygen-containing" Si (Figure 1, curve 1). Comparison of DLTS spectra in irradiated control and doped samples shows that the presence of Yb in the Si bulk leads to a significant decrease in the concentration of both types of radiation defects. The concentrations of both A-centers and E-centers in the irradiated n-Si<Yb> are almost an order of magnitude lower compared to the irradiated control samples (Figure 2, curve 2).

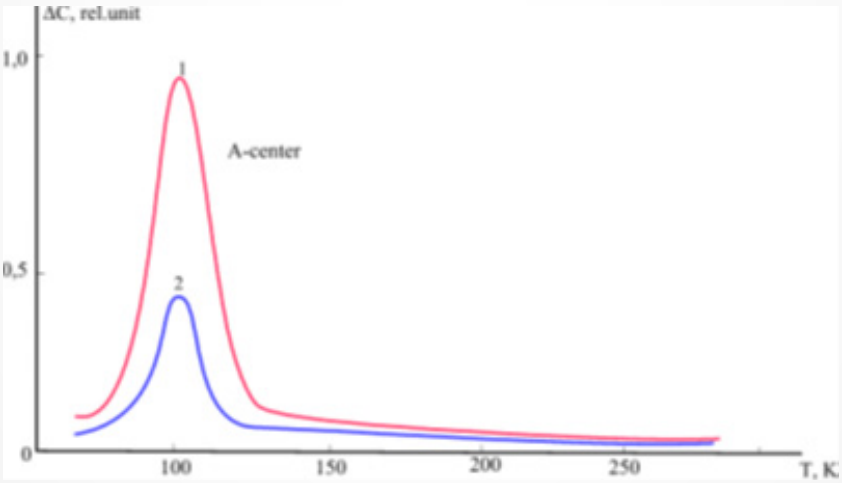

Fig.1. DLTS spectra of the control n-Si samples (1) and n-Si<Yb> samples (2) after irradiation with γ-quanta of 60Co ("oxygen-rich" Si, N0opt ~ 7×1017 cm-3).

Thus, the presence of ytterbium atoms in the silicon bulk significantly reduces the formation efficiency of known radiation defects: A-centers (vacancy-oxygen complexes) and E-centers (vacancy-phosphorus complexes). This effect should apparently be attributed to the specific interactions between ytterbium atoms and the defects introduced by radiation.

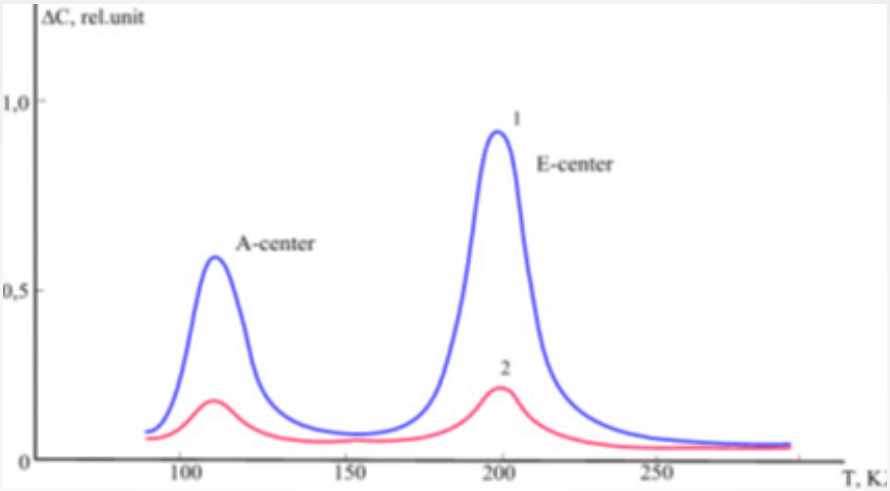

Fig.2. DLTS spectra of the control n-Si samples (1) and n-Si<Yb> samples (2) after irradiation with 60Co γ-quanta ("oxygen-free" Si, N0opt ≈ 1016 cm-3).

An analysis of DLTS spectra was conducted to determine the deep levels formed after electron irradiation of ytterbium atoms introduced into silicon through growth and diffusion, along with gamma radiation. The analysis results show that the introduction of Yb into n-Si during the growth process from solution does not lead to the formation of deep levels (DL) in the silicon's forbidden band. In n-Si samples doped with ytterbium impurity by the diffusion method at Tdif= 1200°C, a single DL with an ionization energy of Ec-0.36 eV was detected. Figure 1 shows typical DLTS spectra of n-Si control samples irradiated with 13 MeV electrons at a beam current of approximately 4 μA (curve 1 - samples of batch I with N_o^opt=8·10^17 ⟦cm⟧^(-3), curve 2 - samples of batch II with N_o^opt=1·10^16 ⟦cm⟧^(-3). Analysis of the DLTS spectra shows that as a result of irradiation in n-Si samples of batch I (with high oxygen content), a new deep level (peak A) is formed with an ionization energy of Ec-0.17 eV and an electron capture cross-section of ≈n = 2·10-14 см2 its parameters coincide with those of the known radiation defect - A-center (vacancy-oxygen complex). In the samples of batch II (with lower oxygen content), two DLs are observed: Ec-0.17 eV (peak A) and Ec-0.43 eV (peak B) with an electron capture cross-section ≈n=1.8≈10-15 см-2, with the second DL being dominant. Its parameters coincide with those of another known radiation defect - the E-center (vacancy-phosphorus complex).

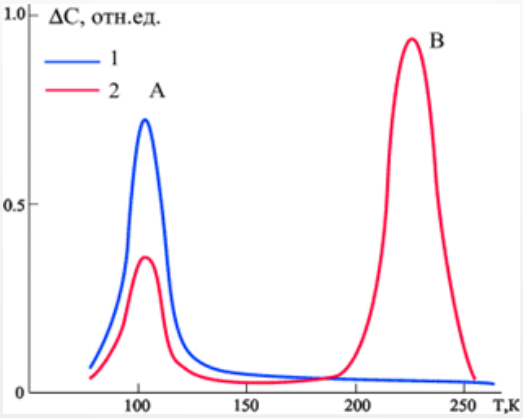

Fig.1. Typical DLTS spectra of Si control samples with different oxygen content after electron irradiation (curve 1:N_o^opt=1·≈10≈^16 ≈cm≈^(-3), curve 2: N_o^opt=8·≈10≈^17 ≈cm≈^(-3)).

Conclusion: Thus, the presence of ytterbium atoms in the silicon bulk significantly reduces the efficiency of formation of known radiation defects: A-centers (vacancy-oxygen complexes) and E-centers (vacancy-phosphorus complexes). The magnitude of this decrease in radiation defect formation efficiency depends on the state of ytterbium atoms in the silicon lattice.

Coalesce Research Group

13th International Conference on

Materials Science & Engineering

October 22-24 2025 | Tashkent, Uzbekistan

DEEP CENTERS AND THEIR INFLUENCE ON THE ELECTROPHYSICAL PROPERTIES OF DYSPROSIUM-DOPED SILICON

Sh.B. Utamuradova and Sh.B. Norkulov*

Institute of Semiconductor Physics and Microelectronics at the National University of Uzbekistan, 20 Yangi Almazar st., Tashkent, 100057, Uzbekistan

Abstract

This paper presents the results of a study of deep energy levels in silicon doped with dysprosium (Dy). Dysprosium atoms were diffused into monocrystalline n-type silicon with a resistivity of ρ = 2÷65 Ω ·cm at a temperature of 1200 °C for 20÷40 h. It was found that the introduction of Dy leads to the formation of three deep levels with ionization energies and corresponding electron capture cross sections: Ec–0.21 eV, $\sigma_n \approx 2.8\times10\text{-}15$cm2; Ec–0.30 eV, $\sigma_n \approx 7.1\times10\text{-}16$ cm2; and Ec–0.41 eV, $\sigma_n \approx 1.7\times10\text{-}15$ cm2. It has been shown that Dy atoms form active centers in the silicon lattice, such as Dy–V, Dy–O, and Dy–V–O complexes, which have a significant influence on the processes of charge carrier capture and emission.

Background: The study of deep energy levels formed during the doping of silicon with rare-earth elements is one of the priority directions in modern semiconductor physics. These levels play a crucial role in the processes of charge carrier recombination and transport, which is especially important for the design and optimization of optoelectronic and microelectronic devices.

Dysprosium (Dy) belongs to the group of rare-earth elements capable of forming stable complexes with vacancies and oxygen atoms in the crystal lattice of silicon, thereby creating localized states within the forbidden band gap[1]. Investigation of the parameters of these centers using the Deep-Level Transient Spectroscopy (DLTS) method makes it possible to determine their energetic characteristics, identify their physical nature, and evaluate their influence on the electrophysical properties of the material[2, 3, 5].

Methods: As the starting material, monocrystalline n-type silicon wafers grown by the Czochralski method with a resistivity of ρ = 2÷65 Ω·cm were used. Doping of silicon with dysprosium (Dy, 99.999%) was carried out by the diffusion method at a temperature of 1200 °C for 20÷40 hours. The diffusion process was performed in vacuum-sealed quartz ampoules under controlled temperature conditions. After thermal treatment, the samples were rapidly cooled (quenched), which made it possible to preserve the defect states formed within the crystal volume[4. 6]. To eliminate the influence of surface defects, a layer with a thickness of 2÷5 μm was removed from the front side of the samples by mechanical and chemical polishing. After surface cleaning, metallic contacts were formed, where gold (Au) was used as a Schottky barrier and antimony (Sb) served as an ohmic contact.

Results: In the control n-type silicon sample, the DLTS spectrum exhibited a single peak at a temperature of approximately 110 K, which corresponds to the A-center — a vacancy–oxygen (V–O) complex — with an activation energy of Ec – 0.21 eV and an electron capture cross section of $\sigma_n \approx 2.8\times10\text{-}15$ cm2. No other deep levels were detected in the control sample.

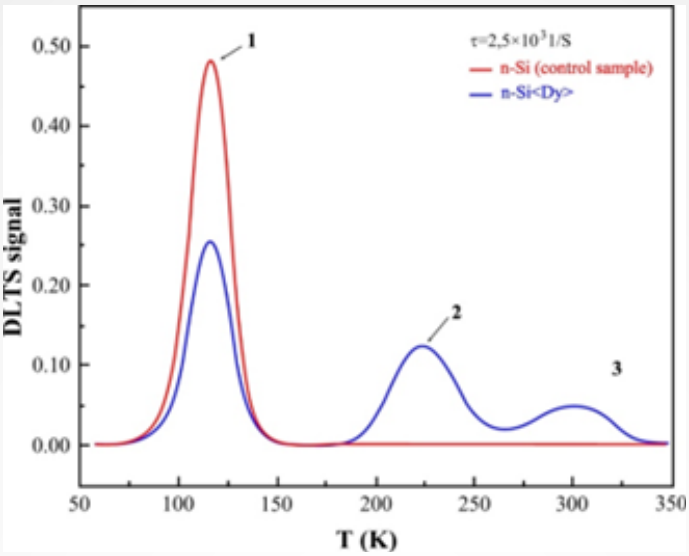

Fig. 1. DLTS spectra of control and dysprosium-doped silicon samples

After dysprosium diffusion in the n-Si< Dy > samples, the DLTS spectra revealed the appearance of three distinct peaks corresponding to different deep levels (Fig. 1). The first peak (~110 K) corresponds to the A-center level with Ec – 0.21 eV the second peak (~220 K) corresponds to a level with Ec – 0.30 eV and an electron capture cross section of $\sigma_n \approx 7.1\times10\text{-}16$ cm2 and the third peak (~300 K) corresponds to a level with Ec – 0.41 eV and $\sigma_n \approx 1.7\times10\text{-}15$ см2.The dependences of $\ln(\tau T2/e)$ on 1/kT (Fig. 2) made it possible to accurately determine the energetic parameters of the detected centers. The obtained data indicate that Dy atoms introduced into the Si lattice interact with point defects, forming complexes of the Dy–V and Dy–O types, as well as triple Dy–V–O complexes. These centers create traps within the forbidden band gap that can effectively capture and emit electrons, thereby influencing the carrier lifetime and recombination processes.

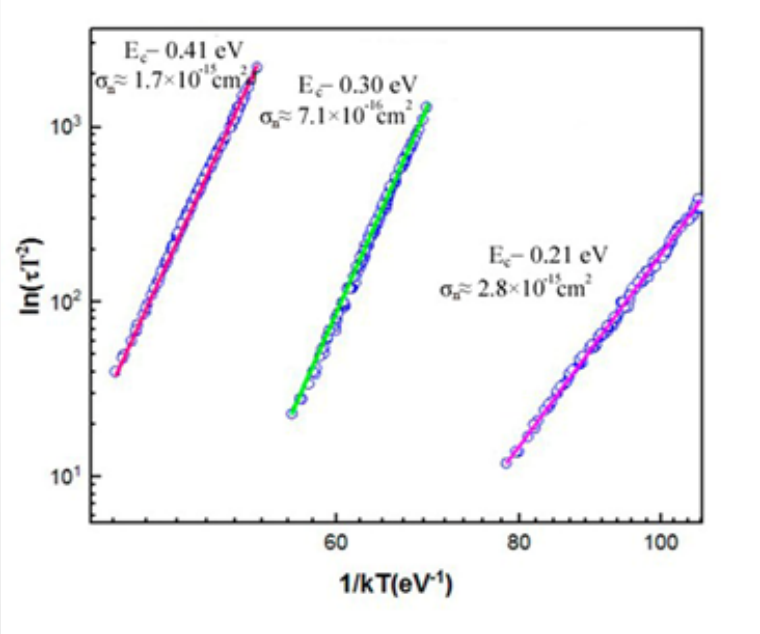

Fig. 2. Arrhenius plot for the n-Si< Dy > sample obtained from DLTS analysis

Thus, the identified energy levels reflect the active participation of Dy atoms in the formation of defect complexes, which play a key role in the processes of carrier capture and relaxation in silicon.

Conclusion: The DLTS studies have shown that the introduction of dysprosium atoms into monocrystalline silicon leads to the formation of new deep energy levels within the forbidden band gap. In contrast to the initial n-type sample, in which only one level corresponding to the A-center (vacancy–oxygen, V–O) with an ionization energy of Ec – 0.21 eV is observed, this level is also preserved in the Dy-doped sample n-Si< Dy >. However, two additional deep levels with ionization energies of Ec – 0.30eV and Ec–0.41 eV were newly detected. The appearance of these levels indicates the formation of new defect complexes of the Dy–V, Dy–O, and Dy–V–O types, which have a significant impact on the processes of charge carrier capture and emission. These centers modify the nature of relaxation and recombination processes, which is manifested in an increase in resistivity and variations in the C–V characteristics of the structures.

Thus, dysprosium is an effective element for controlling the defect structure of silicon. The obtained results are of practical importance for the development of silicon-based structures with tunable electronic and optoelectronic properties used in photodetectors and light-emitting devices. The study confirms the promising potential of rare-earth elements for the purposeful modification of the defect structure of silicon and optimization of its functional characteristics.

THE ROLE AND IMPORTANCE OF CAPACITIVE SEMICONDUCTOR ELECTRONIC MODULES IN MODERN PROTECTION SYSTEMS

Sherali E. Murodov
Institute of Semiconductor Physics and Microelectronics at the National University of Uzbekistan

Abstract

Background: Capacitive semiconductor modules play a vital role in ensuring high-efficiency and reliable energy conversion and control in modern electronic systems. These modules are primarily composed of semiconductor materials and are designed to operate with high power and efficiency. They are widely used in power electronics, energy storage systems, automation, and control systems. This article presents a scientific analysis of capacitive semiconductor modules, including their operating principles, types, and practical applications.

Objective: Capacitive Semiconductor Modules (CSMs) are semiconductor devices capable of managing high efficiency and power. Their structure and operating principles possess unique characteristics that make them suitable for advanced energy systems.

Methodology: These modules are mainly developed using semiconductor transistors such as MOSFETs (Metal-Oxide-Semiconductor Field-Effect Transistors) and IGBTs (Insulated-Gate Bipolar Transistors). They are used to control high power, improve energy efficiency, and ensure stable system operation. CSMs are commonly applied in power electronics, energy systems, industrial automation, transportation systems, and other fields. This article explores these modules from a deep scientific perspective.

Results:Benefits and Advantages of Capacitive Semiconductor Modules

Capacitive semiconductor modules offer several advantages:

High Efficiency: They reduce energy losses and improve system performance, which is crucial for energy-saving and power management systems.

Fast Response: Their ability to operate at high speeds ensures quick system reactions.

High Power Control: Suitable for managing high power and voltage, making them ideal for industrial and energy systems.

Compactness and Integration: Their small size allows easy integration, enhancing system efficiency.

Conclusion: Capacitive semiconductor modules have become an integral part of modern electronics and energy systems. Their operating principles and capabilities make them highly effective in high-efficiency and energy management applications. With ongoing technological advancements, these modules are expected to become even more efficient in the future.

THE ROLE AND IMPORTANCE OF SEMICONDUCTOR MODULES IN ENSURING TECHNICAL SAFETY OF FACILITIES

Sunnatillo Sh. Rashidov
Ministry of Internal Affairs of the Republic of Uzbekistan Department for Supporting the Activities of Military Structures Lead of the Division of Innovative Technologies

Abstract

Background: Technical safety issues are among the most critical areas in modern industry, energy, transportation, information technology, and production processes. For any facility to operate safely, prevent emergency situations, and protect human life, reliable control and protection systems are essential. From this perspective, semiconductor modules (diodes, transistors, thyristors, MOSFETs, IGBTs, etc.) are considered key components in ensuring technical safety. The Role of Semiconductor Modules in Technical Safety
Electrical Safety: Mitigating sudden voltage fluctuations.Automatically disconnecting in case of overload.Protecting against short circuits.
Automated Control: Processing signals from sensors.Rapid response in emergency situations.Reducing human error.
Energy Efficiency: Minimizing electrical energy losses.Managing heat and optimizing cooling systems. Ensuring safety in renewable energy sources.
Monitoring and Diagnostics: Real-time monitoring of device operation.
Early detection of malfunctions.Enabling scheduled preventive maintenance.Semiconductor modules are based on the phenomenon of the p-n junction, which allows electric current to flow in only one irection.
Objective: Semiconductors possess unique electrical properties that make them essential for controlling electric current. The energy gap (bandgap) present in silicon and other semiconductors determines their conductivity. The abundance of electrons and holes in semiconductors allows them to be classified as n-type or p-type. These characteristics enable semiconductor elements to be widely used in various electronic and protection systems.
Methods: Semiconductor Protection Systems: Semiconductor protection systems play a significant role in ensuring safety in electrical energy and other systems. These systems are typically designed to detect changes in electrical power, short circuits, or other undesirable events. They operate primarily using semiconductor materials (such as silicon) and are capable of responding at high speeds, thereby contributing to the uninterrupted operation of power networks.
Results:
Advantages of Semiconductor Protection Systems
Semiconductor protection systems offer the following key benefits:
High-Speed Operation: Semiconductor materials enable rapid response, allowing quick mitigation of potentially catastrophic events in energy systems.

Coalesce Research Group

13th International Conference on

Materials Science & Engineering

October 22-24 2025 | Tashkent, Uzbekistan

KINETICS OF CLEARANCE ON BISMUTH FILMS IN THE CDTE$_2$ LIGHT-SENSITIVE SYSTEM

Sh. B. Utamuradova[1] and B.Z. Khaydarov[2*]

[1]*Research Institute of Semiconductor Physics and Microelectronics at the National University of Uzbekistan*

[2]*Fergana State University, Uzbekistan*

Abstract

The light-sensitive system (CdTe-SnO2), with a thickness ranging from 10 to 100 μm, is unique. It is successfully used in infrared technology. However, the physical mechanisms of the processes within it remain largely unknown. This study experimentally investigates the effect of a discharge on bismuth films on the light-sensitive system's recording element. Under the influence of an electric field of up to 107 V/m, charged particles illuminate the bismuth film, causing its thickness to change exponentially. The experimental results are in satisfactory agreement with the theoretical calculations.

Background. The thin photosensitive system (10–100 μm) has a wide range of applications in infrared technology [1–4]. However, the physical mechanisms of the processes occurring in the gas-discharge cell have not yet been fully revealed. Furthermore, the conclusions of studies conducted in such systems are sometimes contradictory [5–7]. Therefore, any research conducted to clarify the physical mechanisms in light-sensitive systems is valuable. This study presents the results of a detailed investigation into a gas discharge with a bismuth film.

Experimental methodology. Flat glass electrodes coated with transparent SnO2 were placed in the photosensitive system. One of these electrodes was a glass plate with a bismuth layer. Discharge was carried out at the connection between the glass electrodes using an alternating voltage of 1–2 kV at a frequency of 7 kHz. To ensure uniform discharge across the electrode area, a buffer layer of mica (2) with a thickness of 10-40 μm was pressed against the transparent electrode from the discharge side. This mica plate acts as a distributed reactive resistance, performing the same function in the system as a semiconductor photoelectrode. A beam of LG-75 laser light passed through the cell. The intensity of the beam at its output was measured by a silicon photodiode of the FD-24K type. Changes in the intensity of the laser beam passing through the cell could be used to judge changes in the optical density of the bismuth layer under the action of the gas discharge.

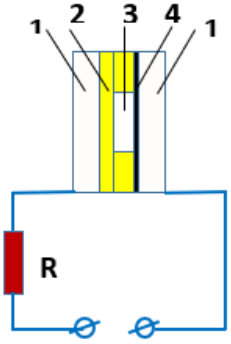

Figure 2: Principal scheme of the experimental setup. 1 - glass plates with conductive SnO_2 coatings, 2 - mica plate, 3 - gas-discharge gap, 4 - bismuth film, $R_б$ - ballast resistance.

Theory: Light of intensity J0 passing through a plate of thickness x0, with an absorption coefficient α, is attenuated according to the law of

$$J=J_0 \exp[-\alpha(x_0-vt)] \quad (1)$$

where J is the intensity of transmitted light, v is the rate at which the thickness of the absorbing medium changes and t is time. Thus, in the simplest case where only the film thickness decreases at a constant rate v as a result of the action of the gas discharge plasma, we obtain exponential curves of the form J = f(t). Such curves of light emission kinetics, calculated for different initial layer thicknesses (ho), are shown in Fig. 2. As the discharge current increases, so does the rate of change of the film thickness (v). The corresponding series of J(t) curves plotted for different values of v are shown in Fig. 3. Clearly, in real conditions, the above simple relations can be significantly more complicated. For example, the velocity v may depend on the layer thickness in a complex way rather than being constant. Furthermore, it is possible that, during the discharge process, the film is not only removed but also undergoes changes in its absorption coefficient due to chemical transformations. Without carrying out more complicated calculations, let us now consider the obtained experimental dependencies.

Experimental results: Figure 4 shows the luminescence kinetics curves of bismuth films with the same optical density, which were sputtered onto a SnO2 surface, a 2 μm thick polystyrene lacquer layer covering the SnO2 surface, and a polystyrene film. As can be seen from the figure, the material of the substrate on which the bismuth layer is deposited significantly affects the luminescence rate.

Discussion of results and conclusions: Based on the above results, we can conclude that, unlike the calculated results, the experimental kinetics curves show a smoother approach to the final state of full

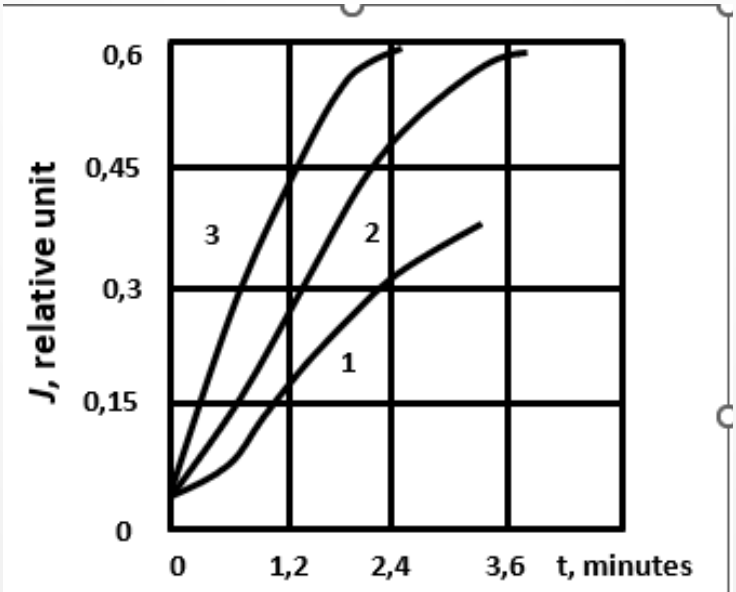

Figure 4: Enlightenment kinetics of Bismuth films at the same optical density: 1 – on an SnO_2 surface; 2 – on a polystyrene lacquer layer covering an SnO_2 surface; and 3 – on a polystyrene film.

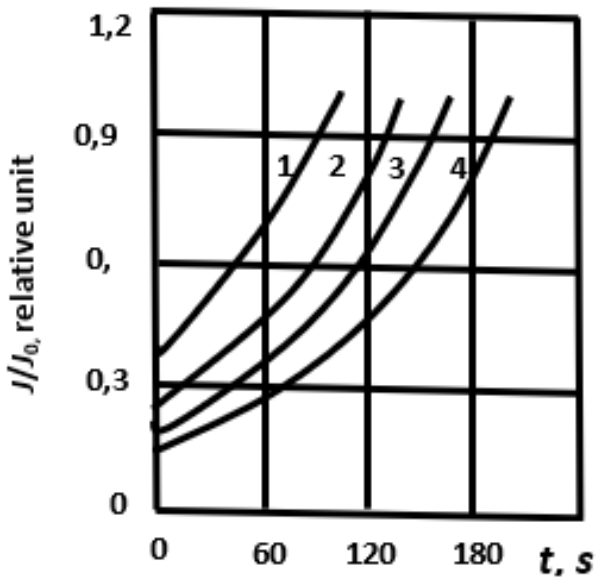

Figure 2: Kinetics of the change in layer optical density at a constant rate of layer thickness change ($v = 10^{-7}$ cm/s) and with different initial layer thicknesses (x_0): 1 – 10^{-5} cm, 2 – 1.4×10^{-5} cm, 3 – 1.7×10^{-5} cm,

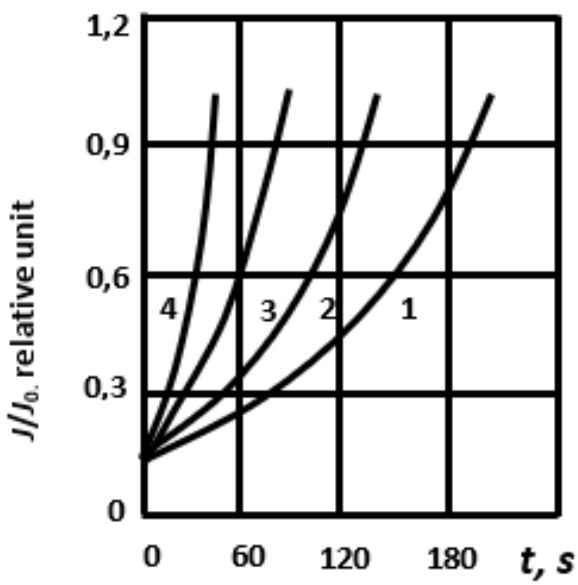

Figure 3: Kinetics of the change in layer optical density at a constant layer thickness of $x_0 = 2 \times 10^{-5}$ cm and at different rates of change in layer thickness v. v is equal to: 1 – 10^{-7} cm/s; 2 – 1.4×10^{-7} cm/s; 3 – 2.4×10^{-7}

lumenisation. This may be due to some non-uniformity in bismuth evaporation, which was not taken into account in the calculation. Another distinctive feature of the kinetics curves compared to the calculations is the presence of a small initial 'jump' in transparency, the cause of which remains unclear. In any case, this sharp increase in photodiode current is unrelated to its response to the discharge glow, as was specifically verified in the experiment. Furthermore, it can be concluded that the active components of the discharge are adsorbed onto the surface of the film and react with the bismuth to form transparent, oxide-type compounds. Brightening occurs not only due to cathodic atomization, but also due to the apparent chemical interaction between active discharge components and bismuth atoms. As shown in Fig. 4, only in the first case (curve 1) is the kinetics close to the calculated kinetics at the initial sites. In the second (curve 2) and third (curve 3) cases, the lumenisation rate is much higher and changes almost discontinuously at the initial site. The average values of α_v for these three cases is 2.9×10−2 s−1, 3.3×10−2 s−1 and 6×10−2 s−1, respectively. The influence of the substrate on the properties of thin films is multifaceted. In this case, it seems to us that the heat dissipation of the bismuth layer plays a significant role in the lumenisation process. Any processes leading to lumenisation, such as cathodic sputtering, chemical reactions and the thermal evaporation of bismuth atoms, intensify with increasing temperature. The thermal conductivity of polystyrene is much lower than that of SnO2 and glass. The layer temperature depends heavily on the thermal conductivity of the substrate. It seems that the increase in lumenization rate on thermally insulating polystyrene substrates is related to this.

Coalesce Research Group

13th International Conference on

Materials Science & Engineering

October 22-24 2025 | Tashkent, Uzbekistan

THEORETICAL CALCULATION OF PHOTODETECTOR PARAMETER SELECTION FOR A GAS-DISCHARGE CELL

Sh. B. Utamuradova[1] and Z. Khaydarov[2*]

[1]Research Institute of Semiconductor Physics and Microelectronics at the National University of Uzbekistan

[2]Fergana State University, Uzbekistan

Abstract

This paper presents the results of theoretical calculations of the stationary lifetime and stationary impurity photoconductivity, as well as the time of decline after switching off the light depending on the position of the Fermi level. It is shown that with increasing light intensity, the impurity photoconductivity increases in all regions of equilibrium concentration, and at very high light intensities, the impurity photoconductivity tends to a limiting value. The character of change of the stationary lifetime at high level of optical excitation was observed such that it decreases in the region of weak filling with increasing optical excitation intensity J. And also from the performed calculations, it appears that the relaxation time depends weakly on the light intensity.

Background: The gas-discharge cell has found quite a wide application in optical photo registration, in particular, spatial and temporal diagnostics of laser radiation and thermal fields of various objects in the infrared (IR) region [1-10]. However, the use of photoelectrodes in a gas-discharge cell with a small value of specific conductivity, less than 107 Ohm·cm [5] and at a high level of optical excitation is a difficult task in IR imaging. The absence of theoretical prerequisites for the analysis of photoconductivity with lifetime of equilibrium and nonequilibrium carriers, as well as the concentration of photo carriers at high level of optical excitation from impurity levels makes it more difficult in the development of photodetectors for gas discharge cell in semiconductor photographic ionization chamber (SPIC) [2]. Therefore, it is necessary to analyze the generation and recombination processes in a gas discharge cell with SPIC semiconductor electrodes. In addition, it should be said that in any case it is necessary to provide a temperature range to create photoelectric hysteresis conditions with high resolution and sensitivity of the photographic process in SPIC [2, 3].

Calculation results: The stationary lifetime τL of the excess concentration of carriers Δn (electrons)

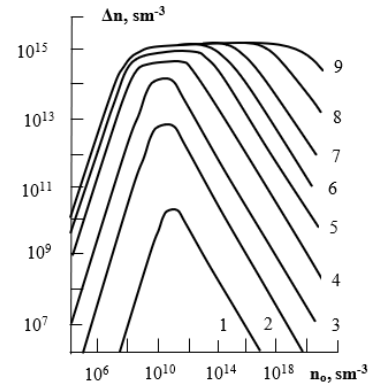

Fig. 1. Dependence of impurity photoconductivity on the Fermi level position at different values of excitation light intensity J. J, photon/(sm²·s): 1 – 10^{13}, 2 – 10^{15}, 3 – 10^{17}, 4 – 10^{19}, 5 – 10^{20}, 6 – 10^{21}, 7 – 10^{22}, 8 – 10^{24}, 9 – 10^{26}. Values of design parameters: M = 10^{15} sm⁻³, N_{cM} = 10^{-9} sm⁻³, γ = 10^{-10} sm³/c, q = 10^{-15} sm².

excited to the conduction band by light with intensity J c of impurity levels having concentration M and energy EM, is expressed by the formula [11]

$1/\tau_L = \gamma(N_{cM}+(MN_{cM})/(N_{cM}+n_0)+ n_0+\Delta n)+qJ$, (1)

where n0 – is the equilibrium concentration of conduction electrons, NcM = Ncexp(EM/kT), Nc – density of states in the conduction zone, γ – recombination coefficient, EM – electron ionization energy, T -thermodynamic temperature.

The value τL is also the characteristic time of photoconductivity rise at switching on the light. Decrease after switching off the light goes with time constant τd

$1/\tau_d = \gamma(N_{cM}+(MN_{cM})/(N_{cM}+n_0)+ n_0+\Delta n_0)$. (2)

The steady-state concentration is defined by the expression

$\Delta n=1/2\ (N_{cM}+(MN_{cM})/(N_{cM}+n_0)+qJ/\gamma)\ \sqrt{([1+(4Mn_0\ qJ)/(N_{cM}+n_0)]/[\gamma(N_{cM}+(MN_{cM})/(N_{cM}+n_0)+n_0+qJ/\gamma)^2]}$. (3)

With the help of (1), (2) and (3) equations it is possible to construct the dependences of: stationary lifetime τL, relaxation decay time after switching off the light τd and stationary carrier concentration Δn on the equilibrium electron concentration no (determining the position of the Fermi level) at different values of optical excitation intensity J. Below these dependencies were plotted using MATLAB software based on the use of calculated parameters.

Fig. 1 shows the results of calculating the dependence of the stationary carrier concentration (impurity photoconductivity), Fig. 2 - the stationary lifetime, and Fig. 3 - the relaxation lifetime on the position of the Fermi level at different values of the optical excitation intensity J.

Discussion: In these figures, three characteristic regions of variation of Δn, τL, and τd can be distinguished: 1) the region of weak filling of M levels (in this example, n0 ≤ 108 sm-3); 2) the region of "medium" filling of M levels

(108 ≤ n0 ≤ 1012 sm-3); and 3) the region of strong filling of M levels (n0 ≥ 1012 sm-3). As the light intensity increases, Δn increases in all the above regions, and at very high light intensities, the impurity photoconductivity tends to a limit value equal to the equilibrium concentration of electrons at the impurity M levels. The top of the Δn(n0) curve becomes hollow at high levels of optical excitation.. With increasing intensity, the "shelf" lengthens toward larger equilibrium concentrations. It is defined by the coordinate

$N0(max) = \sqrt{(MN_{cM}- N_{cM}^2)}$, (4)

the Fermi level decreases toward the valence band ceiling.

The dependence of τL(n0) on formula (1) gives an idea of the nature of the change of the stationary lifetime at high excitation level with the change of the position of the Fermi level. The decrease of the lifetime τL in the region of weak filling, i.e., when the Fermi level is much higher than the emitter level, is directly related to the last term of the sum in formula (1), $\tau L \approx 1/(qJ)$. It can be interpreted as the lifetime of the electron at the emitter level with respect to its interaction with the photon flux of intensity J becomes asymmetric and hollow with respect to the position of the maximum at low level of optical excitation.

The following approximate expressions can be written down for individual parts of the equilibrium filling:

Low occupancy (NcM > n0)

$\Delta n \approx qJ/(\gamma M+qJ)$ $(Mn_0)/(N_{cM}+n_0)$, $[\![\tau]\!]_L \approx 1/(\gamma M+qJ)$, $[\![\tau]\!]_d \approx 1/\gamma M$.

In the area of "medium" filling

$\Delta n \approx (qJMn_0 (N_{cM}+n_0))/(N_{cM} M+qJ(N_{cM}+n_0))$, $[\![\tau]\!]_L \approx (N_{cM}+n_0)/([\![\gamma[N]\!]_{cM} M+qJ(N_{cM}+n_0)])$, $[\![\tau]\!]_d \approx (N_{cM}+n_0)/(\gamma MN_{cM})$.

At full filling and high equilibrium concentration

$\Delta n \approx qMJ/(\gamma n_0+qJ)$ $n_0/(N_{cM}+n_0)$, $[\![\tau]\!]_L \approx 1/(\gamma n_0+qJ)$, $[\![\tau]\!]_d \approx 1/(\gamma n_0)$.

Conclusion: The above process determines the rate of steady-state establishment in the case of very strong optical excitation. In contrast to this rapid process of electron exchange between the zone and impurity levels after switching off the illumination, as can be seen from equation (2), recombination, i.e. τd relatively weakly depends on the light intensity. In this case, recombination can only change by decreasing the nonequilibrium filling and increasing the concentration of electrons in the conduction band. The limits of both (generation and recombination) processes are limited either by the concentration of M levels or by their equilibrium occupancy, i.e., $\Delta n \approx m0$, so the relaxation of the decline in darkness changes relatively weakly with light intensity.

Coalesce Research Group

13th International Conference on

Materials Science & Engineering

October 22-24 2025 | Tashkent, Uzbekistan

OPTICAL AND PHOTOELECTRIC PROPERTIES OF SOLAR CELLS BASED ON P-CDTE-N-CDS AND P-CDTE-N-CDSE HETEROSTRUCTURES WITH DEEP IMPURITY LEVELS

S.M. Otajonov[1], R.N. Ergashev*[2], J.M. Boqirov[3], D.Kh. Najmiddinova[4] and U.Kh. Marufova[5]

[1]Professor at Fergana State University.
[2]Associate Professor, Fergana State University
[3]Master's student, Fergana State University
[4]Independent researcher, Fergana State University
[5]Student, Fergana State University

Abstract

In this paper, we consider the mechanisms of the flow current and photoelectric properties of solar cells manufactured on the basis of strongly mismatched semiconductor p-CdTe-n-CdS and p-CdTe-n-CdSe heterojunctions with a low density of surface states N=3*1011sm-2. It was found that the forward current in heterojunctions is due to tunneling of thermally excited electrons, and at large forward biased currents, thermionic nature.

Background: Heterostructures in the p-CdTe-n-CdS and p-CdTe-n-CdSe systems are promising in terms of practical application in various photoelectric devices [1, 2]. However, their parameters and characteristics are largely determined by the conditions under which the rectifying structure is obtained. The results of experimental studies of the optoelectronic properties of p-CdTe-n-CdS and p-CdTe-n-CdSe GS in relation to the technological modes of their manufacture are described below [3].

Methods: Obtaining a high-quality CdS-CdTe heterostructure using traditional technological methods in high vacuum, despite their different crystal structures (hexagonal and cubic for CdS and CdTe, respectively), as well as a large mismatch in lattice constants (~10%) and thermal expansion coefficients (~10-6 K-1) [4]. The combined effect of these factors leads to a high density of surface states N at the interface, which significantly deteriorates the characteristics of the GS. This can be eliminated by using an optimal production technology. The value of N in CdTe-CdS structures can be significantly reduced by using Group I elements as dopants for their production [5].

Experimental results and their discussion: As a result of processing, a hole-conductivity layer forms on the surface of the initial crystal, the thickness of which is determined by the annealing temperature and time. The study of optical transmission and photosensitivity spectra indicates the formation of a CdSx Te1-x varizone structure, limited on the surface side by a p-CdTe layer and on the crystal volume side by n-CdS [6]. Their concentrations are equal to n=1017 cm-3.

The structures had pronounced diode characteristics with a rectification coefficient of at least 104 at 300 K and a voltage of V =1 V. The transition thickness d0 at zero bias, found from capacitance measurements, depends on the temperature and duration of annealing and is in the range of 0.3÷2 μm. The value of d0 has a relatively weak effect on the spectral distribution of photosensitivity, but it significantly determines the mechanism of current flow, as well as the absolute values of photocurrent and photo-e.m.f. In this regard, the structures under study were conditionally divided into three types: A (d0=0.3÷0.5), B (d0 = 0.5 ÷ 0.1), and C (d0 ≳ 0.1 μm).

The technology used allows obtaining heterostructures with a small number of defects at the interface even for semiconductors with significantly different structures, lattice constants, and thermal expansion coefficients. Such a small Ns has practically no effect on the photosensitivity of the structures under study, but it significantly affects the mechanisms of current flow.

It is clear that as d0 increases, the probability of tunneling decreases for both holes and electrons. As a result, at low forward biases, recombination processes in the space charge region (SCR) become dominant (Fig. 3). The forward current is described by the expression [3]

I=I_gr^0 exp(eV/2kT) (3) The temperature dependence of the cutoff current I_gr^0 (at V=0) in the coordinates In I_gr^0 from 103/T is approximated by a straight line (see the inset in Fig. 3). The activation energy determined from its slope is (1.7 +0.1) eV, which corresponds to the width of the forbidden zone of the CdS_x Te_(1-x) solid solution at x = 0.6 ÷ 0.7. At large direct shifts, the current for both types of structures (A and B) is thermoemissive in nature. At the same time, the current is mainly electronic, since the barrier height on the CdS side is significantly lower than on the CdTe side. The reverse current of the studied heterostructures is determined by the tunneling of electrons from CdTe into CdS, including through impurity levels.

When the barrier thickness is large (d0≳1 μm), processes of current limitation by spatial charge (CLC) begin to play a significant role [5]. The direct I-V curve of such heterostructures is described by the expression I ~ V^m. (4) As can be seen from Fig. 2, up to three sections with different exponents m can be distinguished in the I (V) dependencies. At the smallest displacements up to a certain voltage V_x, m=1, i.e., Ωs law is satisfied. At V > Vx, this dependence is replaced by a quadratic one, and at V > VCFT н1

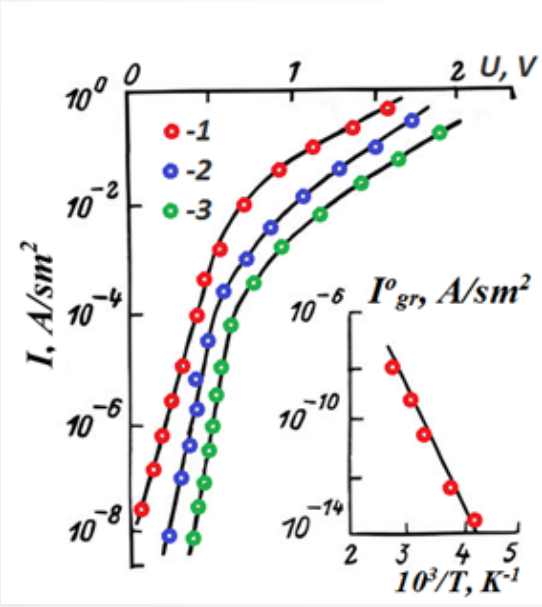

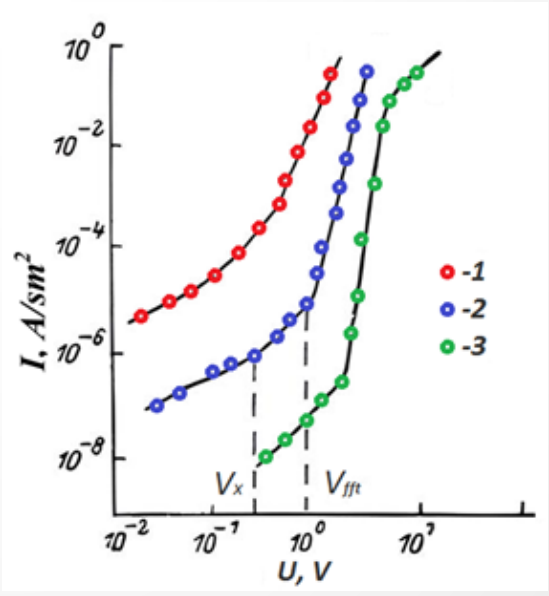

Fig. 1. Straight branches of the B-type HETEROSTRUCTURES VAC at different temperatures. T, K: 1 - 360, 2 - 300, 3 - 240. The inset shows the temperature dependence of the cutoff I_gr^0. Fig. 2. Straight branches of the HETEROSTRUCTURES VAC curve of type B at different temperatures. T, K: 1 - 340, 2 -230, 3 - 130.

(complete filling of traps), m=8÷10.

The studied heterostructures were photosensitive, with the spectrum shape being practically identical for all types of diodes. The low-energy edge of the spectrum is determined by the generation of photo-

carriers in the layer with the smallest band gap, i.e., ~1.3 eV. The sharp drop in photosensitivity in the photon energy range ħω ≳ 2.4 eV is due to their absorption in the CdS crystal bulk. With decreasing temperature, the spectral characteristics shift to the short-wave region, while the shape of the spectrum in the studied temperature range of 100 ÷ 360 K remains practically unchanged [4]. The temperature shift of the long-wave and short-wave edges of the spectral dependence is 4.4·10-4 and 5.2·10-4 eV/K, which is close to the temperature coefficients of change in the band gap width of the CdS0.2 Te0.8 and CdS solutions.

As can be seen in **Fig. 5**, the photosensitivity spectra shift to the long-wave region of the spectrum, indicating that there are deep levels in CdTe responsible for impurity photoconductivity. Analysis of the absorption spectra has determined the activation energies of the deep levels, which are equal to those shown in **Fig**. 3.

Studies have shown that for all heterostructures, the short-circuit photocurrent ISh.cir., as well as the photocurrent in diode mode, linearly depend on the illumination over a wide range of its variation. As the intensity of the incident light increases, the open-circuit voltage Vxx tends toward saturation. At the same time, the absolute values of ISh.cir. and VId significantly depend on the type of structure. They are

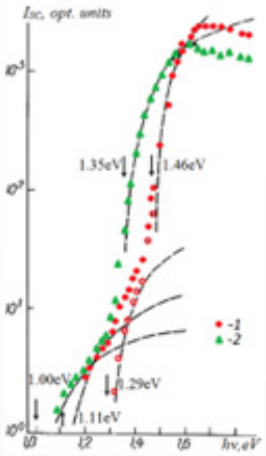

maximal for heterostructures and amount to 20 mA/cm2 and 0.6 V under AM2 conditions. The decrease in VId in the samples is due to an increase in the dark cutoff current Iт0 compared to I_gr^0.

Fig. 3. Ish.cir. spectra for CdTe-CdS heterostructure, under frontal illumination. Experimental points: 1- T = 100 K; 2 - T = 300 K. Dotted line – theory.

Increasing the thickness of the high-resistance varizone layer (type B) leads to an increase in the series resistance limiting Ish.cir. The efficiency of all types of structures is approximately the same and, without the use of brightening coatings, is 0.7÷0.8 el/kv, which confirms the perfection of the interface and the weak influence of defects on the photoelectric properties.

Fig. 3 shows the spectral dependence of the short-circuit current on light energy at different temperatures. The spectra clearly show the activation energies of deep impurity levels located below the conduction band at 1.00 ± 0.03; 1.35 ± 0.03 and 1.17 ± 0.03; 1.29 ± 0.03 eV, respectively. Consequently, with increasing temperature, the thermal generation of charge carriers also increases, and as a result, the effect of additional illumination on the Ish.cir. spectra decreases. For the CdTe-CdS heterostructure, the

dominant level is 1.35 ± 0.03, which suggests that this level is associated with silver or its complex with other point defects.

Conclusions: High photosensitivity combined with a wide linearity range and relatively high speed (less than 1μs at Rn = 100 kΩ) allow the studied heterostructures to be used as photodetectors in the spectral range of 1.3÷2.3 eV due to the presence of deep impurity levels. Note that it covers the radiation range of most industrial LEDs at AIII BV compounds. In addition, these photodiodes are spectrally consistent with the radioluminescence of recently developed scintillators based on AII BVI single crystals. Solar cells based on CdS-CdTe heterostructures have an efficiency of ~22% with a temperature coefficient of 2.5×10-2 %/deg.

Coalesce Research Group

13th International Conference on

Materials Science & Engineering

October 22-24 2025 | Tashkent, Uzbekistan

THERMOELECTRIC GENERATORS FOR POWER SUPPLY OF AUTOMATION EQUIPMENT IN INDUSTRIAL ENTERPRISES

A.M. Kasimaxunova, M.I. Latipova* and M.A. Abdullayeva

Fergana State Technical University, Fergana, Uzbekistan

Abstract

This thesis analyzes the theoretical and practical foundations of using thermoelectric generators (TEG) to supply automation equipment in industrial enterprises with electrical energy. It evaluates the potential of utilizing waste heat flows to generate electricity in order to increase the energy independence of industrial systems and to introduce environmentally friendly energy sources. Experiments were conducted under a temperature difference of 200 K using thermoelectric modules based on BiTeSe–BiSbTe materials. As a result, a thermobattery consisting of ten serially connected blocks generated a voltage of 23.8 V and a current of 0.41 A, producing 4.9 W of power. Calculations demonstrated that such a TEG system can serve as a stable power source for small industrial computers and IoT networks. To increase output power, it is recommended to increase the number of parallel-connected modules or to widen the temperature gradient to 250–300 K. The findings indicate that energy sources based on TEGs can be effectively applied in industrial automation, monitoring systems, and waste-heat recovery units. This approach represents an energy-efficient, environmentally clean, and low-maintenance solution of practical value for industrial facilities.

Background: In recent years, the growing automation of industrial processes has increased the demand for reliable energy sources. In particular, maintaining stable electricity supply at remote industrial sites or in processes generating substantial waste heat has become a pressing issue. From this standpoint, thermoelectric generators (TEGs) attract attention as highly efficient alternative technologies capable of directly converting heat into electricity.

These devices operate with heat flows and can generate power wherever a temperature difference exists, thus representing one of the most promising alternative energy sources [1, 2]. Thermoelectric generators operate based on the Seebeck effect, in which an electrical voltage is produced due to a temperature difference between two types of semiconductors. This phenomenon enables the reuse of waste heat from industrial processes, leading to significant energy savings. Therefore, TEGs are considered a promising solution for providing autonomous power to industrial computers, sensor systems, and automatic control units.

Methods: A TEG module consists of two types of semiconductor materials — n-type and p-type elements. When a temperature difference is applied, electron and hole flows create an electromotive force (thermo-EMF). The generated voltage can be determined by:

$E=\alpha \cdot \Delta T$

bu yerda, E – thermoelectric electromotive force (V), α – Seebeck coefficient (V/K),

ΔT – temperature difference between hot and cold sides (K)..

1. Operating principle of a thermoelectric generator.

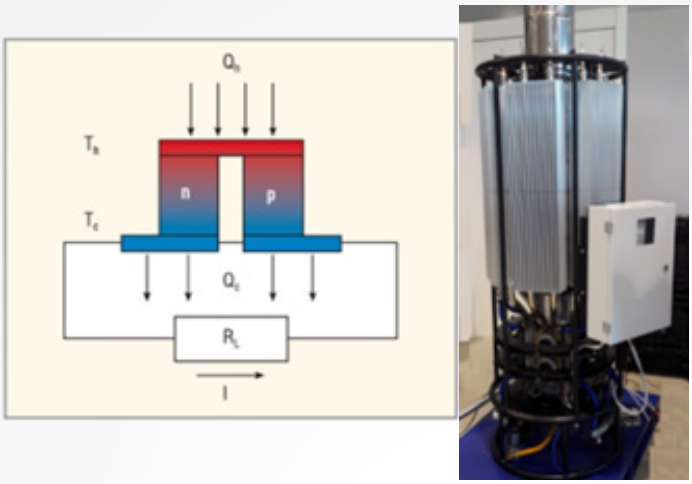

TEG modules are commonly fabricated from semiconductors such as Bi2Te3, PbTe, or SiGe. Thermoelements based on bismuth telluride, selenide, and antimony telluride are most effective within the temperature range of 300–600 K. For the n-type alloy, the composition was: 85 wt% Bi_2Te_3 – 15 wt% Bi_2Se_3 + 0.04 mol% TeI_4, with the following component masses: Bi – 55.186 g, Te – 38.663 g, Se – 6.151g. For the p-type alloy, the composition determined by proportional mixing was: 70 wt% Sb_2Te_3 – 30 wt% Bi_2Te_3 + 0.25 mol% Cd, with Bi – 15.67 g, Te – 57.18 g, Sb – 27.15 g. The thermobattery was assembled from ten serially connected blocks, each containing 60 thermoelectric branches. The height of each branch was 3.3 mm and the cross-sectional area 0.64 mm^2 (30 thermoelements). Samples were cut on an electro-erosion machine and chemically treated. For electrical interconnections, the following alloys were used: (96% Bi – 4% Sb), melting point – 290 °C, and (58% Bi – 42% Sn), melting point – 139 °C [3–5].

Based on the measured electrical parameters:

1. n-tip: σn=1150 Om−1cm−1=1.15×105 S/m, αn=196 μV/K, Zn=2,55×10−3 K−1. p-tip: σp=1000 Om−1cm−1=1.00×105 S/m, αp=200 μV/K, Zp=2,10×10−3 K−1.

For the thermocouple: αcouple=|αp−(−αn)|≈200+196=396 μV/K.

2. Internal resistance

ρ_n=1/σ_n =8,695·10^(-6) Om·m,ρ_p=1/σ_p =1,0·10^(-5) Om·m

R_(leg,n)=ρ_n l/S≈0,04483 Om,〖 R〗_(leg,p)≈0,05156 Om

R_couple=R_(leg,n)+〖 R〗_(leg,p)≈0,09640 Om

R_blok=30·R_couple≈2,8919 Om,R_total=10·R_blok≈28,92 Om

3. Open-circuit voltage and maximum power

V_oc=N·α_couple ΔT=300·3,96·10^(-4) ΔT=0,1188ΔT (V)

P_max=(V_oc^2)/(4R_total),I_max=V_oc/(2R_total),V_load=V_oc/2

Table 1

At ΔT = 200 K, a single thermobattery (10 × 30 pairs) produced ≈ 4.9 W, sufficient to power small IoT/

ΔT (K)	*Voc, (V)*	*Vload (V)*	*Imax (A)*	*Pmax (W)*
100	*11.88*	*5.94*	*0.205*	1.22
150	*17.82*	*8.91*	*0.308*	*2.75*
200	*23.76*	*11.88*	0.411	4.88

sensor or PLC systems. To supply a full industrial computer (≥ 15–25 W), 4–6 such thermobatteries can be connected in parallel, or the temperature difference can be increased accordingly.

Results: In the experiments, a BiTeSe–BiSbTe-based TEG composed of 10 blocks was tested. Each block contained 30 pairs of p- and n-type thermoelements with 3.3 mm legs and 0.64 mm^2 cross-sections.

The hot side temperature was 250 °C (523 K), and the cold side 50 °C (323 K), giving ΔT = 200 K. The obtained parameters were:

Internal resistance Rtot≈28,9 Om;

Open-circuit voltage Voc≈23,8 V;

Current at maximum power Imax≈0,41 A;

Output power Pmax≈4,9 W.

Thus, the thermobattery generated approximately 24 V and 0.4 A (≈ 5 W) under 200 K temperature difference — enough to power an industrial control module or IoT device. By connecting 6–8 such TEG units in parallel, total output can reach 25–35 W, ensuring stable operation of industrial computers (CPU + interface blocks)..

The TEG system designed for industrial computers consists of: A heat collection unit capturing waste heat from technological devices (furnaces, motors, pipelines, etc., with surface temperature 200–400 K); The TEG module, converting thermal to electrical energy; A cooling block (radiator) maintaining the temperature gradient; A power management module (inverter or DC-DC converter) stabilizing output voltage for computer systems.

Fig. 2. Structural diagram of the industrial TEG system.

The results confirm that thermoelectric generators are an efficient solution for ensuring energy autonomy in industrial automation systems. They require no mechanical maintenance compared to diesel generators or backup batteries and are environmentally clean.

TEG systems can be effectively applied in:

remote monitoring of oil and gas pipelines and pumping stations;

waste-heat recovery from furnaces and boilers;

continuous power supply for industrial IoT devices and sensor networks.

Conclusion: Thermoelectric generators play an important role in achieving energy independence of industrial facilities by converting waste heat into electrical energy. According to the study, TEG-based systems can operate continuously for 24 hours, generating 30–40 W of power, and are compatible with various heat sources. In case of main power interruptions, they ensure uninterrupted power supply for automated control systems. Hence, TEG implementation for powering industrial computers, IoT devices, and thermal technologies represents a high-efficiency and environmentally clean solution in the field of alternative energy.

INFLUENCE OF γ-QUANTA ON THE ELECTROPHYSICAL PARAMETERS OF SILICON AVALANCHE TRANSIT TIME DIODES

Abdreymov A.A.[1], Dauletmuratov B.K.[2], Tagaev M.B.[1*] and Sharibaev M.B.[1]
[1]*Berdakh Karakalpak State University, Nukus, Uzbekistan*
[2]*Azhiniyaz Nukus State Pedagogical Institute, Nukus, Uzbekistan*

Abstract

This study investigates the effects of dose and intensity of 60Co γ-radiation on the electrical characteristics of industrial silicon avalanche transit time diodes (ATTDs). Modern microelectronics demand high reliability of semiconductor devices, especially under aggressive environments such as radiation-intensive fields including space, nuclear energy, and medical applications. Traditional thermal treatments for impurity gettering often introduce undesirable side effects, prompting the exploration of a non-thermal methods such as ionizing radiation exposure. Using a controlled γ-source of 60Co emitting photons at 1.17 and 1.33 MeV, ATTDs were irradiated at dose rates of 3 Gy/s and 20 Gy/s across a broad integral dose range (103 to 5×106 Gy). Electrical measurements, including low-frequency current-voltage characteristics and temperature-dependent reverse currents, were conducted alongside diffusion length assessments of minority carriers via electron beam-induced current (EBIC) microscopy. Results reveal that low to moderate γ-doses reduce the thermally generated reverse saturation current and increase the diffusion length and minority carrier lifetime in the n-region, indicating effective radiation-induced defect annealing or gettering without thermal processing. Controversially, doses exceeding a threshold (~8×105 Gy at 3 Gy/s) lead to device degradation manifested by increased tunneling current and reduced carrier lifetimes due to the formation of radiation-induced recombination centers and structural defects. Moreover, higher dose rates shift the beneficial dose range toward lower integral doses, emphasizing the critical role of irradiation intensity. These findings demonstrate the potential of controlled γ-radiation exposure as an non-thermal technique for defect engineering in silicon ATTDs, offering pathways to enhance device performance and radiation hardness.

Research Objective: The aim of this study is to determine γ-irradiation regimes under which it is possible to improve the electrophysical parameters of avalanche transit time diodes without the use of high-temperature processing, through non-thermal gettering of defects and impurities.

Experimental Procedure

Irradiation of silicon ATTDs was carried out using a 60Co γ-source with energy peaks at 1.17 and 1.33 MeV

[1–5]. The dose rate was 3 and 20 Gy/s. The total doses ranged from 103 to 5×106 Gy. Electrophysical parameters were measured before and after irradiation. Low-frequency current-voltage characteristics (I–V curves) were recorded, the temperature dependence of reverse current (within the range 77–350 K) was analyzed, and the diffusion length of minority carriers Lp was measured using the induced current method in an electron microscope.

Results and Discussion (continued): A decrease in the γ-irradiation dose (from 10^3 to 8×10^5 Gy at a dose rate of 3 Gy/s) leads to:

– a decrease in reverse thermogeneration current (ITG),

– an increase in the minority carrier lifetime and diffusion length in the n-layer,

– a reduction in the concentration of recombination centers (Nt) in the p–n junction region.

Exceeding the threshold dose (> 8×105 Gy) results in degradation of the diode characteristics, including:

– an increase in thermotunneling current,

– a decrease in Lp and τp due to the formation of complex radiation-induced defects.

Irradiation intensity also affects the nature of these changes: at higher intensities (20 Gy/s), the optimal dose range for achieving positive effects shifts toward lower values.

Conclusion: Irradiation of silicon avalanche transit-time diodes with low and moderate γ-radiation doses can be used as a non-thermal method to improve their electrophysical characteristics by reducing recombination losses. At doses exceeding the optimal threshold, device parameters deteriorate due to the accumulation of radiation-induced defects. The method of controlled γ-irradiation appears promising for radiation modification of devices intended for operation in rough environments.

Coalesce Research Group

13th International Conference on

Materials Science & Engineering

October 22-24 2025 | Tashkent, Uzbekistan

INVESTIGATION OF THE OPTICAL AND ELECTRICAL PROPERTIES OF SB_XSE_Y FILMS DEPOSITED AT DIFFERENT SOURCE EVAPORATION TEMPERATURES

T.M. Razykov[1,2], K.M. Kuchkarov[1,2*], S.A. Muzafarova[2], R.T. Yuldoshov[1,2], D.Z. Isakov[1], M.P. Pirimmatov[1], R.R. Khurramov[1], M.A. Mahmudov[1,2], A.S. Matmuratov[1] and B.A.Gulumbayev[1]

[1]Institute of Physics and Technology named after S.A. Azimov, Academy of Sciences of the Republic of Uzbekistan, 2b Chingiz Aitmatov street, Tashkent 100084, Uzbekistan.

[2]Institute of Semiconductors Physics and Microelectronics, Yangi Olmazor Street 20, Tashkent 100057, Uzbekistan

Abstract

In this study, the electrical and optical properties of SbxSey thin films grown by a novel separate-source vapor transport method at various source temperatures were investigated. The results revealed that an increase in source temperature leads to a reduction in selenium content within the SbxSey thin films, which in turn significantly affects their optical and electrical characteristics. The bandgap energy of the samples was found to increase from 1.18 eV to 1.27 eV, while their electrical conductivity varied within the range of 1.14×10^{-5} $(\Omega \cdot m)^{-1}$ to 1.89×10^{-4} $(\Omega \cdot m)^{-1}$. These findings demonstrate the potential of Sb_2Se_3 thin films, fabricated via this method, for the development of high-efficiency solar cells.

Background: In recent years, photovoltaic devices based on crystalline silicon, Cu(In,Ga)Se_2, and CdTe have demonstrated power conversion efficiencies of 27.6%, 23.35%, and 22.2%, respectively, making them the leading materials in the global solar cell market [1]. Despite their widespread application, the large-scale production of photovoltaic modules based on these materials faces significant limitations. The primary drawbacks of silicon as the dominant photovoltaic material include its suboptimal bandgap of 1.1 eV, which is lower than the ideal range of 1.4–1.6 eV, and its relatively low absorption coefficient ($\sim 10^2$ cm^{-1}). Consequently, solar cells must be fabricated with a thickness of 200–300 μm [2], leading to excessive material consumption. Furthermore, the large-scale deployment of CdTe- and Cu(In,Ga)Se_2-based thin-film solar cells is constrained by the scarcity of tellurium (Te) and indium (In), as well as the high cost of gallium (Ga), thereby limiting their commercial scalability [2].

Researchers are currently focusing on the utilization of chalcogenide binary compounds such as Sb2Se3, Sb2S3, and their solid solutions Sb2(Sx,Se1-x)3 (with the chemical formula Sb2X3) as absorbing layers for solar cells [3,4]. These materials possess physical properties such as p-type conductivity, band gap (Eg = 1.1 (1.8 eV)), high absorption coefficient (> 105 cm-1 in the visible region), low melting points (Sb2Se3-612°C, Sb2S3-550°C), and high partial vapor pressure that closely resemble those of Cu(In,Ga)(Se,S)2 [3]. Moreover, the constituent elements of these materials are abundantly available in nature, cost-effective, and exhibit stability under external conditions, along with low toxicity. This enables the production of environmentally friendly and efficient solar modules, paving the way for their widespread industrial-scale manufacturing [5].

In this study, the effect of source temperature on the electrical and optical properties of Sb_2Se_3 thin films grown by a novel separate-source vapor transport method is investigated.

Experimental section: The deposition of Sb_2Se_3 thin films at different source temperatures using the separate-source vapor transport method was carried out as follows. Soda-lime glass (SLG) substrates with dimensions of 2 × 2 cm were cut and thoroughly cleaned. The surface was treated sequentially with soapy water, acetone, a fluoride–nitric acid mixture, and deionized water, followed by ultrasonic cleaning for 10 minutes. Finally, the substrates were dried under a nitrogen gas flow.

The prepared SLG substrates were placed in the growth chamber, and Sb_xSe_y thin films were deposited via vapor transport. High-purity Sb_2Se_3 powder (99.999%, Chemsavers) was used as the evaporation source material. The growth process was carried out for 10 minutes under argon (Ar) atmosphere at a pressure of 7 Pa. During deposition, the substrate temperature was maintained at 400 °C, while the source temperature was varied stepwise at 500, 525, and 550 °C. The deposition rate was approximately 0.1 μm/min. The film thickness was determined using scanning electron microscopy (SEM, JEOL JSM-IT510), and the obtained values are presented in Table 1.

The composition of the thin films grown at different source temperatures was analyzed using energy-dispersive X-ray spectroscopy (EDS, AzTec Advanced, Oxford Instruments), while their optical properties were investigated with a UV–Vis spectrophotometer (UV1900i, Shimadzu).

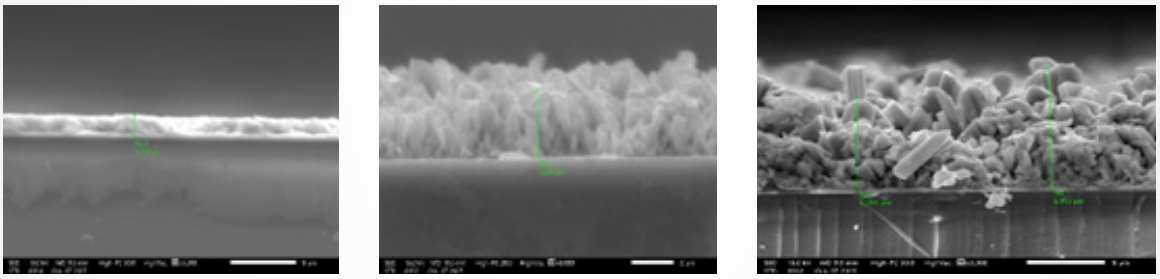

T=500 oC T=525 oC T=550 oC

Figure 1. Microphotograph of the cross-section of SbxSey thin films.

Table 1. Compositional (EDS) results, electrical conductivity, and band gap values of Sb_xSe_y thin films grown at different source temperatures

№	*Substrate temperature (oC)*	*Source temperature (oC)*	*Composition*			*σ (Ω×m)-1*	*Eg (eV)*	*d (mkm)*
			Sb (%)	**Se (%)**	**Sb/Se**			
M54	*400*	*500*	33,7	66,3	0,5083	*6,57×10-5*	*1.18*	*1.7*
M55		*525*	40,1	59,9	0,6694	*1,14×10-5*	*1.23*	*3.3*
M53		*550*	45,2	54,8	0,8248	*1,89×10-4*	*1.27*	*6.2*

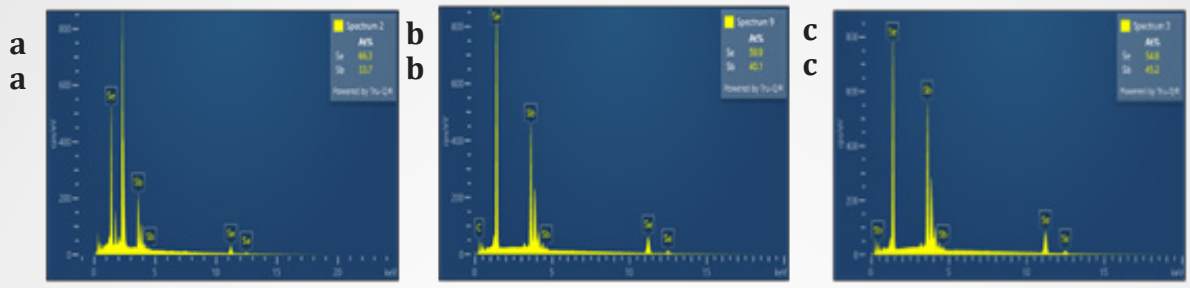

Figure 1: Compositional analysis (EDS) of Sb_xSe_y thin films grown at different source temperatures. (a–c) Correspond to films prepared at 500 °C, 525 °C, and 550 °C, respectively.

Results and Discussion: According to the analysis of energy-dispersive spectroscopy (EDS) results, the variation of source temperature leads to a progressive change in the selenium content of the thin films, as summarized in Table 1, while the corresponding EDS spectra are presented in Figure 1. These results demonstrate that increasing the source temperature enhances the relative fraction of Sb in the Sb_2Se_3 thin films while reducing the Se fraction. Notably, at a source temperature of 525 °C, the Sb/Se ratio approaches the stoichiometric composition of Sb_2Se_3. This indicates that the source temperature is a critical factor during synthesis, playing a decisive role in determining the compositional structure and overall quality of the thin films.

The optical properties of the obtained Sb_2Se_3 thin films were further examined by evaluating the dependence of the absorption coefficient on photon energy, where the main absorption region corresponds to electronic transitions across the band gap. Analysis of the α(hν) plots revealed the presence of direct optical transitions, and the optical band gap (Eg) of the thin films was calculated using the Tauc relation (Eq.1) [6]:

⟦(αhν)⟧^2=A(hν-E_g) (1)

here, hν – represents the incident photon energy, and A – is a constant coefficient.

The optical absorption of Sb_2Se_3 thin films was measured in the 300–1100 nm spectral range. For samples grown at different source temperatures, the absorption spectra exhibited strong absorption in the visible region (λ<1000 nm), which is consistent with the direct band gap nature of Sb_2Se_3. The absorption coefficient was on the order of α=105 sm-1, indicating the material's strong light-harvesting capability. The optical band gap (Eg) values, calculated from Tauc plots, were found to lie within the range of 1.18–1.27 eV, which is in good agreement with reported literature values (Figure 2). The absorption coefficient (α) of Sb_2Se_3 thin films was further determined from the experimental reflectance and transmittance data using the following relation (Eq.2) [7]:

α=-1/d ln⁡((√(⟦(1-R)⟧^4+4T^2 R^2)-⟦(1-R)⟧^2)/(2TR^2)) (2)

Here, d – is the film thickness, R – is the reflectance coefficient, and T – is the transmittance coefficient.

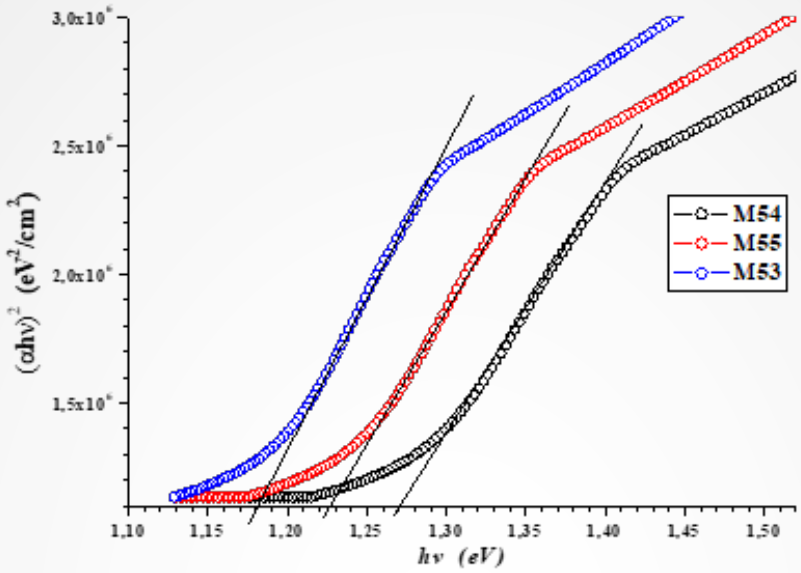

Figure 2. Tauc plots of the deposited SbxSey thin films obtained at different source temperatures

The band gap energy (Eg) was determined by extrapolating the linear portion of the $(\alpha h\nu)^2$ versus hν plot to the abscissa. The spectral dependence of $(\alpha h\nu)^2$–hν and the calculated band gap values for Sb_2Se_3 thin films are presented in Figure 2. The obtained Eg values for different Sb/Se ratios are consistent with those reported in the literature. It was observed that an increase in Se content leads to an increase in the band gap, varying from 1.18 eV to 1.27 eV for SbxSey.

Several factors, including lattice distortions, structural defects, microstructural characteristics, grain size, and compositional fluctuations, strongly influence the variation of the band gap in the synthesized Sb_2Se_3 thin films. These factors affect the energetics of the valence and conduction bands, thereby resulting in either broadening or narrowing of Eg. The band gap is also dependent on the Sb/Se ratio and the synthesis temperature. Thermodynamic processes, phase transitions, or changes between amorphous and crystalline states induced by increasing temperature can significantly alter Eg.

When the Sb/Se ratio increases, leading to Sb-rich compositions, the material deviates from stoichiometry. The ideal stoichiometric composition of Sb_2Se_3 corresponds to Sb/Se = 2:3; however, excess Sb or Se deficiency results in the formation of donor-type defects such as Se vacancies (VSe) and Sb interstitials (Sb_i). These donor defects introduce localized energy levels within the crystal lattice, typically near the conduction band, but in some cases sufficiently close to the valence band. If the donor levels lie near the valence band, band gap narrowing can occur, as electrons transition from the valence band to the donor states and then to the conduction band. This mechanism reduces the effective Eg required for photon absorption or electrical excitation [8,9].

The electrical properties of Sb_2Se_3 thin films were measured under cryostat conditions using the sandwich method. Based on the measured resistance values, the electrical conductivity was calculated according to Equation (3):

$$\sigma=1/\rho=l/(R\cdot A) \quad (3)$$

here: ρ – resistivity (Ω·cm), R – experimentally measured resistance (Ω), l – film thickness (cm), A – electrode surface area (cm^2). The calculated results are presented in table 1.

The minimum conductivity was observed in the stoichiometric composition, which can be attributed to the fact that the Sb_2Se_3 thin film in this state exhibits the characteristics of an intrinsic semiconductor. In intrinsic semiconductor materials, the conductivity is significantly lower compared to doped semiconductors. In contrast, when the composition is enriched with either Sb or Se, the films demonstrate n-type and p-type conductivity, respectively, leading to an increase in overall conductivity. This trend is consistent with the findings obtained in the present study.

Conclusion: In conclusion, it can be noted that with an increase in the source temperature during the growth of SbxSey thin films, a decrease in Se content was observed, which in turn affected their optical and electrical properties. The band gap values of the samples increased from 1.18 eV to 1.27 eV with the rise in Se concentration, while their conductivity varied in the range of 1.14×10^{-5} $(\Omega\cdot m)^{-1}$ to 1.89×10^{-4} $(\Omega\cdot m)^{-1}$. These findings indicate that the obtained Sb_2Se_3 thin films hold great potential for the fabrication of high-efficiency solar cells.

COMBINED DIFFUSION OF GA AND P MIXTURE ATOMS IN SILICON

N.F.Zikrillaev, M.B.Tagaev, Kh.S.Turekeev*, U.Y.Tajimuratov and M.U.Yo'ldoshova
Karakalpak State University. Uzbekistan.

Abstract

In this work, the results of experimental studies of the morphology and composition of the silicon surface using a scanning electron microscope are presented. As can be seen from the research results, when impurity atoms of gallium and phosphorus are simultaneously diffused into silicon, binary compounds are formed on the silicon surface.

Introduction: One of the promising directions in the rapidly developing field of electronics and photovoltaics in the world today is the creation of nanoclusters, including binary elementary cells, in the volume and on the surface of semiconductor materials by selecting elements of groups III, V and II, VI as impurities. From a practical point of view, the discovery of new materials containing binary elementary cells (BEC) with fundamentally different properties from the original material in silicon is an urgent task of the world scientific community. At the same time, the problem of studying the electrophysical and photoelectric properties of new materials and saving high-quality silicon material is relevant. It also leads to the emergence of new semiconductor devices in the fields of electronics, materials science, and photovoltaics by expanding the material's functionality by creating BEC structures in the crystal lattice. Scientific research methods. Currently, in the world, great importance is attached to the creation of nanoscale clusters based on silicon material, radically changing the physical properties of the material, studying its properties, and manufacturing photocells and infrared sensors based on new materials. In this regard, targeted scientific research, including the following scientific studies, is one of the important tasks: introduction of the technology for obtaining samples with complete elimination of surface corrosion by low-temperature diffusion doping of silicon material using elements of groups III, V and II, VI as impurities; Si2AIIIBV and Si2AIIBVI determination of acceptable pairing atoms in the silicon lattice with the participation of elements of groups III,V and II,VI for obtaining binary cells; determination of the control of the electrophysical and photoelectric properties of silicon by forming BEC with the structure Si2AIIIBV and Si2AIIBVI determination of the properties of silicon with the participation of elements of groups III, Determination of the presence of short-circuit current density and open-circuit voltage values in the infrared region in a silicon sample containing Si2AIIIBV and Si2AIIBVI BEC; Development and creation of photocells from silicon material containing Si2AIIIBV and Si2AIIBVI BEC.
For the joint diffusion of impurity atoms of gallium and phosphorus into silicon, a powder obtained by grinding a pure gallium phosphide crystal of the FGECH-1-17 brand was used. After the necessary mechanical and chemical treatment of the silicon samples, gallium phosphide powder was sprayed and diffused from the gas phase at T=1250 °C for a time t=2 hours.

Results. Table 1 and Figure 1 show the composition of the GaP film on the silicon surface, determined using a scanning electron microscope.

Table 1.

Element	*Mass %*	*Atom %*
Si	*90.62±0.23*	*94.12±0.24*
P	*3.74±0.08*	*3.52±0.07*
To	*5.65±0.18*	*2.36±0.08*

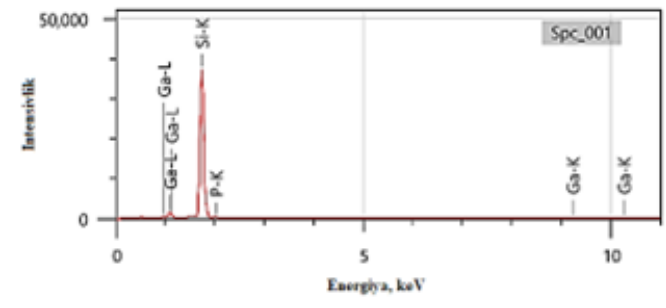

Figure 1. Elemental composition of the thin layer of gallium phosphide formed on the silicon surface

Conclusion: When studying a silicon sample sprayed with phosphorus and gallium impurity atoms using a scanning electron microscope, it turned out that impurity atoms Ga and P are sprayed on the silicon surface in a close ratio to each other. Such scientific results lead to the assumption that Si2GaP type binary compounds are formed in silicon.

Coalesce Research Group

13th International Conference on

Materials Science & Engineering

October 22-24 2025 | Tashkent, Uzbekistan

INFLUENCE OF TEMPERATURE AND MAGNETIC FIELD ON THE DENSITY OF ENERGY STATES IN THE CONDUCTION BAND OF QUANTUM WELL SEMICONDUCTOR MATERIALS

M.G. Dadamirzaev*, U.I. Erkaboev, M.G. and Dadamirzaev

Namangan State Technical University, Namangan, Uzbekistan

Abstract

This study is dedicated to the theoretical analysis of the dependence of the two-dimensional density of energy states in the conduction band of quantum-well semiconductors on temperature and magnetic field. Parabolic and non-parabolic dispersion laws were compared using examples of narrow-gap (InAs) and wide-gap (AlxGa1-xAs) quantum wells. As the temperature increases, the Landau levels smearing, and the oscillations gradually transform into a continuous spectrum.

Background: The variation of charge carrier energy in the allowed bands of a narrow-band quantum well under a strong magnetic field significantly affects the two-dimensional density of energy states . This provides detailed information on the discrete level arrangement of electrons and holes in the quantum well and on the distribution of charge carriers.

The dependence of the density of energy states of narrow-band quantum wells on magnetic field and temperature has not been sufficiently studied. The energy of electrons and holes in narrow-band quantum wells obeys a non-parabolic dispersion law.

Methods: For the quadratic dispersion law, the dependence of the density of energy states of quantum wells on magnetic field and temperature has been thoroughly investigated in [1]. As a result, a new model was proposed [2]:

$$N_{S,Z}^{2d}\left(E,B,T,d\right)=\sum_{N_L,N_Z}^{\infty}\frac{eB}{\pi\mathrm{h}}\cdot\frac{1}{kT}\cdot\exp\left(-\frac{\left(E-\left(\left(N_L+\frac{1}{2}\right)\mathrm{h}\omega_c+\frac{\pi^2\mathrm{h}^2}{2m^*d^2}n_Z^2\right)\right)^2}{\left(kT\right)^2}\right)$$

The expression for the dependence of the energy of free electrons in the conduction band of a narrow-gap quantum well on the magnetic field:

$$E_n^{2d,nonparab}(E_g(B,d),B,d,n_z,N_{Lc})=-\frac{E_g(B,d)}{2}+\frac{1}{2}\sqrt{(E_g(B,d))^2+4E_g(B,d)[(N_{Lc}+\frac{1}{2})\mathrm{h}\omega_{cc}+\frac{\pi^2\mathrm{h}^2}{2md^2}n_z^2]}$$

if the term $\left(\left(N_L+\frac{1}{2}\right)\hbar\omega_c+\frac{\pi^2\hbar^2}{2md^2}n_z^2\right)$ in expression (3) is replaced by

$-\frac{E_g(B,d)}{2}+\frac{1}{2}\sqrt{(E_g(B,d))^2+4E_g(B,d)[(N_{Lc}+\frac{1}{2})\hbar\omega_{cc}+\frac{\pi^2\hbar^2}{2md^2}n_z^2]}$ from expression (2), the follo

wing expression is obtained:

$$N_{s,z}^{c,2d}(E,B,T,d)=\sum_{N_L,n_e}^{\infty}\frac{eB}{\pi\hbar}\cdot\frac{1}{kT}\cdot\exp\left(-\frac{\left(E+\frac{E_g(B,d)}{2}-\frac{1}{2}\sqrt{(E_g(B,d))^2+4E_g(B,d)\left(\left(N_L^e+\frac{1}{2}\right)\hbar\omega_c^e+\frac{\pi^2\hbar^2}{2m^*d^2}n_e^2\right)}\right)^2}{(kT)^2}\right)$$

Results: This expression represents the formula for determining the density of energy states in the conduction band of a narrow-band quantum well. Figure 1 compares the dependence of the two-dimensional density of energy states in the conduction band on magnetic field at constant temperature (T = const) for parabolic (wide-band) and non-parabolic (narrow-band) dispersion laws. It can be seen that the energy dependence of the effective mass of electrons in the narrow-band quantum well, the discrete Landau levels become compressed (deformed) within the same energy interval. The graphs for the narrow-band InAs [3] and wide-band GaAs/$Al_xGa_{1-x}As$/GaAs (quantum well $Al_xGa_{1-x}As$) [4] structures are presented. Oscillations were calculated for T = 1.5 K, B = 3 T, d=5 nm ($Al_xGa_{1-x}As$), and d=4 nm (InAs).

Figure 2 presents the temperature dependence of oscillations in the two-dimensional density of energy states in the conduction band for $Al_xGa_{1-x}As$ and InAs quantum wells. For $Al_xGa_{1-x}As$, the dispersion law is parabolic, while for InAs, it is non-parabolic. The application of the Gaussian statistical function to these materials demonstrates that as the temperature increases, the discrete Landau levels smear out. However, comparison of Figures 2(a) and 2(b) shows that in InAs quantum wells, oscillations transition into a continuous spectrum at lower temperatures compared to $Al_xGa_{1-x}As$ wells.

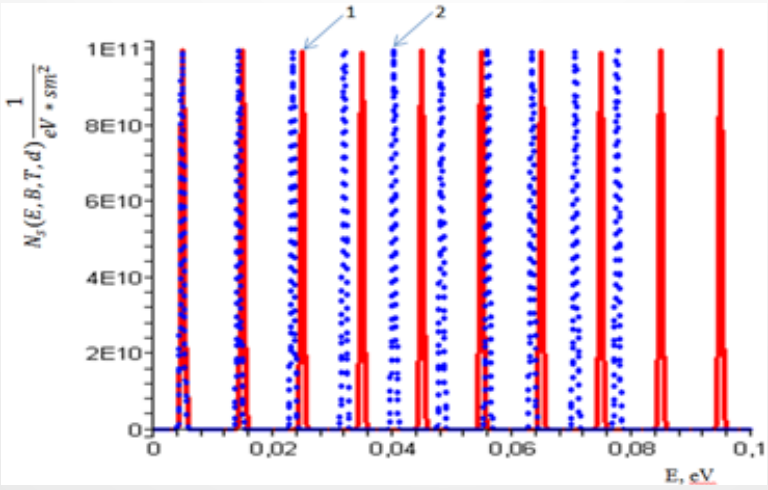

Figure 1. The density of energy states in the conduction band of wide-gap and narrow-gap quantum wells for parabolic and non-parabolic dispersion laws.

Parabolic: $Al_xGa_{1-x}As$, T = 4.2 K, B = 10 T, d = 5 nm

Non-parabolic: InAs, T = 4.2 K, B = 10 T, d = 4 nm

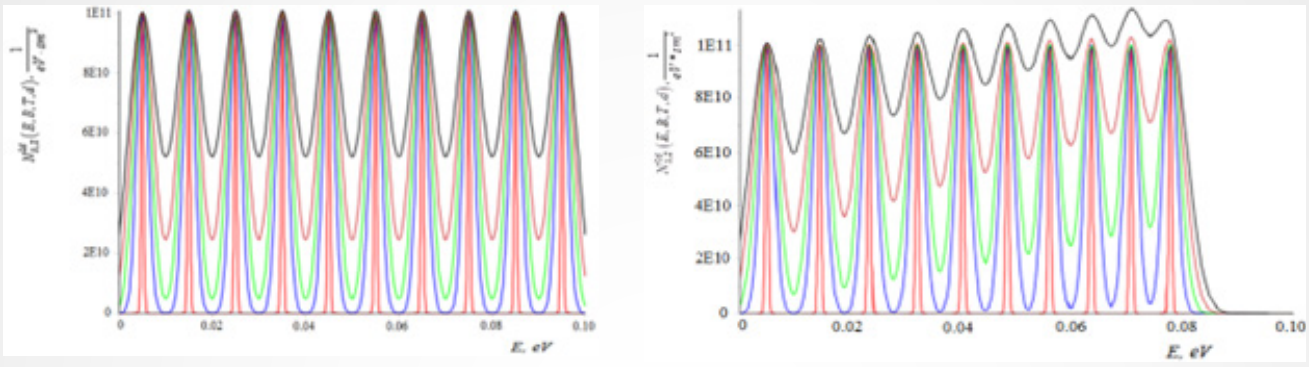

a) Parabolic. AlxGa1-xAs.

------- T=5 K, B=10 Tl, d=5 nm,

------- T=20 K, B=10 Tl, d=5 nm,

------ T=30 K, B=10 Tl, d=5 nm,

------- T=40 K, B=10 Tl, d=5 nm,

------- T=50 K, B=10 Tl, d=5 nm

b) Non-parabolic. InAs.

------- T=5 K, B=10 Tl, d=4 nm,

------- T=20 K, B=10 Tl, d=4 nm,

------- T=30 K, B=10 Tl, d=4 nm,

------- T=40 K, B=10 Tl, d=4 nm,

------- T=50 K, B=10 Tl, d=4 nm

Figure 2. (a) Oscillations of the temperature-dependent variation of the density of energy states in the conduction band of a wide-gap quantum well for a parabolic dispersion law.

(b) Oscillations of the temperature-dependent variation of the density of energy states in the conduction band of a narrow-gap quantum well for a non-parabolic dispersion law.

Conclusion: According to the research results, the two-dimensional density of energy states in the conduction band of narrow-band quantum wells undergoes significant changes under the influence of temperature and magnetic field. An increase in magnetic field quantizes the energy spectrum of charge carriers, enhancing the discreteness of Landau levels. An increase in temperature, on the other hand, leads to the smearing of these levels and the transition of oscillations into a continuous spectrum. Due to the non-parabolic dispersion law, the density of energy states in narrow-band (InAs) quantum wells exhibits much higher sensitivity compared to that in wide-band ($Al_xGa_{1-x}As$) quantum wells.

Coalesce Research Group

13th International Conference on

Materials Science & Engineering

October 22-24 2025 | Tashkent, Uzbekistan

γ-AL_2O_3 AND DEHYDRATION OF ALCOHOLS

N.M.Aliyeva[1], U.A.Karimova*[1], A.A.Aliyeva[1], F.E.Mamedov[1], F.M.Hasanova[1] and N.F.Alverdiyeva[2]

[1]Academician Y.H. Mammadaliyev Institute of Petrochemical Processes of the Ministry of Science and Education of the Republic of Azerbaijan, AZ 1025, Baku, 30 Khojaly ave.
[2]Azerbaijan State University of Economics

Abstract

γ-Al2O3 (gamma-aluminum oxide) possesses a semi-crystalline, defect-rich spinel-type structure. The oxygen atoms form a densely packed cubic lattice, while Al^{3+} ions occupy both tetrahedral and octahedral positions. These structural features contribute to the catalyst high surface area and catalytic activity [1]. The particle size varies depending on synthesis and calcination conditions; according to XRD analysis, the crystallite sizes typically range between 3–20 nm. These nanocrystallites may aggregate into larger structures measuring 250–300 nm, as observed by TEM/SEM [2, 3]. The presence of surface vacancies and structural defects increases the number of active sites, thereby enhancing catalytic performance [1, 4]. γ-Al2O3 exhibits high catalytic activity in the dehydration of ethanol and propanol.

Alcohol molecules are adsorbed onto the catalyst surface, where water is removed via Brønsted and Lewis acid sites, resulting in the formation of ethylene, propylene, and other alkenes [1, 3]. The reaction rate and selectivity depend on the surface properties of the catalyst, temperature, and the composition of the reaction medium. The reaction atmosphere may consist of pure alcohol vapor, alcohol mixed with an inert gas (N2, Ar), oxygen-containing air, or steam [2, 4]. The ratio of Brønsted to Lewis acid sites significantly affects the conversion and selectivity. Metal additives and surface modifications can further enhance catalyst activity, reduce by-product formation, and improve the process in terms of both economic and environmental efficiency [5, 6].

Objective: The thesis aims to evaluate the catalytic efficiency of the γ-Al2O3 catalyst in the conversion of alcohols to hydrocarbons and to study the influence of surface properties on this process.

Methods: Chromatographic γ-Al2O3 catalyst samples were characterized using thermal analysis (TGA/DTG, STA 449 F3 Yupiter), X-ray diffraction (XRD TD3500 (China)) and scanning electron microscopy (SEM, Hitachi S-3400N). The catalytic decomposition of alcohols (ethanol and propanol) was carried out in a specialized reactor system, and the products were analyzed using gas chromatography.

Results: Due to its high surface area and abundance of active sites, the γ-Al2O3 catalyst demonstrated effective catalytic performance in the adsorption and dehydrogenation reactions of ethanol and propanol. The catalyst showed high conversion and selectivity in the transformation of alcohols into hydrocarbons. Thermal analysis confirmed its thermostability and structural stability. These properties suggest that γ-Al2O3-based catalysts are promising materials for the conversion of alcohols into hydrocarbons.

Discussion: Based on XRD phase analysis and SEM results, the catalyst exhibits a semi-crystalline structure and consists of nanoscale, homogeneous particles. Thermal analyses confirmed the stability of the catalyst up to 800 °C, which indicates its potential for use in advanced industrial applications. The study findings show that the large surface area and high number of active sites in γ-Al2O3 significantly contribute to the high yield of olefins in the dehydration of ethyl and propyl alcohols. Comparative analyses revealed that γ-Al2O3 achieves high conversion rates and selectivity in the dehydration processes of

both ethanol and propanol. During these processes, both alcohols are adsorbed on the γ-Al2O3 surface via Brønsted and Lewis acid sites, and with increasing temperature, water molecules are removed, resulting in ethylene and propylene as the main products. A small amount of by-products was also observed during these reactions (Tab. 1).

Parameter	*Ethanol*	*Propanol*
Main product	*Ehylene*	*Propene*
Conversion rate (%)	*85–90*	*88–93*
Selectivity (%)	*92–95*	*90–94*
Optimal reaction temperature (°C)	*300–350*	*350–400*
Active site type	*Brønsted acid*	*Brønsted and Lewis*
By-products	*Diethyl ester*	*Isobutene, butadiene*
Thermal stability	*High*	*High*

Table 1. Dehydration of Ethanol and Propanol over γ-Al2O3

As is evident from the table, the reaction conditions and the ratio of active sites directly influence both conversion and selectivity. The presented results demonstrate that the γ-Al2O3 catalyst provides high conversion and selectivity in the dehydration of both ethanol and propanol. The primary product of ethanol is ethylene, while for propanol it is propene and this outcome is closely related to the type of active sites on the catalyst and the reaction temperature. The relatively low amount of by-products highlights the catalyst specificity and the controllable nature of the reaction. In future studies, metal additives and surface modifications could be employed to enhance catalyst activity and extend coke resistance, offering promising directions for further research.

Coalesce Research Group

13th International Conference on

Materials Science & Engineering

October 22-24 2025 | Tashkent, Uzbekistan

MORPHOLOGICAL CHARACTERIZATION OF $(GAAS)_{1-X-Y}(GE2)_X(ZNSE)_Y$ SOLID SOLUTIONS

S.Z. Zaynobidinov*[1], A.Y. Boboyev[1], I.M. Soliyev[2] and U.R. Karimberdiyev[1]

[1]*Andijan State University, Andijan, Uzbekistan*

[2]*Andijan State Pedagogical Institute, Andijan, Uzbekistan*

Abstract

This study presents the results of morphological investigations of $(GaAs)_{1-x-y}(Ge2)_x(ZnSe)_y$ solid solutions containing ZnSe quantum dots, grown on GaAs substrates by the liquid-phase epitaxy (LPE) method. The development of micro- and nanotechnologies has intensified interest in the fabrication of semiconductor quantum-sized nanostructures with controllable physical properties for advanced optoelectronic applications. In this work, epitaxial layers were grown from a tin-based melt solution in a hydrogen atmosphere purified by palladium. The grown layers exhibited n-type conductivity with a specific resistance of 250 Ω·cm and a thickness of 350 μm, while the epitaxial films possessed p-type conductivity with a specific resistance of 0.1 Ω·cm and a thickness of about 10 μm. The surface morphology of the epitaxial films was analyzed using an industrial atomic force microscope (AFM, "Solver-NEXT"), which provided three-dimensional images and local conductivity maps. The results revealed the formation of self-assembled ZnSe nanostructures on the film surface in the form of dome-shaped quantum dots with lateral sizes of 55–60 nm and heights of 13–15 nm. The lattice constant of the ZnSe nanocrystallites exceeded that of GaAs by approximately 0.22%, indicating elastic strain within the epitaxial layer. Local conductivity mapping showed that the ZnSe nanoislands exhibit higher conductivity compared to the surrounding matrix, due to the larger bandgap of ZnSe facilitating charge transport through the quantum dots. The obtained results confirm that the LPE technique enables self-assembly of high-density, uniform quantum-sized nano-objects on the film surface. The density, shape, and dimensions of these nanostructures are strongly influenced by the crystallization temperature, cooling rate, and technological parameters. These findings demonstrate that ZnSe quantum dots formed in (GaAs)1-x-y(Ge2) x(ZnSe)y solid solutions are promising for use in next-generation optoelectronic devices, photodetectors, and quantum light-emitting structures.

Background: The rapid development of micro- and nanotechnology has stimulated the need for scientific research in many areas, including the formation of nano-objects with controllable properties, the creation of quantum-sized nanocrystals (semiconductor quantum dots and wells), and their wide application in electronic devices. In this regard, the present study presents the results of electron microscopic analysis of ZnSe quantum dot-containing (GaAs)1-x-y(Ge2)x(ZnSe)y solid solutions grown on GaAs substrates [1, pp. 60–66]. Such research objects and the quantum dots (nano-objects) formed in them exhibit unique physical properties related to their atomic-scale energy spectra, generating strong interest among scientists and specialists working in optoelectronics.

Methods: The objective of the study was to investigate the surface morphology of ZnSe quantum dot-containing (GaAs)1-x-y(Ge2)x(ZnSe)y solid solutions grown on GaAs substrates using a scanning probe microscope. For experimental investigation, epitaxial layers were grown on GaAs substrates from a tin-based melt solution by the liquid-phase epitaxy (LPE) method in a hydrogen atmosphere purified with palladium. The grown epitaxial layers exhibited a specific resistance of 250 Ω·cm, a thickness of

350 μm, and n-type conductivity. The initial crystal nucleation temperature was 730 °C, and the cooling rate of the melt was approximately 1 °C per minute. The resulting epitaxial films had a thickness of 10 μm, a specific resistance of 0.1 Ω·cm, and p-type conductivity.

The surface morphology of ZnSe quantum dot-containing (GaAs)1-x-y(Ge2)x(ZnSe)y solid solutions was studied using a "Solver-NEXT" industrial atomic force microscope (AFM). This instrument allows measurement of surface relief and potential distribution. The scanning speed was optimized for surface areas of 256 × 256 pixels. Figure 1a presents the three-dimensional AFM image of the surface of the ZnSe quantum dot-containing (GaAs)1-x-y(Ge2)x(ZnSe)y solid solution. It can be seen that the epitaxial film surface contains nanostructures of various shapes and sizes.

Results: Analysis of the obtained results showed that the nanostructures appear in the form of nanoislands with base diameters of 55–60 nm and heights of 13–15 nm. The formation of such layers occurs through the multilayer growth of semiconductors whose lattice constants differ from that of the substrate, leading to the self-organization of nearly uniform nanoislands (quantum dots) on the surface [2]. It was established that the formation of quantum dots of another phase on the film surface helps to relieve the microstrain of the substrate's crystal lattice. For GaAs/ZnSe and GaAs/Ge systems, the lattice mismatch (< 1%) makes it possible to form ZnSe and Ge quantum dots on the GaAs surface. Furthermore, the lattice constant of the ZnSe nanocrystallites formed in the epitaxial layers exceeds the tabulated value by approximately 0.22%, which indicates elastic deformation of the base crystal lattice [3].

According to AFM results, during growth the ZnSe nanostructures on the surface of (GaAs)1-x-y(Ge2)x solid solutions exhibit a dome-like geometry (dome islands) [2, p. 124], with a lateral dimension of 55–60 nm (Fig. 1a). Figure 1b presents the local conductivity map of ZnSe nano-objects formed on the surface of (GaAs)1-x-y(Ge2)x epitaxial films obtained using contact AFM methods. Measurements of the local specific resistance of these nano-objects were performed simultaneously with the acquisition of topographic data.

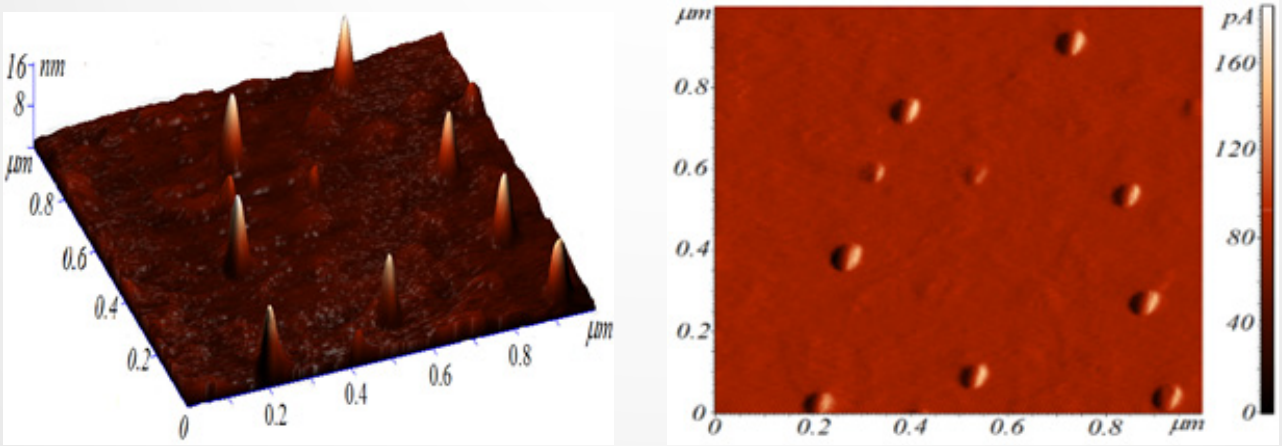

a b

Figure 1. AFM three-dimensional image of the ZnSe nano-object-containing surface of (GaAs)1-x-y(Ge2)x solid solutions (a) and the local conductivity map of ZnSe nano-objects (b) [4, pp. 56–59].

From the figure, it can be observed that the brighter areas correspond to higher current values, indi-

cating regions of lower specific resistance. The analysis confirms that ZnSe nanoislands demonstrate higher conductivity compared to the $(GaAs)_{1-x}(Ge_2)_x$ solid solutions. Since these nanoislands consist of ZnSe molecules whose bandgap is wider than that of GaAs or Ge, the transfer of charge carriers through the nano-objects becomes easier.

The experimental results confirm that during liquid-phase epitaxial growth, a sufficiently dense and uniform ensemble of quantum-sized objects with high conductivity can be self-assembled on the film surface. Therefore, it can be stated that ZnSe quantum dots (nano-objects) can be obtained on the surface of (GaAs)1-x-y(Ge2)x(ZnSe)y epitaxial films by the LPE method. It is also established that the density, geometric shape, and size of the self-assembled quantum dots depend significantly on the crystal growth temperature, the cooling rate of the melt, and technological parameters [5].

AFM data demonstrated that the ZnSe nanostructures on the surface of (GaAs)1-x-y(Ge2)x solid solutions appear as dome-shaped nanoislands with lateral sizes of 55–60 nm. Moreover, experimental studies revealed the mechanism of self-formation of quantum-sized nano-objects with high surface density and uniform morphology in the LPE-grown solid solutions.

Conclusion: During the study, the growth conditions, morphological, X-ray structural, and electrical properties of ZnSe quantum dot-containing (GaAs)1-x-y(Ge2)x(ZnSe)y solid solutions grown on GaAs substrates by liquid-phase epitaxy were thoroughly investigated. AFM analysis clearly demonstrated the self-formation of quantum-sized nano-objects (quantum dots) on the epitaxial film surface.

The ZnSe nanostructures formed on the surface of the epitaxial layers exhibit dome-shaped morphology with lateral dimensions of 55–60 nm and heights of 13–15 nm. These nanostructures possess a high degree of crystallinity, and their lattice constant exceeds that of the GaAs substrate by about 0.22%, indicating the presence of elastic deformation in the layer.

The experimental results show that the liquid-phase epitaxy method allows the self-assembly of quantum-sized objects whose density and morphology can be controlled by adjusting the crystallization temperature, cooling rate, and technological parameters. Thus, the ZnSe quantum dots formed in the (GaAs)1-x-y(Ge2)x(ZnSe)y solid solutions, due to their stable morphology, high conductivity, and favorable energetic properties, can be considered promising materials for the development of future optoelectronic devices, photodetectors, and quantum light-emitting sources.

Coalesce Research Group

13th International Conference on
Materials Science & Engineering
October 22-24 2025 | Tashkent, Uzbekistan

MORPHOLOGY OF NICKEL IMPURITY ACCUMULATIONS IN SILICON

Nozimjon Turgunov and Shirin Sobirova*
Institute of Semiconductor Physics and Microelectronics at the National University of Uzbekistan named after Mirzo Ulugbek, Tashkent, Uzbekistan

Abstract

This paper presents the results of studies on the morphological parameters of nickel impurity accumulations in silicon obtained by electron probe microscopy. It was revealed that the size, geometric shape, and chemical composition of nickel impurity accumulations formed in surface layers and bulk silicon during high-temperature diffusion doping mainly depend on the cooling rate of samples after diffusion annealing. It is shown that, in addition to nickel impurity atoms, technological impurities such as iron and chromium are also present in the volume of the accumulations.

Background: The study of the behavior of impurity atoms during the formation of various defect structures is one of the relevant problems in modern microelectronics. The results of previous experimental studies [1–3] have shown that during diffusion doping of silicon single crystals with fast-diffusing 3d-group elements at high temperatures (T>1000 °C), defect structures are formed that can exist in thermodynamic equilibrium or nonequilibrium states within the bulk of the sample. The thermodynamic state of impurity atom accumulations mainly depends on the cooling rate after diffusion annealing. In [4], the interaction between oxygen atoms and impurity accumulations was considered, and it was found that after diffusion doping of silicon single crystals, the number of electrically active O2 atoms in the sample decreases by several orders of magnitude. Hence, it was established that electrically active atoms of uncontrolled impurities actively interact with the main dopant atoms during diffusion, forming various compounds. To determine the significance and quantity of technological impurity atoms in the formation process of impurity accumulations, experimental studies were carried out, and their results are presented in this paper.

Methods: For the experiments, n-Si<Ni> samples were obtained from monocrystalline silicon of the KEF type with electron conductivity and a specific resistance of 10 Ωohm·cm, grown by the Czochralski method. The p-Si<Ni> samples were made from monocrystalline silicon of the KDB type with hole conductivity and a specific resistance of $\acute{\rho}$=5 Ohm·cm.

All samples prepared for study were parallelepipeds with dimensions of 8.4.2 mm. Diffusion of nickel impurity atoms into silicon was carried out in a horizontal resistance furnace of the SUOL-4 type in the temperature range of 1250 °C. The furnace temperature was measured and controlled by a platinum–platinum-rhodium thermocouple, maintained constant within ±3 K. After diffusion annealing, the samples were cooled at different rates. Morphological parameters of nickel impurity accumulations in silicon were studied using an electron probe microanalyzer “Superprobe JXA-8800R” with EDS Link ISIS-300.

Results: The structural analysis of impurity accumulations in n-Si<Ni> samples cooled rapidly (υcool=400 °C/s) after diffusion annealing showed the presence of accumulations up to ~1 μm in size. Electron microscopy revealed that such accumulations consist of several nickel silicide layers and have needle-like, disk-like, or complex polyhedral shapes close to spherical. The accumulation density in the samples was about ~10^5 cm^{-3}.

Microstructural analyses of impurity accumulations in n-Si<Ni> samples obtained with slow cooling at υcool = 1 °C/s after diffusion annealing revealed that impurity accumulations up to ~8 μm in size, primarily spherical, are formed within their bulk. The density of impurity accumulations within the bulk of the n-Si<Ni> samples is ~6·103 cm-3.

Table 1 shows the dependence of the accumulation size on the cooling rate in n-Si<Ni> and p-Si<Ni> samples after diffusion annealing. As can be seen, the growth of impurity accumulations in silicon single crystals mainly depends on the cooling rate: the lower the υcool, the higher the probability of forming thermodynamically stable accumulations of various shapes and larger sizes.

Table 1. Dependence of impurity accumulation size on cooling rate

υcool Cooling rate (°C/s)	*Maximum sizes of impurity accumulations by diameter (μm)*	
	n-Si<Ni>	*p-Si<Ni>*
1	*8*	*2*
10	*6*	*1.5*
100	*5*	*1.2*
200	*3*	*0.5*
300	*1.5*	*0.3*
400	*1*	*0.2*

The analysis of the chemical composition of the silicide layers within the accumulations in nickel-doped silicon samples showed that, depending on the accumulation size and shape, the impurity atom concentration varies significantly. In n-Si<Ni> samples, the nickel atom content in the central region of large accumulations ($d \geq 5.10^{-6}$ m) reached ~75%, while in smaller accumulations ($d \leq 0.5.10^{-6}$ m) it was about ~25%. Comprehensive analysis of the silicide composition revealed the ratio of impurity atoms to matrix atoms in each silicide shell. Figure 1 presents the dependence of the impurity atom concentration on accumulation diameter for an n-Si<Ni> accumulation with $d=8.10^{-6}$ m. As seen, the nickel atoms are distributed non-uniformly: their maximum concentration lies at the accumulation center and decreases toward the periphery.

Fig. 1. Distribution of Ni atoms by accumulation diameter with size d=8 μm.

Further investigation of the gettering properties of impurity accumulations in n- and p-type Si<Ni> samples revealed the presence of technological impurities such as Fe and Cr within the accumulations.

The data presented in Figure 2 show that the amount of uncontrolled impurity atoms within the accumulation depends on its diameter. At high temperatures, most uncontrolled impurity atoms become electrically active and influence the accumulation formation process.

Fig. 2. Distribution of uncontrolled impurity atoms by the diameter of impurity accumulations: A) in the n-Si<Ni> sample for an impurity accumulation of size d=8 μm; B) in the p-Si<Ni> sample for an impurity accumulation of size d=0.8 μm.

Microstructural analysis showed a non-uniform distribution of uncontrolled impurity,atoms across the accumulation volume their concentration is highest at the accumulation center and decreases toward the outer shells. The distribution of uncontrolled impurity atoms (Fe, Cr, etc.) across the accumulation diameter follows the same pattern as the distribution of the main impurity (Ni), suggesting that such impurities significantly affect both the kinetics of silicide formation and the nucleation and growth of silicide layers.

Conclusion: Based on the obtained results, it can be assumed that the growth of impurity accumulationsbeginsfrom the outer shell. The formation of SixNiy compounds occurs in the following sequence: initially, silicides with the lowest concentration of impurity atoms are formed, followed by those with increasing nickel content. Technological impurities are present within all impurity accumulations, and their distribution across the accumulation diameter follows the same pattern as that of the main impurity atoms. This indicates that uncontrolled impurities (such as Fe, Cr, and others) play a significant role during diffusion doping of silicon, influencing both the kinetics of silicide formation and the nucleation and growth of various silicide layers.

OPTOELECTRONIC DEVICE FOR INFORMATION PROTECTION IN FIBER-OPTIC COMMUNICATION LINES

Kuldashov O.Kh and Nabiev D.O*.
Research Institute of Semiconductor Physics and Microelectronics at the National University of Uzbekistan

Abstract

All possible unauthorized accesses to fiber-optic communication systems were analyzed, and destructive, non-destructive, and optical-radio wave methods of data collection were considered.
An optoelectronic method for countering unauthorized data collection and modern technical means for unauthorized data collection in fiber-optic communication systems was developed.
An optoelectronic device implementing an optoelectronic method for countering unauthorized data collection and modern technical means for unauthorized data collection in fiber-optic communication systems was developed.

Introduction: Recently, one of the most promising and developing areas of communication network construction in the world is fiber-optic communication lines (FOCL). The priority area of development of the transport network of Uzbekistan is the transition of the network to the widespread use of FOCL and the implementation of work to provide all populated areas of the republic with a fiber-optic network, access to high-speed Internet for all households, and coverage of all international and national highways with mobileThroughout the world, considerable attention is paid to ensuring information security-the state of protection of society's information environment, ensuring its formation, use, and development in the interests of citizens, organizations, and the state. In recent years, the Republic of Uzbekistan has implemented a set of measures to improve its information security.

In light of the above, the development of effective methods and technical means for protecting information in fiber-optic communication lines (FOCLs) is a pressing issue.

Analysis of possible information leakage channels. An analysis of existing methods and means for covertly intercepting information in fiber-optic communication systems (FOCS) revealed that a new generation of technical means for information intelligence (TMIS) is being developed for covertly intercepting information from FOCS [1]. The operating principle of all known TMIS is based on recording the portion of optical radiation scattered by the surface of the fiber-optic line's cladding.

An analysis of potential information leakage channels in fiber-optic communication systems revealed the following methods of data extraction [2]:

1. Destructive data extraction methods – based on the use of fiber-optic splitters, which are activated by cutting the fiber-optic line.
2. Non-destructive data extraction methods – based on recording optical radiation scattered on the surface of the fiber-optic line.
3. Optical-radio wave methods – in which the optical radiation extracted from the surface of the fiber-optic line is converted into a high-frequency electrical signal.

Destructive methods and means for data extraction in fiber-optic communication lines are more reliable and simpler than other methods.

The use of fiber-optic splitters in a fiber-optic communication line ensures sufficient intensity of optical radiation emitted from the fiber. This, in turn, ensures reliable operation of the photodetector, as well as the covert data extraction device.

Non-destructive methods extract data without damaging the optical fiber. They use specialized equipment that records the small portion of the signal energy dissipated through the fiber [3].
Non-destructive methods are covert, as they have virtually no effect on the parameters of the radiation propagating through the fiber, but they have low sensitivity.
Optical-radio wave data collection methods are based on the principle of converting optical radiation into a high-frequency electrical signal, which is emitted by an antenna as electromagnetic radiation [4].
This method of data collection utilizes optical-radio wave bugs, which are pre-installed in the fiber-optic communication line (FOCL) by the manufacturer. These bugs can be installed in any segment of the FOCL (optical splitters, patch cords, optical couplings, optical regenerators, optical amplifiers, etc.).
Optoelectronic method of information protection. An optoelectronic method for counteracting unauthorized information retrieval and modern technical means in fiber-optic communication systems is proposed.
The fiber-optic communication line (FOCL) carrying the information signal is irradiated by a noise-like optical signal at the receiver, which propagates along the entire length of the fiber-optic communication line in the opposite direction of the information signal. Thus, a mixed signal is formed in the FOCL, consisting of the information signal and the noise-like signal. Therefore, if information is intercepted unauthorizedly from any section of the FOCL, the signal received by the intruders will be a mixed signal and cannot be separated from the information signal due to the unknown nature of the change in the noise-like signal.
At the receiving end of the fiber-optic communication line, the noise-like signal in the mixed signal is compensated by the same noise-like signal irradiated by the fiber-optic communication line. To achieve this, in the transmitting end of the fiber-optic communication line, the transmitted information signal uc(t) is converted into optical radiation pc(t) and focused onto the input of the fiber-optic communication line, which has two outputs at the receiving end of the fiber-optic communication line. The information signal, converted into optical radiation, travels the entire length of the fiber-optic line and is focused from the first output onto the sensitive area of the radiation receiver.
From the receiving part, an optical noise-like signal pn(t) is introduced from the second output of the fiber-optic line, which propagates in the opposite direction of the information signal along the entire length of the fiber-optic line.
In this case, the total optical signal acts on the sensitive area of the radiation receiver:

$$p_f(t) = p_c(t) + p_n(t) \quad (1)$$

According to expression (1), a photoelectric signal will be generated at the output of the radiation receiver:

$$u_f(t) = u_c(t) + u_n(t) \quad (2)$$

where $u_c(t)$ – information signal at the output of the radiation receiver $u_n(t)$ – noise-like signal at the output of the radiation receiver.
To compensate for the noise-like electrical signal, the phase-inverted noise-like electrical signal from the output of the noise-like signal source is added to the mixed electrical signals in expression (2).
Then we have $u_f(t) = u_c(t) + u_n(t) - u_n0(t)$ (3)
where $u_n0(t)$ - phase-inverted noise-like electrical signal.
Given that $u_n(t) = u_n0(t)$ on the basis we have:

$$u_f(t) = u_c(t) \quad (4)$$

Using the proposed method for protecting an information signal from unauthorized access in a fiber-optic communication line, a noise signal is generated at the receiving end before the sum signal is formed and transmitted to the transmitting end of the fiber-optic communication line for mixing with the in-

formation signal. At the receiving end, during the process of shifting the delayed inverse noise signal toward the sum signal, a complete phase match occurs between the noise signal and its inverse signal. As a result, the noise signal is completely compensated, the information signal is isolated, and information in the fiber-optic communication line is protected from unauthorized access.

Optoelectronic device for information protection in fiber-optic communication lines

Figure 1 shows a block diagram of an optoelectronic device implementing the proposed method of protecting an information signal from unauthorized access in a fiber-optic communication line. The optoelectronic device implementing the proposed method of protecting an information signal from unauthorized access in fiber-optic communication lines comprises, on the transmitting side 1, an information signal generator 2, a mixer 3, a source 4 of transmitted optical radiation, a noise signal photodetector 5, a directional coupler 6 with inputs 6-2 and an output 6-1, a fiber-optic communication line 7, on the receiving side 8, a directional coupler 9 with an input 9-1 and an output 9-2, a sum signal photodetector 10, a mixer 11, delay lines 12, an inverse noise signal generator 13, a source 14 of noise optical radiation and a noise signal generator 15.

Fig. 1. Block diagram of the optoelectronic information security device

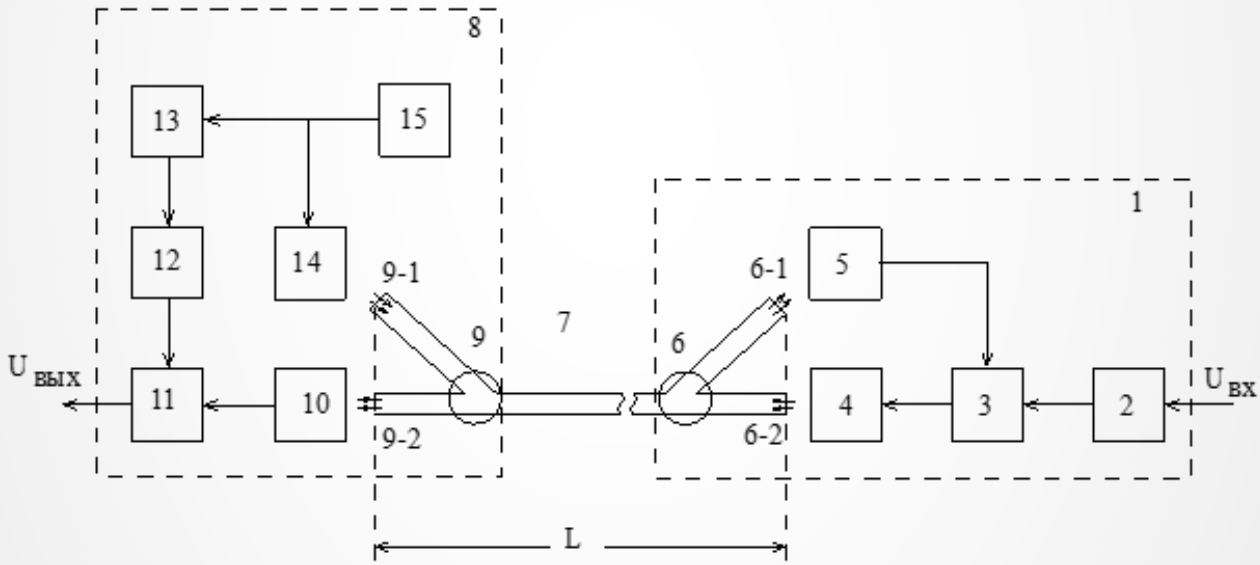

When implementing the proposed method of protecting an information signal from unauthorized access in a fiber-optic communication line, the following operations are performed:

- on the receiving side 8 of the fiber-optic communication line 7:

1) using generator 15, a noise signal is generated;

2) using inverter 13, an inverse noise signal is generated;

3) using delay line 12, the inverse noise signal is delayed for a time ,

4) the noise signal modulates the transmitted noise optical radiation in the optical radiation source 14,

5) through the input 9-1 of the directional coupler 9, the transmitted noise optical radiation is introduced into the fiber-optic communication line 7,

4) the noise signal modulates the transmitted noise optical radiation in the optical radiation source 14,

5) through the input 9-1 of the directional coupler 9, the transmitted noise optical radiation is introduced into the fiber-optic communication line 7,

1) using the generator 2, the transmitted information signal is generated,

2) through the output 6-1 of the directional coupler 6, the received noise optical radiation is output from

the fiber-optic communication line 7,
3) using the photodetector 5, a noise signal is generated from the received noise optical radiation,
4) a sum signal is generated by mixing the information and noise signals using the mixer 3,
5) the transmitted optical radiation is modulated with the sum signal in the source 4 of the transmitted optical radiation,
6) through the input 6-2 of the directional coupler 6, the transmitted optical radiation is introduced into the fiber-optic communication line 7,
- on the receiving side 8 of the fiber-optic communication line 7:
1) the received optical radiation is output from the fiber-optic communication line 7 through the output 9-2 of the directional coupler 9,
2) a sum signal is formed from the received optical radiation using the photodetector 10,
3) an information signal is isolated by mixing the delayed inverse noise signal with the sum signal using the mixer 11.

Conclusion: All possible unauthorized accesses to fiber-optic systems were analyzed, and destructive and non-destructive data retrieval methods, as well as optical-radio wave methods, were considered.
An optoelectronic method for countering unauthorized data retrieval was developed, using modern technical means in fiber-optic systems.
An optoelectronic device implementing an optoelectronic method for countering unauthorized data retrieval and using modern technical means in fiber-optic systems was developed.

Coalesce Research Group

13th International Conference on

Materials Science & Engineering

October 22-24 2025 | Tashkent, Uzbekistan

STUDY OF THE OPTICAL PROPERTIES OF COTTON FIBERS

A.T. Mamadalimov*[1], A.A. Lebedev[2], N.K. Khakimova[1], D.E. Khazratov[1], S.U. Umarova[4], Sh.M. Norbekov[3] and D.A. Azimova[1]

[1]Research Institute of Semiconductor Physics and Microelectronics under the National University of Uzbekistan

[2]A.F. Ioffe Physical-Technical Institute of the Russian Academy of Sciences

[3]Tashkent Institute of Management and Economics

[4]Karshi State University

Abstract

In this article, we present the results of optical microscopy analysis of fine-fiber cotton fibers, undoped and doped with various chemical elements, as well as the results of photoluminescence spectra of samples treated with $KMnO_4$ and iodine. High optical activity was observed in the sample doped with $KMnO_4$. The results of the study confirm the potential of the fibers for use in optoelectronic devices.

Background: At present, research on the physicochemical properties of cotton fibers is developing more rapidly than that of other natural fibers. This is due to the wide use of cotton fibers in various branches of industry. A thorough study of their physical properties provides opportunities for creating new electronic and optoelectronic elements [1–6]. In recent years, extensive research has been conducted to convert natural fibers into electrically conductive materials. Uzbek scientists were the first to discover the semiconducting properties of cotton and silk fibers [7–10]. Studies have shown that the structure of cotton fibers is formed on the nanoscale and that various physical phenomena occur within them [11–12]. Cotton fiber has a helical structure consisting of crystalline and amorphous regions. This has been confirmed by its birefringence and moisture absorption properties. Mature cotton fibers consist of three layers: an outer protective layer, a secondary layer composed of pure cellulose, and a central canal (lumen). During the sample preparation process, the fibers were washed, dried, and doped in chemical element solutions. The diffusion process was carried out at a temperature of 75–80°C for 5 hours. As a result of doping, chemical bonds were formed between the active functional groups on the fiber surface, leading to the formation of new complex compounds. These modifications significantly altered the electrical and optical properties of the fibers.

Methods: After processing the cotton fibers, an electrically conductive glue based on graphite and liquid glass is prepared to obtain ohmic contacts. The graphite crushed like powder particles, is mixed with liquid glass until it becomes thick. The prepared cotton fiber is cut into 0.5 cm pieces, placed in a special clamp, and a copper wire about 7-8 cm long is placed on both sides and hardened using the prepared glue. The resistance of such an electrically conductive glue is 3·102 ohm for a 1 cm long and 20μm thick film. In order for our contact to harden to an ideal state, it is placed in a drying chamber at 80 0C for at least 30 minutes. Thus, the samples are placed parallel to each other, the total weight of the fibers is 3.0-3.5 mg, the number of fibers is 7000-8000, the sample length is 5 mm. In the process of carrying out this work, modern methods and devices were used that allow for high-precision measurement of the dependence of the electrical conductivity of cotton fibers on temperature, energy activation at deep levels, optical properties (on an “MP-6” optical microscope) and photoluminescence spectrum (Fluorescent spectrometer model Cary Eclipse).

Results: Cotton fibers possess a nanostructure formed during their growth, which is closely related to

cellulose synthesis. The selected "Surkhon-104" fibers were examined under an optical microscope. The results showed that the fibers displayed various colors (red, yellow, green, blue), reflecting their degree of maturity. Mature fibers were chosen for further optical and electrophysical analysis. After washing with distilled water, the external appearance of the fibers remained almost unchanged — they retained their natural white color and structure. Under different lighting conditions, the fiber surface exhibited color changes: in white light, the fibers appeared bright white, while under red light they took on a pinkish hue. This effect is due to the spectral reflection properties of cotton fibers — they reflect white light uniformly but absorb most wavelengths except red. This effect is clearly visible only when white objects are illuminated by red light sources. The surface structure of the sample remains the same, only the visual perception of color changes when exposed to a certain spectrum of light. Analysis of natural fibers through their optical properties and microscope images is crucial for identifying physical and morphological changes. The natural spiral structure in pure cotton fibers is clearly visible and remains after washing with distilled water, while the color depends on the type of light: white light gives a pure white tone, and red light imparts a reddish-pink hue.

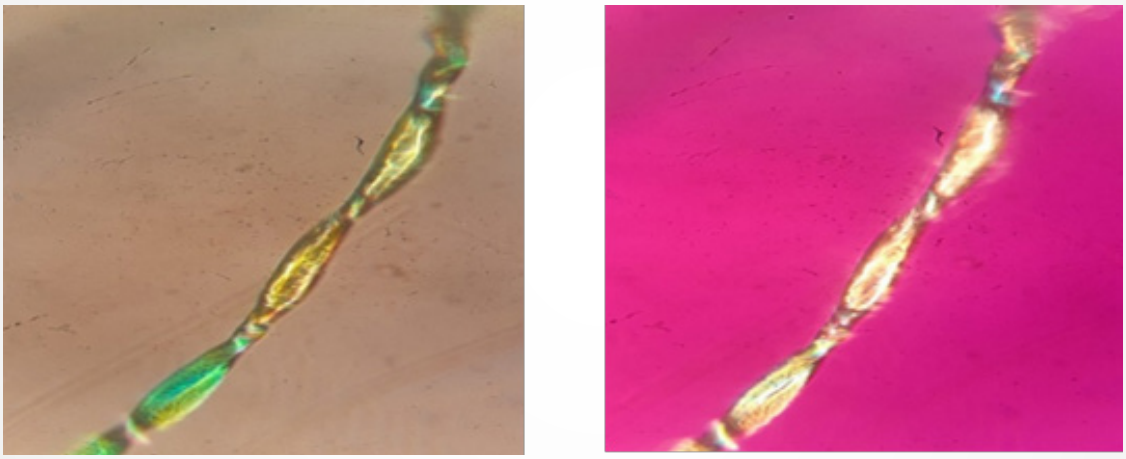

A B

Fig.1. Image of unwashed fine-fiber cotton of the "Surkhon-104" variety under white (A) and red light (B)

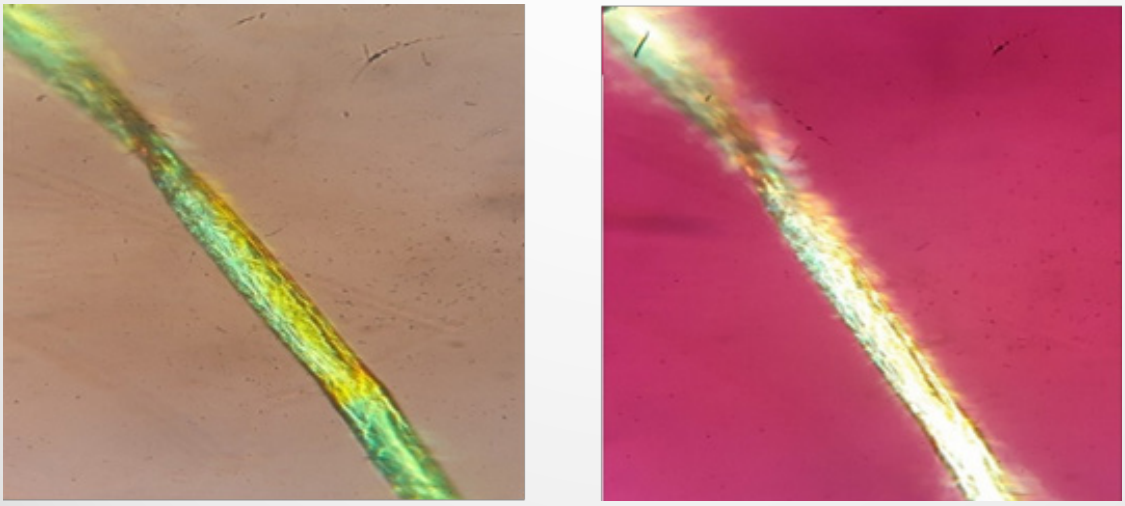

A B

Fig 2. Image of fine-fiber washed cotton of the "Surkhon-104" variety under white (A) and red light (B)

Changes color from orange to brown under white light due to the formation of a complex with iodine. The fiber surface becomes opaque and colored areas are observed. The refractive index increases, increasing contrast. When iodine is added to the fiber, the fiber absorbs more light, so light transmission is reduced. Under red light, iodine absorbs red light weakly, but the surface is iodized, so the color appears dark reddish or brown. Iodine forms a complex with cellulose, which increases the electrical conductivity of the fiber and changes the optical properties (figures 1 and 2). Based on the results of studying cotton fibers of the "Surkhon-104" variety in an "MP-6" optical microscope, it was determined that the surface of the alloyed cotton fibers is covered with alloying elements is rough, uneven, sometimes has cracks or grains. In this case, alloying elements form chemical bonds with the molecules of the fiber at high temperatures. Each dopant atom disrupts the lattice periodicity around its location, and creates surfaces for electrons or holes. As a result of introducing dopants into cotton fibers, on their surface: Chemical bonds are formed. The surface morphology changes (roughness, surface area increases); Electrical conductivity and optical properties improve; Interaction with the environment increases. This allows them to be used as semiconductors, sensors, and electrotechnical materials. To increase the electrical conductivity of semiconductors or to give them a certain function, dopants are purposefully added to semiconductor materials. Dopant atoms replace the main atoms of the crystal lattice or are located between the lattice nodes and form levels. Based on the above data, we conducted experiments, namely, the electrophysical properties of fine-fiber cotton fibers of the "Surxon-104" grade was investigated. Four different types of samples were prepared for the experiment. The first was prepared from pure, that is, untreated cotton fibers and its voltammogram (VAX) was examined. In this case, a voltage was applied in the range from 0 to 100 V, as it can be seen from the 1st straight line in figure 3, the current strength was Imax≤1nA that is we can see that a very small amount of current is passing through. Our second sample was prepared by doping cotton fibers with a 1% alcohol solution of C27H34N2O4C (brilliant blue). In this case, the introduced substance is soaked in cotton fibers (30 minutes at a temperature of 28-30 0C). Then it is heated in a diffusion furnace to a temperature of 90 0C for 5 hours, the water molecules in the dopant evaporate and the dopant atoms diffuse into the cotton fibers. These dopant atoms settle in the vacant nodes or between the nodes. The voltage applied to the second samples was from 0 to 100 V, the current strength was Imax≤10 nA (figure 3, 2nd straight line). After doping cotton fibers with C27H34N2O4C (brilliant blue), we can observe sharp changes in the current flow in the VAX process.

Our third sample is the KMnO4 concentration of cotton fibers of the "Surkhon-104" variety. The doped cotton fibers were prepared by doping with a 1.5% solution of KMnO4. The dopant soaking process lasted for 30 minutes at a temperature of 27 0C, and the diffusion process was carried out in a diffusion furnace at a temperature of 90 0C for 5 hours. When the voltage was increased from 0 to 100 V, the current strength was Imax≤46nA. From the straight line shown in figure 3 we can see that the current strength in cotton fibers doped with KMnO4 increased by several 10 times compared to undoped cotton fibers. This demonstrates the properties characteristic of dopant semiconductors. The fourth sample, "Surkhon-104" cotton fibers, was treated with Ca(H2PO4)2 was prepared by alloying with a 5% solution of calcium dihydrogen phosphate in distilled water. The soaking process of the insert lasted for 30 minutes at a temperature of 27 0C and the diffusion process continued for 5 hours at a temperature of 90 0C in a diffusion furnace. When the applied voltage was applied from 0 to 100 V, the current strength was Imax<80 nA (figure 3, straight line 4). We can observe that when we alloyed Ca(H2PO4)2 with calcium dihydrogen phosphate, the current passing through the sample was higher than when it was alloyed with **brilliant blue.**

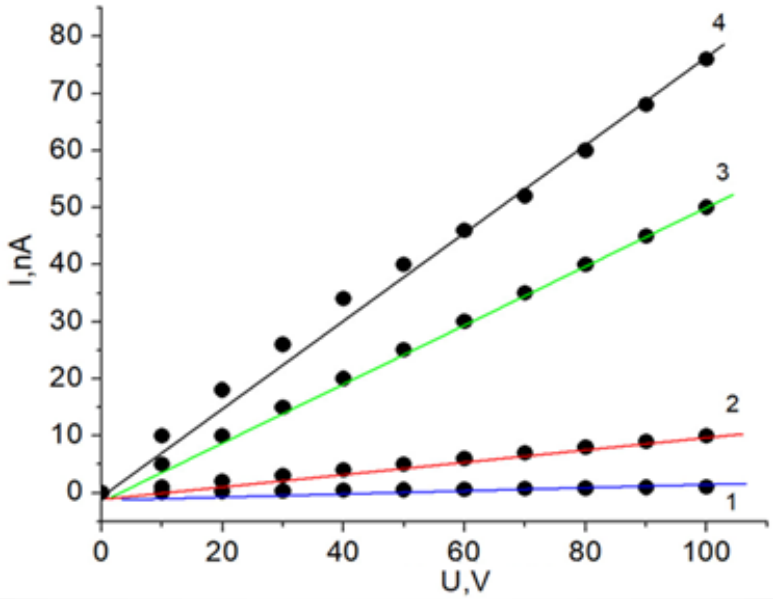

Fig.3: Volt-ampere characteristics of fine-fiber cotton fibers "Surkhon-104" T=300K, first test sample alloyed with2-$C_{27}H_{34}N_2O_4C$, doped with$_3$-$KMnO_4$, alloyed with $_4$-$Ca(H_2PO_4)_2$

The samples were exposed to monochromatic ultraviolet light using a xenon lamp, as a result of which the electrons in the sample hν absorbed a quantized amount of energy and transferred from lower energy levels to higher energy levels according to the selection rule. The electrons are in higher levels for a short time, and then, returning to their original state, emit the absorbed energy in the form of photons. It is known from the results obtained that maximum was observed in the photoluminescence spectrum at different wavelengths. The study of the photoluminescence properties of organic materials, in particular, natural fibers, has become an important scientific direction today, as the need for environmentally friendly and sustainable materials increases. Cotton fibers are composed of a natural polymer cellulose, and its internal structure and defect states exhibit different photoluminescence (FL) spectra when interacting with light. In this study the optical activity of cotton fibers was analyzed in depth based on the results of FL spectra measured in the range of 1350–1600 nm. In this study, it was investigated how cotton fibers of "Surkhon-18" and "Surkhon-104" types change their photoluminescence properties after various chemical treatments. Changes in energy states and band gap widths were observed through samples modified with $KMnO_4$ and iodine substances. In the study, the FL spectra of the following samples were recorded in the range of 1300–1600 nm. In figure 4, sample 1: "Surkhon-18" cotton fiber doped with $KMnO_4$ (potassium permanganate), sample 2: "Surkhon-18" cotton fiber treated with 5% solution of iodine in alcohol, sample 3: "Surkhon-104" cotton fiber treated with a 5% solution of iodine in alcohol. The FL spectra recorded by spectroscopy were expressed in relative units. The maximum intensity and maximum emission wavelength were determined for each sample and the deep levels located in the forbidden zone of the material were identified.

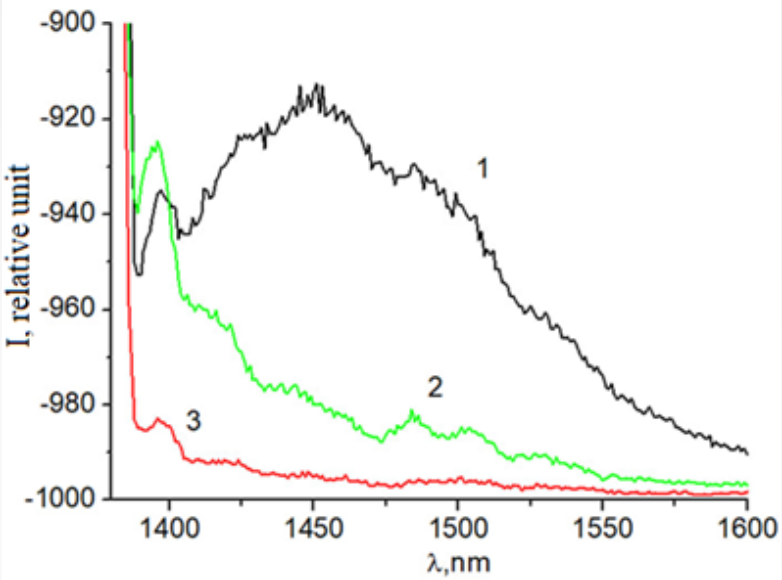

Fig. 4. Photoluminescence spectra of "Surkhon-18" cotton fibers doped with KMnO4 (potassium permanganate) (1), 5% iodine solution in alcohol "Surkhon-18" (2) and 5% iodine solution in alcohol "Surkhon-104" (3)

As can be seen in figure 4, in sample 1 ("Surkhon-18" doped with $KMnO_4$), the light spectrum has a high-intensity FL maximum located in the range of approximately 1450–1470 nm. In sample 2 (iodine-treated Surkhon-18), the light spectrum is reduced, the FL maximum is broader, i.e. in the range of 1450–1500 nm. Sample 3 (I-treated "Surxon-104"): The spectrum has the lowest intensity, the FL maximum is weak.

The energy activation of deep levels located in the forbidden zone, according to preliminary results, is estimated by the following formula:

$E = hc / \lambda$ where $h = 6.626 \times 10^{-34}$ J·s, $c = 3 \times 10^{8}$ m/s, λ – FL maximum wavelength (m):

Sample λ (nm) Eg (eV)

Sample	*λ (nm)*	*Eg (eV)*
1	*1450*	*0.86*
2	*1480*	*0.84*
3	*1500*	*0.83*

Conclusion: From the above results, we can conclude that, based on the results of studying cotton fibers of the "Surkhon-104" variety in an "MP–6" optical microscope, it was determined that different spectral rays were scattered from their surface. We observed that the surface of the alloyed cotton fibers was covered with alloying elements. In this case, the alloying elements form chemical bonds with the molecules of the fiber at high temperatures. It was observed that the current passing through our samples

alloyed with different alloys changed dramatically and became different. So, by introducing impurities into cotton fibers, we can control their electrical conductivity. The introduction of impurities is the most important process for increasing the electrical conductivity of semiconductors and using them for certain purposes. $KMnO_4$ ions stabilize the energy states of the fibers and enhance photon emission. Iodine treatment reduced the spectral intensity. When comparing "Surxon-18" and "Surxon-104", a weak response to iodine was observed in "Surxon-104" fibers. The Surkhon-18 sample doped with $KMnO_4$ had the highest FL intensity. Iodine treatment generally leads to a decrease in FL. The values of the deep levels in the forbidden zone vary between samples. The result opens up possibilities for the application of cotton fibers in optoelectronics and sensor technologies. This work was carried out at the Research Institute of Semiconductor Physics and Microelectronics under the National University of Uzbekistan under the fundamental grant FL-9524115084 on the topic "Creating the scientific foundations of organic semiconductor electronic devices".

Coalesce Research Group

13th International Conference on

Materials Science & Engineering

October 22-24 2025 | Tashkent, Uzbekistan

PHYSICAL PROCESS OF TEMPERATURE DISTRIBUTION AS A TIME DEPENDENCE IN A SOLID, WITH A NON-STATIONARY HEAT FLOW

A.M. Kasimakhunova*[1], Xiaohua Li[2], Q.Sh. Mamarasulov and R.A. Nurdinova

[1]*Ferghana State Technical University, Uzbekistan*

[2]*South China University of Technology, China*

Abstract

This paper presents analytical models describing the temperature distribution over time under the influence of heat flux in semi-infinite solids. The moments of arrival of pulsed heat flux during transient heating by illumination of hot junctions of a thermocouple are considered in order to identify physical processes occurring in the bulk of semiconductor materials. The influence of heat pulsations on the output electrical parameters of a thermoelectric converter is studied. For theoretical studies, the object under study is assumed to be a semi-infinite solid. This eliminates the importance of the cooling conditions of the cold ends of a solid semiconductor body, where it can be considered an accumulator of thermal energy. From a physical standpoint, this is explained as follows: the second end of the thermocouple remains virtually unheated due to the lack of heat input from the hot junctions. Duhamel's assumptions are used, and the obtained results are compared. The difference in the results of stable illumination and transient illumination is analyzed. The phenomena occurring are discussed from a physical standpoint. The amount of heat that has not yet been converted into electrical energy is shown. To thermally excite the crystal lattice of the thermocouple's leg material, it must first "saturate" the material's heat capacity and distribute a stable temperature along the converter's legs. The formulas were implemented dynamically in the Simulink environment, and the nature of temperature changes over time was analyzed. Calculations were performed in real time using a Simulink model for simple parameters. The problem was solved in two ways: in the first case, a formulated mathematical problem was considered with conditions for the independence of the physical parameters of the thermoelectric converter under consideration from temperature. In this case, the equations were solved using the operational method and, based on the proportionality of temperature change and thermoelectric force, the following two problems were posed. The essence of the first problem was to determine the change in emf and temperature difference for a given law of heat flux change, and the second problem, conversely, was to determine the required law of heat flux change over time for given values of emf and ΔT. The second method used the functional dependence of temperature and heat flow.As a result of the research, the values of the parameters under consideration were compared for cases of stationary and non-stationary lighting.

Background: It is well known that many results on temperature distribution along a given length and material as a function of time are typically described by a linear relationship. In some cases, they may deviate slightly from linearity. The reason for this deviation is explained by the electrophysical properties of the material. However, in nature, there are situations in which the effect of temperature on a solid is not always uniform and continuous. It is very important to study the influence of temperature on propagation along a body, either under the influence of an unstable heat flow or a pulsed one. In our opinion, according to [1], in the latter case, this relationship changes significantly. Therefore, precise mathematical calculations using modeling are attractive to researchers studying physical processes in the volume of a solid.

Methods: When solving the problem using modeling, a semi-infinite solid body is considered from a physical perspective, but this is crucial for practical applications. Within such bodies, heat propagates in

only one direction, and its boundaries on opposite sides do not influence each other [2-4]. In this method, the temperature distribution was considered specifically for this semi-infinite moment of the body under consideration. The following mathematical expressions were used as the basis for the theoretical calculation [5,6]:

$T(0,t)=(2q\_0)/(\lambda\sqrt{\pi a})\ \sqrt{t}$ (1)

or, in integral form:

$\Delta T(t)=2/(\lambda\sqrt{\pi})\ \int\_0^t q\_0/\sqrt{\tau}\ d\tau,$ (2)

$E(t)=a\cdot\Delta T(t)$ (3)

where T(0,t) is the body surface temperature (K); q0 is the constant heat flux (W/m^2); λ is the thermal conductivity of the material being studied (W/m·K); a is the heat transfer coefficient (m^2/s); t is the duration (time) (s). This is explained by a good representation of the temperature distribution on the body's surface under the influence of heat flow. These expressions easily allow one to obtain theoretical results for any time range.

Figure 1 shows a Simulink model showing the temperature distribution as a function of time on a semi-infinite solid.

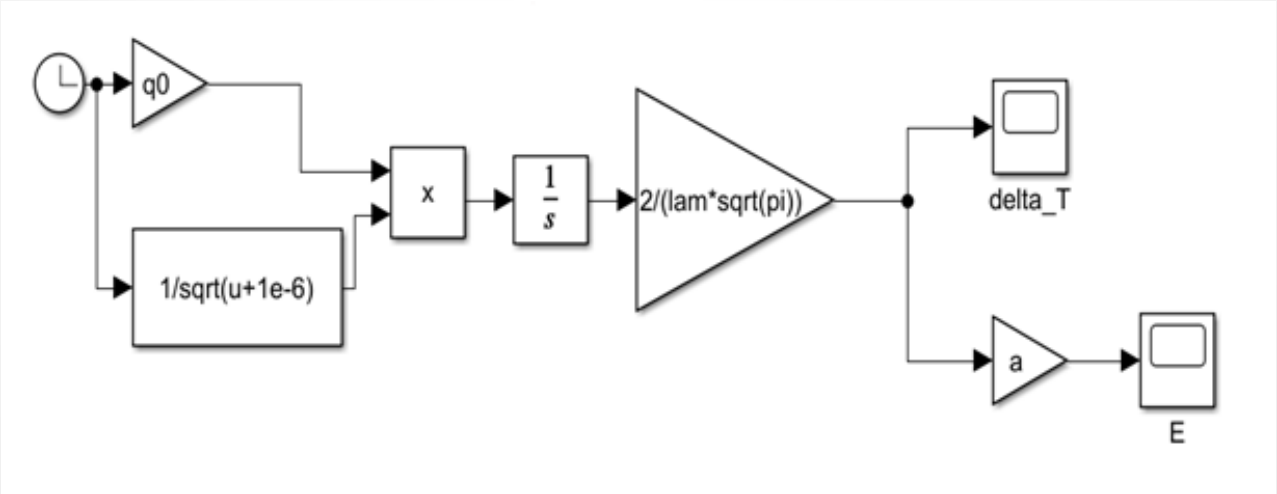

Fig. 1. Simulink model showing temperature distribution on a floor of infinite solids. The model consists of the following main blocks: Input: time t; Square root block: √t : Gain blocks: amplification by the constant $(2q\_0)/(\lambda\sqrt{\pi})$; Output: surface temperature T(0,t).In the model used, physical parameters are introduced as given parameters (for example, in the case we are considering, q0=500 W/m^2, λ=200 W/m•K, a = 1.2•10-5 m^2/s. These parameters can be any based on the selected material).

Results: In our case, we considered the case of thermoelectric material branches. This is explained by the importance of studying heat transfer from the hot to cold junctions of the branches, which allows us to estimate the electrical energy yield. Figure 2 shows the graphical dependences of the temperature distribution along the surface of the solid over time (left figure) and the process of electromotive force generation.

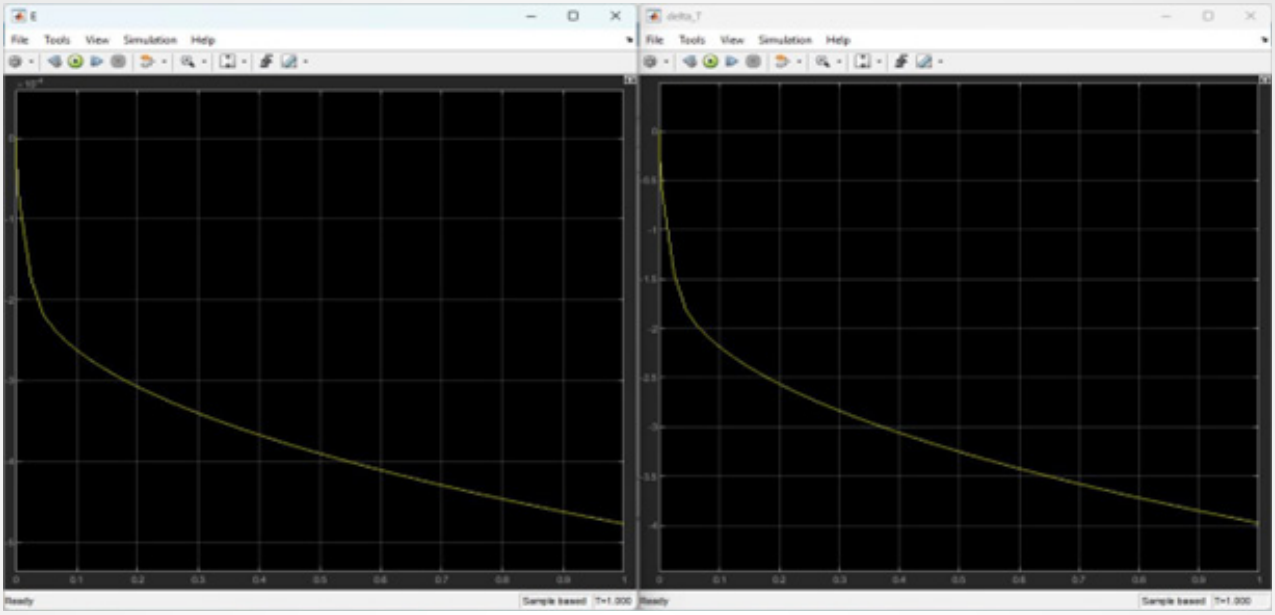

Fig. 2. Dependences of temperature distribution along the length of a solid body over time (left figure) and the process of generation of electromotive force (right figure).

The graph shows that under pulsed, non-stationary illumination, unlike irradiation with steady-state radiation, the temperature on the surface and near the illuminated portion of the hot junction of the thermocouple legs reaches a maximum. This is followed by a sharp drop in temperature (Fig. 2a). The deeper the heat penetrates, the less noticeable the heating becomes. This indicates incomplete excitation of the charge carriers due to the short duration of the light pulse. Moreover, the heat flux is a linearly decreasing function of time, that is:

$$q(t) = q_0\left(1 - \frac{t}{t_0}\right) \qquad [4]$$

If, based on the well-known Duhamel theorem, we assume q for the heat flux density, we can formulate Duhamel's mathematical expression and obtain a solution for the case q=q(t):

$$\Delta T(0,t)\big|_{q=q(t)} = \tilde{\Delta T}(0,t) = \frac{1}{\sqrt{\pi}} \cdot \frac{\sqrt{c}}{\chi} \int_0^t \frac{q(\tau)}{\sqrt{t-\tau}} \cdot d\tau \qquad [5]$$

where τ is the integrating variable and t is the elapsed time.

According to formula (5), the following can be concluded:

$$\tilde{\Delta T}(0,t) = \frac{2\sqrt{c}}{\sqrt{\pi\chi}} q_0 \sqrt{t_0} \left[\sqrt{\frac{t}{t_0}} - \frac{2}{3} \sqrt[3]{\left(\frac{t}{t_0}\right)^2} \right] \qquad [6]$$

and, having checked (6) for an extremum, we obtain a result that shows that it reaches its maximum at t = t0/2. A similar relationship (Fig. 2b) is observed when plotting the thermal emf coefficient versus time. Electrons located on the illuminated side of the branch are the most mobile, due to the efficient absorption of light photons. This pattern dictates strict criteria for selecting the geometric dimensions of thermoelectric converter branches when used under pulsed lighting conditions (for example, when converting lightning energy into electricity).

Conclusion: Based on the results of the conducted studies, it was established that the spectral collection coefficient of charge carriers Q(t) = If(t)/qEo is initially characterized by an increase in Q(t). According to the dependence t<<τ, a2Dτ<<1, it is determined by the radiation parameters. In this case, the service life of the semiconductor charge carrier is independent of the relaxation parameter, but is a function of the kinetic diffusion coefficient. The obtained dependences of temperature on the quantity and quality of the incoming heat flux, using a modeling method in the bulk of a solid, show that this physical process differs significantly with varying heat flux. Consequently, it affects the formation of electromotive forces and the nature of charge carrier mobility.

Coalesce Research Group

13th International Conference on
Materials Science & Engineering
October 22-24 2025 | Tashkent, Uzbekistan

PHOTOCATALYTIC, STRUCTURAL AND OPTICAL PROPERTIES OF UNDOPED AND DOPED ZINC OXIDE NANOSTRUCTURES

A.S. Esbergenova*[1], I.A. Rakhmatullaev[2]

[1]*Research Institute of Semiconductor Physics and Microelectronics under the National University of Uzbekistan*

[2]*Alfraganus University, Tashkent, Uzbekistan*

Abstract

This paper describes the specific features of doping ZnO nanostructures with transition metals for efficient absorption of visible solar radiation. Results are presented on the influence of transition metal impurities (dopants) on the structure and electronic properties of ZnO nanostructures to enhance photocatalytic efficiency. It was found that ZnO doped with Cu and Fe exhibited the best photocatalytic activity.

Introduction: Doping with cations is essential for effectively modulating the optoelectronic properties of semiconductor photocatalysts and thereby enhancing their photocatalytic activity in order to improve the photocatalytic activity of [1]. Moreover, transition metal doping in ZnO crystal lattice is one of the well-known strategies for tuning the band gap of ZnO to make it a visible-light-active photocatalyst [2].

Methods: In this work, we investigated the effect of varying concentrations (0% - 10%) of Fe and Cu dopants on the optoelectronic properties and photocatalytic efficacy of ZnO nanostructures synthesized through the hydrothermal route. The ZnO nanostructures were obtained as precipitates through a chemical precipitation reaction between zinc nitrate (Zn(NO3)2·6H2O) solutions and a KOH alkali solution at 70°C. The resulting precipitate was filtered and dried. To synthesize doped samples, appropriate amounts of FeSO4 and Cu(NO3)2·6H2O were added to the hydrothermal solution. A combination of experimental and theoretical approaches was employed for this investigation.

Results and discussion: Density functional theory (DFT) calculations were utilized to elucidate the location and nature of localized energy levels within the bandgap of ZnO induced by Cu and Fe impurities. The photocatalytic efficiency of both undoped and Fe/Cu doped ZnO nanostructures was assessed by monitoring the degradation of aqueous methylene blue (MB) solution under visible light irradiation.

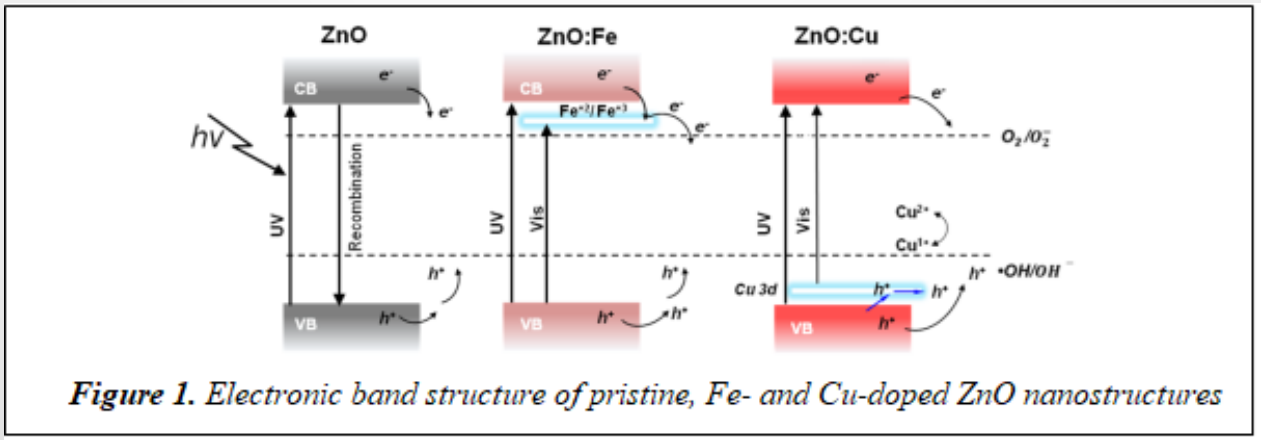

Figure 1. *Electronic band structure of pristine, Fe- and Cu-doped ZnO nanostructures*

The combination of theoretical and experimental findings allowed us to conclude that the introduction of Fe and Cu impurities can enhance the photocatalytic activity of ZnO under visible light (see Fig. 1). The enhancement by Fe impurities is attributed to the formation of small donor levels below the conduction band, with the contribution from the Fe 3d state. Specifically, the newly formed impurity level in the electronic structure of ZnO facilitates visible light absorption through the O 2p → Fe 3d transition and suppresses the recombination of photogenerated charge carriers by capturing electrons from the conduction band. In the case of Cu, the formation of small acceptor levels near the valence band maximum of ZnO facilitates visible light absorption through Cu 3d → Zn 2p and Cu 3d → O 2p transitions and suppresses charge carrier recombination by capturing photoexcited holes. As light strikes ZnO NPs, the valence band electrons are triggered and dispersed into the conduction band. The hydroxyl radicals generated by the valence band holes in ZnO then react with water, resulting in dye degradation through the direct oxidation mechanism. By absorbing the ZnO conduction band electrons, the impurity Cu2+ and Fe2+ ions produce Cu+ and Fe3+ ions. The Cu+ and Fe3+ ions formed are then transferred an electron into atmospheric oxygen, generating superoxide radicals and Cu2+ again. By introducing Cu+ and Fe3+ ions into the ZnO crystal structure, the electrons were captured by the defect band, and photo-induced charge carrier coupling was suppressed. As the superoxide radical combines with the water molecule, it releases H2O2, which results in the formation of hydroxyl radicals [13]. The hydroxyl radicals created readily interact with dye molecules, which then degrading the of methylene blue in an aqueous solution [3].

Conclusion: Thus, among the various concentrations of dopant elements, 1% Fe and 3% Cu were found to be favorable, exhibiting the highest photocatalytic activity in the degradation of methylene blue in an aqueous solution, owing to the beneficially modulated optoelectronic structure.

Coalesce Research Group

13th International Conference on

Materials Science & Engineering

October 22-24 2025 | Tashkent, Uzbekistan

FORMATION OF CU-NI-SN PRECURSORS ON A FLEXIBLE METAL FOIL TO OBTAIN SEMICONDUCTOR $CU_2NISN(S,SE)_4$ THIN FILMS

Sharifa Utamuradova[1], Kakhramon Fayzullaev*[1] and Aliona Stanchik[2]

[1]*Institute of Semiconductor Physics and Microelectronics at the National University of Uzbekistan named after Mirzo Ulugbek, Tashkent, Uzbekistan*

[2]*Scientific-Practical Materials Research Centre, National Academy of Sciences of Belarus, Minsk, Republic of Belarus*

Abstract

The paper presents the results of a study of the phase composition and morphology of Cu-Ni-Sn precursors obtained by magnetron sputtering, depending on the elemental composition and type of substrates (Ti-foil and glass/Mo). The established patterns of formation of Cu-Ni-Sn precursors on various types of substrates will allow synthesizing semiconductor $Cu_2NiSn(S,Se)_4$ thin films, which are used to create efficient thin-film solar cells of a new generation.

Background: Copper compounds such as $Cu_2NiSn(S,Se)_4$ (CNTSSe) can be promising materials for thin-film photovoltaics due to their physical properties [1-3]. In particular, this is necessary for the creation of flexible solar cells, which, compared to conventional solar cells (on glass substrates), offer a high power-to-weight ratio, mechanical flexibility, functionality, and cost-effective production. The achieved efficiency of conventional solar cells based on Cu2NiSnS4 films is 17.06%, demonstrating their high potential despite falling short of the theoretical limit (~33%). To improve the achievable efficiency of CNTSSe-based solar cells, a deeper understanding of the synthesis process, compositional control, morphology, and other fundamental aspects of their active layers, and especially the CNTSSe layer itself, is essential. This represents an open area for research and improvement.

Objective: To obtain Cu-Ni-Sn precursors by magnetron sputtering on titanium foil substrates, and study their morphology, elemental and phase composition. The precursors will be used to produce thin films of CNTSSe by high-temperature treatment in chalcogen vapor.

Methods: The Cu-Ni-Sn precursors were obtained by layer-by-layer magnetron sputtering at room temperature on titanium foil. Magnetron sputtering was performed using an ORTUS-700 magnetron sputtering system (Izovac LLC, Belarus). Planar copper, tin, and nickel targets with a diameter of 10 cm were used as the source of deposited materials. The process start pressure was about 3 × 10–3 Pa. The sputtering parameters for copper, tin, and nickel were set as follows: 200 W and 60 sccm of Ar; 60 W and 60 sccm of Ar; 130 W and 90 sccm of Ar, respectively.

The elemental composition and microphotographs of the precursors were obtained using X-ray spectral microanalysis and scanning electron microscopy on a ZEISSEVO instrument (Zeiss, Oberkochen, Germany). The phase composition of the precursors were studied using an X-ray diffractometer DRON-3M with CuKα radiation. Analysis of the phase composition was performed using the program Match.

Results: Three series of Cu-Ni-Sn precursors with different component ratios were obtained (Table 1). The precursor component ratios were varied by changing the thickness of the deposited Sn layer (from 150 nm to 225 nm) without changing the thicknesses of the Cu and Ni layers (150 nm and 75 nm, respectively). All precursors were Cu-poor. The first series had a Ni-rich composition, while the second and third series, on the contrary, were Ni-poor. The precursors of the first and second series had the closest composition to stoichiometry.

Series number	Elemental composition, at.%			Atomic ratio	
	Cu	Sn	Ni	Cu/(Sn+Ni)	Sn/Ni
N1	46.4	25.3	28.3	0.87	0.89
N2	44.0	28.1	27.9	0.79	1.01
N3	38.2	34.9	26.8	0.62	1.30

Figure 1 shows the X-ray diffraction patterns of Cu-Ni-Sn precursors obtained on a Ti-foil substrate. In all cases, the Cu-Ni-Sn precursors were polycrystalline in nature and had a multiphase composition, regardless of the elemental ratio.

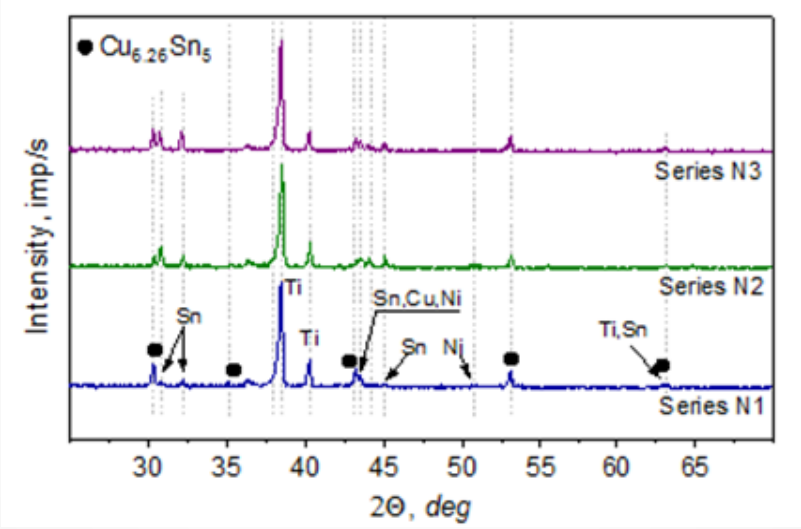

Figure 1. X-ray diffraction patterns of Cu-Ni-Sn precursors obtained on a Ti-foil substrate. The X-ray patterns shows the series number of the precursors

The X-ray diffraction patterns of all Cu-Ni-Sn precursors contain reflections from Ti (card number: 96-900-8518), the substrate material. The X-ray diffraction pattern of the Cu-Ni-Sn N1 series precursors contains reflections from the elemental phases of tetragonal Sn (card number: 00-086-2264), cubic Cu (card number: 96-901-3022), and the binary phase Cu6.26Sn5 with a hexagonal structure (card number: 00-047-1575). Furthermore, the existence of an elemental phase of cubic Ni is possible (card number: 96-901-3030).

The X-ray diffraction patterns for precursors in N2 and N3 series are very similar to those for precursors in N1 series. However, the X-ray diffraction patterns for N2 and N3 series show increased intensity of reflections from the Sn phase and the binary Cu6.26Sn5 phase, which is due to the increased tin content in these samples (Table 1).

Scanning electron microscopy showed that the precursors have similar Cu-Ni-Sn layer surface morphology regardless of elemental composition. Figure 2 shows a typical micrograph of the precursor layer at

an angle, using N3 series as an example. It can be seen that the precursor layer is characterized by a collection of nanocrystals and larger crystals reaching several hundred nanometers in size. However, it can be noted that the large faceted crystals on the surface of the N2 and N3 series precursors were larger and more densely packed than in the case of the N1 series precursor.

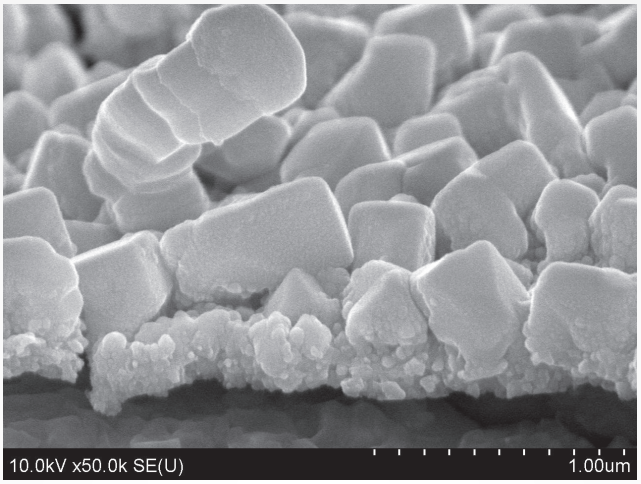

Figure 2. Typical micrograph of Cu-Ni-Sn precursors (series N3) on a titanium foil substrate

Conclusion: The Cu-Ni-Sn precursors were obtained using layer-by-layer magnetron sputtering on a Ti-foil substrate. In all cases, the precursors were characterized by a polycrystalline nature, multiphase composition, and similar morphology. The Cu-Ni-Sn precursors contained both elemental metallic phases (copper, tin, and nickel) and a binary Cu6.26Sn5 phase. It was established that the phase composition of the precursors depends weakly on the ratio of their constituent elements. These results will allow us to optimize magnetron sputtering of precursors to obtain light-absorbing thin Cu2NiSn(S,Se)4 films with the required properties for creating efficient flexible solar cells of the new generation.

Coalesce Research Group

13th International Conference on

Materials Science & Engineering

October 22-24 2025 | Tashkent, Uzbekistan

NANOCRYSTALS PRODUCED BY NUCLEAR REACTIONS IN LITHIUM FLUORIDE CRYSTALS

E.M. Ibragimova* and Sh.N. Buzrikov

Institute of Nuclear Physics of Uzbekistan Academy of Sciences, Tashkent, Uzbekistan

Abstract

Lately the global interest to Li-compounds has increased more, since Li is the source of generating Tritium (the long-living beta-emitting isotope) in blanket of ”pure” thermonuclear reactors by exothermic 6Li(n,α)3H reaction discovered by Rutherford. Now this reaction is applied also for diagnosis of Li-based batteries by detecting alpha- and beta-emission. The widest gap ionic LiF crystals have been used for 70 years as a slow neutron dosimeter and thermo-luminescence dosimeter of absorbed X- and gamma-ray, despite quite a low dose limit.

The goal of this research was to find out what chemical compounds and crystal structures appear in the tracks of a few MeV energy alpha and tritium. To study other possible nuclear reactions with 6Li, 7Li and 19F, we irradiated in the research water-cooled uranium fission reactor with the neutron flux 1014 n/cm2s to fluencies 1015 – 1018 n/cm2 and monitored alpha-beta-gamma-activity for a few years. Since the neutron flux is accompanied by γ–quanta emission of nuclear recoils (gamma-flux 37 Gy/s), the contribution of gamma-induced nuclear reactions was evaluated by means of irradiation in the shut-down reactor for 100 hours and also by 60Co γ–quanta (1.17 and 1.33 MeV) at dose rate ~10 Gy/s to high doses 107 Gy. And the effect of beta-emitting recoils was studied by exposure to electron beams accelerated to 4-5 MeV at beam current density 0.4÷3 μA/cm2 to fluencies 1014 – 1017 e/cm2. No post-irradiation alpha-beta-gamma-emission was detected after the gamma- and electron irradiation.

Using SEM and SPM we found square pyramidal micro-size tracks (1-5 μm) also nano-size hillocks (10-300 nm) inside the tracks and on the exposed surface in all the examined conditions of irradiations, which size depends mostly on the impact neutron, electron and gamma-quanta energy, while the distance between the tracks depended on the flux and accumulated fluency. By means of energy dispersion spectroscopy (EDS) installed in SEM we studied micro-local element composition inside nuclear tracks and between them in the surface micro-layer and found irradiation induced impurity Boron, Carbon and Oxygen atoms. It should be noted that K-lines of B and C are not well resolved. These element ions, also Hydrogen, were detected in FTIR spectra as additional lines of chemical bonds Li-H, B-H, B-O, and no carbon bonds were found, while Li-F bond line decreased. Taking into account EDS and FTIR data, we carried out X-ray diffraction analysis of crystal structure and phase composition by using HighScore FullProf codes, and data base PDF–2013 and 2019. Nanocrystal phases of LiH, LiT, BH4, LiBH2 and complicate compound (LiF)2(B2O3)3 were identified. Suggested nuclear reactions in the reactor: $^{19}F_9 + t \rightarrow 2\ ^{10}B_5$; $^{7}Li_3 + {}^{4}\alpha_2 \rightarrow {}^{11}B_5$; with 4-5 MeV electrons: $^{19}F_9 + \rightarrow\beta\ ^{3}He_2 + {}^{16}O_8$; $^{7}Li_3 + \beta \rightarrow {}^{4}He_2 + {}^{3}He_2$; with γ–quanta: nuclear excitation with electron-positron pair emission and nuclear reaction of transmutation via compound-nucleus (LiFH)→(BO) followed by chemical compound B2O3 as nano-crystallites. Thus, the participation of nuclear reaction products in the mechanism of chemical composition changing and nanocrystalline phase transformation in irradiated crystals is confirmed experimentally.

Coalesce Research Group

13th International Conference on

Materials Science & Engineering

October 22-24 2025 | Tashkent, Uzbekistan

PRELIMINARY TESTING OF A PHOTOVOLTAIC INSTALLATION WITH A DUAL-AXIS SOLAR TRACKING SYSTEM

O.F. Tukfatullin, E.D. Muxamediyev, S.A. Daminov*, K.A. Djumamuratov and D.A. Fatkullaev

Institute of Semiconductor Physics and Microelectronics at the National University of Uzbekistan named after Mirzo Ulugbek Uzbekistan, Uzbekistan

Abstract

This paper presents the design and preliminary testing of a photovoltaic installation equipped with a dual-axis solar tracking system. To ensure the highest measurement accuracy, the electrical parameters of the photovoltaic module with the tracking system are compared with those of an identical stationary module fixed at an inclination angle of 42° relative to the horizontal surface. The study describes the measurement equipment developed for the simultaneous monitoring of current and voltage generated by the photovoltaic modules. A preliminary evaluation of the efficiency of the solar tracking system has been performed.

Background: In the context of the global transition to renewable energy sources, solar energy occupies one of the leading positions due to its environmental friendliness, inexhaustibility, and availability. However, the performance of photovoltaic modules (PVMs) is limited by their stationary configuration, which leads to reduced electricity generation throughout the day and throughout the year [1]. In this regard, the development and implementation of technologies aimed at improving the utilization of solar radiation — in particular, solar tracking systems — represent a relevant and important research direction. The use of such systems makes it possible to increase the amount of electricity generated by dynamically adjusting the orientation of PVMs toward the Sun, which makes them particularly promising for modern photovoltaic installations [2]. The aim of this study is to conduct preliminary tests of a PVM equipped with a solar tracking device in order to assess its performance compared with that of a stationary module. The obtained results are expected to contribute to the advancement of photovoltaic technologies by improving their energy yield, competitiveness, and potential for widespread application in various regions.

Methods: A photovoltaic installation equipped with a dual-axis solar tracking system was developed for testing. The tracking system is designed to increase the power output of the PVM by adjusting its spatial orientation according to the Sun's position. The installation employs a monocrystalline silicon PVM with a nominal power of 50 W (Standard Test Conditions: AM 1.5, 1000 W/m^2, 25 °C). An identical module was used as a control sample, fixed in a stationary position at an angle of 42° to the horizontal surface. Rotation of the PV module in the tracking system is achieved using linear actuators, one for each rotational axis. It should be noted that the use of linear actuators introduces certain mechanical constraints, including a limited range of angular movement for both axes [3]. In addition to the PV module and actuators, the system includes rotation mechanisms along both axes, a drive controller, a solar tracking sensor, and a power supply unit. The system can be powered autonomously by the PVM itself through a charge controller and a rechargeable battery, ensuring full operational independence. The operating principle of the system is based on maintaining the normal vector of the PVM surface as closely aligned as possible with the direction of solar radiation. For this purpose, the tracking sensor is rigidly attached to the module body so that its optical axis is parallel to the module's surface normal. The tracking sensor consists of four identical optoelectronic channels whose sensitive elements are photodiodes.

The photodiodes are positioned on the faces of a four-sided pyramid and operate in short-circuit mode. Their photocurrents are converted into voltages, which are processed by the actuator controller to determine the direction and magnitude of the module's rotation. During testing, it was necessary to measure key electrical parameters of the PV modules, such as short-circuit current and open-circuit voltage. To ensure experimental reliability, measurements were taken continuously over extended periods, with data accumulation, storage, and subsequent analysis. For this purpose, a current and voltage measuring device was developed to record parameters in two independent DC circuits, enabling direct comparison of the energy performance of the tracking and stationary PVMs under identical solar irradiance conditions. In addition, the meter is equipped with a digital interface supporting up to six DS18B20 temperature sensors, which enhances the system's ability to monitor environmental parameters and assess the thermal behavior of PVMs during testing.

Results: During the experimental study, the dependence of the short-circuit current (ISC) of the PVM equipped with a solar tracking system was investigated and compared

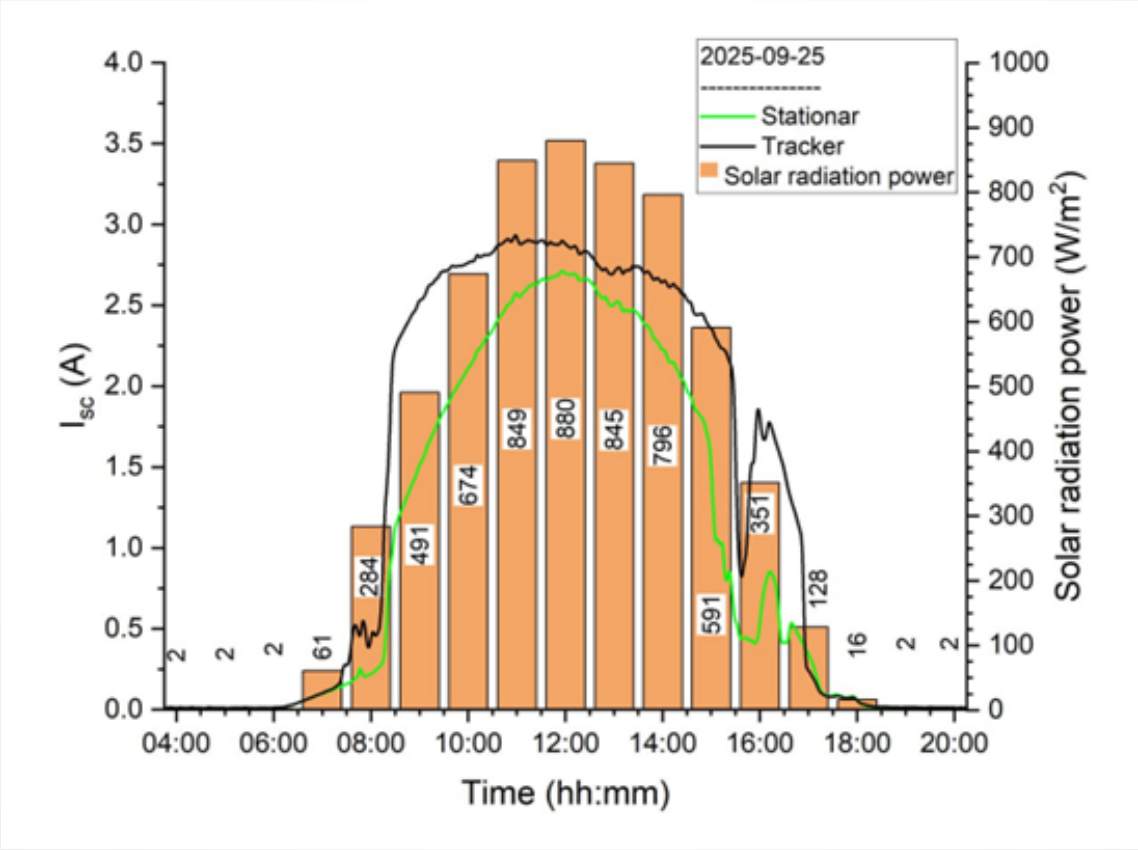

(a)

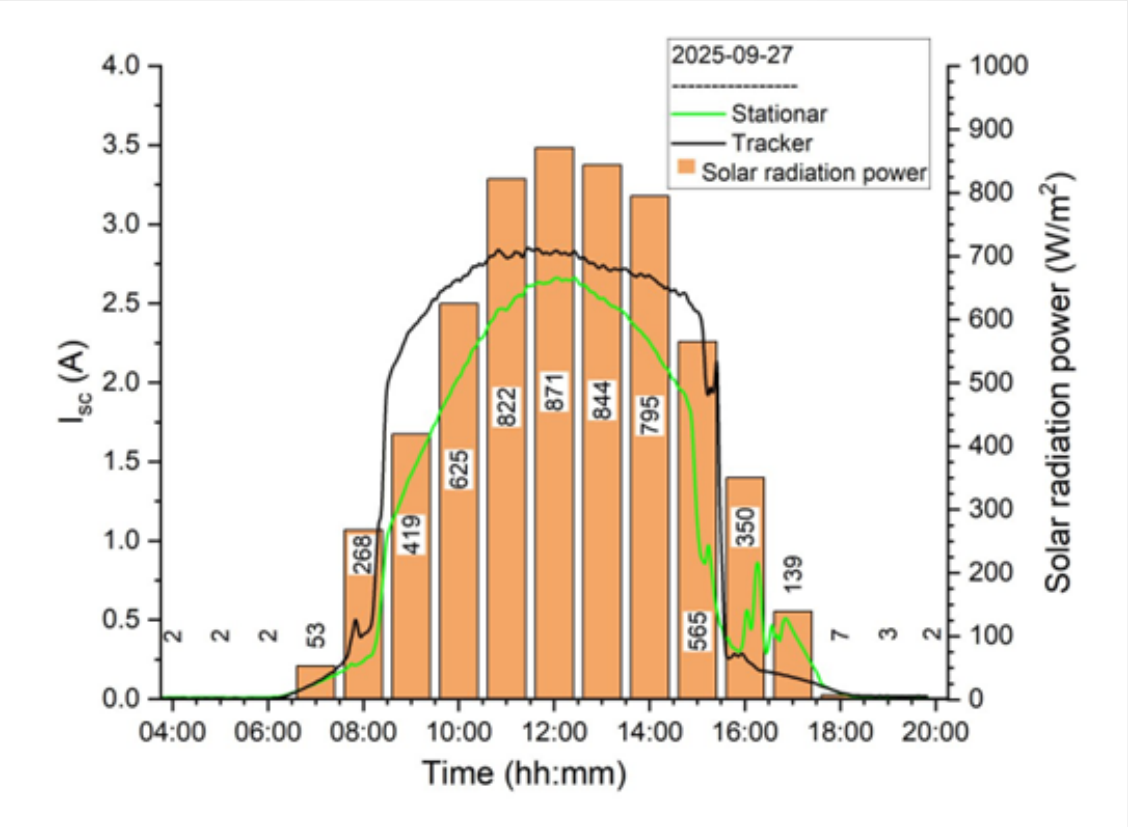

(b)

Fig. 1. Variation of photovoltaic module short-circuit current with solar irradiance

with that of an identical stationary module. The experiments were conducted at the heliopolygon of the Institute of Semiconductor Physics and Microelectronics (Tashkent). Representative measurement results obtained on September 25 and 27, 2025, are presented above (Fig. 1). The solar irradiance data were recorded using a YJ-SR100 pyranometer installed in a horizontal position. The results demonstrated that the PVM with the solar tracking system consistently exhibited higher short-circuit current values throughout the observation period compared to the stationary module. This enhancement is primarily attributed to the optimized angle of incidence of solar radiation on the surface of the photovoltaic cells during daylight hours. The most pronounced difference in current output between the two systems was observed during the morning and evening periods, confirming the effectiveness of the tracking mechanism in increasing the overall energy yield of photovoltaic installations.

Conclusion: Preliminary testing of the PVM equipped with a solar tracking device demonstrated a noticeable increase in its energy output compared to an identical stationary module, even when accounting for the energy consumption of the tracking system. The results confirm that the implementation of solar tracking technology provides a more uniform distribution of power generation throughout the day, across different seasons, and under varying weather conditions. This contributes to a more stable and predictable energy supply, which is a critical factor in enhancing the reliability and overall performance of photovoltaic installations.

Coalesce Research Group

13th International Conference on

Materials Science & Engineering

October 22-24 2025 | Tashkent, Uzbekistan

INVESTIGATION OF THE TEMPERATURE-DEPENDENT PHOTOVOLTAIC BEHAVIOR OF SILICON HETEROJUNCTION SOLAR CELLS WITH GALLIUM- AND PHOSPHOROUS-DOPED SILICON SUBSTRATES

Sh.B. Utamuradova, O.K. Ataboev* and F.R. Yuldoshov

Institute of Semiconductor Physics and Microelectronics at the National University of Uzbekistan named after Mirzo Ulugbek, Tashkent, Uzbekistan

Abstract

In this study, the temperature dependence of the photovoltaic (PV) performance of silicon heterojunction (HJT) SCs fabricated on Gallium- and Phosphorus-doped crystalline silicon (c-Si) substrates was investigated under the AM0 spectrum in the temperature range of 173–373 K. The experimental results show that the short-circuit current density (J_sc) of both cell types increases linearly with temperature, exhibiting positive temperature coefficients of 0.054%/K for n-type and 0.058%/K for p-type substrates, whereas the open-circuit voltage (V_OC) decreases. For n-type HJT SCs, V_OC demonstrates a more complex behavior: it increases from 0.547 V at 373 K to 0.693 V at 223 K, after which the rise slows, reaching 0.815 V at 173 K. Based on experimental results, the temperature coefficient of the maximum output power (P_max) was determined to be -0.31%/K for n-type and -0.20%/K for p-type HJT SCs.

Background: Over the past few decades, solar PV modules based on single-crystalline silicon technology have become the dominance in the PV market, currently representing for over 95% of the global share due to mature fabrication technology, abundant raw materials and cost-effectiveness [1]. Among various silicon-based PV technologies, Si HJT SCs have attracted considerable attention due to their excellent surface passivation and high open-circuit voltages enabled by intrinsic hydrogenated amorphous silicon (a-Si:H) layers. Recently, HJT SCs have achieved conversion efficiencies of up to 27.3% [2]. These advantages make HJT SCs highly attractive not only for terrestrial applications but also for space applications, where efficiency and stability are critical. In recent years, HJT SCs have attracted growing interest for space missions – particularly for Low Earth Orbit (LEO, 500–2000 km) [3]. However, SCs operating in LEO are subjected not only to high-energy particle radiation but also to extreme temperature fluctuations. Considering the above, studying the temperature dependence of the PV performances of HJT SCs fabricated on Gallium (p-type) and Phosphorous doped (n-type) Si substrates under AM0 spectrum (136.7 mW/cm^2) in the temperature range of 173–373 K is one of the urgent tasks.

Methods: Sample preparation To conduct study, HJT SCs (Fig. 1) were created on n- and p-type Czochralski (Cz) grown c-Si substrates. Prior to depositing a-Si:H layers on the n- and p-type c-Si substrates, the substrates underwent a wet chemical cleaning procedure. After, thin intrinsic a-Si:H layers were deposited on both front and rear surfaces of the textured substrates by PECVD. Using the same method to form p-n-junction, p- and n-type a-Si:H layers were deposited on the front side of the i-α-Si:H coated n- and p-type c-Si substrates, respectively. Simultaneously, to create the back-surface field, n- and p-type a-Si:H layers were deposited on the rear sides of i-α-Si:H deposited n- and p-type c-Si substrates. All a-Si:H layers were deposited at a low temperature of 180–185°C and a frequency of 40.68 MHz. Further, transparent conductive oxide layers (ITO – 90 wt.% In2O3 and 10 wt.% SnO2) were deposited on the front and rear surfaces of the photosensitive heterostructures. Finally, silver (Ag) busbar-type contacts were screen-printed onto both the front and rear sides of the photosensitive heterostructures at low temperature **(Fig. 1).**

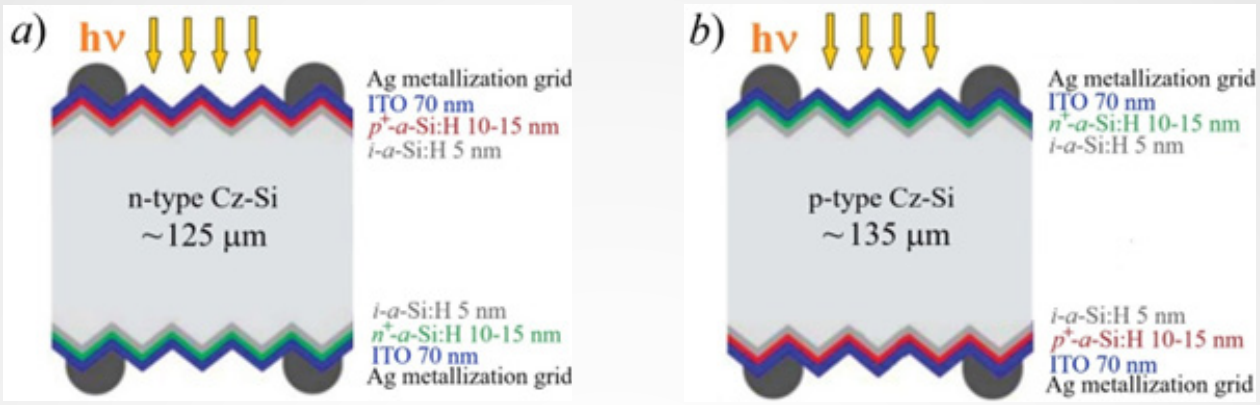

Fig. 1. A cross-sectional view of the finished HJT SCs based on n-type (a) and p-type (b) c-Si substrates.

To perform experiment, both n- and p-type c-Si samples with an area of 1 × 1 cm2 were cut from a high-efficiency HJT SCs with full-area dimensions of 15.6 × 15.6 cm2. No additional passivation was applied to the lateral surfaces, and edge isolation was not performed. A solid-state "MiniMaker2" diode laser with a wavelength of 1064 nm and a maximum power of 20 W was used for cutting the samples.

Characterization and measurement of performances

To study the effect of temperature on the output PV performance of HJT SCs, light J-V curves were measured using a liquid nitrogen cryostat (Janis VPF-100) in the temperature range of 173–373 K, in 20 K increments. During the measurements, the samples were illuminated using a class AAA pulsed solar simulator (SS-80AAA simulator) under AM0 spectral conditions (136.7 mW/cm2). The J_SC and V_OC were recorded using a Keithley SM2460 Source Meter.

For the investigation about 20 HJT SCs samples of each type conductivity were fabricated, which have similar parameters within a margin of error of no more than 2%. From these, two samples with 1x1 cm2 area – one based on n-type and the other on p-type c-Si were selected for temperature-dependence measurements.

Results: Fig. 2 presents temperature dependence of J_SC of HJT SCs based on n-type (curve 1) and p-type (curve 2) c-Si substrates under AM0 spectrum (136.7 mW/cm2). The J_SC values were determined from the experimentally measured light J-V curves. The experimental results demonstrate a linear increase in the J_SC with increasing temperature for both types of HJT SCs.

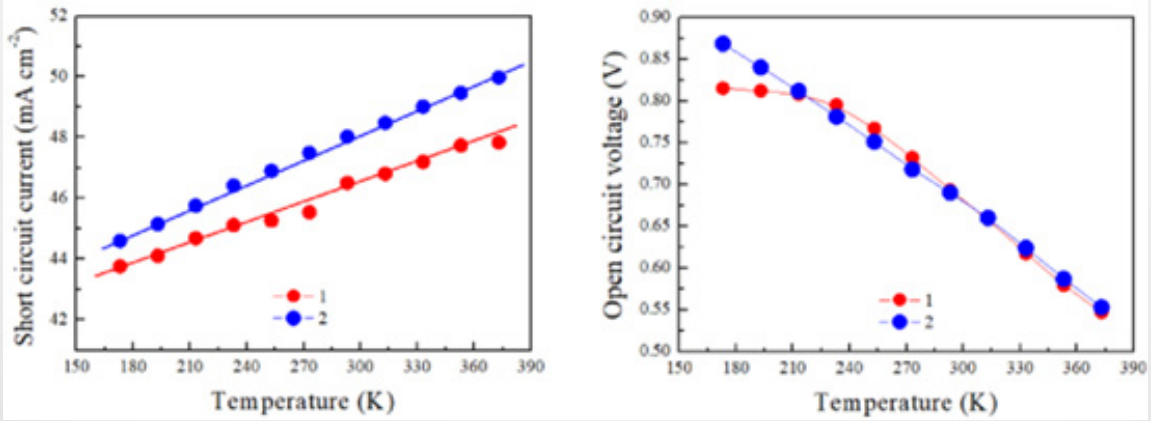

Fig. 2. Temperature dependence of J_SC and V_OC of HJT SCs based on n-type (curve 1) and p-type (curve 2) c-Si substrates under AM0 spectrum (136.7 mW/cm2).

As illustrated in Fig. 2, the J_SC of p-type HJT SCs (curve 2) is higher than that of cells based on n-type substrate (curve 1). This difference is presumably attributed to the variation in substrate thickness: the p-type wafer has a thickness of ~135 μm, which is approximately 10 μm greater than that of the n-type wafer (~125 μm). It is well established that photons with longer wavelengths - particularly those in the near-infrared region are more effectively absorbed in thicker substrates, whereas in thinner substrates they are more likely to transmit through without generating electron-hole pairs.

Based on the experimental results, the temperature coefficients of the short-circuit current density (TCJ_sc) was extracted from the slope of the linear region of J_SC versus temperature characteristics for HJT SCs based on n-type and p-type c-Si substrates. The calculated TCJ_sc values are 0.054%/K and 0.058%/K for n-type and p-type c-Si substrates, respectively.

Also, in the Fig. 2 presents experimental results of V_OC (T). As seen in Fig. 2, the experimental V_OC (T), demonstrates more complex behavior for HJT SCs based on n-type c-Si (curve 1), whereas for p-type c-Si-based HJT SCs, V_OC (T) exhibits an approximately linear dependence (curve 2). As shown in Fig. 2, the V_OC for n-type HJT SCs decreases linearly from 0.693 V to 0.547 V as the temperature increases from 293 K to 373 K. When the SC is cooled from 293 K to 173 K, the value of V_OC initially exhibits a linear rise, reaching 0.795 V at 233 K, after which the increase slows down and approaches saturation. For p-type HJT SCs, the V_OC increases linearly from 0.553 V to 0.8684 V as the temperature decreases from 373 K to 173 K.

Fig. 3 shows the temperature dependence of the maximum output power P_max (T) for n- (curve 1) and p-type (curve 2) HJT SCs under 136.7 mW/cm^2. P_max is determined by the product of J_sc, V_oc and FF.

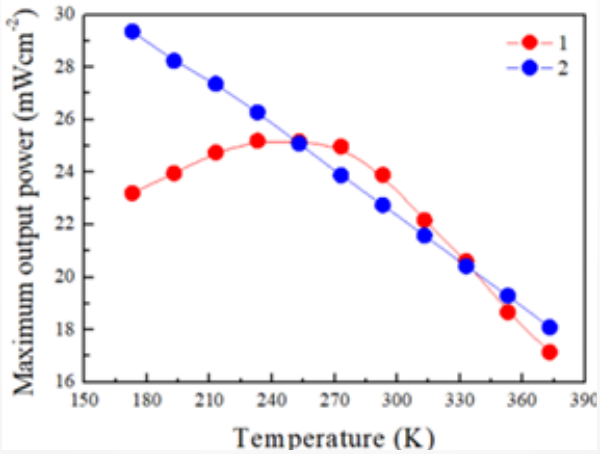

Fig. 3. Temperature dependence of the maximum output power of n- (curve 1) and p-type (curve 2) HJT SCs under AM0 spectrum (136.7 mW/cm2).

As shown in **Fig. 3** (curve 1), the P_max of n-type c-Si HJT SCs decreases linearly from ~25 mW/cm2 to ~17.2 mW/cm2 with increasing temperature from 273 K to 373 K. Upon cooling SCs from 273 K to 173 K, P_max initially exhibits a slight increase, reaching a peak of ~25.2 mW/cm2 at 233 K, followed by a linear decline to ~23.2 mW/cm2. In the studied temperature range, P_max of p-type c-Si HJT SCs (curve 2) exhibits a linear decrease, declining from ~29.4 mW/cm^2 at 173 K to ~18.1 mW/cm^2 at 373 K. The

temperature coefficients of the P_max (TCP_max) for n-type c-Si HJT SCs were evaluated to be -0.31%/K in the 273–373 K range and -0.15%/K in the 173–233 K range, while the corresponding coefficient for p-type c-Si HJT SCs was -0.2%/K over the 173–373 K interval. These results demonstrate that the investigated p-type c-Si HJT SCs exhibit the modest TCP_max among various silicon-based PV technologies.

Conclusion: This study presents a comprehensive investigation of the temperature dependence of the PV performance of HJT SCs fabricated on Gallium- (p-type) and Phosphorus-(n-type) doped c-Si wafers under AM0 spectrum (136.7 mW/cm2) in the temperature range of 173–373 K. The short-circuit current density of both cell types increases linearly with temperature, exhibiting positive temperature coefficients of 0.054 %/K for n-type and 0.058 %/K for p-type substrates. The open-circuit voltage (V_OC) demonstrates a distinct behavior for each cell type. For n-type HJT SCs, V_OC shows a complex, non-linear dependence: it increases from 0.547 V at 373 K to 0.693 V at 223 K, beyond which the rate of increase diminishes, saturating near 0.815 V at 173 K. In contrast, the V_OC for the p-type SCs decreases linearly from 0.868 V at 173 K to 0.553 V at 373 K.

Day-2
Keynote Presentations

ENHANCING MATERIALS SOUNDNESS IN DIFFERENT PROJECTS (PERFORMANCE , QUALITY, & LIFE CYCLE COSTING) THROUGH THE VALUE ANALYSIS TOOLS

Jamal Alduaij
Kuwait University, Kuwait

Abstract

Execution program and decisions in the projects industry (Infrastructure, Services, ICT, Manufacturing, Construction, Systems, etc.) are strongly attached to the expected returns; in the areas of economics, equity, and environment, or the so called 3e's of the sustainability measures. Deep analysis of those measures and criteria is the decisive tool in project directions for a successful result. Professional societies, practitioners, and researchers in the project material development fields monitored the outcomes of such projects and the levels of satisfactions. Technical, behavioral, and managerial factors (i.e. Communications, resource planning, time and cost estimations, requirements, criteria, administration, scope, and information), will be studied as principal signs of steadiness in the performance of projects. The sustainability aspects are the focus of the project program since they are the measures of how comprehensive the project is as a human product and activity, to serve in the three highlighted aspects. This presentation is targeting professionals' activities which are concerned with the development of proper materials in the projects through enhancing their soundness in all the project phases. Project materials, as human activities, are tremendously vital and crucial in our daily life. Value Analysis as an impact assessment tool will be implemented to deal with these activities for the said enhancement under the Sustainable Assessment Systems (SAS). Categories as the main sustainability indicators will be implemented and integrated according to the project materials requirements under these standards.

Biography

Jamal Alduaij is Civil Engineering with a Ph.D. from Colorado University. He is the Chairman of the consulting firm GCC Bureau and has held various managerial positions in academic, professional, and administrative fields. His specialty and experience fall in Project Development and Control under Sustainability Assessment Standards, Planning and Design of large-scale projects, and Project Assessment in different phases through Value Analysis Methodology. He has supervised several services and constructional projects, conferences, forums, symposiums, workshops, seminars, and career development programs, and has published several research papers and articles.

MACHINE LEARNING FOR LOGISTICS AND TRANSPORTATION ENGINEERING-GENDER DISPARITIES IN RURAL MOTORCYCLE ACCIDENTS: A NEURAL NETWORK ANALYSIS OF TRAVEL BEHAVIOR IMPACT

Ittirit Mohamad
King Mongkut's University of Technology Thonburi, Thailand

Abstract

Gender Road Accident Safety Machine learning Neural network Comparative analysis Prediction model Risk assessment Rural Road accidents involving motorcycle riders present a formidable challenge to road safety globally. This study offers a comprehensive gender-based comparative analysis of rural road accidents among motorcycle riders, aimed at illuminating factors contributing to accidents and discerning potential gender disparities in accident rates and severity. Employing a sophisticated Neural Network approach, the research delves into the intricate relationship between various variables and accident outcomes, with a specific emphasis on identifying gender-specific patterns. For female riders, the ANN model demonstrates impressive overall accuracy (CA) of 92 %, indicating its capability to correctly classify accident outcomes. Precision, which measures the model's ability to avoid false positives, stands at a commendable 90.8 %. Moreover, the model exhibits high recall (92 %) and F1 score (88.4 %), indicating its effectiveness in identifying both fatal and non-fatal accidents among female riders. Additionally, the Matthews Correlation Coefficient (MCC) of 0.132 suggests a moderate level of agreement between the predicted and actual outcomes. Upon further examination, it is evident that the model performs exceptionally well in predicting non-fatal accidents for female riders, achieving a precision, recall, and F1 score of 92 %, 99.9 %, and 95.8 %, respectively. However, its performance in predicted fatalities is relatively lower, with a precision of 75.6 % and recall of 2.6 %, resulting in a lower F1 score of 5.0 %. Despite this disparity, the MCC remains consistent at 0.132, indicating a balanced performance across both classes. The findings reveal valuable insights for policymakers and road safety practitioners, providing avenues for the development of targeted interventions and the enhancement of safety measures for motorcycle riders on rural roads. By addressing the gap in understanding gender-related differences in travel habits and accident risks, this research contributes to ongoing efforts to mitigate the impact of road accidents and promote safer travel environments for all road users

Biography

Ittirit Mohamad brings over a decade of industry experience, having served as an Engineering Quality Data Analytics Manager at a world-leading data storage company. He later earned a Commercial Pilot License (CPL) and a Doctor of Engineering degree, with a research focus on big data analytics and machine learning applications in logistics, smart manufacturing (Future Factory), and transportation engineering. Currently, he is a Lecturer in the Department of Production Engineering, Faculty of Engineering, King Mongkut's University of Technology.

NECESSARY REVISION OF CARBON SOLID STATE AND RAMAN SPECTROSCOPY FUNDAMENTALS FOR COMPREHENSIVE MASTERING OF MORE PERFORMING ADVANCED MATERIALS APPLICATIONS

Stephane NEUVILLE
Independent Scientific Consultant, France

Abstract

Considering the important potential of more advanced carbon materials for many different domains including mechanical and tribological applications, energy and electrochemical energy storage and conversion and nanotechnologies, their applications used to be hampered by several non-mastered and non-understood effects basing on non-satisfactory established fundamentals of the achievement and characterizing of more performing material structure. They have been very often confronted to conflictual interpretation of Raman spectroscopy and to some non-understood and/or little-known specific phase transformation, especially when these materials correspond to a wide distribution of different homogeneous or more complex polymorph crystalline and amorphous structures with frequently both quite poor and non-reproducible outstanding properties. Thus, needing to be revised to some extent. Much confusing the established definition of carbon Raman D and G bands and when some essential aspects used to be often neglected or incorrectly considered, especially concerning the hypothetical concept of Raman D' and G' peaks specific to atomic disorder, the superimposition of different substructures bands , the internal stress causing shifts of Raman signals which have then to be differently assigned, the locality of some specific phonon breathing modes, the role of atomic disorder on band broadening and last but not least, different sorts of phase transitions with either exothermal or endothermal atomic rearrangements. Last one corresponding to some almost ignored electronic quantum energy activation effects. Clearing comprehensively these aspects is expected to provide the perspectives of well mastered processes for many more performing application domains and particularly the achievement of more efficient production of green hydrogen and cheaper renewable energy, which can then be used for competitive modern transportation systems.

Biography

Stephane NEUVILLE obtained a degree in physics at INPG Grenoble with Louis Neel in 1970. After 25 years combined industrial and R&D field experience closely associated to General and Export Marketing and Sales Management with different international deep tech companies and technical and export manager positions in high-tech industries (RIBER, LEYBOLD, ITT, ALCATEL etc.) concerning many high-tech domains including vacuum plasma and coatings, scientific analytical instruments, microelectronics, nuclear, renewable energy, transportation systems and mechanical applications etc. For which he used to closely combine interactive R&D with financial and marketing realism and significant business developments. In 1996, PhD at Ecole Polytechnic (X) and Management diploma. He developed then deeper scientific expertise and acting over 15 years as an independent consultant during which he revisited also theoretic scientific and applied solid state fundamentals. In 2017, he received an ELSEVIER Award for recently developed outstanding scientific expertise in more advanced deeptech carbon materials. Being requested over100 times now, as an invited speaker and/or for plenary lectures and cession chairman positions for all sorts of international scientific conferences. With main published papers on applied and fundamental subjects concerning improved applications for different sorts of Energy and especially the different sorts of renewable energies. Becoming thus an expert being often requested for reviews of newly produced scientific results (nearly 2000 times since last ten years) and especially concerning some aspects of better understood carbon material mastering with higher combined properties including characterizing and process selections.

Coalesce Research Group

13th International Conference on

Materials Science & Engineering

October 22-24 2025 | Tashkent, Uzbekistan

IMITATION MODELING. THE BEHAVIOR ANALYSIS OF THE MIXTURE OF TWO OPPOSITELY CHARGED POLYELECTROLYTES WITH THE HELP OF A MACROSCOPIC MECHANICAL SYSTEM

Arkadii Arinstein

Technion Israel Institute of Technology, Israel

Abstract

Objective: To realize the idea of imitation modelling proposed by us recently, a mechanical system consisting of identical quantity of two type springs (20 ones of each type) having different elasticities and equilibrium lengths, was fabricated. To mimic a polymer network, all springs should be connected in such a manner that a quadrangular lattice will be formed, in doing so each node of this lattice should contain two springs of each type. As a result of such restriction, the springs of the one type form chains at any allowable spring distribution, and these chains can be considered as "polymer macromolecules".

Methods: Each random system configuration generated by computer, was assembled inside of metallic frame and photographed with further analysis with the help of the computer program including pattern recognition, image analysis. As a result, the system parameters (energy and order parameter) were calculated and collected for 256 generated configurations, differed by system orientational ordering when more springs of the one type are orientated along one direction (for example, along x- axis), whereas the orientation along other direction (along y-axis) is preferable for the other type springs.

Results: The statistical analysis of obtained data allows one to derive the dependence of the system energy vs. spatial distribution of the system springs (more exactly, their orientational ordering).

Using the obtained dependence, the statistical weight of each system state characterized by energy and orientational ordering, can be calculated (more exactly, the state portion corresponding to a narrow range of the above system parameters). Thereafter the system entropy as well as the free energy can be introduced, and the minimum of last corresponds to the system equilibrium state.

Conclusion: The above examining allows one to verify experimentally the outcomes of theoretical model analyzing the self-ordering in a 2D two-component system modelling the behavior of a mixture of two oppositely charged polyelectrolytes.

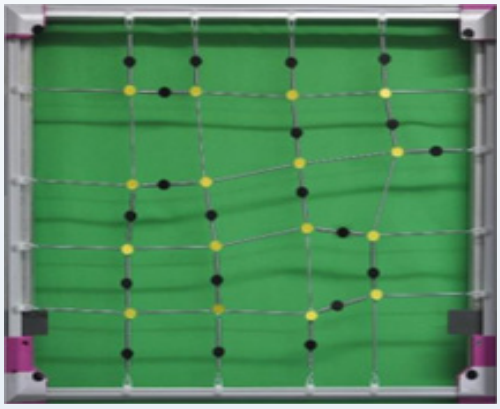

Biography

Arkadii Arinstein received his MSc degree in Theoretical Physics from Tomsk State University in 1977 and PhD degree in Theoretical and Mathematical Physics from the Landau Institute for Theoretical Physics of the USSR Academy of Sciences in Moscow in 1982. For many years he worked in the Semenov Institute for Chemical Physics of the Russian Academy of Sciences in Moscow, where received DSc (habilitation) degree in Chemical Physics in 1995. Now he is the Research-Professor Associate at the Technion-Israel Institute of Technology. Arinstein's re-search interests include statistical physics of polymers, non-linear phenomena in disordered systems. Last 20 years his research is related with nanotechnology and are devoted to polymer nanofibers.

Day-2
Oral Presentations

THEORETICAL AND SPECTRAL CHARACTERIZATION OF BIOLOGICALLY ACTIVE LN(III) COMPLEXES

Irena Kostova
Medical University, Bulgaria

Abstract

Extensive efforts are continually being put into research of complex compounds for medicinal purposes. Lanthanide-based coordination complexes of biologically active ligands have become the source of research and development for potential drug candidates with anticancer and antioxidant activity for last decades.

In the present study a series of bioactive complexes have been synthesized and thoroughly investigated. The physicochemical characterization of the newly obtained lanthanide(III) complexes has been performed using theoretical, spectroscopic and analytical techniques. The computational modelling supported by experimental results can explain the molecular structures, vibrational assignments, reactive sites and structural properties. In this context, to help the binding mode elucidation in the complexes, detailed vibrational analysis was performed on the basis of comparison of experimental (FT-IR, FT-Raman) vibrational spectra of the ligands and Ln(III) complexes with the DFT theory prediction.

The current study was carried out to evaluate the anticancer and antioxidant properties of the Ln(III) complexes. The in vitro cytotoxic activity of the studied compounds against cancer cell lines was determined by MTT assay. Taken together the results from the antineoplastic and antioxidant screenings give us reason to conclude that the lanthanide(III) complexes proved to be active cytotoxic and antioxidant agents and strengthen the potential of the complexes as a resource for the discovery of novel anticancer and antioxidant agents.

Acknowledgments: The administrative support received by the European Union-NextGenerationEU, through the National Recovery and Resilience Plan of the Republic of Bulgaria, project No. BG-RRP-2.004-0004-C01 is greatly acknowledged.

Biography

Kostova is one of the World's Top 1% of scientists according to Stanford University's ranking of scientists with the greatest contribution to the development of modern science. She graduated from Mendeleev University with the highest grade. Defended her PhD and DSc theses at MU-Sofia where she is currently a full professor. Author of hundreds of publications with high impact factor, several textbooks and monographs with thousands of citations. Lecturer at renowned European universities. Member of organizing committees of over 40 international conferences. Editor of 9 prestigious international scientific journals, a member of the Editorial Boards of over 25 international journals and a reviewer for high-ranking journals. She has created and maintains collaborations with a number of European universities in joint research projects and programs.

MORPHOLOGICAL CHARACTERISTICS OF NEMATIC DROPLETS DOPED WITH METAL NANOPARTICLES

Makhsudov Barot Islomovich
Tajik National University, Tajikistan

Abstract

Background: Polymer-encapsulated liquid crystal systems (PDLCs) are considered promising optical materials for optimization and use in display devices. Advances in this research field depend on the development of advanced materials with a low threshold field and high contrast ratio. When an electric field is applied, the director (the preferred orientation of molecules inside the droplet) of the liquid crystals aligns along the field, resulting in a transition from a state with strong scattering to a transparent state. However, due to the low contrast ratio and switching characteristics, the use of PDLC materials in display devices is limited. Therefore, to improve the contrast ratio, the use of liquid crystals doped with metal nanoparticles (NPs) has been proposed.

Objective: To investigate the electro-optical properties of a PDLC cell using cadmium sulfide (CdS) metal nanoparticles.

Methods: Polarization optical microscopy (POM) and differential scanning calorimetry (DSC).

Results: It was found that PDLC with a low concentration of nanoparticles significantly alters the optical properties (transmittance, threshold voltage, contrast and absorption coefficients) of the studied materials. It was established that, with constant UV radiation intensity, the concentration of the dye can be optimized to ensure a uniform droplet size, higher transmittance, and increased contrast ratio. Using the Beer-Lambert equation, absorption and extinction coefficients were obtained by measuring the transmittance of the PDLC cells. It was discovered that the liquid crystal droplets in the PDLC cells predominantly adopt a bipolar configuration. A higher concentration of metal nanoparticles leads to a decrease in the clearing temperature and a reduction in transmittance due to a lower order parameter caused by thermal fluctuations. Numerical calculations showed that the maximum contrast ratio for the PDLC cells with nanoparticles content is 2.55 times higher than the minimum contrast ratio of the films in their initial state.

Conclusion: Possible mechanisms for the implementation of the obtained results are proposed for the creation of flexible liquid crystal display elements used in environmentally friendly technologies.

Biography

Makhsudov Barot Islomovich – Doctor of Physical and Mathematical Sciences, Professor, Head of the Department of Nuclear Physics at Tajik National University. He is an expert in the fields of laser physics, optoelectronics, and photonics. Makhsudov B.I.'s research work primarily focuses on the development of new advanced materials for applications in micro- and nanoelectronics. He is the author of more than 180 scientific articles, 12 monographs, and educational-methodical guides. Under the supervision of Professor Makhsudov B.I., 6 PhD theses and 3 doctoral dissertations have been defended.

DEFECT ENGINEERING OF $PBWO_4$ SINGLE CRYSTALS BY HEAVY XE IONS

Ainash Abdrakhmetova
L.N. Gumilyov Eurasian National University, Kazakhstan

Abstract

In this work, the optical properties, radiation damage, and recovery processes of lead tungstate ($PbWO_4$) single crystals are investigated, with particular emphasis on the effects of heavy-ion irradiation and the mechanisms of intrinsic photoluminescence. $PbWO_4$ crystals are widely used in high-energy physics experiments as scintillation materials due to their high density, short radiation length, and radiation resistance. However, irradiation with high-energy Xe ions significantly modifies their optical and luminescent characteristics through the formation of radiation-induced defects.

Irradiation of the single crystals was carried out with Xe^{132} ions at an energy of 220 MeV using the DC-60 accelerator at fluences ranging from 1×10^{11} to 1×10^{14} ions/cm^2. Optical absorption and transmission spectra were measured before and after irradiation, and stepwise thermal annealing was performed within the temperature range of 340–910 K. At low and medium fluences, partial degradation of optical transparency and a shift of the absorption edge were observed, which were partially reversed upon annealing. At high fluences ($\geq1\times10^{13}$ ions/cm^2), irreversible damage occurred: the transparency was not restored even after thermal treatment, indicating the formation of stable defect complexes and critical structural degradation.

Additionally, the photoluminescence kinetics of non-irradiated crystals was studied under pulsed laser excitation (λ = 320 nm) at 300 K. Time-resolved measurements revealed a biexponential decay: the fast component ($\tau_1 \approx 7.37$ ns, ~47%) is associated with direct radiative transitions, while the slow component ($\tau_2 \approx 27.75$ ns, ~53%) corresponds to longer recombination processes. The emission maximum was located near 440 nm, attributable to charge-transfer transitions within the $[WO_4]^{2-}$ oxyanion complex and the relaxation of localized excitons.

Irradiation with heavy ions substantially alters the defect structure and optical behavior of $PbWO_4$. While radiation-induced defects can be partially removed by annealing at low and medium fluences, high fluences lead to irreversible structural breakdown. Controlled defect engineering via ion irradiation combined with thermal treatment thus offers new opportunities to enhance radiation tolerance and tailor the properties of $PbWO_4$, establishing it as a model material for the design of next-generation scintillators.

The work was carried out within the framework of the grant project AP25794899 of the Ministry of Science and Higher Education of the Republic of Kazakhstan.

Biography

Ainash Abdrakhmetova is a PhD and Senior Lecturer at the Department of Technical Physics, L.N. Gumilyov Eurasian National University, Astana, Kazakhstan. She received her Master's degree in Physics with honors in 2009 and her PhD in Physics in 2013. Her doctoral research was devoted to the study of oxygen-containing impurities and their effects on the luminescent properties of lithium fluoride crystals. She is a co-author of the innovative patent "Scintillation material – LiF-TiO_2 crystal" (2015) and the author of more than 30 scientific and methodological works, including 7 papers published in journals indexed in Web of Science and Scopus. Her research interests include radiation damage, defect engineering, and optical properties of scintillation materials such as $PbWO_4$ under heavy-ion irradiation. At present, she is the principal investigator of the project "Radiation Resistance of Scintillation Crystals to Heavy Ion Exposure" funded by the Ministry of Higher Education and Science of the Republic of Kazakhstan.

Coalesce Research Group

13th International Conference on

Materials Science & Engineering

October 22-24 2025 | Tashkent, Uzbekistan

PREPARATION OF ZWITTERIONIC SOLID POLYMER ELECTROLYTES FOR LITHIUM-ION BATTERIES

Chien-Hsiang Chang
National Cheng Kung University, Taiwan

Abstract

Background: Solid polymer electrolytes for high electrochemical performance lithium-ion batteries have attracted much attention due to their low flammability and high safety. However, solid polymer electrolytes are still a long way from commercialization due to their low ionic conductivity and lithium transference number.

Objective: To focus on separator coatings and zwitterionic monomers added to solid polymer electrolytes to improve battery performance.

Methods: Sulfonated polyetheretherketone (sPEEK) was coated on non-woven cellulose fibers as separators. Polyethylene glycol methyl ether methacrylate (PEGMEMA) was used as the main electrolyte matrix, and PEGMEMA was combined with zwitterionic monomer sulfobetaine methacrylate (SBMA) to prepare a solid polymer electrolyte precursor. Zwitterionic solid polymer electrolytes were then prepared by in-situ polymerization and applied to lithium metal batteries.

Results: The use of the sPEEK-coated cellulose separators could improve ionic conductivity. However, as the amount of sPEEK coating on the cellulose was increased, the porosity of the separator was decreased. The zwitterionic SBMA on the copolymer side chains could promote the dissociation of lithium salts and the transport of lithium ions, thereby reducing the cathode interfacial impedance.

Conclusion: The battery assembled with sPEEK-coated cellulose separator made of proper amount of sPEEK solution and liquid electrolyte had good performance. The battery with good performance and cycle stability could be fabricated by using the solid polymer electrolyte containing an appropriate amount of SBMA.

Biography

Chang received his Ph.D. degree in 1993 in Chemical Engineering at Purdue University, USA. His research interest is colloid and surface chemistry. Dr. Chang is now working as a professor at the Department of Chemical Engineering and vice dean of the College of Engineering, National Cheng Kung University, Tainan, Taiwan and serving as an Associate Technical Editor of the Journal of Surfactants and Detergents.

NOVEL HEM-BASED CATALYSTS FOR ENERGY AND ENVIRONMENTAL APPLICATIONS

Miran Čeh
Jožef Stefan Institute, Slovenia.

Abstract

Background: High-entropy materials (HEMs), including medium- and high-entropy alloys (MEAs and HEAs) as well as high-entropy oxides (HEOs), have recently attracted attention for their promissing catalytic properties. These materials, composed of three or more elements randomly distributed in a single-phase lattice, exhibit lattice distortions and uneven electron distribution between metals of different valences and oxygen vacancies in the case of HEOs. These features may enhance various catalytic reactions, positioning these materials as promising new catalysts.

Objective: To use HEMs (MEAs, HEAs, HEOs) with various compositions as catalysts for hydrogen evolution reaction (HER) and for tetracycline degradation.

Methods: HEM materials tested in our studies (Cantor-based MEAs and HEAs: CoFeNi, CoFeNiMn, CoFeNiCr, CoFeNiMnCr; HEA with the composition TaNbHfZrTi) were either used as pristine materials in catalytic experiments or were previously anodized in custom made electrolytic cells and subsequently heat treated in order to either form a thin layer of HEO on the surface of pristine materials or to induce growth of ordered HEO nanotubes arrays similarly as in anodically treated metal titanium.

Results: Cantor-based MEAs and HEAs used in HER demonstrated promising activity when benchmarked against Pt foil. Tafel slope analysis showed that lower slopes were observed for alloys containing multiple matrix phases. All samples showed high electrochemical stability in alkaline environments, some composition were stable even in acidic environment. TaNbHfZrTi HEA, used for photo-, electro-, and photoelectrocatalytic (PEC) degradation studies of tetracycline, showed that the most efficient was photoelectrocatalytic (PEC) degradation of tetracycline, which yielded up to 86% degradation of tetracycline after three reuse cycles over a three-hour period.

Conclusion: Our results emphasize the potential of HEMs as efficient and durable (photo)electrocatalysts. Their adjustable properties, driven by high-entropy design principles, offer new strategies for using these materials in various catalytic applications for energy and in environment.

Biography

Miran Čeh has large expertise in investigation of structure and chemical composition of materials using advanced electron microscopy techniques on micro-, nano and atomic level. More recently he is involved in studies of new generation materials for catalytic applications. He is scientific advisor at the Nanostructured Materials Dpt. at the JSI, full professor at the Faculty of Chemistry and Chemical Engineering at the UniversityMaribor and at the Jožef Stefan International Postgraduate School. He is also the head of the Center for Electron Microscopy and Microanalysis Center (CEMM) at the JSI.

THE MECHANISM OF HETEROGENEOUS ALKALINE DEACETYLATION OF CHITIN

Svetlana Derkach
Murmansk Arctic University, Russia

Abstract

Background: Chitosan is obtained based on the chitin deacetylation reaction (acetamide group hydrolysis reaction), which is accompanied by the cleavage of the acetyl group from the structural unit of chitin with the formation of an amino group.

Objective: The analysis of experimental results on the study of alkaline heterogeneous deacetylation of chitin, obtained by the authors, as well as published in the scientific literature, is carried out.

Methods: A detailed analysis of the reaction kinetics is carried out taking into account the influence of reaction reversibility, crystallinity and porosity of chitin, changes in the morphology of chitin during washing, alkali concentration, diffusion of hydroxide ions, hydration of reacting particles.

Results: It is shown that the rate of deacetylation of chitin increases with a decrease in the degree of hydration of hydroxide ions in an aqueous highly concentrated alkali solution. At an alkali concentration below the limit of complete hydration, the reaction practically does not occur. Hypotheses are put forward to explain the decrease in the rate (inhibition) of the reaction in the second flat section of the kinetic curve. The first hypothesis is the formation of "free" water, leading to the hydration of chitin molecules and a decrease in the reaction rate. The second hypothesis postulates the formation of a stable amide anion of chitosan, which prevents the nucleophilic attack of the chitin macromolecule by hydroxide ions.

Conclusion: Establishing the mechanism of the chitin deacetylation reaction is of practical importance for the development of chitosan production technologies, and also makes a theoretical contribution to understanding the role of the solvent and hydration processes when considering the kinetics of heterogeneous reactions. The work is supported by Russian Science Foundation, project No 25-16-00064.

Biography

Svetlana Derkach, Doctor of Science, Professor, Professor of Chemistry Department of Murmansk Arctic University, Chief Researcher of the Laboratory "Chemistry and Technology of Marine Bioresources", Murmansk, Russia. S. Derkach is the head of the scientific direction of the university: "Properties of multicomponent systems containing surfactants and biopolymers; development of compositions for practical application"; the head of the master's program "Physical and Colloid Chemistry"; author of 10 monographic reviews and monographs, author of more than 150 scientific articles in the field of biopolymer chemistry and their application; expert of the Russian Science Foundation, the head of international scientific projects in the field of biopolymer.

Coalesce Research Group

13th International Conference on

Materials Science & Engineering

October 22-24 2025 | Tashkent, Uzbekistan

VALORIZATION OF MINING AND METALLURGICAL WASTE FROM METAL EXTRACTION: GLOBAL TRENDS AND INITIATIVES

Irina Marinova
Bulgarian Academy of Sciences, Bulgaria

Abstract

Background: In recent decades, many national strategies and policies around the world have embraced the principles of the circular economy, which promote the utilization of industrial waste, including mining and metallurgical waste, for the recovery of secondary raw materials, products, and energy (e.g., European Commission, 2015). The concept of a circular economy arises from the recognition of the planet's finite natural resources, the environmental degradation caused by human activity, the need for sustainable economic development, and the anticipated growth of the global population, which will lead to increased consumption of natural resources.

Objective: The objective of this work is to highlight global experiences in the valorization of mining and metallurgical waste derived from metal extraction processes.

Methods: The authors critically review the literature on tailings dams and heaps, which are used to store large volumes of ground barren rock, metallurgical slag, and related by-products.

Results: The review demonstrates that mining and metallurgical waste can serve as substitutes for non-renewable natural resources, which are continuously being consumed and depleted. Furthermore, their utilization can help reduce CO_2 emissions that contribute to climate change. In addition, recycling such waste conserves agricultural land and water, lowers energy consumption, and enhances the supply of critical and strategic raw materials, including rare earth elements.

Conclusion: Research conducted at various scientific institutions worldwide has shown that mining and metallurgical waste from metal extraction can be effectively used as an additive in the production of geopolymers, cement, concrete, mortar, ceramics, insulation, and fireproofing materials. It is also a potential source for the extraction of critical and strategic raw materials, such as rare earth elements.

Biography

Irina Marinova possesses strong field and research experience in the exploration of base metal and gold deposits in Bulgaria. Her careful examination of mineral textures in the field, mines, and hand specimens, combined with a solid understanding of their mineralogical, chemical, and microscopic characteristics, has enabled her to develop genetic models that are valuable for mineral exploration. Her most notable contributions have been published in prestigious journals such as Mineralium Deposita and Geology of Ore Deposits. Over the past year, she has focused her research on mining and metallurgical waste from metal extraction, with an emphasis on their recycling and valorization.

Coalesce Research Group

13th International Conference on

Materials Science & Engineering

October 22-24 2025 | Tashkent, Uzbekistan

ORIENTATION-DEPENDENT DEFECT FORMATION IN $MGAL_2O_4$ CRYSTALS UNDER SWIFT HEAVY ION IRRADIATION

Abdirash Akilbekov

L N Gumilyov Eurasian National University, Kazakhstan

Abstract

Background: Magnesium aluminate spinel ($MgAl_2O_4$, MAS) is a wide bandgap dielectric (Eg ≈ 8 eV) used as a substrate for light-emitting devices and as a model system for studying radiation–matter interactions. Swift heavy ion (SHI) irradiation produces a variety of point and extended defects in MAS, which can be analyzed by optical spectroscopy and electron paramagnetic resonance (EPR). The crystallographic orientation plays a сукефшт role, with the (111) plane containing "wells" ion-free channels extending through the unit cell-potentially affecting defect formation.

Objective: To investigate the features of defect generation in $MgAl_2O_4$ single crystals with different crystallographic orientations ((100), (110), and (111)) under 220 MeV Xe ion irradiation.

Methods: Single crystals of MAS with orientations (100), (110), and (111) were irradiated under SHI. Optical absorption in the VUV–UV range was measured using a Thompson polarizer, while EPR spectroscopy was employed to identify irradiation-induced paramagnetic centers and assess angular and azimuthal dependencies.

Results: Optical absorption spectra of pristine and irradiated samples revealed characteristic F and F^+ centers and additional optically active defects below 4.5 eV. For (100) and (110) orientations, absorption intensity between 3.5–4.5 eV increased upon rotating the polarizer by 90°, an effect absent in the (111) plane. EPR spectra showed additional signals between the third and fourth Mn^{2+} hyperfine bands, attributed to vacancies trapping unpaired carriers. These signals demonstrated angular and azimuthal dependencies, similar to those previously observed under neutron irradiation, confirming orientation-sensitive defect formation.

Conclusion: Defect generation in MAS under SHI irradiation depends strongly on crystallographic orientation. The anisotropy of optical and EPR responses highlights the role of lattice geometry in controlling radiation-induced defects, offering insights for radiation-hard materials and spinel-based optoelectronic applications.

Biography

Akilbekov is a specialist in solid-state radiation physics with extensive experience in research, teaching, and postgraduate training. He completed his internship and postgraduate studies at the Institute of Physics, Academy of Sciences of Estonia, defending his Candidate of Sciences degree in 1985 and his doctoral dissertation in 2004 on "Stabilization and Association of Radiation Defects in Face-Centered Alkaline Halide Crystals." His current research focuses on the modification of dielectric properties under ion irradiation, optical spectroscopy, pulsed cathodoluminescence, track technology, and template synthesis of nanomaterials. He is the author and co-author of more than 100 scientific papers and has supervised 1 Candidate of Sciences and 15 PhD graduates. Prof. Akilbekov is the recipient of the Satpayev State Prize (2020) and was recognized as The Best University Lecturer in 2007, 2012, and 2022.

WASTE MULLITE USED FOR REFRACTORY LINING OF THE COMBUSTION FURNACE

René Sommr
SMS CZ s.r.o., Czech Republic

Abstract

Background: Incineration of industrial waste is one of the operations where it is necessary to follow the technological process and regime in a suitable type of equipment. Given the diversity of waste, it is also necessary to choose an appropriate material for the furnace lining that can withstand high temperatures and a reducing environment.

Objective: Utilization of coal waste ash containing "mullite" to create a new active layer of the combustion furnace lining.

Methods: The choice of material for lining the inner layer of an industrial combustion furnace is crucial, as the material can melt onto the walls. Based on the development, we have verified that a suitable material is waste ash from the combustion of black coal from the Silesian Basin in the Czech Republic. This ash contains up to 70% mullite. We measured the thermal conductivity of the prepared test sample. The value was from 0.5 to 0.6 ($W.m^{-1}.K^{-1}$). The specific weight of the lining was 1744 $kg.m^{-3}$. The thermal expansion was ±0.5% at a temperature of around 1200°C. The resulting flue gases are then freed from sulphide at high temperature. CaO has proven itself as a sorbent at a temperature of 750 to 800°C.

Results: We created the corresponding parts of the lining for an industrial combustion furnace according to the project. The furnace was equipped with an internal heat source. After burning the lining, we burned the waste ion exchanger with an active sulfo group as part of the warranty tests. The resulting exhaust gases contained 0.8 to 0.96% of sulfane. These flue gases were passed through a CaO layer. After flue gas desulfurization, the flue gases were fed into cogeneration.

Conclusion: The main objective of the project was to use waste ash for furnace lining with subsequent assessment of environmental impacts.

Biography

René Sommr and the company SMS CZ Technology has been dealing with the issue of waste incineration for almost 20 years. The incineration unit itself is a high-tech device that presents a wide range of modern knowledge in the field of materials, the combustion process, its management and achieves the maximum degree of burnout of the combustible part of the waste. A completely separate and comprehensive issue of waste incineration is also the extraction of heat and its use and, in particular, the cleaning of flue gases from the combustion process. This part of the technology is designed completely individually, with the choice mainly being made between the so-called "dry or wet" cleaning, or even a combination of both systems. The most basic basis for the combustion technology project is the operational economic and ecological aspect with an impact on the environment.

HIGH-ENTROPY SHAPE MEMORY ALLOYS FOR HIGH OR CRYOGENIC TEMPERATURES APPLICATIONS

Aleksei Sibirev
Saint-Petersburg State University, Russia

Abstract

Background: High-entropy shape memory alloys (HESMAs) are unique materials that combine the high yield strength and exceptional mechanical strength of high-entropy alloys with the shape memory effect and superelasticity of traditional shape memory alloys. The Ti-Hf-Zr-Ni-Cu-Co system is considered particularly promising for applications across a wide range of temperatures.

Objective: Characterization of 16 senary Ti-Hf-Zr-Ni-Cu-Co alloys with varying compositions.

Methods: Ti-Hf-Zr-Ni-Cu-Co alloys were synthesized in a vacuum arc furnace under an argon atmosphere. Their martensitic transformations were investigated via differential scanning calorimetry (DSC) and electrical resistivity measurements, while the microstructure was characterized using SEM/TEM. The alloys' functional properties were evaluated through a series of mechanical tests.

Results: It was found that the alloy with the equal concentrations of the Hf, Zr, Cu and Co atoms were characterized by a high a yield limit for dislocation slip and underwent the martensitic transformation at extremely low temperature. This made possible them to demonstrate the superelasticity in a wide temperature range from -150°C to 0°C. It was observed that if the concentration of the Hf significantly exceeded the concentration of the Ti and Zr atoms, it increased the transformation temperature. Such alloys reveled the shape memory effect at high temperatures (over 200°C). The alloy with high concentration of the Hf and Ni atoms compared to the Ti, Zr, Cu and Co atoms demonstrated the shape memory effect at temperatures over 500°C.

Conclusion: Ti-Hf-Zr-Ni-Cu-Co senary alloys demonstrate martensitic transformation over a wide temperature range and possess superior functional properties compared to traditional shape memory alloys.

Biography

Alexey Sibirev is a Lead Researcher in the Department of Physical Mechanics at Saint Petersburg State University. A specialist in materials science with over a decade of experience, his research is centered on smart and functional materials, particularly shape memory alloys (SMAs). Dr. Sibirev has a strong experimental background, specializing in the mechanical testing and thermomechanical characterization of alloys like TiNi and novel multi-component systems such as Ti-Hf-Zr-Ni-Cu-Co. He has successfully led multiple national research grants, including projects from the Russian Science Foundation, and has authored over 30 scientific publications in reputable international journals. His work focuses on understanding martensitic transformations and functional fatigue to improve the performance and stability of SMA-based actuators and devices.

THERMAL CYCLING STABILITY OF THE FUNCTIONAL PROPERTIES OF THE NITI-BASED SHAPE MEMORY ALLOYS

Natalia Resnina
Saint-Petersburg State University, Russia

Abstract

The NiTi-based shape memory alloys are perspective for space and aircraft engineering due to their unique possibility to recover a large unelastic strain (up to 10 %) on heating or unloading and generate a high recovery stress (up to 500 – 1000 MPa). One of widely used applications is repeat action actuators. For such devices, the thermal stability of the shape memory alloy properties on thermal cycling is a key factor. The NiTi-based shape memory alloys demonstrate a weak thermal stability of the functional properties on thermal cycling. Thus, there is a great challenge to improve the thermal cycling stability. In the present study, the influence of possible reasons such as chemical composition, grain size, defect density, yield limit for dislocation slip, ordering on the variation in the martensitic transformation temperatures were investigated in the binary, ternary, quaternary and senary NiTi-based alloys. The samples were in as cast state or as melt spun ribbons which were subjected to crystallization to transform the amorphous state to crystalline. All samples were subjected to 500 thermal cycles in a temperature range of the martensitic transformation. The martensitic transformations were studied by differential scanning calorimetry and resistivity measurements. The dislocation density was measured by X-ray analysis, resistivity measurement and electron back scattering diffraction. It was found that the chemical composition did not affect the thermal cycling stability of the martensitic transformations. It was first observed the absence in the correlation between the dislocation density variation and reduction in the martensitic transformation temperatures on thermal cycling. It was first found that thermal cycling led to the disordering of the NiTi phase that decreased the transformation temperatures. Two compositions of quaternary alloys which showed the perfect stability of the recoverable strain variation on thermal cycling (at least on 500 cycles) were found which might be successfully used for application in microelectronics. The study was supported by Russian Science Foundation (# 23-19-00280).

Biography

Resnina Natalia has her expertise in experimental study of the relation between the structure, martensitic transformations, functional and mechanical behaviour in the NiTi-based shape memory alloys. Last ten years, her scientific interest was focused on a study of the martensitic transformation and shape memory behaviour in the multi-component NiTi-based shape memory alloys including the high-entropy shape memory alloys. It was found the influence of the configuration entropy on the structure, temperatures of the martensitic transformations, mechanical properties and the shape memory effects in the Ti-Hf-Zr-Ni-Cu-Co alloys. One of the main scientific interest is a study of the ways for improvement of the thermal cycling stability of the functional properties of the NiTi-based alloys. She is the member of Advisory Committee of the International conference on the martensitic transformation (ICOMAT) and co-chair of the conference "Shape memory alloys".

Day-2
E-Poster Presentations

INNOVATIVE SENSOR TECHNOLOGIES FOR HEAVY METAL ION DETECTION IN WATER: THE ROLE OF IOT IN SUSTAINABLE WATER RESOURCE MANAGEMENT

Babankumar S. Bansod
CSIR - Central Scientific Instrument Organisation, India

Abstract

Heavy metal ion contamination poses a serious threat to both human health and the environment, underscoring the need for precise and real-time monitoring solutions. This study presents recent innovations in sensor technologies developed for detecting heavy metal ions in aquatic systems. It examines the transformative impact of the Internet of Things (IoT) on advancing water resource management.

Recent advancements in electrochemical, optical, and biosensor technologies have enabled the development of highly sensitive and selective platforms capable of detecting trace concentrations of toxic metal ions. These advancements offer significant benefits in terms of sensitivity, specificity, miniaturisation, and cost-effectiveness.

Furthermore, the integration of IoT-based sensor networks facilitates continuous, real-time monitoring of water quality. By enabling seamless data acquisition, analysis, and transmission to centralised systems, IoT technologies empower data-driven decision-making and timely interventions to mitigate contamination and optimise resource distribution.

This work underscores the synergistic interplay between advanced sensor innovations and IoT frameworks in addressing the challenges of heavy metal pollution and ensuring the sustainable management of water resources. Leveraging these combined technologies can safeguard public health, protect ecosystems, and support a resilient and equitable water future.

Biography

Babankumar S. Bansod is a leading Senior Principal Scientist at CSIR-CSIO, Chandigarh, dedicated to developing innovative electrochemical devices and sensors. His primary focus lies in creating real-time water quality monitoring solutions, particularly for detecting toxic heavy metal ions in water. Dr Bansod's proposed sensor scheme holds immense potential for deployment at water distribution and treatment plants in both urban and rural settings. This system would enable real-time water quality monitoring through an IoT-enabled cloud-based network. The user interface could include mobile applications and other software systems for easy access to crucial water quality data.

PTNPS-COATED GOLD SURFACE FOR HIGH-PERFORMANCE ELECTROCHEMICAL SENSING OF LEAD IN ENVIRONMENTAL SAMPLES

Monika Antil
CSIR-Central Scientific Instrument Organization, India

Abstract

Background: Lead ion (Pb2+) contamination is a critical environmental and public health concern, driving the urgent need for highly sensitive and selective detection methodologies. Traditional methods often fall short in terms of on-site applicability and detection limits, highlighting a gap in current monitoring capabilities.

Objective: Our primary objective was to develop and thoroughly characterise an innovative, highly effective electrochemical sensor for the ultra-sensitive and selective detection of Pb2+ at trace levels in real-world environmental samples.

Methods: We engineered a sophisticated sensing platform centred on a gold electrode ingeniously coated with citrate-capped platinum nanoparticles (PtNPs). This unique architecture significantly amplifies the electrode's surface area and catalytic activity, crucial for enhancing sensitivity and accelerating electron transfer kinetics. The sensor's electrochemical performance was rigorously assessed using square wave voltammetry (SWV), a highly sensitive technique. We meticulously evaluated key analytical parameters, including detection limit, sensitivity, linear dynamic range, and selectivity against common interfering ions. To validate its practical utility, the developed sensor was applied to the analysis of real-world groundwater samples collected from a polluted area in Panipat, India.

Results: The developed sensor demonstrated exceptional analytical performance, achieving an impressive detection limit of 0.024 μM for Pb^{2+}, confirming its capability for detecting even trace-level concentrations. It exhibited high sensitivity (38.4 μA μM^{-1}) and a robust linear range (0.1–0.5 μM) with an excellent correlation coefficient (R2=0.98, RMSEC 0.02), ensuring precise and accurate quantification. Crucially, the sensor displayed remarkable selectivity, effectively distinguishing Pb^{2+} from common interfering substances often found in environmental matrices.

Conclusion: This robust and repeatable electrochemical sensing platform, which synergistically combines the advantages of PtNPs on a gold substrate with the high sensitivity of SWV, represents a promising and practical solution for effective on-site environmental monitoring of lead contamination.

Biography

Monika Antil is a distinguished Prime Minister Fellow and Research Scholar at CSIR-Central Scientific Instruments Organisation (CSIR-CSIO), Chandigarh, pursuing her Ph.D. in Chemical Science through the Academy of Scientific and Innovative Research (AcSIR) since 2020. She holds an M.Tech (8.79 CGPA) in Chemical Engineering from Deenbandhu Chhotu Ram University of Science & Technology. Her research focuses on developing advanced electrochemical sensors for in-situ multi- analyte heavy metal detection in water, specifically employing electrodes, electrochemical techniques, and nanomaterials. Monika has presented at over 21 national and international conferences, boasts 34 publications/workshops, and has received numerous accolades, including the Prime Minister Award – 2022, the Young Scientist Award in Engineering 2024 and the Young Scientist Award 2025. She is a lifetime member of four professional societies, including the Catalysis Society of India.

Coalesce Research Group

13th International Conference on

Materials Science & Engineering

October 22-24 2025 | Tashkent, Uzbekistan

THE EFFECT OF MECHANICAL ACTIVATION ON THE STRUCTURAL AND PHASE STATES AND HYDROGEN ABSORPTION PROPERTIES OF THE LANI$_5$ INTERMETALLIC COMPOUND

Nassyrova Anar

NJSC East Kazakhstan University Named after Sarsen Amanzholov, Kazakhstan

Abstract

The paper provides an overview of a number of studies on the use of alloys and intermetallic compounds for hydrogen storage. These materials have long been considered as a promising component of hydrogen energy due to their ability to form stable hydrides. Among them, the intermetallic compound Lani$_5$ occupies a particularly important place, which is characterized by a high reversible hydrogen absorption capacity and good cyclic stability at moderate temperatures and pressures. The latest achievements in the field of development and optimization of intermetallic compounds of type Ab$_5$ are analyzed. These compounds, in particular LaNi$_5$ and its doped analogues, are widely used due to the possibility of adjusting their properties by replacing elements. The paper also provides an overview of methods for the synthesis and modification of Ab$_5$ alloys aimed at increasing their efficiency in hydrogen technologies. Both traditional production methods (melting in arc and induction furnaces) and modern technological approaches, including spark plasma sintering and mechanical activation, are considered. A review of the scientific literature has shown that mechanical activation is an effective method of modifying the intermetallic compound LaNi$_5$ in order to improve its hydrogen-absorbing properties. According to a number of studies, the effect of high-energy ball grinding leads to significant changes in the microstructure of the material. To increase the efficiency of LaNI$_5$'s practical application in hydrogen energy, further comprehensive studies are needed to establish the relationships between the parameters of mechanical processing, structural characteristics and functional properties of the material. The aim of this work is to use mechanical activation to modify the microstructure of a material, reduce the size of crystallites, increase the density of defects, and promote the formation of amorphous or nanostructured.

Background: Hydrogen is an efficient and environmentally friendly energy carrier, and the separation of this gas from mixtures is a promising area of membrane technology. Hydride-forming metals, whose permeability to other gases is very low, have a unique selectivity with respect to hydrogen. Hydrogen transfer begins with the dissociation of H_2 molecules into atoms on the metal surface, which subsequently diffuse into the membrane volume, followed by recombination and desorption. Among the thermometallides containing rare earth elements, LaNi$_5$ type alloys are the most well-known. After the discovery of the hydride-forming ability of LaNi$_5$ in 1970, a real breakthrough began in the research of hydride-forming ICS. The subsequent surge in research led to the widespread use of nickel-metal hydride (Ni-MH) batteries and the development of technologies for hydrogen storage.

LaNi$_5$ is a typical representative of hydride-forming ICS of the AB5 class. This compound forms LaNi$_5$H$_6$ hydride at room temperature and pressures slightly higher than atmospheric (from 1.6 atm). This hydrogen content corresponds to 1.38% by weight. The hydride decomposes easily with a slight increase in temperature or with a decrease in pressure to form the initial IMC and hydrogen. LaNi$_5$ contains 1.5

times more hydrogen atoms per unit volume than liquid hydrogen. At room temperature, the intermetallic compound is saturated with hydrogen in less than 10 minutes, and most of the gas is absorbed in the first 3-5 minutes. Like other ICS of the AB5 composition, $LaNi_5$ has a high hydrogen storage density, resistance to gas impurities and multiple hydrogenation-dehydrogenation cycles.

Objective: To analyze the literature and determine the effect of mechanical activation on the structure and water-absorbing properties of metal hydrides based on the intermetallic compound $Lani_5$ in order to increase their efficiency for use in hydrogen storage systems.

Methods: The hydrides of intermetallic compounds have been well studied and are already widely used in practice. Intermetallides of the AB5 type (for example, $LaNi_5$), AB2 (for example, ZrV2), A2B (for example, Ti2Ni), and AB (for example, TiFe) containing rare earth and/or transition metal atoms are of interest for hydrogen storage. Hydrides are usually easily formed by the interaction of these compounds with hydrogen at 290-475K and pressures 0.1-1.0 MPa. Hydrogen desorption for a number of compounds occurs at 475-775K (and even at temperatures close to room temperature) and pressures 0.01-0.2 MPa. Hydrides have a high volume density in hydrogen, but the mass capacity does not exceed 3%. Partial replacement of the main components A and B with various elements (Ti, V, Cr, Mn, Ni, Fe, Co, Y, Ce, Cu, Zn, etc.) and even additives such as oxygen, nitrogen, carbon (for example, to Ti_2Ni) can slightly increase the sorption capacity, improve the characteristics and reduce the cost.

During the mechanical activation treatment, the position of the characteristic peaks remains unchanged. This means that after 1 and 3 minutes of processing in a ball mill, the crystal structure of the IMC is preserved. However, with an increase in the time of mechanical activation, the characteristic peaks widen, which indicates a regular decrease in the size of the coherent scattering regions of the DCR and an increase in the concentration of microstress ε [**Table 1**]. This effect is especially noticeable after 3 minutes of machining.

The characteristic peaks of hydrides are shifted relative to the peaks of non-hydrogenated compounds, which indicates a significant change in the parameters of the crystal lattice. The volume of the unit cell increases after hydrogenation, which is associated with the incorporation of hydrogen atoms into the structure. The different peak displacement indicates a different maximum composition of the hydride in the case of each IMC. For $LaNi_{4.8}Al_{0.2}$ and $LaNi_{2.5}Co_{2.4}Mn_{0.1}$, the relative volume increase is 15-20%, indicating the presence of a β-hydride phase. For alloys with an equilibrium hydrogen desorption pressure exceeding atmospheric pressure ($LaNi_5$ and $La_{0.7}Ce_{0.3}Ni_{4.5}Cu_{0.5}$), two coexisting phases with different hydrogen contents were found – α-solid solution and β-hydride. In the case of mechanically activated alloys, there is a smaller increase in the volume of the unit cell after hydrogenation than for the initial samples. This is typical for all studied ICS.

Results: To determine the structural parameters of the hydride phases, hydrogen-saturated samples were placed in liquid nitrogen under pressure, and then kept in air at the same temperature (77 K) for 1-2 hours. This treatment leads to passivation of the surface and prevents decomposition of the hydride for several hours, which is sufficient for X-ray phase analysis. The morphology of intermetallic powders changes in the same way during mechanical activation for all studied ICS. Exposure to hydrogen leads to visible dispersion of IC particles. As the processing time in the ball mill increases, the content of small, shapeless particles increases.

All compounds, including hydrides, have a hexagonal structure with the space group P6/mmm ($CaCu_5$

type). Alloying $LaNi_5$ with other metals does not lead to the appearance of additional phases. The authors of the work show that among the new technologies being developed for hydrogen purification and storage for autonomous energy, devices and systems based on the use of reversible metal hydrides (MG) – intermetallic compounds (IMS) capable of selectively and reversibly absorbing hydrogen can become economically acceptable and safe.

A series of laboratory samples of the AB5 type based on $LaNi_5$ with partial substitution of La for Ce, Ni for Fe, Mn, Al, Sn and other metals was prepared by melting initial stoichiometric weights of pure metals in an electric arc furnace in an argon atmosphere. To achieve uniformity of composition, each sample was melted at least 3 times. The purity of the starting metals was at least 99.5%.

In a literature review on the crystal structure of $LaNi_5H_6$, hydrogen atoms are arranged in octahedral nodes coordinated by two La atoms and four Ni atoms; tetrahedral nodes are coordinated by two La atoms and two Ni atoms. In octahedral and tetrahedral nodes, the concentration of hydrogen atoms is 96% in 3c (octahedral nodes) and 52% in 6d (tetrahedral nodes) in the spatial group P31m (No. 157), respectively. The weight and volume densities of $LaNi_5$ hydrogen are 1.38 wt.% and 92 kgN^2/m^3, respectively. Despite the higher volume density of $LaNi_5$ hydrogen compared to gaseous and liquid hydrogen (less than 70 kg^2/m^3), it is necessary to improve the low weight density of hydrogen. The properties of hydrogen storage by LaNi5-based alloys, including cycles of hydrogen absorption and desorption reactions, crystal structures, microstructures, and morphology, were studied.

Conclusion: This paper provides an overview of recent studies of the $LANI_5$ intermetallic compound, one of the most promising materials of the ab_5 type for hydrogen storage. The physicochemical properties of this compound, its ability to form stable reversible hydrides, as well as current trends in structural modifications to improve hydrogen absorption characteristics are reviewed.

The main attention is paid to the effect of mechanical activation on the structural and phase states of $LaNi_5$, as a result, on its interaction with hydrogen. It has been established that mechanical activation can significantly change the microstructure of the material by reducing the size of crystallites, increasing the density of defects and partial amorphization. These changes contribute to improving the kinetics of hydrogen absorption and desorption, as well as increasing the specific hydrogen capacity.

An analysis of recent achievements has shown that the most effective results can be achieved with the combined use of mechanical activation and alloying. Replacing nickel with other elements such as Co, Mn, Al, and Fe allows fine-tuning the thermodynamic parameters of interaction with hydrogen and increasing the material's resistance to degradation during repeated cycles.

Thus, the analysis of the work performed shows the prospects of using mechanical activation as a method of increasing the efficiency of $LaNi_5$-based materials in hydrogen energy. The data obtained can be used in the development of highly efficient hydrogen storage systems and the creation of materials with specified characteristics.

The present work was carried out as part of the implementation of the objectives of the IRN project No. PCF -BR21882200 targeted program financing of the Science Committee of the Ministry of Science and Higher Education of the Republic of Kazakhstan.

Biography

I, Nassyrova Anar Kenzhebekkyzy, was born on October 26, 1992 in the East Kazakhstan region. She graduated from high school in 2009. In 2009, she entered the «Sarsen Amanzholov East Kazakhstan University» at the Faculty of Natural Sciences and Technology, specializing in 5B071000 – «6B07101 Materials science and technology of new materials». In 2015, she enrolled in a magistracy degree in the specialty 6M012000 – Professional training».On October 15, 2019, I am currently working at the NJSC «Sarsen Amanzholov East Kazakhstan University» as a teacher (lecturer).

Since 2023, he has been a senior lecturer. I teach various disciplines such as Mechatronics and Electronics, Composite Materials, Three-dimensional processing of materials, etc. at the Department of Physics and Technology.

List of scientific and methodological works: textbook-2, international article-5, KKSON-1.

In 2024, the doctoral 8D05301 – «Physics» of the Department of Physics and Technology of the NJSC «Sarsen Amanzholov East Kazakhstan University».

Coalesce Research Group

13th International Conference on

Materials Science & Engineering

October 22-24 2025 | Tashkent, Uzbekistan

EFFECT OF ACIDIC ENVIRONMENT ON THE STRUCTURE OF COMPOSITE COATINGS BASED ON SUPERMOLECULAR POLYETHYLENE

Perassyl Zhanimkhan

Sarsen Amanzholov East Kazakhstan University, Kazakhstan

Abstract

Background: In this paper, the influence of an acidic environment on the structure of composite coatings based on super-high molecular weight polyethylene (UHMWPE) modified with a mineral filler of the diabase type is investigated. It was found that the introduction of 10% diabase into the UHMWPE Matrix significantly increases the resistance of the composite coating to corrosive environments, which is confirmed by a minimum level of swelling compared to pure UHMWPE and composites with a high filler content. Scanning electron microscopy (SEM) showed a uniform distribution of diabase in the coating structure and the absence of defects such as sintering and cracks. Infrared spectroscopy (AFS) and X-ray diffraction analysis methods revealed a decrease in the degree of crystallinity of coatings under the influence of acids, but no significant changes in the chemical structure of the materials were recorded, which confirms their resistance to chemical decomposition. Composites containing 10% diabase showed the best chemical resistance, which is associated with the formation of a barrier structure that prevents the diffusion of acids.

With the help of a number of experimental methods, the effect of an acidic environment on the microstructure of UHMWPE and composite samples with a diabase-type mineral filler based on it was studied. It was found that pure UHMWPE and UHMWPE composite samples containing 10% diabase have the best resistance to acidic environments. The results show that UHMWPE and composites based on it do not decompose under the influence of aggressive media and indicate the low reactivity of the material under study to acids. However, with an increase in diabase, the resistance of UHMWPE composite to the effects of an acidic environment is somewhat reduced. This seems to be due to a decrease in the proportion of UHMWPE matrix material in the composite.

It was also found that after exposure to an aggressive environment, the crystallinity of pure UHMWPE decreases from 67 to 52%, and for a composite UHMWPE with a 10% diabase filler-from 60 to 49%. IR spectroscopy of UHMWPE samples and composites based on it did not reveal significant changes or shifts in the main peaks under the chemical influence of aggressive media.

Objective: Introduction of diabase into the matrix of ultra-high molecular weight polyethylene (UHMWPE) with filler for the manufacture of coatings resistant to aggressive environments.

Methods: As the main material for the production of coatings, UHMWPE commercial powder (Yangzhou Guotai Fiberglass Co., Ltd.), density 930 kg/m^3, molecular weight 2·106 mol-1, TB = 135-150°C, bulk density >0.4 g/cm^3 is obtained. As a filler – contains 10, 20, 30 and 40 drunk. % dispersed powder used mineral diabase. The average size of diabase particles is 14 microns.

The coatings were obtained by the gas-flame method, respectively. Standard aluminum foil was used as a substrate. For subsequent tests and research, the coatings were mechanically separated from the substrate. The resulting samples will have a square shape dimensions 50×50×1mm.

Results: When UHMWPE samples are exposed to acids (H_2SO and HCl) for a long time, the chemical

resistance results are shown. However, changes in the degree of swelling and mass of samples increase with an increase in the amount of acids and the duration of their action, which leads to the diffusion of acid molecules in the polymer and partial degradation of the material.

At the level of 10% diabase, the coating shows the best resistance (degree of swelling 0.00598 G), which is due to the uniform distribution of the filler and increased barrier properties. With an increase in diabase up to 20%, the chemical resistance of the coating remains high, however, due to the initial destruction of intermolecular bonds in the matrix, the level of edema increases to 0.01564 G. In 30% and 40% diabase, the chemical resistance decreases sharply (the swelling rate is 0.0329 G and 0.058 g, respectively). This is due to the excess amount of filler, which causes defects in the structure of the coating, increases porosity and allows the acid to penetrate deeper.

The results of the study of the surface of composite coatings based on UHMWPE by IR spectroscopy are presented. In the IR spectra, deformation oscillations of groups C–H at 2915 cm^{-1}, 2844 cm^{-1} and valence oscillations of groups C–H at 1560 cm^{-1} are manifested. Also, carbonyl functional groups can be observed at 1248 cm^{-1}, and the peak of 721 cm^{-1} shows a double C=C bond, the above bands are characteristic of the initial UHMWPE absorption bands as shown in the work.

The X-ray diffraction pattern shows two intense reflections (110) $2\theta = 21.76°$ and (200) 24.15°, which characterize the crystalline part of the UHMWPE structure with an orthorhombic lattice [4]. Due to their complex chemical composition, diabase peaks have a low intensity. The most intense diabase reflexes (004), (420) and (111) are observed at diffraction angles of 12.49°, 25.11° and 27.91°, respectively.

From the analysis of X-ray diffraction data to chemical exposure, it was found that the degree of crystallinity of a pure UHMWPE sample is 67%, and for a composite based on UHMWPE, the degree of crystallinity of a diabase filler in the amount of 10% drunk is 60%. After chemical exposure, the percentage of crystallinity of samples from UHMWPE and the composite based on it decreases and is 52 and 49%, respectively. Acids can cause ion deposition on the surface of UHMWPE, which can lead to the formation of surface films or deposits that reduce the degree of crystallinity of the material as it turned out, as a result of radiation-chemical effects, the degree of crystallization of the polymer can be significantly reduced.

On the surface of UHMWPE samples with diabase filler, minor changes are observed after exposure to an aggressive environment. The continuous structure of the polymer matrix is preserved, which confirms its morphological stability. The preservation of the structure can be explained by chemical inertness and the high molecular weight of UHMWPE, which interferes with the diffusion of aggressive agents. These results are consistent with the data presented in the literature, which shows the high resistance of UHMWPE to chemical degradation.

Conclusion: With the help of a number of experimental methods, the effect of an acidic environment on the microstructure of UHMWPE and composite samples with a diabase-type mineral filler based on it was studied. It was found that pure UHMWPE and UHMWPE composite samples containing 10 diabase have the best resistance to acidic environments. The results show that UHMWPE and composites based on it do not decompose under the influence of aggressive media and indicate the low reactivity of the material under study to acids. However, with an increase in diabase, the resistance of UHMWPE composite to the effects of an acidic environment is somewhat reduced. This seems to be due to a decrease in the proportion of UHMWPE matrix material in the composite.

It was also found that after exposure to an aggressive environment, the crystallinity of pure UHMWPE decreases from 67 to 52%, and for a composite UHMWPE with a 10% diabase filler-from 60 to 49%. IR spectroscopy of UHMWPE samples and composites based on it did not reveal significant changes or shifts in the main peaks under the chemical influence of aggressive media. This suggests that UHMWPE and the composites based on it did not undergo significant degradation under the influence of the chemical environment. The absence of visible defects on the surface of the sample also indicates that the microstructure of the composite material does not undergo significant chemical degradation or corrosion when exposed to an acidic environment. In our opinion, due to the high average resistance, structural changes in UHMWPE and its diabase filler composites occur to a lesser extent than other polymers, which makes it attractive for use in aggressive environments.

Biography

Zhanimkhan – Project Engineer, Sarsen Amanzholov East Kazakhstan University, 070002, Ust-Kamenogorsk, Kazakhstan.

Coalesce Research Group

13th International Conference on

Materials Science & Engineering

October 22-24 2025 | Tashkent, Uzbekistan

INVESTIGATION OF INTERGRANULAR CORROSION RESISTANCE IN WELDED DISSIMILAR STAINLESS STEELS 12X18H10T AND AISI 316

Eldos Akbolatov

Institute of Atomic Energy Branch RSE NNC RK, Kazakhstan

Abstract

Background: Welded joints of dissimilar austenitic stainless steels are widely used where combined performance properties are required, such as corrosion resistance, heat resistance, and mechanical strength. Steel 12X18H10T contains titanium, which stabilizes the microstructure and prevents chromium carbide formation, enhancing intergranular corrosion (IGC) resistance at 500–850 °C. AISI 316, enriched with molybdenum, offers excellent pitting corrosion resistance. Such welded joints are found in heat exchangers, pipelines, and reactors operating under high temperatures and aggressive environments, where the heat resistance of 12X18H10T and the corrosion resistance of AISI 316 are both needed. Despite good weldability, joining these dissimilar steels presents challenges, especially the risk of IGC and brittle phase formation in the weld.

Objective: To experimentally determine the ferrite phase content in the weld metal and evaluate the susceptibility to IGC of dissimilar austenitic stainless steel welds between 12X18H10T and AISI 316.

Methods: Test samples were welded using a Fronius MagicWave 230i TIG welding machine. Radiographic nondestructive testing was applied. Ferrite content was measured with a Ferritscope FMP30. IGC susceptibility was assessed using the AMU method (GOST 6032-2017). Microstructure was analyzed on a TM4000Plus Hitachi scanning electron microscope.

Results: The ferrite content in the weld metal ranged between 2.78% and 3.70%. The weld metal and heat-affected zone (HAZ) showed dendritic structures oriented along the heat dissipation direction, with austenite filling the interdendritic spaces. Corrosion damage was observed along the fusion line on the AISI 316 side, where metal degradation was most intense. This region exhibited austenite with a high density of chromium carbides, particularly along grain boundaries.

Conclusion: The fusion line on the AISI 316 side of the dissimilar weld showed lower corrosion resistance, potentially reducing overall joint strength. Further studies are needed on post-weld heat treatment and mechanical performance optimization.

Biography

Eldos Akbolatov is an engineer at the Institute of Atomic Energy, National Nuclear Center of the Republic of Kazakhstan, and a second-year PhD student. He works in the field of metal processing and welding, specializing in the study of welding issues for stainless steels and zirconium alloys used in the nuclear industry. His research interests include welding of dissimilar materials, optimization of welding technologies to improve the corrosion and mechanical resistance of joints, and investigation of the effects of welding parameters on the microstructure and properties of weld metal. Eldos is involved in developing welding technologies for complex systems and experimental devices, including equipment designed to operate under extreme conditions of high temperature, pressure, and aggressive environments. He is the author of several publications in scientific journals and conferences and actively collaborates with industrial enterprises and research institutes to implement innovative welding solutions.

Coalesce Research Group

Bookmark The Dates

15th International Conference on

MATERIALS SCIENCE AND ENGINEERING

October 28-29, 2026 | **Dubai, UAE**

Vote of Thanks

We extend our sincere gratitude to all speakers, delegates, and participants whose presence and contributions made this conference a meaningful and successful gathering. Our heartfelt thanks also go to the organizing committee, sponsors, and partners for their invaluable support. We look forward to continued collaboration and future engagements.

Scan QR for Conference Book

Phone: +1-718-543-9362 | E-Mail: materialscience@conferencesecretary.com